Toughening of Rigid Silicone Resins

by

Bizhong Zhu

Bachelor of Science, Polymer Synthesis, 1985
Master of Engineering, Polymer Materials, 1988
Chengdu University of Science and Technology, China

Submitted to the Department of Materials Science and Engineering in Partial Fulfillment of the Requirements for the Degree of

DOCTOR OF PHILOSOPHY IN POLYMERS
at the
MASSACHUSETTS INSTITUTE OF TECHNOLOGY

September 1997

Signature of Author: _____
Department of Materials Science and Engineering
August 8, 1997

Certified by: _____
Frederick J. McGarry
Professor of Polymer Engineering
Thesis Supervisor

Accepted by: _____
Linn W. Hobbs
John F. Elliot Professor of Materials
Chairman, Departmental Committee on Graduate Students

Toughening of Rigid Silicone Resins

by

Bizhong Zhu

Submitted to the Department of Materials Science and Engineering
on August 8, 1997 in Partial Fulfillment of the
Requirements for the Degree of Doctor of Philosophy in Polymers

ABSTRACT

Rigid silicone resins are too brittle for structural applications. Previous efforts to toughen them have been unsuccessful, due to the highly crosslinked nature of the resin. A new two step approach has been proposed and followed in this study. The Phase I step improves the resin network mobility by incorporating short rubber chain into it, and the Phase II step facilitates matrix plastic deformation by separate rubber particles of appropriate type and size.

Triethoxy silyl or phenyl dimethoxy silyl terminated PDMS were prepared by end capping silanol terminated PDMS with TEOS or methyl trimethoxy silane, and their structure and chain length verified by FT-IR, ^{1}H and ^{29}Si NMR. The compatibility of the PDMS with the resin pre-polymer was studied by ternary phase diagrams. The functionalized PDMS was coupled with the resin pre-polymer with no self condensation of the PDMS and minimum chain scission. This pre-cure coupling was essential.

Casting techniques were developed which enabled the investigation of mechanical properties and fracture behavior of the cured system. The coupled Phase I rubbers (DP 8-57) significantly increased the K_{Ic}, the G_{Ic}, the strain at break, and the strength. Longer Phase I chains were more effective than shorter ones due to less restricted chain motion. Second phase particles were formed by coupling long chain PDMS (DP 246-586) with the resin. The appropriate Phase I/II combination was 7 to 9 times more effective than the Phase I alone, while Phase II alone was harmful. The appropriate particle size was in the submicron range, comparable to the resin nodular size, 60 to 80 nm in diameter. By effective Phase I/II combinations, K_{Ic} of the resin was increased by 220%, and G_{Ic} by 900%, with a modulus drop of 25%. The thermal stability of the PDMS modified resin was unchanged. The enhanced network mobility, and the successful engagement of the resin nodules in the plastic deformation process by the rubber particles were identified as the toughening mechanisms. Use of rigid silicone resins for structural purposes has been made possible by this method of incorporating PDMS.

Thesis advisor: Frederick J. McGarry
Title: Professor of Polymer Engineering

To my parents and my wife

Acknowledgments

I wish to thank Professor F. J. McGarry for his invaluable guidance in the course of this research. Especially appreciated is his encouragement when I was frustrated in the lab. He is not only an academic advisor but also a personal model from whom I have learned so much!

Professor Michael Rubner and Professor Dietmar Seyferth in the Chemistry Department are thanked for their priceless help as members of my thesis committee. I owe an apology to them for trying repeatedly to set up meetings at short notice.

Many people at MIT have offered their generous help. Among them Arthur Rodulph and Steve Rodulph of the Civil Engineering Department, and Timothy McClure at the Center of Materials Science and Engineering deserve special thanks. They have made my work so much easier it is safe to say I would still have been at the Phase I of my research if it were not for them.

I also want to thank Dow Corning Corporation for financial support which made this work possible. Dr. Dimitris Katsoulis and John Keryk at Dow Corning have given whatever they can possibly supply, including and far beyond materials, ideas, and even experimental work, to expedite the project. I am really excited that I will become a colleague of them.

It has been an extremely pleasant experience working in Professor McGarry's group. Diane Rose has been taking care of all the administrative work for us. She even typed for us our research reports I, II, III and...., who knows what follows, that I almost felt guilty. Dr. Carmon Bautista read my thesis very carefully and made excellent comments. UROP students Jason Pinto, Kum Ming Woo, graduate students Deborah-Ann Spense, Lan Hoang, Anand Raghunathan, and student researcher Greg Zelenka worked with me on the project. Working with them has been as enjoyable as it is fruitful. Drs. Ramnath Subramaniam and Edward Shaffer, Rizwan Gul, Caroline Lee, and Mavyn McAlliff are thanked for their help in the lab.

Table of contents

List of Illustrations and Figures

List of Tables

Chapter 1. Background and Strategy

1.1. Introduction.

Toughening of polymers has become so widely practiced that for each engineering plastic several toughened versions can be found[1-14]. There are two main routes to a toughened polymer: the manipulation of the molecular composition and architecture, and the incorporation of second phase toughening particles. For thermoplastics the first route controls the stiffness and tacticity of the chain as well as the molecular weight and its distribution. For thermosetts it changes the crosslink density, its distribution and the chain structure between crosslinks. The second route makes a more complete use of the intrinsic toughness of a polymer. A number of ways have been identified as successful; among them the incorporation of rubbery particles is most widely practiced. The particles controllably alter stress distribution, relieve stress triaxiality ahead of a crack, and induce plastic deformation in numerous places instead of a few localized areas[15]. In addition to the incorporation of rubbery particles, other means such as the use of reinforcement, inorganic fillers, and low molecular weight plasticizers can also hinder the growth of a crack and help promote plastic deformation. Transformation of crystal domains from one form to another may also help slow crack initiation and propagation.

Enhanced toughness has tremendously broadened the use of many polymers. Examples include High Impact Polystyrene[16-19], rubber toughened epoxy resins[20-29], plasticized and rubber toughened Polyvinyl Chloride[30], toughened unsaturated polyesters[31, 32], Poly Methyl Methacrylate[33-38], Polyamides[11, 13, 39-43], Polyacetal[12], Polyethylene[44-46], Polycarbonate[47, 48], and many others[49-51].

It has been sought to apply the general polymer toughening principles in rigid silicone resins. Efforts to toughen them started decades ago when rubber toughening of polystyrene became successful, but the conclusion was made that rigid silicone resins could not be toughened in a similar manner.

Silicone resins are among the best heat and fire resistant polymers and have found wide applications where such properties are desired. However they are highly crosslinked, possessing mainly a T or Q structure. Their rigidity depends on the crosslink density and the substitutions on the silicon atoms. A high modulus is obtained only by using more Q structure, or by combining the highly crosslinked T structure with a high percentage of bulky substituents such as phenyl. A higher fraction of Q structure or bulky substituents leads to the very brittle nature of rigid silicone resins, which severely restricts their use. It is the primary goal of this research to show that rigid silicone resins can be substantially toughened by applying the general polymer toughening principles, essentially without loss of thermal stability.

In this Chapter, the toughening mechanisms found in organic polymers and the underlying principles will be reviewed. A brief discussion on silicone resin chemistry and the past toughening experience will be given. Finally, a strategy to toughen rigid silicone resins will be proposed based on these principles and on past experience.

1.2. Principles of Polymer Toughening.

1.2.1. Stress blunting around a crack tip.

The fracture of epoxy resins has been extensively studied and the following three crack growth modes have been observed: brittle stable growth, unstable stick-slip growth and ductile stable growth[52-56]. At low temperature or relatively fast displacement rates, the crack grows at a constant load. The fracture toughness is low and almost independent of the test rate and temperature within a certain range. At a higher temperature and slower rate, the crack grows in a stick-slip manner and the fracture toughness, K_I, corresponding to the crack arrest stress, is found to be the same as the K_I for the onset of brittle stable growth at lower temperature and faster rate. At even

higher test temperature, the crack grows in a stable ductile manner, involving extensive plastic flow. It has been found that under the above test conditions the crack tip has been blunted to various degrees. Higher temperature and lower displacement rate allow more crack tip blunting and thus higher measured fracture toughness.

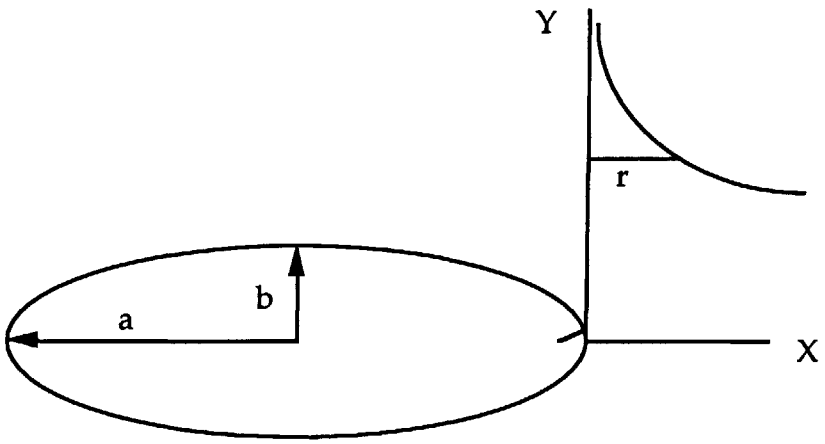

Figure1. 1. Schematic diagram of an elliptical hole in an infinite sheet.

Blunting prevents or delays crack growth by reducing the stress concentration at the crack tip. Although more sophisticated solutions for the stress distribution around a crack tip are available, the following approach serves the purpose to explain the effect of crack tip blunting. If the crack tip has a finite radius of curvature, i.e. $\rho << a$, the stress distribution in the vicinity of the tip ($r << a$) can be approximated by the solution for an elliptical hole in an infinite body shown in Figure 1.1[57, 52-54]:

$$\sigma_{yy} = \frac{\sigma_0 \sqrt{a}}{\sqrt{2r}} \frac{(1+\rho/r)}{(1+\rho/2r)^{3/2}} \tag{1.1}$$

where σ_0 is the applied tensile stress far from the elliptical hole, ρ the radius of curvature of the tip, r the distance from the tip, a is half of the major axis of

the elliptical hole and σ_{yy} the stress in the Y direction.

Based on the observation that during stick-slip crack growth, the crack is initiated at a distance ahead of the crack front and grows back toward the front, a critical stress level, σ_c, at a critical distance c, from the crack front, has been proposed as the fracture criterion. This is equivalent to a critical stress intensity factor, K_C, thus:

$$\sigma_c = \frac{\sigma_0\sqrt{a}}{\sqrt{2c}}\frac{(1+\rho/c)}{(1+\rho/2c)^{3/2}} \tag{1.2}$$

σ_c is a monotonically decreasing function of ρ if ρ/c is greater than 1. If ρ/c is greater than 1, as the crack tip radius of curvature ρ increases, higher external force, σ_0, must be applied to bring σ_c to the critical level. Macroscopically the specimen will exhibit a higher fracture toughness. The measured fracture toughness, K_{Ic}, is related to the applied tensile stress by:

$$K_{Ic} = \sigma_0\sqrt{\pi a} \tag{1.3}$$

and $K_{Ic}^{'}$, the criterion for the growth of a sharp crack without blunting, is:

$$K_{Ic}^{'} = \sigma_c\sqrt{2\pi c} \tag{1.4}$$

thus from (1.2):

$$\frac{K_{Ic}}{K_{Ic}^{'}} = \frac{(1+\rho/2c)^{3/2}}{(1+\rho/c)} \tag{1.5}$$

The quantity $\frac{K_{Ic}}{K_{Ic}^{'}}$ is the ratio of the fracture toughness measured when the crack tip is effectively blunted to that measured when the crack tip remains sharp during the test. It goes through a minimum when ρ/c equals one and then rises monotonically with ρ/c. For a given fracture criterion σ_c and c, an effectively blunted crack tip with a larger radius of curvature will start growing at a higher measured K_{Ic}. Plastic flow of material in the area close to the crack tip is required to blunt the crack tip. When toughened, the mobility of the polymer chain can be enhanced, or the constraint can be relieved to increase the plastic flow.

1.2.2. Energy consideration.

In some cases an energy analysis may better elucidate the underlying toughening principles, although it is essentially equivalent to the above stress analysis. Based on the minimum potential energy theorem, Griffith[58] proposed the well known rupture criterion for brittle solids: the total potential energy of an elastically strained body is diminished by the introduction of a crack. This is equivalent to saying that the release of elastically stored energy in the body by the introduction of a crack is greater or equal to the energy required to create the new surfaces of the crack. Considering only surface tension as the energy required to create the crack surface, the stress required to initiate a crack is:

for plane stress:
$$\sigma = \sqrt{\frac{2E\gamma}{\pi a}} \tag{1.6}$$

and for plane strain:
$$\sigma = \sqrt{\frac{2E\gamma}{\pi(1-\nu^2)a}} \tag{1.7}$$

where E is the Young's modulus, γ the surface tension and ν Poisson's ratio. This relation holds well for very brittle materials such as glass. Irwin[59, 60] and Orowan extended Griffith's theory and replaced γ by the fracture work per unit crack extension, which included the surface energy and the plastic work. Typically in polymers, it has been found that the surface energy, γ, only amounts to a few percent of the fracture work. For a linear elastic body, when the energy dissipation mechanisms are confined in a relatively small region close to the crack tip, Griffith's equation (1.6) may be extended to include any energy dissipation:

$$\sigma = \sqrt{\frac{2EG}{\pi a}} \tag{1.8}$$

where G is the sum of all energy dissipation per unit area of crack growth. Extensive crack tip plastic deformation increases G and the stress to initiate a crack.

1.3. Toughening Mechanisms.

1.3.1. Rubber particle induced crazing and shear yielding.

Rubber particles are often used to toughen polymers. The role of the particles in a rigid polymer matrix is three fold: (1) due to thermal expansion mismatch residual stresses are built up inside and outside the particles, as a result of cooling after the curing cycle; (2) under a uniform remote stress field, the inclusion creates a stress concentration which is confined to less than a few diameters away from the surface of the particle; (3) the rubber particle can deform, cavitate and introduce a new energy dissipating mechanism into the system. The disturbance of the stress field by the particles may suppress crazing and facilitate yielding, or it may simply induce crazing or yielding in numerous places, instead of just a few when the rubber particles are absent. Therefore great mechanical energy can be consumed before the material fractures.

The residual stress due to the thermal expansion mismatch was derived by J. Selsing[61]. In the matrix at a distance r from the particle:

$$\sigma_r = -2\sigma_t = -P\frac{R^3}{r^3} \tag{1.9}$$

where R is the radius of the particle, σ_r is the stress along the radial direction, and σ_t is the stress along the tangential direction. P is negative and is the hydrostatic pressure created inside the particle:

$$P = \frac{\Delta\alpha \cdot \Delta T}{\frac{1+\nu_1}{2E_1} + \frac{1-2\nu_2}{E_2}} \tag{1.10}$$

where $\Delta\alpha$ is the difference of thermal expansion coefficients of the matrix and the dispersed particle, ΔT is the cooling temperature range, E_1 and ν_1 the Young's modulus and Poisson's ratio of the matrix, E_2 and ν_2 those of the rubber. Usually polymers are either processed or cured at relatively high temperature and cooled down to the service temperature. The rubber in the polymer matrix, having a higher thermal expansion coefficient, creates a negative pressure inside the particle, a compressive stress along the tangential

direction in the matrix and a tensile stress in the radial direction in the matrix. The tangential compressive stress in the matrix and the negative pressure in the particle are important. The former will generally facilitate yielding under tensile loading and the latter may facilitate cavitation of the particle and relieve the stress triaxiality constraint. In many rubber toughened polymers the separate domain is not pure rubber, but as long as the separate domain has a higher thermal expansion coefficient than the matrix, a similar residual stress state will be created.

For an isotropic, homogeneous solid under load, the stress around a spherical inclusion in it was derived by Goodier[62]. The final expression is rather complicated and covers the variation from a void to an ideal rigid particle. At one extreme, in the case of the void, under a uniform tensile stress σ_0, the highest stress concentration is at the equator of the sphere and is $^{45}/_{22}\sigma_0$. If the spherical inclusion is filled with a material having a Young's modulus 1/4 that of the matrix and the same Poisson's ratio, this stress concentration is lowered by approximately 20%. Therefore a rubbery inclusion in a rigid polymer matrix will create a stress concentration at the equator of the particle between 1.9 to 2 times of the average tensile stress.

When a polymer sample with rubbery inclusion is stretched, crazing will be initiated by the stress concentration around the rubber particle, if the craze stress is lower than the yield stress under the specific stress condition. This has been observed by many authors[5, 7, 64-67]. When the yield stress is lower than the craze stress, as is usually the case for polycarbonate at room temperature, the stress concentration will initiate shear yielding. This has also been verified both experimentally[5, 7, 68-70] and by numerical simulation[7]. Since large numbers of rubber particles usually are incorporated into the polymer matrix, crazing or yielding can be initiated in numerous places rather than a few when impurities dominate. Much more energy can be consumed.

There are several requirements that have to be satisfied for the rubber particles to be effective. The above analysis is a simplified one. The adhesion between the particle and the polymer matrix is assumed to be perfect; the initiation of crazing and shear yielding is assumed to be determined only by

the local stress concentration, which according to Goodier's and Selsing's analysis is independent of the particle diameter; rubber particles are assumed to be far apart from each other. In reality the distance between particles is not always greater than four times the particle diameter, so concentrated stress fields may overlap. The adhesion between particles and matrix has been found to be extremely important. Often chemical linkage has to be established at the interface of the particle and the matrix, or the particle should be formed in situ by precipitation from a homogeneous solution to ensure good adhesion. When adhesion is poor, the particles function much like voids, which create a stress concentration without the ability to inhibit or retard the development of a crack. Particle diameter also is a major factor determining toughening efficiency[7, 19, 20]. It has been proposed that the size of the stress field mismatch created by the presence of the particles should be comparable to the scale of the plastic deformation involved. For example, crazing usually involves larger scale plastic flow of material than shear banding thus larger particles will be more effective in initiating crazing and smaller ones are better for shear banding. There is an optimal particle size for each specific matrix system.

The modulus of the spherical inclusion is also important. According to Goodier's analysis, in going from a lower to one higher than the matrix, in a uniform tensile stress field, the stress at the equator goes from increased tension to less than the average stress. And according to equation (1.9), the thermal stress in the matrix becomes tensile tangential to the sphere surface and compressive normal to the sphere surface, which is more likely to suppress yielding.

1.3.2. Rubber particle cavitation.

Under plane strain condition a crack opening force creates a triaxial tensile stress state ahead of the crack tip. Combined with the thermal stress inside the particle, this facilitates cavitation of the particle and the cavity may grow plastically[81-84]. As a result of the cavitation, the triaxiality of the stress state is relieved and yielding is facilitated. The cavitation process, creating

new surfaces, and the subsequent plastic growth of cavities convert mechanical energy into heat or surface energy.

The tendency of the particle to cavitate under the triaxial tensile stress is determined by the diameter of the particle. Dompas obtained a criterion for particle cavitation [71, 80, 84] based on an energy analysis. The hydrostatic strain energy built up in the rubber particle should be large enough to supply the energy of the surface area created by the cavitation process. With a given hydrostatic strain, the particle diameter above which cavitation will take place is:

$$d_0 = \frac{12(\gamma_r + \Gamma_{sc})}{K_r \Delta^{4/3}} \tag{1.11}$$

where γ_r is the rubber surface energy, Γ_{sc} is the energy required to break chemical bonds per unit area of rubber, K_r is the rubber bulk modulus, and Δ is the relative volume strain of the particle. According to (1.11), for a small particle, the volume strain of the particle should reach a high value in order for the particle to cavitate. However the volume strain of the particle is restricted by the strain that the matrix can achieve without fracture. Therefore for a specific system, there is a critical value of the particle diameter below which cavitation will not take place and above which it will. This has been verified in numerous systems. When the particles do cavitate, as they often do in modified epoxy resins, the process dissipates much energy and the matrix is greatly toughened.

1.3.3. Rubber bridging of the crack surfaces.

In highly crosslinked thermosetts, rubber bridging of the crack flanks may be important. The bridging particle extends much more than the matrix resin and its contribution to the fracture toughness is the energy stored and dissipated by the extended rubber before it breaks. Kunz-Douglass and collegues[85] analyzed this in highly crosslinked epoxy and proposed a useful model to account for the contribution to the toughness of epoxy resins. Based on their analysis, the rubber particles will elongate and tear at a certain elongation. Tearing will start at the boundary of the crack surface and the

elongated rubber particle when the stored strain energy release rate of the debonded rubber is equal to or higher than the energy absorbing rate by the new surfaces created by debonding and tearing. A critical extension ratio, λ_t, at which tearing will start, can be obtained through the relation:

$$\lambda_t^2 - \frac{4}{\lambda_t} + 3 = \frac{4\Gamma_t}{\overline{G}\overline{R}} \tag{1.12}$$

where Γ_t is the tear energy of the rubber, $\overline{G}$ the average or effective shear modulus of the rubber and $\overline{R}$ the average rubber particle diameter. This relation predicts that the critical extension ratio will be higher for smaller particles, which is verified by experiments within the diameter range from 2 to 30 microns. The contribution of a particle to the toughness of the system is the energy used to stretch the particle to the tear point:

$$\Delta G_{IC} = \left[\frac{\lambda_t^2 + 2/\lambda_t - 3}{\lambda_t^2 - 4/\lambda_t + 3}\right] 4\Gamma_t V_p \tag{1.13}$$

where V_p is the volume fraction of the rubber particles. The predicted results agree reasonably well with the toughening effect obtained with a highly crosslinked epoxy but with more ductile matrices the agreement was not so good. In ductile matrices the rubber particles induce more effective mechanisms to toughen the resin.

A drawback of this model is its prediction that the bridging contribution has little dependence on rubber particle size, which contradicts experimental observations. An examination of equations (1.12) and (1.13) may disclose the reason. In equation (1.13), the quantity in the bracket will be practically independent on λ_t if λ_t is higher than 4. Equation (1.12), however, will predict a λ_t well above 30 for particles of 0.5 micron in diameter, if a typical value of 400 J/m^2 is used for Γ_t and 3 MN/m^2 for $\overline{G}$, as cited in Kunz-Douglass' paper. If a typical Γ_t value for bulk rubbers, between 10^3 to 10^4 J/m^2, is used, the predicted λ_t will easily exceed hundreds, which is far higher than the possible ultimate elongation of any rubber. Therefore modification should be made to this model. If we equate λ_t to 10, the typical ultimate extension achievable by a rubber, we can obtain an approximate value of 5

microns as the rubber particle diameter above which this model holds. Below this limit this model will fail.

1.3.4. Brittle-ductile transition.

The yield stresses of most glassy polymers are similar so their toughness depends on how much they extend before fracture. This is determined by the density of chain entanglements or crosslinks. If the matrix is capable of large extension but does not do so, then plastic constraint and strain localization may be the reasons. The constraint can be relieved and plastic flow restored. Such a brittle to ductile transition is observed when the matrix ligament thickness between rubber particles is below a critical value[86-100]. The phenomenon is explained by a plane strain-plane stress transition. Wu[86-90, 92] modeled the brittle to ductile transition in rubber toughened Nylon-66 as the percolation of the thin matrix ligaments in which a plane strain-plane stress transition and yielding take place. Below the critical ligament thickness, the stress concentration due to individual particles overlap and yielding is more effectively promoted. When connectivity of the local yielding zone around particles can be achieved, yielding will propagate through the entire area. The yielding of thin ligaments also relieves the constraint on thick ligaments and initiates the yielding of the latter. Cavitation of rubber particles more effectively relieves the constraint but it is not necessary because of the stress volume overlap. Smaller particles are more effective in reducing matrix ligament thickness, but if matrix crazing is the predominant energy dissipating mechanism an optimal particle size is expected. Relatively large particles are required to initiate crazes but the matrix ligament thickness should be reduced below the critical level to prevent easy catastrophic failure of matrix ligaments between crazes. Agglomeraion of particles is detrimental to rubber toughening because of the large matrix ligament thickness between such concentrations.

Percolation models will apply only to quasi-ductile matrices, which include polymers theoretically capable of large extension. van der Sanden[93-100] showed the critical thickness is strongly dependent on the crosslink or entanglement density of the matrix, and increases as the entanglement or

crosslink density increases. Also, increasing the entanglement or crosslink density decreases the magnitude of the toughness differential at the transition. If the crosslink density is high, no brittle to ductile transition is observed.

1.3.5. Cold drawing.

In certain blends of brittle and ductile thermoplastics, with the former the minor and the latter the major component, a toughness higher than both sometimes can be obtained[101-103]. This has been attributed to the cold drawing of the brittle particles. During bulk deformation a large compressive stress is created on the brittle particle, which suppresses crazing of the brittle polymer and facilitates yielding. (Generally a brittle thermoplastic will go through a brittle-ductile transition with rising temperature or pressure[104, 105].) For some brittle thermoplastics, the transition pressure P_c has been measured. According to Goodier's stress analysis, when a spherical inclusion of higher elastic modulus and smaller Poisson's ratio is present, a compressive stress will be created at the equator of the particle if the plate containing the particle is uniaxially stretched. It has been shown[101-103] that when this compressive stress exceeds the brittle to ductile transition pressure of the polymer particle, the particle will undergo large plastic deformation and toughen the ductile matrix.

1.3.6. Phase transformation toughening.

Phase transformation toughening is practiced in metals and ceramics. In semicrystalline polymers, stress induced phase transformations also can occur. For example, PBT undergoes a reversible α (helix) to β (planar zig-zag) transformation upon loading[104], with a density change from 1.40 to 1.29 g/cm^3. Volume expansion accompanies this density change. In ceramics a similar volume expansion of partially stabilized zirconia creates compressive stress on the crack tip which opposes the crack opening stress. If the volume expansion in PBT could be utilized, a similar toughening effect might be

expected. However in polymers the degree of crystallinity also plays a very important role and the drawing at the crack tip may increase the crystallinity and cause a volume contraction. The result would be a competition between the expansion from the phase transformation and the contraction from the increase of crystallinity. Isotactic polypropylene undergoes a stress induced phase transformation from β(hexagonal) to α(monoclinic) with a density change from 0.921 to 0.936 g/cm^3, a net volume contraction, so during transformation stress shielding due to a volume expansion cannot occur. There has been no evidence that stress induced phase transformations in polymers function as an effective toughening mechanism, but there are discussions in the literature about its potential. If phase transformation toughening could be made to work in polymers, it would offer an advantage over rubber toughening: no decreases of strength, modulus and heat stability.

1.3.7. Plasticization and flexibilization.

Plasticization is probably the oldest technique to make a brittle polymer more flexible and useful[106]. First, mixing a high boiling point, inert, compatible organic liquid into a bulk polymer reduces the interchain interaction and provides more free volume. A second method copolymerizes a flexible comonomer into the backbone or grafts it to the backbone of a polymer to get higher chain flexibility or to reduce the interchain interactions. The first is called external plasticization and the second internal plasticization. The most common example of external plasticization is polyvinyl chloride, while internal plasticization has been done with many polymers to make them tougher. In contrast to PVC, where the modulus decreases greatly when plasticized, a small amount of internal plasticization with low molecular weight species can plasticize a crack tip area and increase the toughness significantly with little loss of modulus.

It has been shown[107-109] that the intrinsic plastic flow capability of the matrix itself is a critical factor in determining how effectively a polymer can be toughened by rubber particles. If a matrix is too brittle it must be plasticized or flexibilized to render it toughenable by rubber particles, otherwise the particles will be ineffective. External plasticization lowers the yield stress and

modulus. In highly crosslinked thermosetts, internal plasticization reduces the crosslink density and flexibilizes the network, often at the cost of thermal stability.

1.3. 8. Discussion.

Among the mechanisms discussed, rubber particle induced plastic deformation and particle cavitation have proved to be effective in toughening polymers. However these mechanisms can work only when certain requirements are met. The particles cannot induce plastic deformation if the matrix is inherently unable to flow, because of high entanglement or crosslink density. If this is the case internal plasticization is necessary, and it must be done without a severe drop in the modulus of elasticity or in the high temperature resistance of the material. The structure and properties of any dispersed rubber particles also must suit the specific polymer. Only when energy dissipation mechanisms are functioning in a synergistic manner will the polymer be effectively toughened.

1.4. Toughening of Rigid Silicone Resins.

A brief review of the silicone resin chemistry and the past toughening efforts is necessary. This will help understand the toughenability of the original resins and illustrate possible toughening mechanisms. Based also on past work of other researchers, the strategy followed in this research will be explained.

1.4.1. Silicone resins and their applications.

There are two major types of silicones: linear and branched or crosslinked. Their composition can be expressed as $(R^1_xR^2_ySiO_{(4-x-y)/2})_n$, where

R^1 and R^2 are alkyl or aryl substituents. While most often there are only one or two substituents, more can be introduced. By far the most important silicone material is rubber, or linear and crosslinked polydimethyl siloxane. Other major silicone products include silicone oils and silicone resins. The former is a low molecular weight linear polysiloxane, while the latter is a highly crosslinked polysiloxane produced mainly from T or Q structure.

Silicone oils, rubbers, and resins have found applications in almost every branch of industry because of their unique properties. The silicon-oxygen bond is slightly stronger than carbon-carbon one and inert to oxygen, so all silicone backbones have excellent thermal and oxidation resistance. The large bond angle around oxygen, the length of the Si-O bond and the larger size of the silicon atom combine to produce a low rotation energy barrier and a very flexible backbone chain. Because of this, silicones have a very low Tg and their physical properties do not change much with temperature. The combination of low Tg, low variation of properties with temperature, and excellent thermal and oxidation resistance makes silicones useful over a wide temperature range. Shielding the dipolar Si-O bond with organic substituents affords water repellence where moisture penetration needs to be stopped. The longer Si-O bond length, the easier rotation and the larger silicon atom, however, also increase the van der Waals distance between chains and reduce the van der Waals interchain interactions. This leads to the lower mechanical properties of silicones. To counter this silicone rubbers rely heavily on silica reinforcement in combination with slight crosslinking, while silicone resins utilize crosslinking reactions forming predominantly T structures.

There are two main types of silicone resins utilizing different crosslinking reactions: condensation between silanol ends, and hydrosilylation of vinyl with SiH termination. Good progress has been made in the past few decades to optimize the properties of resins for broad areas of applications: coatings[109-117], pre-ceramics[118-120], insulating materials for electric motors, glass fiber reinforced electrical panels[117,120,121], and more recently adhesives for cosmetics, electronic packaging[122-127] and resist materials for microlithography[128]. However no silicone resins have been suitable for structural uses, for two reasons: low rigidity and strength, and easy crack initiation and propagation. With a small substituent like methyl

on each silicon, even pure T structure is very soft and has a glass transition at ~40 °C. Bulkier substituents must be introduced to increase the Tg and the elastic modulus. Usually phenyl groups are used for this purpose, tightening the crosslinked network due to steric hindrance. However the tight network allows very little deformation and cooperative flow, leading to bonds being broken individually and to low fracture toughness. This is the cause of the very brittle nature of the high phenyl T resins. Copolymerization of phenyl T with methyl T and di functional monomers have been used to balance rigidity and toughness, but the fact that all the rigid silicone resins remain brittle, after so many efforts to improve them, indicates that this approach has reached its limit. A new material philosophy, both at the molecular and the network structure level, is needed.

The continuing search for cheaper, safer, higher performance, longer lasting, and easier to use thermal and fire resistant polymers both for structural and for non structural uses justifies the effort to utilize silicone resins. One example is the High Speed Civil Transport project being studied collaboratively by Boeing and NASA. A new passenger aircraft operating at Mach 2.4, the extensive use of polymer composite is essential to reduce the weight of the aircraft, and the thermal resistance requirement of the polymer matrix is very stringent. The polymer matrix must be able to sustain 177 °C for 60,000 hours without any loss of weight or mechanical properties. To date no organic polymer has met this requirement but silicone resins are promising candidates at least in terms of their thermal stability. The problem is their fracture toughness: this needs to be improved significantly.

1.4.2. Background.

Efforts to toughen rigid silicone resins date back to the early 1970s, as recorded in the internal research reports of Dow Corning Corporation, though no publication in the open literature can be found. The processes and results are summarized in Table 1.1.

The only experiment which showed some increase in fracture energy, marked in the table with a star, was an incompletely cured resin, as specified

by the author. All the other experiments were unsuccessful, producing no increase in strength and fracture energy. (The increase of fracture energy from a incompletely cured resin was meaningless.) An approach similar to the toughening of epoxy resins, i.e., the incorporation of reactive short chain rubber segments, was used repeatedly. In all these studies, hydrosilylation cure resins were used except the study of the condensation cure resin laminates.

Table 1.1. Summary of previous work.

Year	Resin Type	Toughening Agent	Process	Results and Comments
1974	Addition cure*	short PDMS chain, vinyl terminated	capped with crosslinker, and mixed into the resin	no conclusive toughening*, from 3 point bending and fracture energy test of opaque castings.
1974	Addition cure	short PDMS chain, vinyl terminated	dispersed into resin solution by the help of surfactant	no toughening, the same test methods as above
1974	condensation	short PDMS chain, hydroxyl terminated	dispersed with surfactant or reacted in with KOH	no toughening, from 3 point bending of reinforced laminates
1978	Addition cure	Silicone rubber particles	particles formed by emulsion polymerization and mixed in.	no toughening, according to impact strength of opaque castings

Sources: Dow Corning Reports, 1974-I0030-4238, 3664 (1970), 1973-I0030-4129, 3723, (1970), 1978-I0030-4831.

The reason why none of the experiments listed in Table 1.1 increased the fracture toughness was that the capability of the resin to undergo plastic flow is very low. In a typical resin, the crosslink density is high, which is necessary to achieve acceptable strength and modulus values but this severely restricts the molecular mobility of the structure. The role of second phase rubber particles in a resin matrix is to utilize the inherent matrix toughness more efficiently by creating stress concentrations and a larger plastic zone at a crack tip. A very brittle matrix renders the dispersed rubber particles ineffective. For example, highly crosslinked epoxy resins also have frustrated many researchers trying to toughen them. In the studies summarized in Table 1.1, second phase rubber particles were formed in all experiments but there was no increase in fracture resistance. Only when the network capability for plastic flow is increased will rubber particles toughen the resin, (provided that other requirements such as particle size, interfacial adhesion, etc. are also satisfied.) It was the goal of this research to toughen rigid silicone resins, by altering the structure of the network and then using second phase particles to exploit the alteration.

1.4.3. Toughening Strategy.

It is clear to toughen a rigid silicone resin first the intrinsic plastic deformation capability of the network must be increased and then the enhanced flow capability should be exploited as fully as possible. The network flow capability can be enhanced by enlarging the less constrained molecular loops of the network, which can be done either by copolymerizing with more di functional monomers, for example dimethyl dichlorosilane or methyl phenyl dichlorosilane, or by reacting short linear chains into the network. Copolymerization with more di functional monomers is known to reduce the elastic modulus and strength and is not a good choice. Incorporating short linear chains into the network selectively enlarges some loops of the network, which introduces the required mobility when stressed, while the many unaffected tightly connected loops retain the desired elastic modulus. Therefore to increase the intrinsic flow capability, short chain PDMS

segments were functionalized and reacted into the resin network in modest concentration levels.

A condensation cure resin, 4-3136 binder resin produced commercially by Dow Corning, was used as the model resin to demonstrate the effectiveness of toughening. It was chosen because: 1) as a commercially successful laminate binder resin it has the best mechanical properties among rigid condensation cure silicone resins when used as composite matrix; 2) condensation cure resins are more difficult to work with and methods developed and principles demonstrated with condensation resins should be applicable to addition cure resins. This resin has the composition: $(PhSiO_{3/2})_{0.40}(MeSiO_{3/2})_{0.45}(Ph_2SiO)_{0.10}(PhMeSiO)_{0.05}$. It is synthesized by cohydrolyzing a mixture of corresponding amounts of phenyl trichlorosilane, methyl trichlorosilane, diphenyl dichlorosilane, phenyl methyl dichlorosilane in the presence of excess amount of water and acid, and polymerizing the hydrolyzate to a certain extent in the presence of a base. The product is a pre-polymer with a number average molecular weight of about 1500, with a highly branched structure and dangling silanol ends for further curing or reaction. The linear rubbery segments to be reacted into the network were polydimethyl siloxane (PDMS). The excellent thermal stability of the PDMS chain and its availability are the major reasons why it is chosen. Proper functional groups were introduced at the ends of the PDMS chains and proper reaction routes were explored to couple the PDMS chains into the resin network. Phase separation was avoided with these short chains being in the resin network, which were called Phase I rubbers.

After the plastic deformation capability of the resin network was increased effectively by the Phase I PDMS segments, second phase rubbery particles were introduced into the same matrix. These were called Phase II rubbers. The cooperation of the concentrated stress fields due to the Phase II particles and the matrix plastic flow will enable the resin to consume much more mechanical energy before fracture and show much higher fracture toughness. This has been found to be true when done correctly and the details will be discussed in the following sections.

Chapter 2. Functional PDMS: synthesis, characterization and reaction with silicone resins.

2.1. Introduction.

The Phase I step uses short PDMS chains to increase the plastic flow capability of the resin network. To alter the network structure the short PDMS chains must be reacted into it, and suitable functionalities must exist at the chain ends.

Short PDMS chains are available from specialized chemical suppliers with a variety of functional ends and a DP from a few to a few thousands. They are often used as room temperature vulcanizable (RTV) silicone rubbers, as pre-polymers to silicone rubber emulsions, and as chain blocks in organic polymers. PDMS toughened thermosetts[1 to 16], Polysiloxane-imides[17 to 23] and other siloxane-organic copolymers[24 to 34] are a few examples where they are used. However the available functionalities are not suitable for the subsequent coupling with the resin pre-polymer bearing silanol ends. For example halosilanes and acyloxy silanes are hydrolytically unstable and produce acids after coupling with silanol which will catalyze further condensation[35 to 39]. Hydride termination requires a special catalyst and produces hydrogen gas. Therefore new termination has to be introduced to the PDMS ends.

There are certain requirements for the coupling reaction between the PDMS segments and the resin pre-polymer. First the architecture of the segments must not be changed by the coupling reaction. Second the coupling reaction cannot involve catalysts damaging the heat stability of the resin, or causing difficulty in the subsequent handling of the resin, during which shaping will take place.

For the following reasons methoxy or ethoxy termination is chosen. The coupling reaction can be promoted by the same catalyst as for the resin curing reaction, and the reactivity can be altered over a wide range by changing the number and the size of the alkoxy groups. The by-products released from the coupling reaction are low boiling point, non-toxic alcohol

which can be readily removed from the reaction system. To maximize the possibility that the PDMS ends are coupled with the resin blocks, up to three methoxy or ethoxy groups can be attached to each PDMS end. If only one or two of them are used during the coupling reaction, the remaining ones will be utilized in the subsequent curing reaction. The incomplete utilization of functional ends, expected in the reaction of relatively large molecular weight species, will not cause any problem.

In this Chapter, the end capping of silanol terminated PDMS either by TEOS or by phenyl trimethoxy silane, producing triethoxy silyl or phenyl dimethoxy silyl terminated PDMS, will be investigated and the structure of the final products will be characterized. The coupling reaction of the functionalized PDMS with the resin pre-polymer will be analyzed, and the impact of reaction routes on the properties of cured resins will be discussed. An optimal reaction route will be determined.

2.2. Experimental.

2.2.1. Materials.

The chemicals used in the experiments, their suppliers and grades are listed in Table 2.1. They are used as received without further purification.

Table 2.1. Materials used to synthesize functionalized PDMS.

Name	Supplier	Comments
Tetraethtyl Orthosilicate	Pfaltz & Bauer, Inc.	99% pure
Potassium Acetate	Aldrich	99+% pure
Phenyl trimethoxy silane	United Chemical Technologies, Inc.	i.e. Petrarch Silanes and Silicones.
PA fluid	Dow Corning Corp.	Silanol terminated PDMS of DP 14.
KP-80 fluid	Dow Corning Corp.	Silanol terminated PDMS of DP 55.
PA2 fluid	Gelest, Inc.	Silanol terminated PDMS of DP 6.
Other PDMS fluids	Gelest, Inc.	Silanol terminated PDMS of DP 246, 375, 586.
4-3136 binder resin	Dow Corning Corp.	Condensation silicone resin with silanol ends.
Titanium Tetrabutoxide	Aldrich	99% pure

2.2.2. Methods.

2.2.2.1. Preparation of triethoxy and dimethoxy silyl terminated PDMS.

PDMS of DP 14, triethoxy silyl terminated. A 500 ml three necked, round bottomed Pyrex glass flask was equipped with a stirrer, a condenser, and a Dean Stark trap under the condenser. The flask was connected to a

vacuum system through the condenser. 100 g of PA fluid (a silanol terminated PDMS of DP 14) and 190 g of tetraethyl orthosilicate (TEOS) were mixed in the flask and 0.29 g of potassium acetate was added. The mixture was heated slowly under nitrogen while stirring. When the temperature reached 115 °C volatile substances were distilled out, condensed, and collected in the trap. The collected volatile substances were removed continually and finally there were only negligible collectable volatile substances. The temperature was maintained at 120 to 146 °C. From time to time samples were taken from the flask and checked by FT-IR. The completion of the reaction was indicated by the disappearance of the silanol ends. After the completion of the reaction the excess TEOS was removed by vacuum distillation. The mechanical stirrer was replaced by a magnetic one, and the position of the condenser was changed so that the condensed TEOS could be collected in a separate flask. The system was sealed and vacuum was applied through the collector. After the required vacuum was reached the mixture was slowly heated while being stirred, and the unreacted TEOS was removed. Finally the liquid left in the reactor was filtered to remove the solid potassium acetate and a clean, transparent, colorless liquid was obtained.

PDMS of other DP or termination. For PDMS of other DP the process was the same except for the weight of TEOS. The molar ratio of TEOS to PDMS was maintained at ten. When the DP of the PDMS was large, the viscosity became high and the final step to remove the residual TEOS was difficult. A Rotary Evaporator was better to ensure a complete removal of the residual end capper.

The other termination was phenyl dimethoxy silyl, and it was obtained by phenyl trimethoxy silane end capping. The same process was also used for this except for the molar ratio between the end capper and the PDMS. A ratio of twenty was maintained to overcome the self condensation due to the higher moisture sensitivity of the methoxy groups.

The designations of the prepared functional PDMS, their DP, and the functionalities are listed in Table 2.2.

Table 2.2. Functional PDMS.

Name	Targeted DP	Actual DP	Type of end group
PAE	16	16.5	triethoxy silyl
PAE2	8	8.05	triethoxy silyl
KPE	57	58.9	triethoxy silyl
PAM	16	16.7	phenyl dimethoxy silyl
Others	~246, ~375, ~586	~246, ~374, ~586	triethoxy silyl

2.2.2.2. Construction of room temperature ternary phase diagrams.

The turbidity of the mixture of 4-3136 resin/toluene/functionalized rubber was taken as the criterion of phase separation and the homogeneous/heterogeneous boundary was determined by a turbidity titration. For all PDMS, the turbidity transition was sharp enough for unaided eyes to detect accurately. However it was noticed that the lower the degree of polymerization of PDMS, the less obvious the turbidity transition and the harder for unaided eyes to detect the accurate transition. To construct a phase diagram, two series of solutions were prepared. One series was the 4-3136 resin solution in toluene with concentrations from 5 wt.% to 80 wt.%, at a 5 wt.% interval. Another series was PDMS solution in toluene of the same concentrations. Two steps were needed to complete the construction of a room temperature ternary phase diagram. In the first step, PDMS was added to a 4-3136 resin toluene solution of known concentration so that the composition moved along a straight line towards the pure PDMS corner until the turbidity transition was encountered. Starting with the resin solutions of different concentrations, points along the homogeneous/heterogeneous boundary could be determined and a half of the curve was obtained. The second step was to obtain the other half of the curve. For this the PDMS solutions in toluene were used. Into these solutions a 60 wt.% 4-3136 toluene solution was added gradually so that the composition moved along a curved trajectory on the phase diagram towards the pure resin corner until the homogeneous/heterogeneous boundary was encountered. In the same way as in step 1, points on the boundary curve were determined and the other half of the boundary was obtained. This method assumed that either the phase

diagram was rather simple, or in the case of a complex phase diagram the part of interest to us would be obtained.

2.2.2.3. Coupling reaction of the functionalized PDMS with 4-3136 resin pre-polymer.

The coupling reaction between the functionalized PDMS and the resin pre-polymer can be carried out in two different ways: concurrent with, and before the curing of the resin. The former is called a co-reaction, and the later a pre-reaction.

To co-react the resin and the PDMS they were simply mixed and cured together.

To pre-react the resin blocks with the rubber segments, they were dissolved in a toluene solution and heated in the presence of a catalyst, titanium tetrabutoxide. A three necked, round bottomed flask equipped with a mechanical stirrer, a condenser and an electric heating mantle was used. The catalyst level was 0.1 to 0.2%. An appropriate amount of toluene determined by the phase diagram was added to compatiblize the resin pre-polymer and the PDMS. The reaction temperature was 95 °C and it was maintained for 28 hours.

2.2.3. Characterization and testing.

FT-IR. Transmission absorption IR spectra were obtained by a Nicolet Magna-IR 860 Spectrometer. To obtain a spectrum, liquids of relatively high viscosity were coated onto a KBr plate and low viscosity liquids were contained in a fixed liquid cell.

^{1}H-NMR. A 360 MHz spectrometer was used to collect ^{1}H spectra from a 50% sample solution in deuterated chloroform. TMS was used as reference and a 5 mm diameter NMR tube was used.

^{29}Si-NMR. ^{29}Si-NMR spectra were obtained from a 30% solution in chloroform-d1 or benzene-d6 using a Varian VXR-200 MHz spectrometer at 39.745 MHz, or 79.456 MHz. NMR tubes of sixteen mm in diameter produced by Wilmad Glass Co. were used. A pulse width of 12.4 μs and a relaxation delay time of 8 s were chosen. Chromium (III) acetylacetonate (0.03M) was used as a paramagnetic relaxation agent.

GPC. The GPC column was packed with polystyrene divinyl benzene beads of 5 μm in diameter and pore type mixed c supp'ied by Polymer Laboratory. The mobile phase was tetrahydrofuran and a refractive index detector was used. A polystyrene standard was used to determine the molecular weight.

Optical Microscopy. A Zeiss optical microscope was used to take pictures of separate particles in an otherwise transparent casting.

SEM. Freshly fractured surfaces were observed under a Cambridge Instrument Stereoscan 240 SEM. The resin surfaces were coated with a thin layer of gold before observation and an acceleration voltage of 10 to 20 KV was used.

Three point bending test. Three point bending test was performed per ASTM standard D 790-92[40].

The cured resin cast plates about 0.125" to 0.18" thick were cut into specimens 2"x0.5" in dimension and polished to a thickness of 0.125 to 0.13 inch. The specimens were polished further until smooth, shiny, and scratch free surfaces were obtained. This was achieved by the following polishing sequence: Grit # 320, 800, 1200, 2400, and 4000 sand papers and then water dispersed alumina powders of 1, 0.3 and 0.05 μm in diameter. The test temperature was 21 °C and a test speed of 1 mm/minute was used. The support span was 38 mm. For each sample at least three specimens were tested.

Force-displacement curves were recorded. The toughness of the cured resin was obtained as the area under the stress-strain curves. The flexural strength was calculated using the peak force as:

$$S=3PL/2bd^2 \quad (2.1)$$

where S is the stress in the outer surface at the mid span, P the maximum load, L the support span, and b, d the width and thickness of the beam. The maximum strain was calculated using the maximum displacement as:

$$\gamma=6Dd/L^2 \quad (2.2)$$

where γ is the strain at break and D is the maximum displacement. The slope of the steepest initial straight-line portion of the load-displacement curve was taken as the Young's modulus.

Casting techniques. Special casting techniques have been developed to make sound, void free castings of condensation cure silicone resins. Details of these techniques will be given in Chapter 3, where the mechanical properties will be discussed.

Fracture toughness testing. The fracture toughness, K_{Ic}, and the critical strain energy release rate, G_{Ic}, were obtained through a fracture toughness test. Details of the test will be discussed in the next chapter.

2.3. Results and Discussion.

2.3.1. Preparation and characterization of functionalized PDMS.

PDMS with silanol termination was end capped with TEOS. The reaction can be depicted as follows.

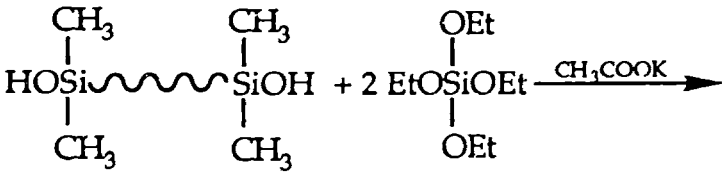

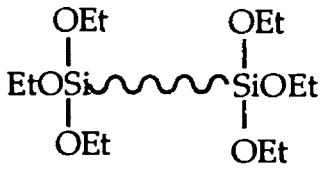

The silanol terminated PDMS was also end capped by phenyl trimethoxy silane, as shown below. This end capped PDMS, however, was less often used in the Phase I toughening of rigid silicone resins, since its toughening effect was similar to that of the triethoxy silyl terminated one but it was more difficult to prepare.

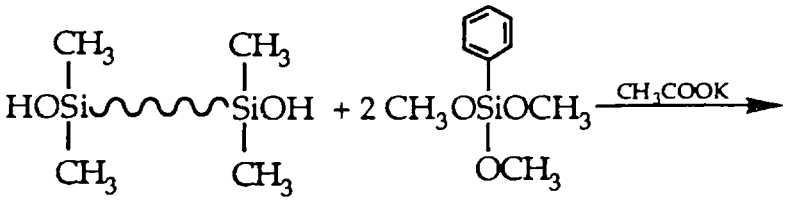

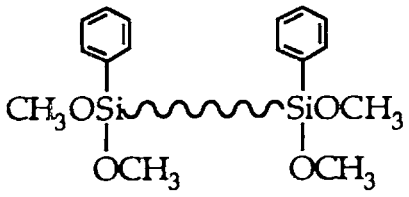

The products obtained by TEOS end capping were purified and their structures characterized by IR, ^{1}H and ^{29}Si NMR analysis.

2.3.1.1. IR Analysis.

FT-IR was used to monitor the end capping of silanol terminated PDMS by tetraethyl orthosilicate. The characteristic hydrogen bonded silanol absorption peak centered at 3312 cm^{-1} was used as an indication whether or not the reaction was complete. Figure 2.1 shows an IR spectrum of PA, a silanol terminated PDMS of DP 14. During the reaction samples were taken from the reactor and IR absorption spectra of the samples were obtained. The completion of the reaction was indicated by the complete disappearance of the silanol absorption peak, see Figure 2.2.

The IR absorption of silicones has been intensively studied[41 to 44]. Reference spectra are available[45] and allow the assignments of most absorption peaks in Figures 2.1 and 2.2. Table 2.3 lists these assignments.

Other changes in the IR spectrum also support a complete end capping reaction. The absorption at ~900 cm^{-1}, of Si-O in SiOH, in addition to the 3312 cm^{-1} peak, disappeared. Two new absorption peaks attributed to the symmetric and asymmetric stretching of methylene at 2940 and 2885 cm^{-1}, and a characteristic, very strong absorption doublet at 1100 to 1080 cm^{-1}, of the stretching of C-O bond of SiOEt linkage, appeared. This characteristic doublet coincided with the antisymmetric stretching of Si-O-Si. At 1180 and 1068 cm^{-1} two absorption peaks of ethoxyl were also seen. The new peak at 1392 cm^{-1} was also consistent with an ethoxylated PDMS. Other absorption peaks in Figure 2.1, due to the side methyl groups and the siloxane backbone, either remained intact or overlapped with the new absorption peaks due to ethoxyl group. No chain structural degradation was visible through IR analysis.

The IR spectra of PDMS of other DP are similar to Figures 2.1 and 2.2 and they are not included.

Table 2.3. Assignment of IR absorption peaks.

Wave number	Assignment	Comments
PA Fluid in Figure 2.1:		
3312 cm^{-1}	Associated OH of SiOH	very broad
2965 cm^{-1}	Antisymmetric stretch of C-H in CH_3	moderate
~2895 cm^{-1}	Symmetric stretch of C-H in CH_3	weak
1414 cm^{-1}	Antisymmetric CH_3 deformation	weak
1262 cm^{-1}	Symmetric CH_3 umbrella deformation	strong and narrow analytically useful
1090 cm^{-1}	Antisymmetric stretch of Si-O-Si	strong and broad
1024 cm^{-1}	Antisymmetric stretch of Si-O-Si	strong and broad
~900 cm^{-1}	Asymmetric SiO stretch of SiOH	moderate-weak relatively broad
860 cm^{-1}	-CH_3 rocking	
799 cm^{-1}	Asymmetric -CH_3 rocking and Si-C stretch	strong
PAE in Figure 2.2 (only those different from Figure 2.1 are listed):		
2940 cm^{-1}	Symmetric stretch of -CH_2-	moderate-weak
2885 cm^{-1}	Asymmetric stretch of -CH_2-	overlap
1393 cm^{-1}	SiOEt (vibration ?)	
1180 cm^{-1}	SiOEt (vibration ?)	analytically useful
1110 - 1080 cm^{-1}	C-O stretch of SiOEt	characteristic doublet of SiOEt
968 cm^{-1}	SiOEt (vibration ?)	analytically useful

2.3.1.2. ^{29}Si and ^{1}H NMR.

^{29}Si and ^{1}H NMR spectra of the triethoxy silyl terminated PDMS are included in Figures 2.3 to 2.7. The chemical shifts and their assignments are listed in Table 2.4. These assignments are based on the knowledge accumulated from the ^{29}Si NMR studies of other workers[43, 46 to 54].

Table 2.4. ^{29}Si chemical shifts and their assignments.

δ(ppm)	Assignment	Comments
0	Me_4Si	Reference
-11.063	$(MeO)Me_2SiO-$	linewidth<0.3 ppm
-12.927	$(EtO)Me_2SiO-$	linewidth<0.2 ppm
-19.349	$(Me_2SiO)_4$ (D_4)	linewidth<0.5 ppm
-20.228 to -22.852	$(Me_2SiO)_n$ (linear or cyclics of n>5)	many narrow peaks severely overlap
-87.644 to -88.850	$(EtO)_3SiO-$	number of peaks and linewidth varies
-94.770 to -95.504	$-O(EtO)_2SiO-$	Self condensation

Due to the shielding effect of the oxygen atoms, silicon nuclei in a siloxane chain usually appear to the right of tetramethyl silane (TMS): two or more oxygen atoms provide higher shielding effect than two methyl groups. If in TMS only one methyl group is replaced by oxygen, the silicon nucleon appears to the left of TMS due to the well known Sagging Effect of the chemical shifts of substituted silicon. However in the case of silicone rubbers and resins, every silicon atom is bonded to at least two oxygen atoms and always appears to the right of TMS. The more oxygen atoms a silicon nucleon is bonded to, the more highly shielded it is. And it will appear at a lower frequency and farther away from TMS. Subsequent bonding with oxygen atoms also affects the shielding effect and allows the determination of end groups and side reaction products.

In Figure 2.3, the ^{29}Si NMR spectrum of a triethoxy silyl terminated PDMS of average DP 8.05 (PAE2) is shown. This spectrum shows that a successful end capping was achieved despite small amounts of side reactions. The average DP was slightly larger than the theoretical value of 8. The triethoxy silyl ends appear as a group of peaks at the vicinity of -88 ppm, with the -88.024 ppm peak dominating, and the others reflecting a spread of chain lengths. The effect of chain length is observable with short segments, but becomes less pronounced and predominantly a single peak appears when the DP of the chain becomes large. PAE2 contained impurities such as trace cyclic D_4, appearing at -19.349 ppm; 2.9% dimethyl ethoxy silyl termination, appearing at -12.927 ppm; and 8.0% dimethyl methoxy silyl termination, appearing at -11.063 ppm. The cyclic structure was possibly formed during the end capping process, and the impurity terminations were from the raw material, a silanol terminated PDMS of average DP 6. Some self condensation occurred as evidenced by the peaks at -94.778 and -95.504 ppm.

The end capping of PA, with a DP of 14, was achieved with minimum self condensation and cyclization, see Figure 2.4. No small cyclics were seen at -19.51 or -9.12 ppm. Silanol ends, originally at -11.5, were completely converted to triethoxy silyl ends, appearing at -87.986 ppm. There were no difunctional and monofunctional impurity ends, in contrast to PAE2. A little self condensation did occur but it only altered the degree of polymerization by as little as 3%, from a theoretical value of 16 to an actual value of 16.5.

Figure 2.5 is the spectrum of a PDMS of DP 55 end capped with TEOS (KPE). The theoretical degree of polymerization was 57, and an actual value of 58.9 was obtained as calculated from this spectrum. A little self condensation, resulting in the slight increase of degree of polymerization, is seen at ~-95 ppm. Impurity traces, seen from the unspecified small peaks at -67.025, -17.951, and ~-13 ppm, also are evident.

Therefore it is clear that the desired PDMS structure was obtained and the lengths of the PDMS chains were basically unchanged, although in some products impurities did exist. The amount of impurities, however, was almost negligible except for PAE2. The impurity end functionalities in PAE2

were able to be utilized in the subsequent coupling reaction with the resin pre-polymer.

The structures of the triethoxy silyl terminated PDMS were also verified by ^1H NMR. The ^1H NMR spectra of PAE and KPE are shown in Figures 2.6 and 2.7. The proton of $SiCH_3$ coincided with the reference TMS. The proton of $SiOCCH_3$ was at 1.1 ppm as a triplet and the $-CH_2-$ proton at 3.7 ppm as a quartet. The use of these spectra was limited since a TMS reference was used and it obscured the quantitative ratio of different protons.

Triethoxy silyl terminated PDMS of other degrees of polymerization up to 586 and methyl dimethoxy silyl terminated PDMS of DP 16 were also prepared and analyzed by ^{29}Si and ^1H NMR and their structures verified.

2.3.2. Coupling reaction of the PDMS segments with the resin pre-polymer.

There are several ways to incorporate the functionalized PDMS into rigid silicone resin networks. These are classified as pre-reaction and co-reaction, according to when the chemical linkage of the PDMS ends with the resin network is established. A pre-reaction establishes the coupling of the functionalized PDMS with the resin pre-polymer before the resin is cured. A co-reaction seeks to couple them while the resin is being cured. The mechanical properties and fracture toughness are the criteria to determine the appropriate route. In the following the pre-reaction will be discussed first, then its impact on resin properties will be contrasted with that of co-reaction. A proper coupling route will be chosen and followed thereafter.

2.3.2.1. Ternary Phase Diagrams.

Despite the compositional similarity, the 4-3136 resin pre-polymer and the PDMS short segments are incompatible due to their macromolecular nature. The Liquid Lattice Theory[55] states that the free energy of mixing is:

$$\Delta F_M = kT[n_1 \ln v_1 + n_2 \ln v_2 + n_3 \ln v_3 + \chi_{12} n_1 v_2 + \chi_{13} n_1 v_3 + \chi_{23} n_2 v_3] \quad (2.1)$$

where ΔF_M is the free energy of mixing per unit volume of solution, n_i the number of molecules of the *i*th component in a unit volume of solution, v_i the volume fraction of the *i*th component in the solution, and χ_{ij} the pairwise interaction parameter which can be expected to be slightly positive. The structural and compositional differences contribute a positive value to the free energy of mixing and make the polymers incompatible. The entropy of mixing depends on the number of molecules, seen in the first three terms in (2.1). In the absence of solvent, the numbers of polymer molecules, n_2 and n_3, are very small due to their polymeric nature, and the entropy of mixing is not enough to compensate for the small interaction difference between dissimilar molecules. As a result, a solvent is always needed to increase the entropy of mixing and to achieve a molecular mixing of the rubber segments with the resin pre-polymer. This is a prerequisite condition for an effective coupling reaction.

The coupling reaction was done in toluene. Among the factors which influence the reaction efficiency, the concentration of the reaction mixture is the most important. The resin pre-polymer and the rubber segments must achieve molecular mixing for the reaction to go effectively. Otherwise phase separation occurs, and effective coupling cannot be expected.

Phase diagrams of the 4-3136 resin/Toluene/PDMS system define the reactant composition windows. Seen in Figure 2.8, (the phase diagram of 4-3136 resin/Toluene/PAE2), there is a small incompatible region at the right lower corner even when the DP of the PDMS chain is only eight. The coupling reaction must be done outside this heterogeneous region. When the DP of the functionalized PDMS is increased to sixteen, the heterogeneous region is enlarged significantly, see Figure 2.9, the 4-3136 resin/PAE/toluene phase diagram. The coupling reaction of PAE with the resin pre-polymer could be done effectively only at a total concentration below 55 wt.%. If the DP of the PDMS is 55 (KPE or KP), the boundary moves up even more and the homogeneous region becomes even smaller, see Figure 2.10. At room temperature, the KPE and 4-3136 resin could be compatiblized only in a toluene solution below 35 wt.%. The coupling reaction was actually done at 95

°C in a 38 wt.% solution regardless of the ratio of KPE to the resin. The elevated temperature lowered the boundary curve on the phase diagram by a few percent.

Figure 2.10 also shows that KPE is made less compatible with the 4-3136 resin by triethoxy silyl end capping. The incompatibility of the 4-3136 resin and the PDMS can also be utilized to control second phase morphology. This will be discussed later.

2.3.2.2. ^{29}Si NMR.

The coupling reaction was studied by ^{29}Si NMR. The spectra are included in Figures 2.11 to 2.18. They showed that (1) a catalyst and an elevated temperature were needed for the coupling reaction; (2) the reaction temperature should not be excessively high, otherwise the removal of volatile substances would diminish the reaction efficiency; and (3) when done correctly, the functionalized PDMS segments were completely coupled with the resin pre-polymer. These conclusions were based on the following experimental results.

The chemical shifts of peaks appearing in Figures 2.11 to 2.18 and their assignments are listed in Table 2.5. These assignments are based on the theoretical and experimental analysis of model compounds[43, 46 to 54]. In addition to the positions of peaks, a linewidth also provides useful information. Silicon nuclei in the PDMS segments usually have narrow peaks on the spectra (Figure 2.16), while those in the resin pre-polymer show a much larger linewidth, due to the multiplicity of environment (Figure 2.11). For the same reason, when the PDMS ends are coupled with resin blocks the resonance peaks of these end nuclei become very broad (Figure 2.14). This serves as a means to distinguish the PDMS reaction with itself and with the resin.

Table 2.5. ^{29}Si chemical shifts and their assignments.

δ(ppm)	Assignment		Comments
0	Me_4Si		Reference
-9.51	$((CH_3)_2SiO)_3$ (D_3)		
-11.1	M^{OZ}		Z=H or R
-19.8 to -21.6	-$OSi(Me_2)O$-	(D)	
-22.8	$PhMe(OH)SiO_{1/2}$	($M^{Ph,OH}$)	
-31.1	-$OSi(PhMe)O$-	(D^{Ph})	broad peak
-37.4	-$OSi(Ph_2)OH$	($M^{Ph_2,OH}$)	broad peak
-41.0	-$OSi(Ph_2)OR$	($M^{Ph_2,OR}$)	trace
-45.9	-$OSi(Ph_2)O$-	(D^{Ph_2})	broad peak
	or -$OSi(Me)(OH)_2$	($M^{(OH)_2}$)	
-54.8	-$OSi(Me)(OH)O$-	(D^{OH})	broad peak
-58.1	-$OSi(Ph)(OH)_2$	($M^{(Ph,OH_2)}$)	broad peak
-63.9	$MeSiO_{3/2}$	(T)	broad peak
-69.9	$HOSi(Ph)O_{2/2}$	($D^{Ph,OH}$)	broad peak
-72.1	$ROSi(Ph)O_{2/2}$	($D^{Ph,OR}$)	broad peak
-78.7	$PhSiO_{3/2}$	(T^{Ph})	broad peak
-85.1	-$OSi(OEt)_2OH$	($M^{(OEt)_2,OH}$)	narrow
-87.8	-$OSi(OEt)_3$	($M^{(OEt)_3}$)	narrow peak
-90.3	$EtO(OH)SiO_{2/2}$	($D^{OH,OEt}$)	broad peak
-92.3	$(EtO)_2SiO_{2/2}$	($D^{(OEt)_2}$)	broad peak
-94.3	-$OSi(OH)_2O$-	($D^{(OH)_2}$)	from self condensation of -$Si(OEt)_3$
-95.2	-$OSi(OEt)_2O$-	($D^{(OEt)_2}$)	from self condensation of -$Si(OEt)_3$
-101.6	$HOSiO_{3/2}$	(T^{OH})	same as above
-102.2	$EtOSiO_{3/2}$	(T^{OEt})	same as above
-110	$SiO_{4/4}$	(Q)	broad

Note: R stands for an unspecified alkyl.

The spectrum of the resin pre-polymer is shown in Figure 2.11. The starting compositions of the resin and those calculated from the NMR spectrum are listed in Table 2.6. At the pre-polymer stage, a higher fraction of methyl T monomer was converted to T network structure than Phenyl T monomer due to less steric hindrance. This led to the compositional and crosslink density heterogeneity in the final cured resin. Approximately one third of the silicon atoms from $MeSiCl_3$, a half of those from $PhSiCl_3$, the majority of those from Ph_2SiCl_2, and a negligible number of those from $PhMeSiCl_3$ remained partially condensed and available for the subsequent coupling reaction.

The spectrum of a mixture of the resin pre-polymer and 10 parts of PAE, shown in Figure 2.12, was simply the superposition of the resin pre-polymer spectrum and the PAE spectrum. Without catalysts and elevated temperatures, no coupling reaction between PAE and the resin pre-polymer occurred.

Table 2.6. Compositions of the resin pre-polymer

Type	Starting materials	Shown by NMR	
$MeSiCl_3$	45 % (mole)	$MeSiO_{3/2}$ (T)	32.4%
		-OSi(Me)(OH)O- (D^{OH})	10.5%
		-OSi(Me)$(OH)_2$ ($M^{(OH)_2}$)	<2.7%
$PhSiCl_3$	40% (mole)	$PhSiO_{3/2}$ (T^{Ph})	20.1%
		$HOSi(Ph)O_{2/2}$ ($D^{Ph,OH}$)	19.6%
		$ROSi(Ph)O_{2/2}$ ($D^{Ph,OR}$)	1.4%
		-OSi(Ph)$(OH)_2$ ($M^{Ph,(OH)_2}$)	2.3%
Ph_2SiCl_2	10% (mole)	-OSi(Ph_2)O- (D^{Ph_2})	<2.7%
		-OSi(Ph_2)OH ($M^{Me_2,OH}$)	5.0%
		-OSi(Ph_2)OR ($M^{Me_2,OR}$)	0.5%
$PhMeSiCl_2$	5% (mole)	-OSi(PhMe)O- (D^{Ph})	4.6%
		$PhMe(OH)SiO_{1/2}$ ($M^{Ph,OH}$)	0.3%

In the presence of the catalyst titanium tetrabutoxide, and at an elevated temperature, the functionalized PDMS and the resin pre-polymer were coupled. The reaction efficiency was affected by a variety of factors including the reactant concentration, the catalyst level, and whether or not volatile materials were removed from the reaction system.

The spectra in Figures 2.13 to 2.15 show the effect of removing volatile materials. Figure 2.13 was a spectrum for the resin pre-polymer coupled with 10 part PAE, when the reaction was done at 105 °C with 0.1 wt.% $Ti(OBu)_4$, and volatile substances were removed from the beginning of the reaction. The removal of volatile substances was controlled by the sweeping nitrogen. A small fraction of the triethoxy silyl ends remained unreacted, indicated by the remaining trace of the -87.8 ppm peak in Fig. 2.13. This was also seen in Figure 2.14, the spectrum of the resin pre-polymer reacted with 20 parts of PAE. The reacted ends were seen at ~-95 and ~-100 ppm. If no volatile substances were removed and the other reaction conditions were kept the same, the triethoxy silyl peak disappeared completely (Figure 2.15), indicating a complete coupling reaction. The absence of peaks in the region from -90 to -95 ppm indicated that at least two of the three ethoxyl groups at each end reacted with the resin pre-polymer. This was also shown by the appearance of the -100 ppm and -110 ppm peaks, correspondingly, for ends with two and three ethoxy groups reacted.

The IR spectra of condensed volatile substances were consistent with a mixture of water and ethanol. The removal of ethanol might facilitate the condensation between the PDMS with the resin, but the removal of water promoted the condensation of silanol with silanol and diminished the number of reaction sites on the resin and led to a less efficient coupling reaction.

During the coupling reaction, side reactions did occur. For example, the appearance of cyclic structure at -19.3 ppm and di methyl silanol ends ($-OSiMe_2OH$) at -11.2 ppm suggested a re-equilibration of PDMS chains, though the extent was negligible.

That the triethoxy end groups reacted mostly with the resin pre-polymer instead of PDMS was further supported by a sluggish self

condensation observed by NMR. In a ^{29}Si NMR spectrum the peaks for the PDMS chain ends coupled with resin blocks were broad due to the multiplicity of their environment, whereas self condensation of rubber segments gave a very narrow, well defined peak(Figure 2.16). The spectrum in Figure 2.16 was for a pure PAE sample after being subjected to the same heat history as a coupling reaction with the catalyst. Mostly the PAE remained intact. The trace side reactions included the self condensation, the re-equilibration of PDMS, and the substituent redistribution. Less than 4% of the total functional ends participated in the self condensation. A trace amount of re-equilibration occurred and the appearance of T units revealed the redistribution of a small number of substituents.

The effective coupling can be more clearly shown by the NMR spectrum of a partially finished reaction(Fig. 2.17). The useful region of Figure 2.17 was replotted with the same region of the PAE and the resin spectra (Figure 2.18). In Figure 2.18, the top spectrum was for pure PAE, the middle for the resin pre-polymer, and the bottom for the reacted resin/PDMS. After the partial reaction, the -87.8 ppm peak almost disappeared. Broad peaks appeared: at -90 ppm, for the PDMS ends with one ethoxyl group reacted with the resin pre-polymer and another hydrolyzed; at -92.3 ppm, for those with one ethoxyl group reacted with resin and the other intact; and at -100 ppm, for those with two ethoxyl groups reacted with the resin block and the other one hydrolyzed.

2.3.2.3. GPC Analysis.

Despite the inconvenience and uncertainty caused by the use of Polystyrene standard, GPC was a useful tool to qualitatively evaluate the molecular size of the resin pre-polymer and its distribution.

In Figures 2-19 to 2-22 are plotted the GPC retention time vs. concentration curves. The weight concentration is shown as the number of counts which corresponds to the refractive index difference between the reference and the sample.

Figure 2.19 is for the neat 4-3136 resin pre-polymer. The curve consists mainly of three peaks, the overlapping peaks at 17.5 and 18.2 minutes, and a small peak at 19.5 minutes.

Figure 2.20 is for a mixture of the resin with 10 parts of PAE. The mixture was not heated, and there was essentially no coupling reaction between the resin pre-polymer and the PDMS, according to NMR studies. The PAE was concealed by the resin pre-polymer peaks, since it had a number average molecular weight of 1415, almost the same as the resin pre-polymer. The M_N of the resin pre-polymer was determined to be 1410. Careful examination showed that PAE slightly broadened the molecular weight distribution, evidenced by the longer high MW tail. The polydispersity, M_w/M_N, was increased from 1.805 to 2.013.

After a pre-reaction the molecular weight was increased and its distribution broadened (Figure 2.21). In Figure 2.21, the GPC curves of the neat resin pre-polymer, and the pre-polymer reacted with different amounts of PAE or PAM, are plotted. The lowest molecular weight peak at 19.5 minutes of the resin pre-polymer disappeared, and the height of the low molecular weight peak next to it, at 18.2 minutes, was reduced. The molecular weight distribution was broadened by consuming the lower molecular weight species of the resin pre-polymer.

It was inferred that re-equilibration occurred during the coupling reaction, based on the number average molecular weights and distributions listed in Table 2.7. The number average molecular weight depended on the reactant mixture concentration. For example, when the resin pre-polymer was reacted with 10 parts of PAE in a 53 wt.% solution, the M_N of the reacted product was higher than when the reaction was done in a 46 wt.% solution. The polydispersity was lowered by a factor of two when the reaction concentration was changed from 53 wt.% to 46 wt.%. When the resin solution was diluted and heated in the presence of titanium tetrabutoxide and a trace amount of water, siloxane bonds were broken and the equilibrium was shifted to the depolymerization direction. This re-equilibration was also evidenced by the effect of the amount of PAE on M_N. When the amount of PAE was increased to 20 parts per hundred parts of resin, the average

molecular weight of the final product and the molecular weight distribution remained unchanged. The PDMS chains, bearing six functional groups at two ends, were actually chain extenders for the resin pre-polymer. The constant molecular weight and distribution were explained by the reduced size of the resin blocks with dilution.

The GPC curves of the resin pre-polymer coupled with KPE are plotted in Figure 2.22. The molecular weight and distributions are listed in Table 2.7. They are also plotted in Figure 2.23. Again the reaction of KPE with the resin increased the molecular weight and broadened the molecular weight distribution. Because of the higher molecular weight of KPE, less resin blocks were coupled with the PDMS ends and the average molecular weight only increased slightly. The molecular weight distributions were broadened but generally were much more narrow than the resin reacted with PAE. This was because of the lower reaction concentration, consistent with a re-equilibration process. Due to this re-equilibration process the number average molecular weight only changed slightly with increasing KPE content (Fig. 2.23a). However the polydispersity increased as the amount of KPE was increased (Fig. 2.23b).

Table 2.7. Average molecular weight and its distribution, calculated from GPC, of 4-3136 resin coupled with different functionalized PDMS

Toughener	Reaction	M_N	M_W/M_N
None	None	1410	1.805
10 parts PAE	None	1507	2.013
10 parts PAE	108 °C, 28 h., 53 wt.%*	3312	15.64
10 parts PAE	108 °C, 28 h., 46 wt.%	3109	7.535
20 parts PAE	108 °C, 28 h., 51 wt.%	3237	13.99
10 parts PAM	108 °C, 28 h., 65 wt.%	3121	10.11
5 parts KPE	95 °C, 28 h., 38 wt.%	2158	3.205
10 parts KPE	95 °C, 28 h., 38 wt.%	2310	3.990
15 parts KPE	95 °C, 28 h., 38 wt.%	2311	4.617
20 parts KPE	95 °C, 28 h., 38 wt.%	2327	5.545

*In toluene solution.

2.3.3. Pre-reaction vs. co-reaction.

The co-reaction route appears simpler: mixing the resin pre-polymer and the PDMS and curing them together. This simple mixing and curing procedure, however, proved to be unsatisfactory.

Cast plates were made from the resin pre-reacted and co-reacted with PAE and tested. The results are plotted in Figures 2.24 to 2.26. The solid diamonds in the Figures are data obtained from co-reacted samples and the open squares from the pre-reacted. When 2 to 8 parts (per 100 parts resin) of PAE was co-reacted into the resin the cast plates showed essentially no change in mechanical properties. The Young's modulus remained constant at 1.70 to 1.86 GPa, the flexural strength at 37.22 MPa, the strain at 2.2 to 2.5%, and the area under the stress-strain curve at 5.5 KJ/m^3. The fracture toughness only increased slightly, from 0.25 to 0.28 $MPam^{1/2}$. When pre-reacted into the resin network, however, 10 and 20 parts of PAE significantly improved the fracture toughness and mechanical properties.

This was attributed to the improved coupling reaction. In a co-reacted system, PAE was not well compatiblized with the resin due to the poor coupling reaction. In Figure 2.28a, separate particles were seen when PAE was co-reacted, in contrast to a homogeneous casting when the PAE was pre-reacted (Figure 2.27). More PAE produced larger particles (Figure 2.28b). The presence of particles was also verified by SEM observation of the freshly fractured surface (Figure 2.29). The particles contracted more than the matrix after cooling and appeared as dents on the fractured surface. They were flat on a polished surface (Figure 2.30) and the rubbery composition of these particles was verified by EDS analysis.

Therefore it is apparent that a pre-reaction is necessary to effectively couple the functional PDMS with the resin pre-polymer. This procedure has been followed throughout this study.

2.4. Conclusions.

Triethoxy silyl terminated PDMS of different DP were synthesized by end capping silanol terminated PDMS segments with TEOS. The degrees of polymerization of these PDMS ranged from 8 to 586. Their structures were verified by FT-IR, ^{1}H NMR, and ^{29}Si NMR. During end capping trace side reactions, e.g., the formation of small rings, and the self condensation of PDMS, were observed but their impact on the chain length was minimal. The end functionalities were pure for most products except for the DP 8, which contained other usable functional groups.

A pre-reaction had to be carried out to couple the Phase I PDMS with the resin pre-polymer before the modified resin was cast. Otherwise no toughening effect could be observed because of the formation of useless second phase particles.

The PDMS segments and the resin pre-polymer were generally incompatible. On a resin/PDMS/toluene ternary phase diagram, the position of the homogeneous/heterogeneous boundary was determined by the degree of polymerization of the PDMS. Higher DP PDMS was less compatible with the resin pre-polymer and the homogeneous region was smaller. This homogeneous region defined a composition window within which the coupling reaction was carried out, since molecular mixing had to be achieved to effectively couple the PDMS segments with the resin pre-polymer.

The functionalized PDMS segments were successfully coupled with the resin pre-polymer with little self condensation and chain scission. The coupling reaction was done in toluene at 95 °C with $Ti(OBu)_4$ as the catalyst. The catalyst level was 0.1 to 0.2 wt.%. Reaction conditions such as temperature and whether or not volatile substances were removed were important. During the pre-reaction, re-equilibration and substituent redistribution occurred. At least two of the three ethoxy groups at each end were coupled to resin blocks by the pre-reaction, the other either reacted with another resin block or was left for the subsequent curing reaction. The molecular weight was increased and its distribution broadened by the pre-reaction.

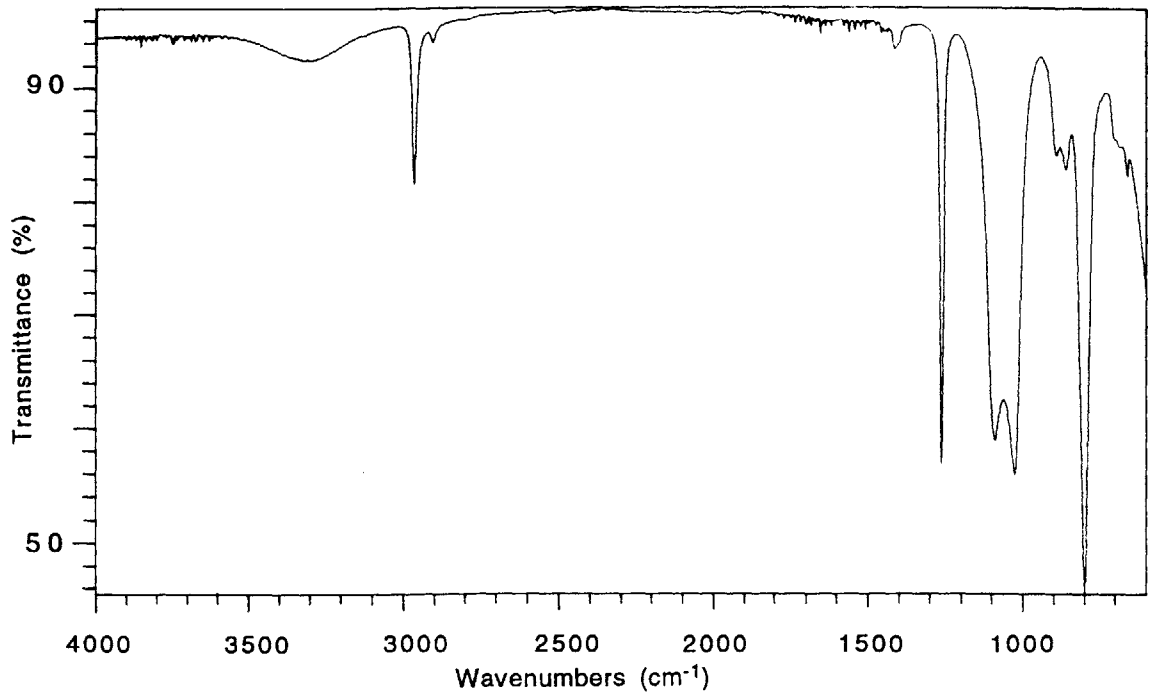

Figure 2.1. IR spectrum of PA fluid, a silanol terminated PDMS of DP 14.

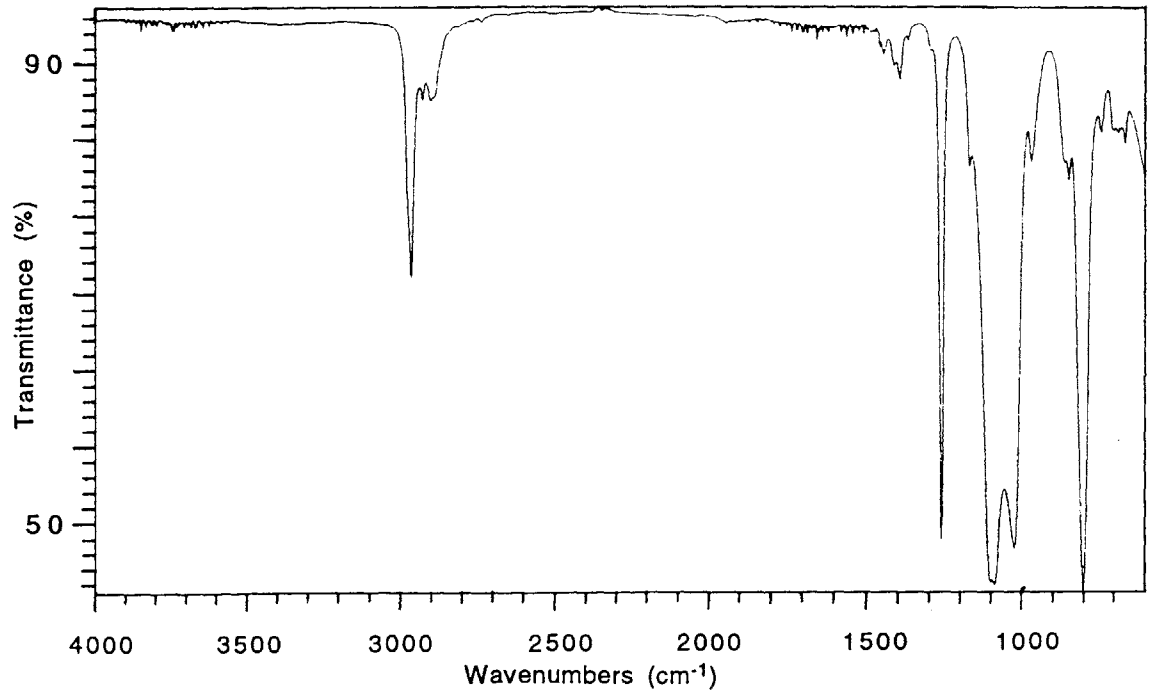

Figure 2..2. IR spectrum of PAE, a triethoxy silyl terminated PDMS of DP 16.5.

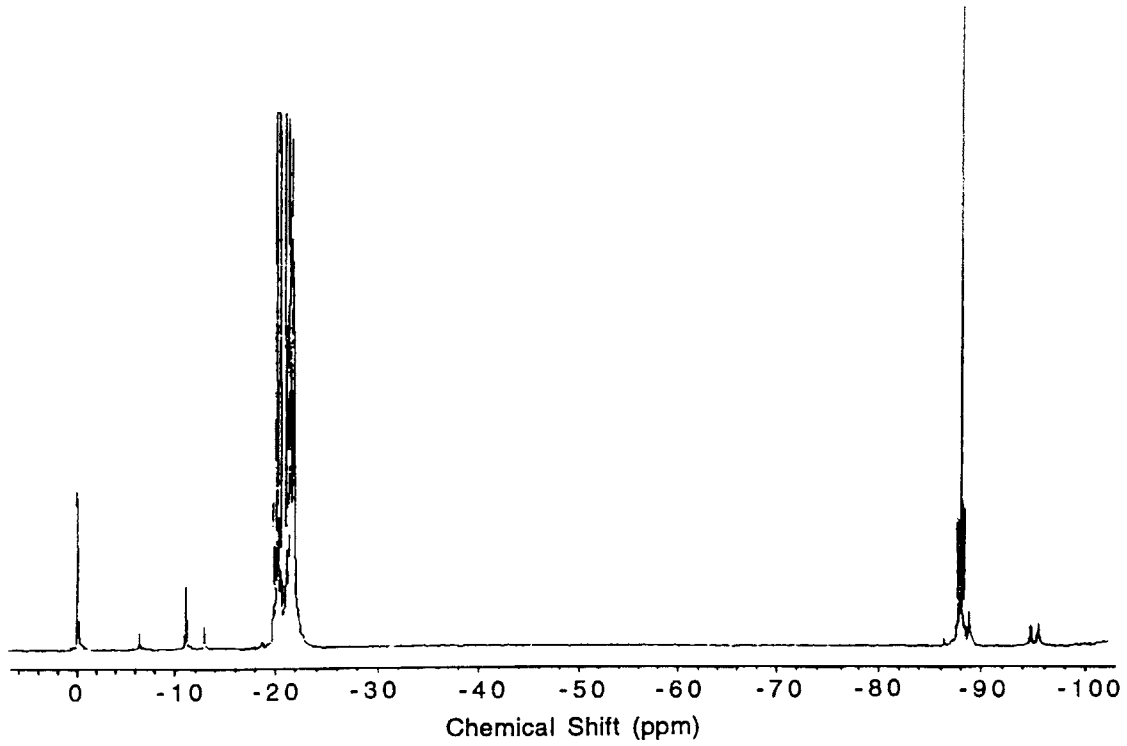

Figure 2.3. ^{29}Si NMR spectrum of PAE2, a triethoxy silyl terminated PDMS of DP 8.05.

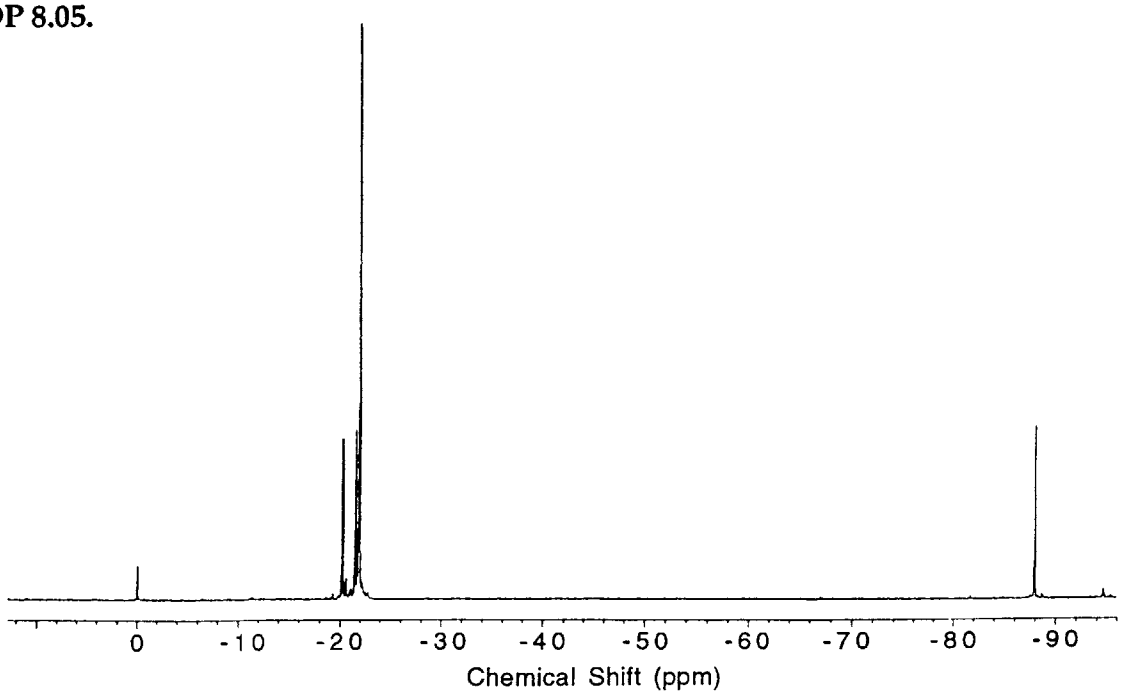

Figure 2.4. ^{29}Si NMR spectrum of PAE, a triethoxy silyl terminated PDMS of DP 16.5.

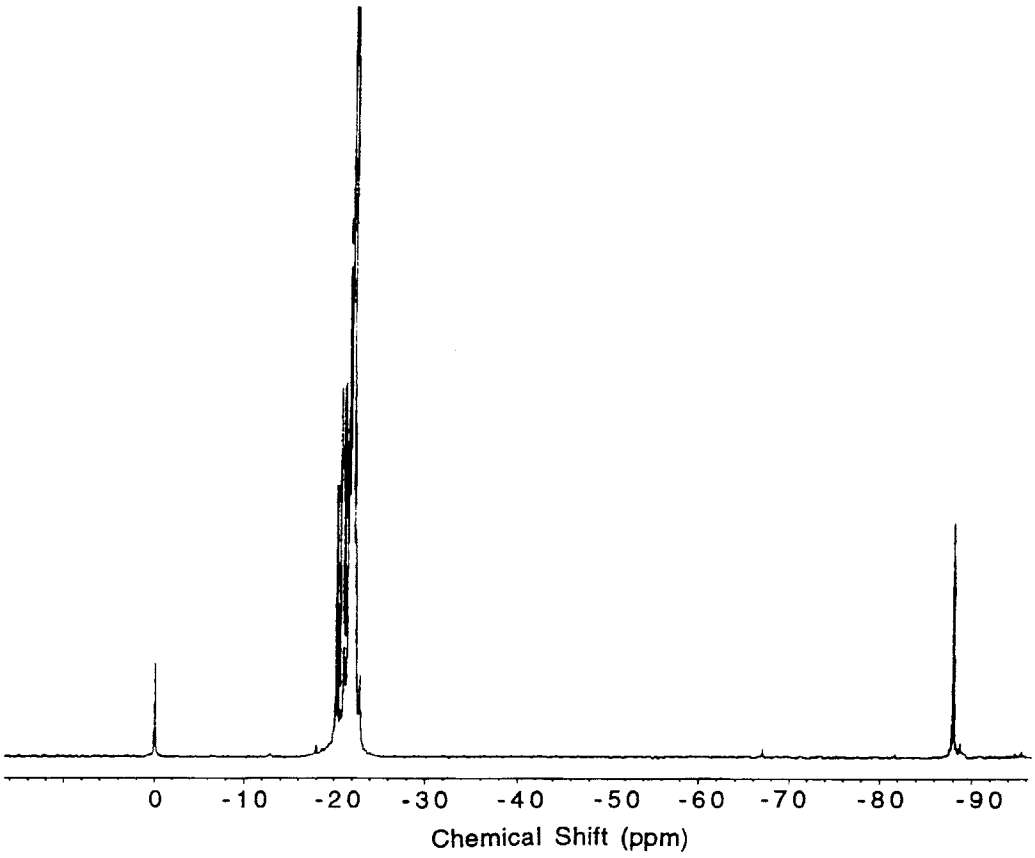

Figure 2.5. ^{29}Si NMR spectrum of KPE, a triethoxy silyl terminated PDMS of DP 58.9.

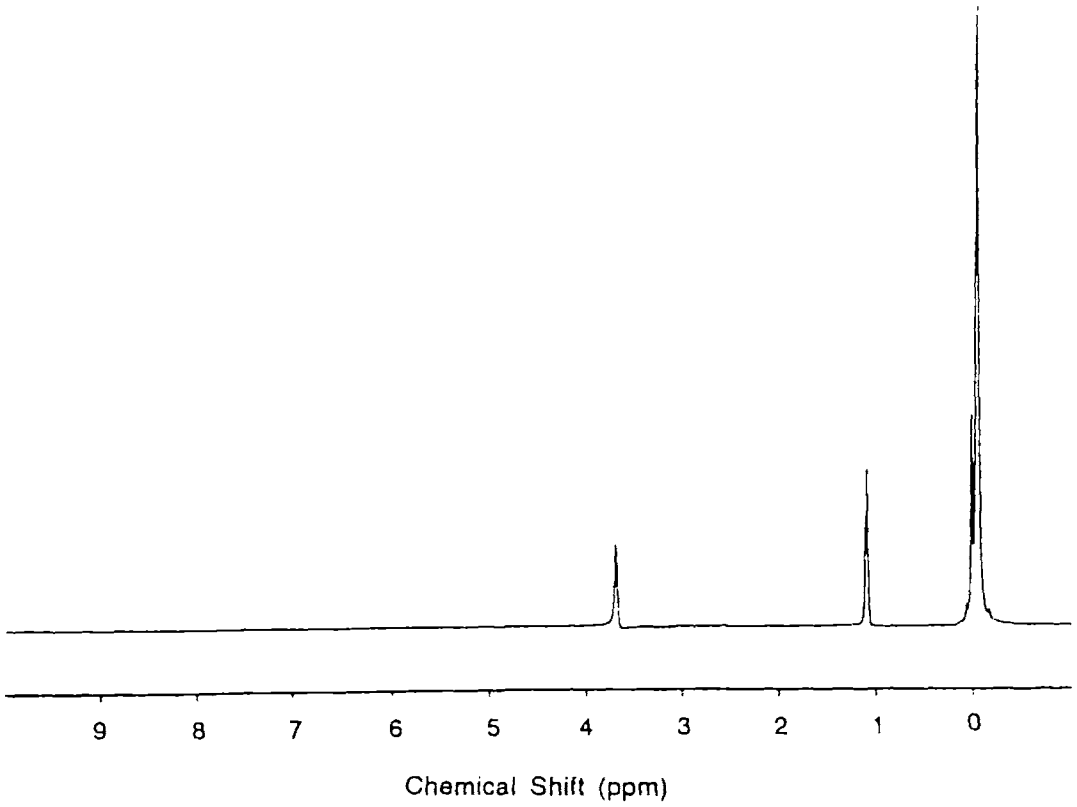

Figure 2.6. ^{1}H NMR spectrum of PAE, a triethoxy silyl terminated PDMS of DP 16.5.

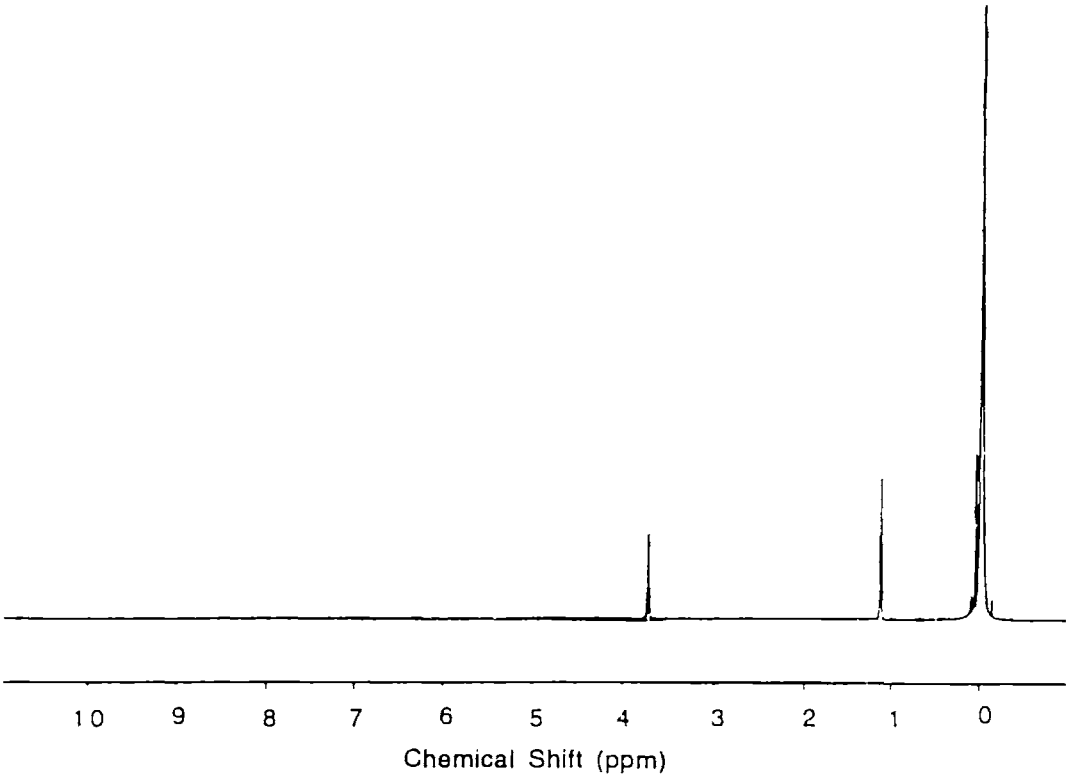

Figure 2.7. ^{1}H NMR spectrum of KPE, a triethoxy silyl terminated PDMS of DP 58.9.

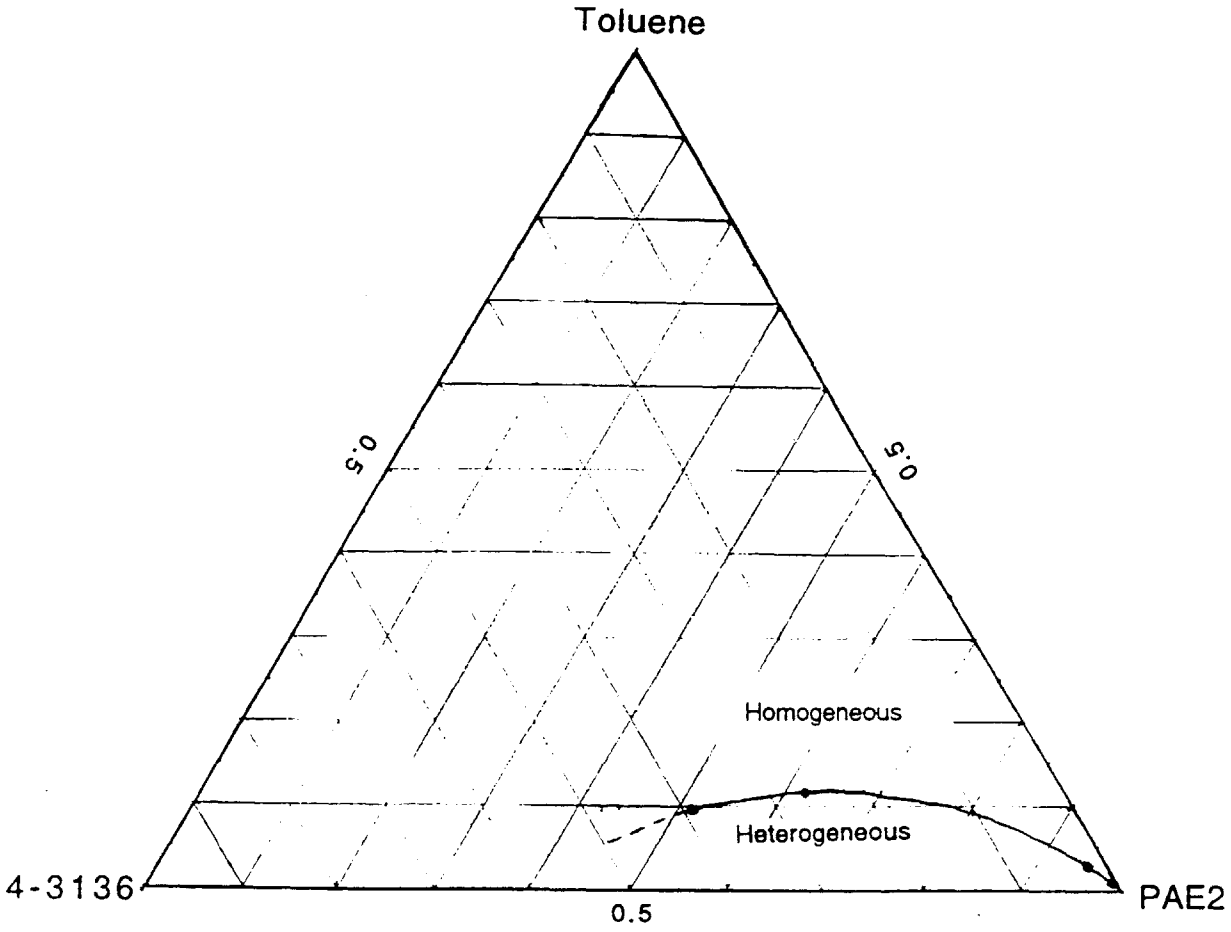

Figure 2.8. Room temperature ternary phase diagram of 4-3136 silicone resin/toluene/PAE2.

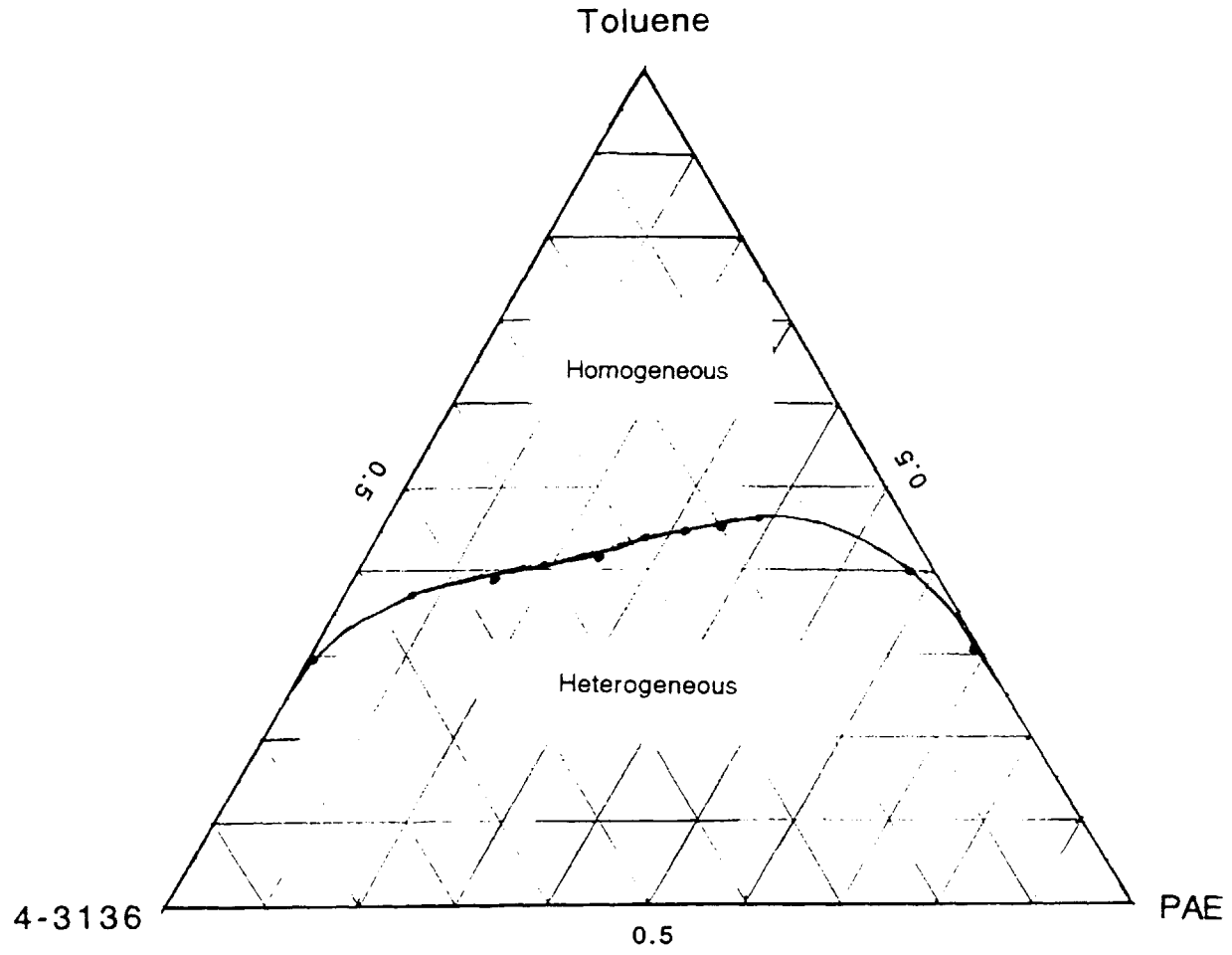

Figure 2.9. Room temperature ternary phase diagram of 4-3136 silicone resin/toluene/PAE.

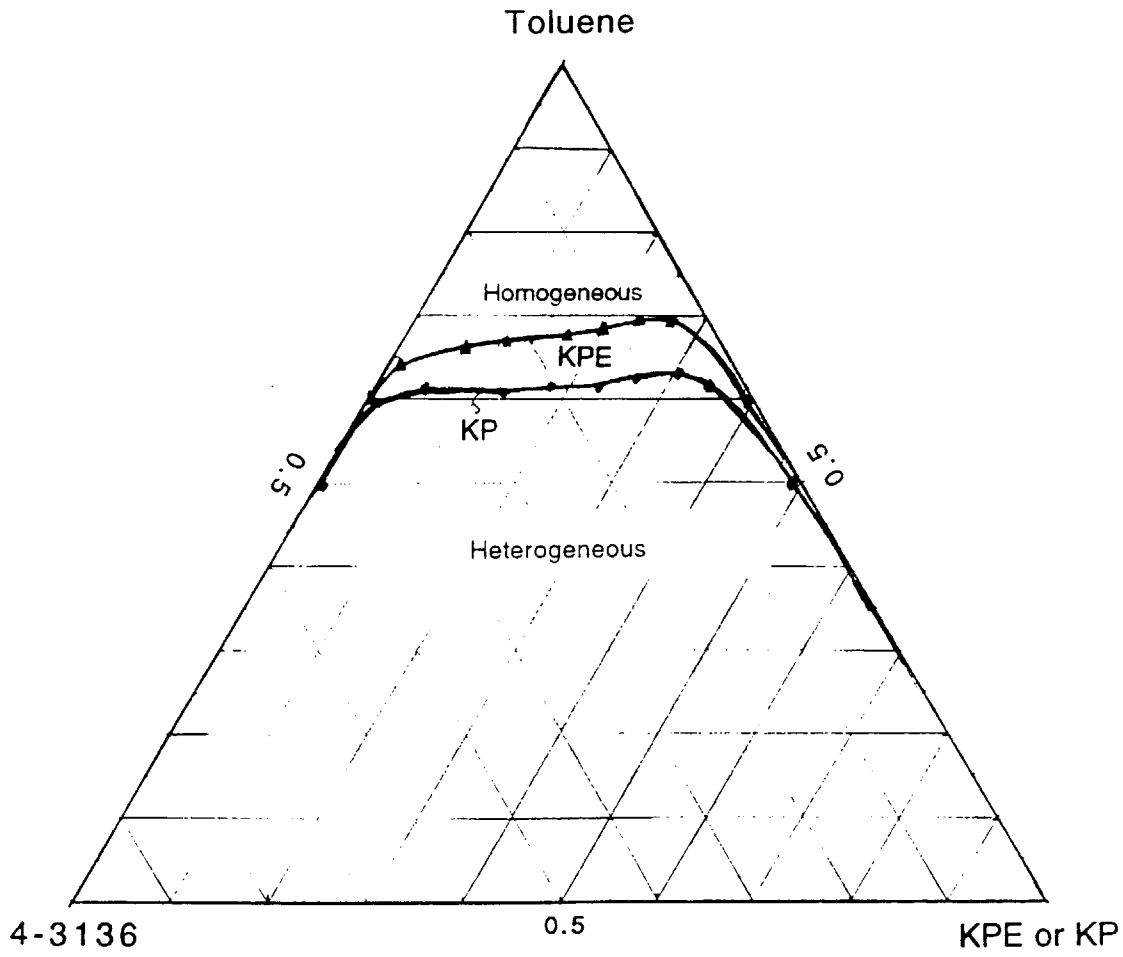

Figure 2.10. Room temperature ternary phase diagram of 4-3136 silicone resin/toluene/KPE or KP-80.

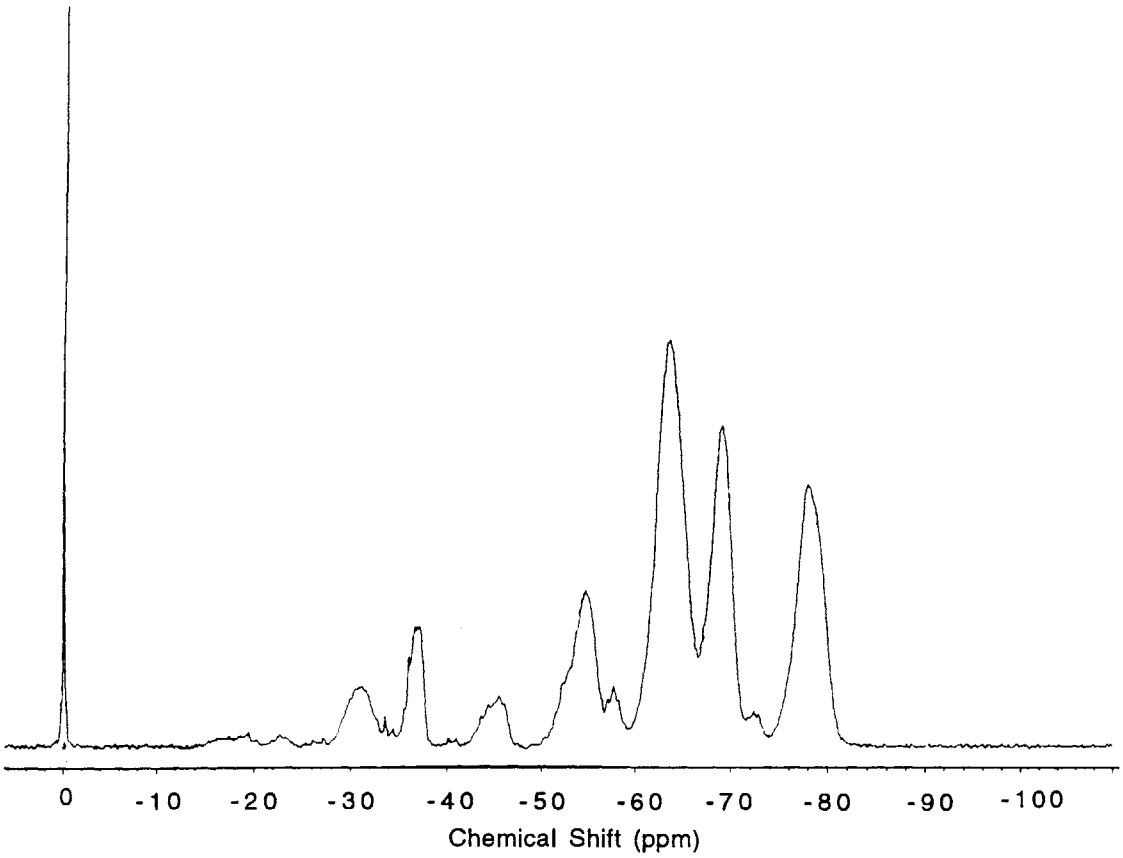

Figure 2.11. ^{29}Si NMR spectrum of the 4-3136 resin pre-polymer.

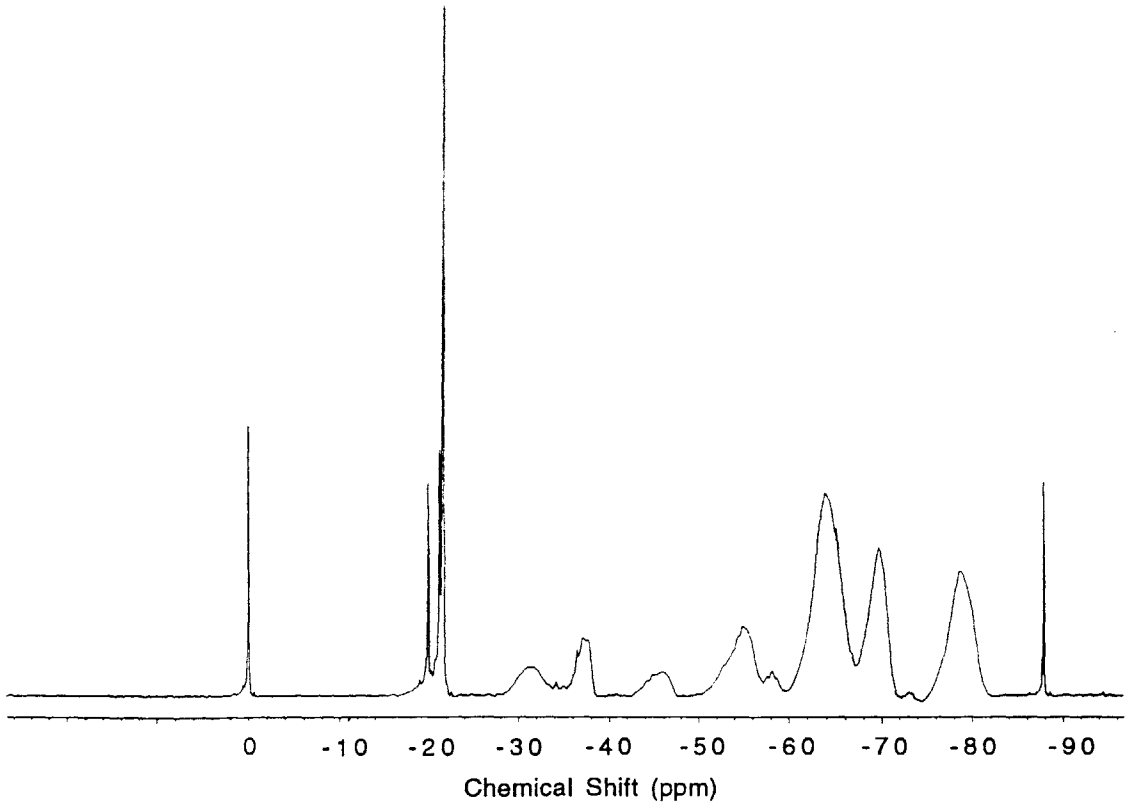

Figure 2.12. ^{29}Si NMR spectrum of a mixture of the 4-3136 resin pre-polymer with 10 part PAE without pre-reaction.

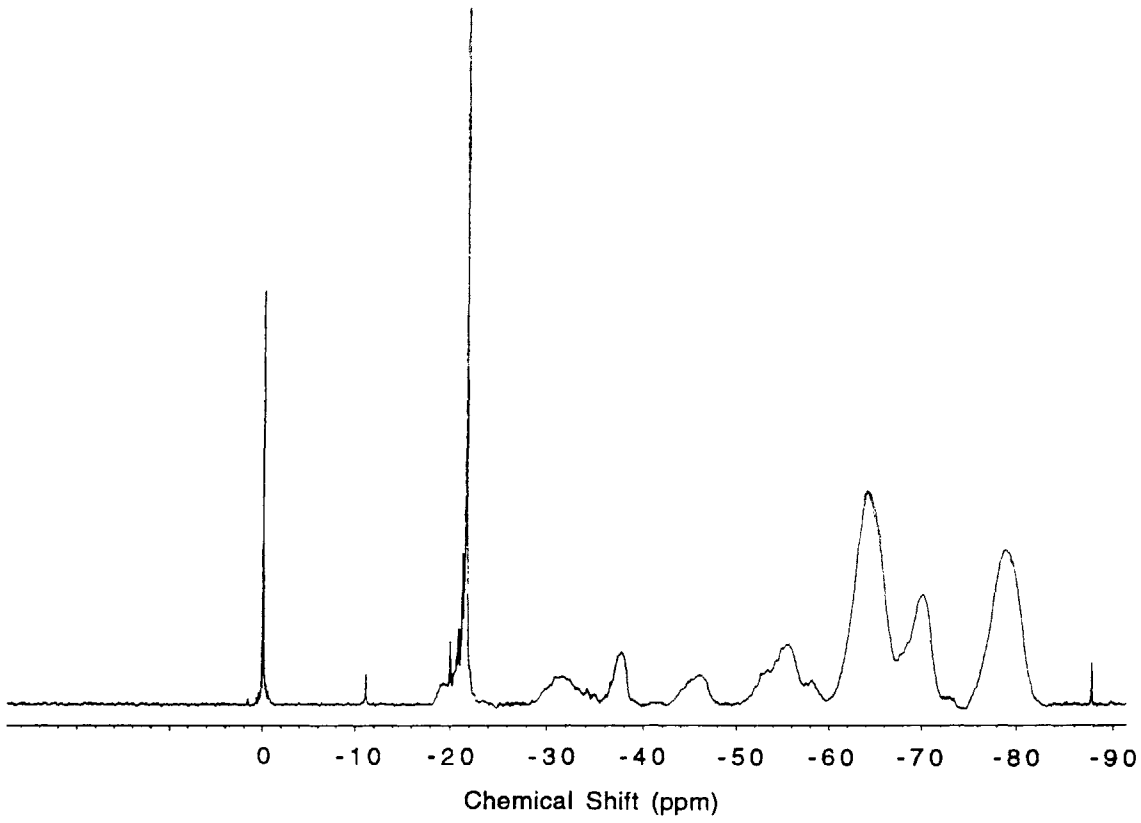

Figure 2.13. ^{29}Si NMR spectrum of the 4-3136 resin pre-polymer coupled with 10 part PAE. Volatile substances were removed from the beginning of the reaction.

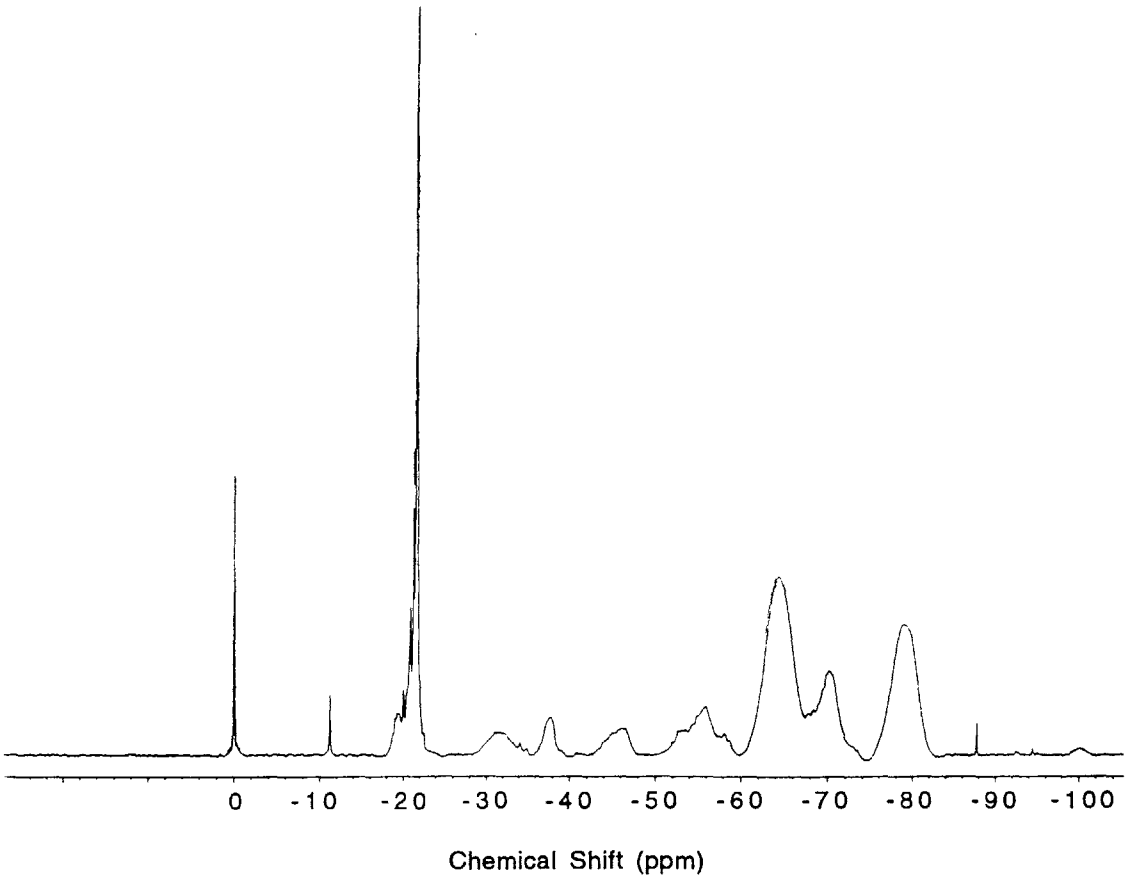

Figure 2.14. ^{29}Si NMR spectrum of the 4-3136 resin pre-polymer coupled with 20 part PAE. Volatile substances were removed from the beginning of the reaction.

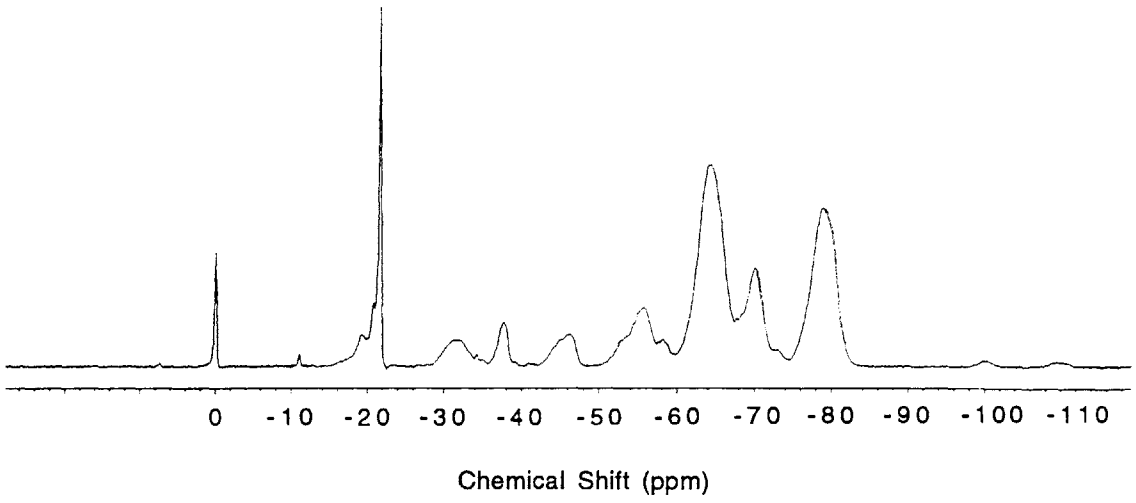

Figure 2.15. ^{29}Si NMR spectrum of the 4-3136 resin pre-polymer coupled with 10 part PAE. No volatile substances were removed from the reaction system.

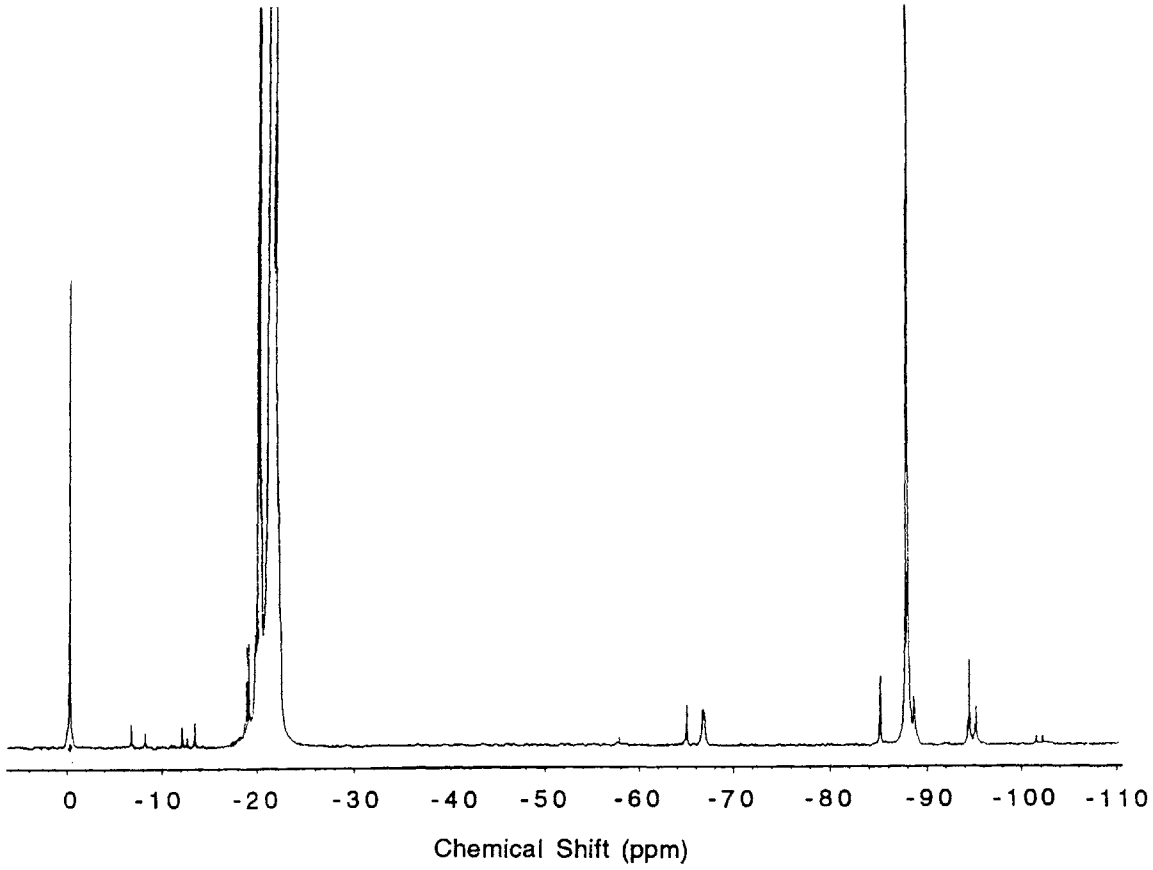

Figure 2.16. ^{29}Si NMR spectrum of PAE after being heated at 105 °C for 28 hours with 0.1 wt.% $Ti(OBu)_4$.

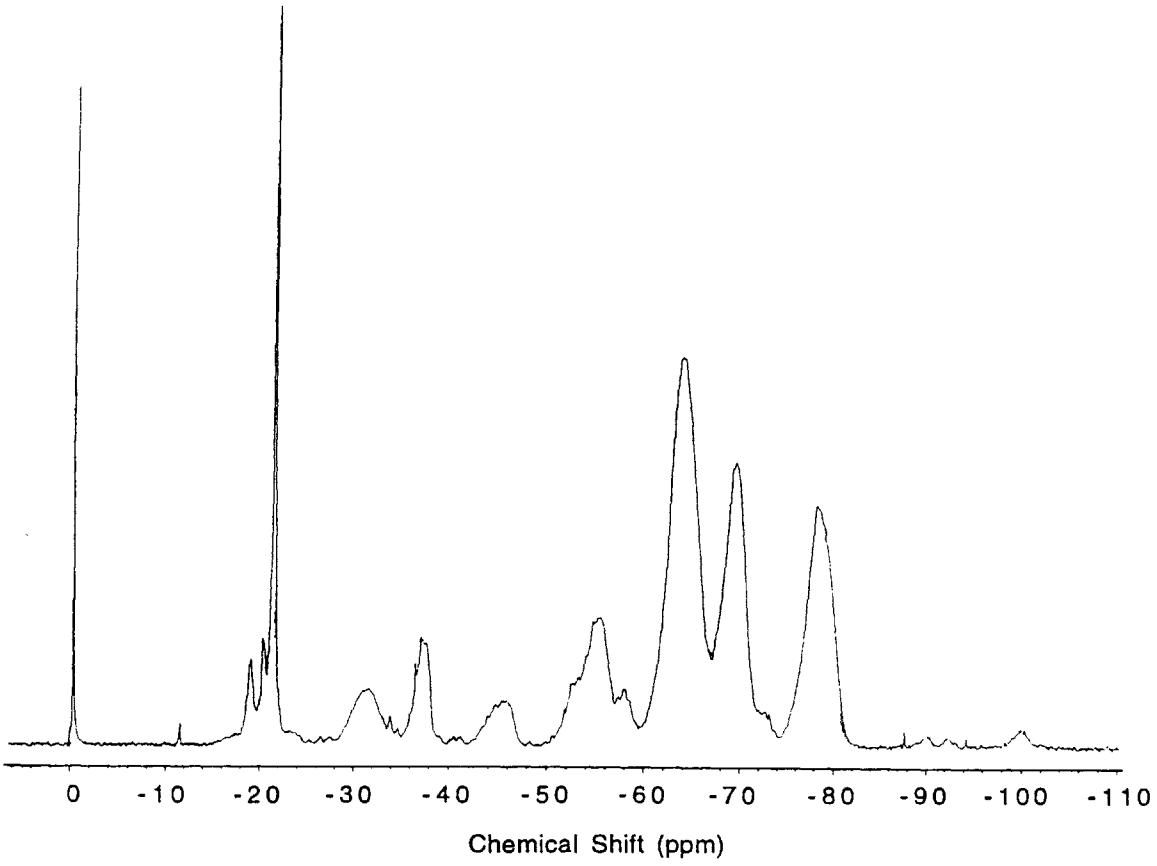

Figure 2.17. ^{29}Si NMR spectrum of the 4-3136 resin coupled with 10 part PAE. The coupling reaction was partially finished.

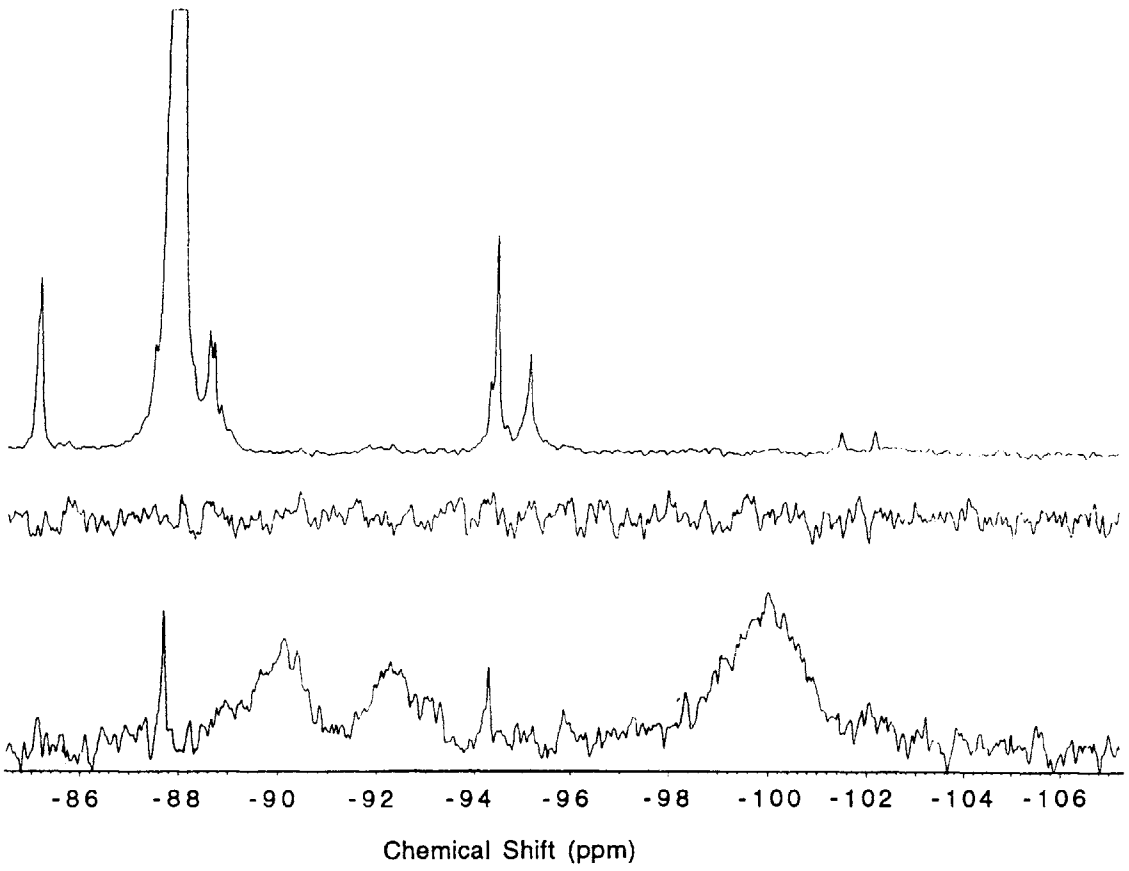

Figure 2.18. Selected regions of Figure 2.16 (top), the spectrum of the 4-3136 resin pre-polymer (middle), and Figure 2.17 (bottom).

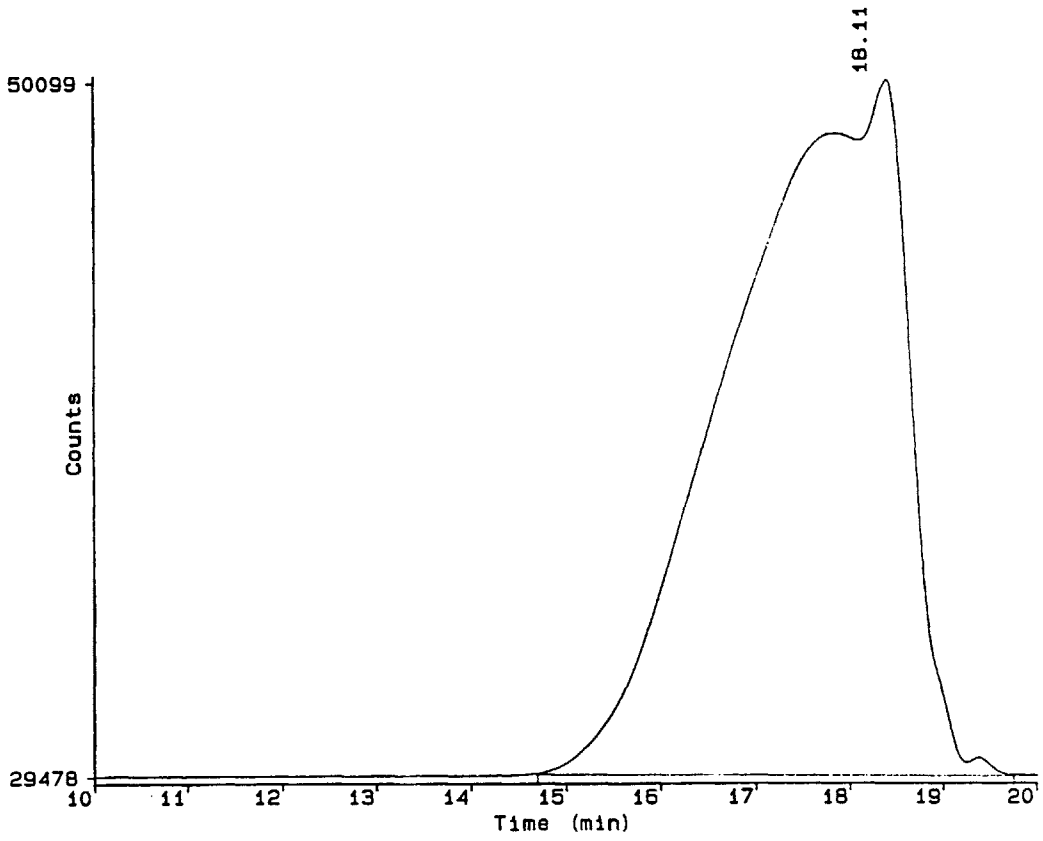

Figure 2.19. GPC retention time vs. concentration curve of the 4-3136 resin pre-polymer.

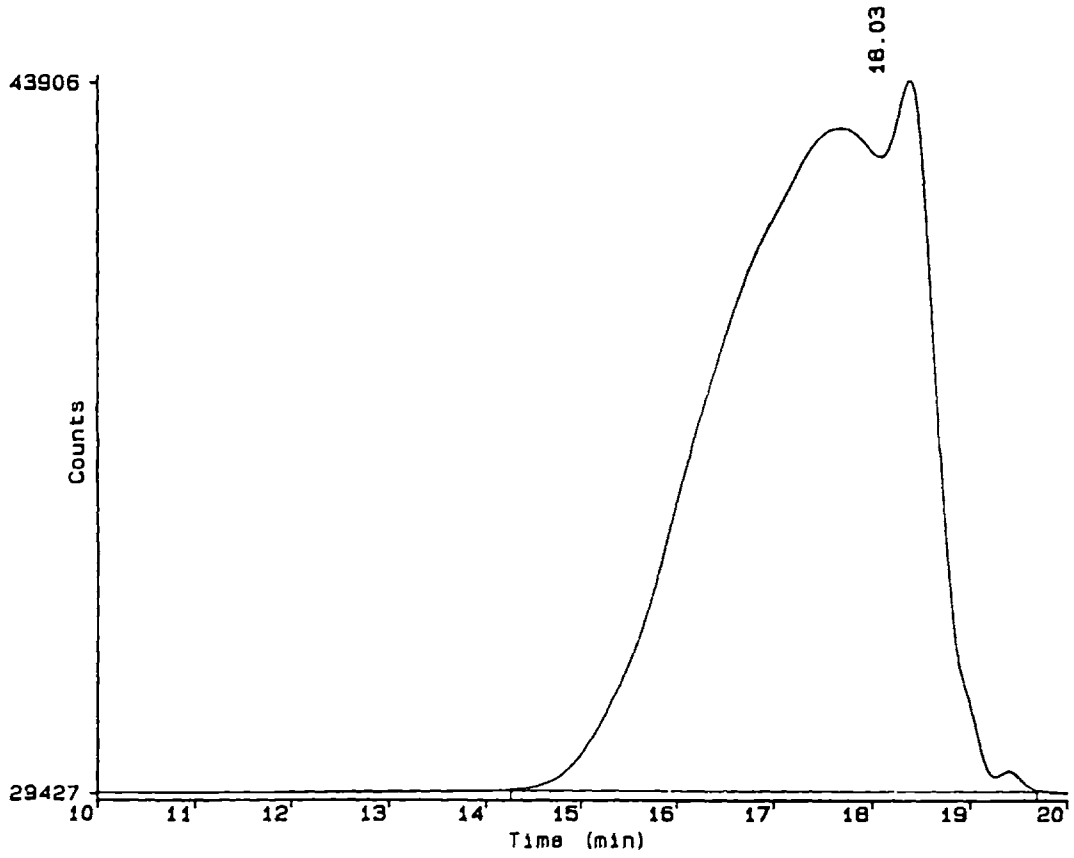

Figure 2.20. GPC retention time vs. concentration curve of a mixture of the 4-3136 resin pre-polymer and 10 part PAE without pre-reaction.

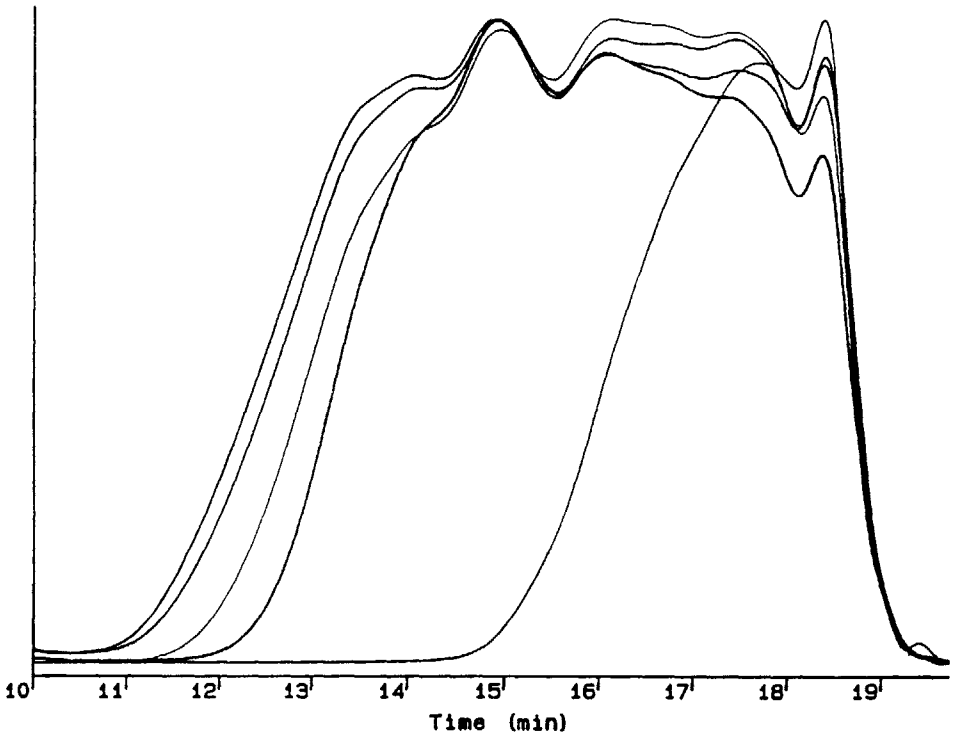

Figure 2.21. GPC retention time vs. concentration curves of the 4-3136 resin pre-polymer coupled with different modifiers in solutions of different concentrations. The modifiers and reaction solution concentrations were, from right to left: no modifier; 10 parts of PAE, 46 wt.%; 10 parts of PAM, 65 wt.%; 10 parts of PAE, 51 wt.%; 20 parts of PAE, 53 wt.%.

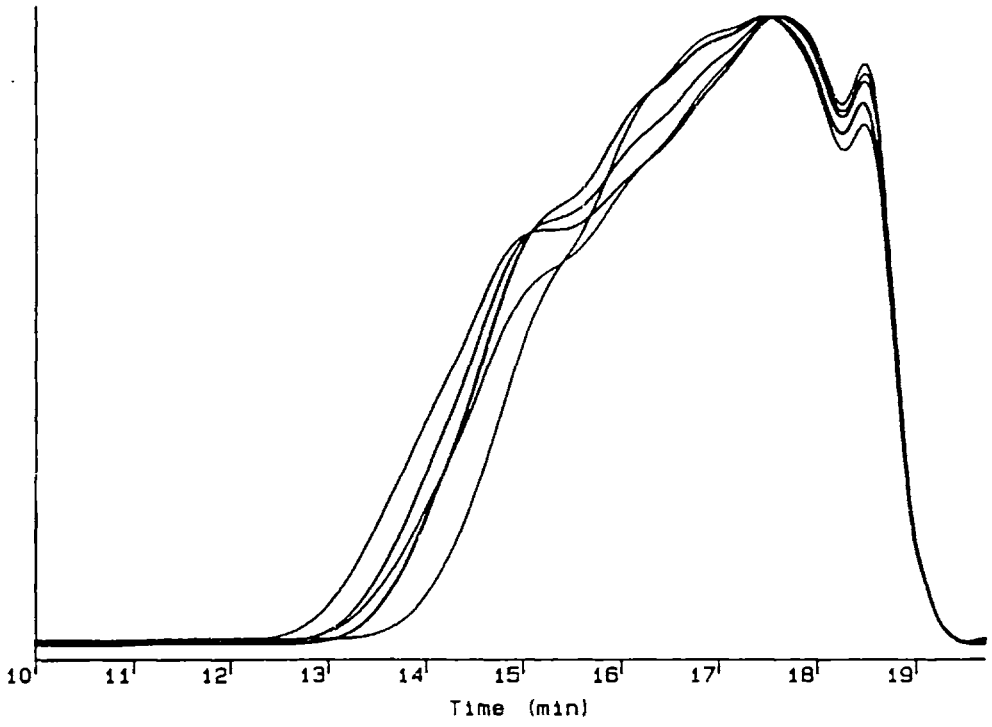

Figure 2.22. GPC retention time vs. concentration curves of the 4-3136 resin pre-polymer coupled with different amounts of KPE. The amounts of KPE were, from right to left: 5, 10 15, 15, and 20 parts.

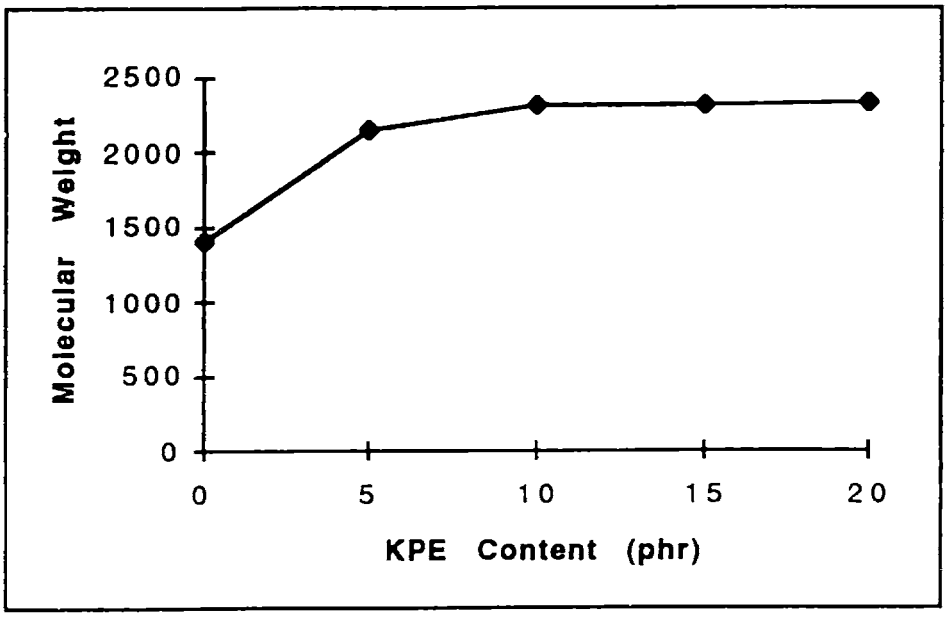

a

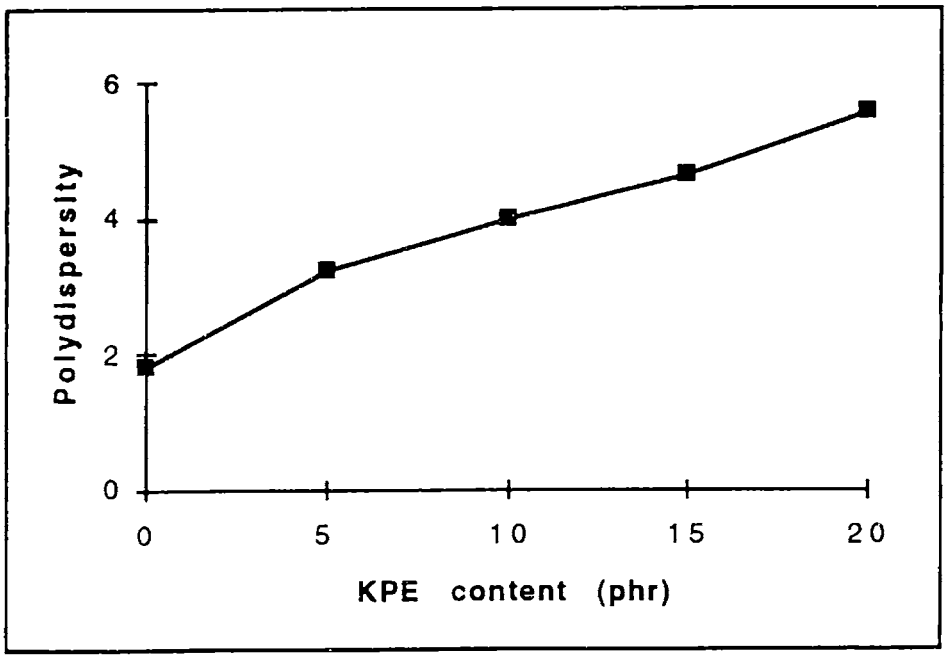

b

Figure 2.23. Number average molecular weight and polydispersity of the 4-3136 resin coupled with various amounts of KPE.

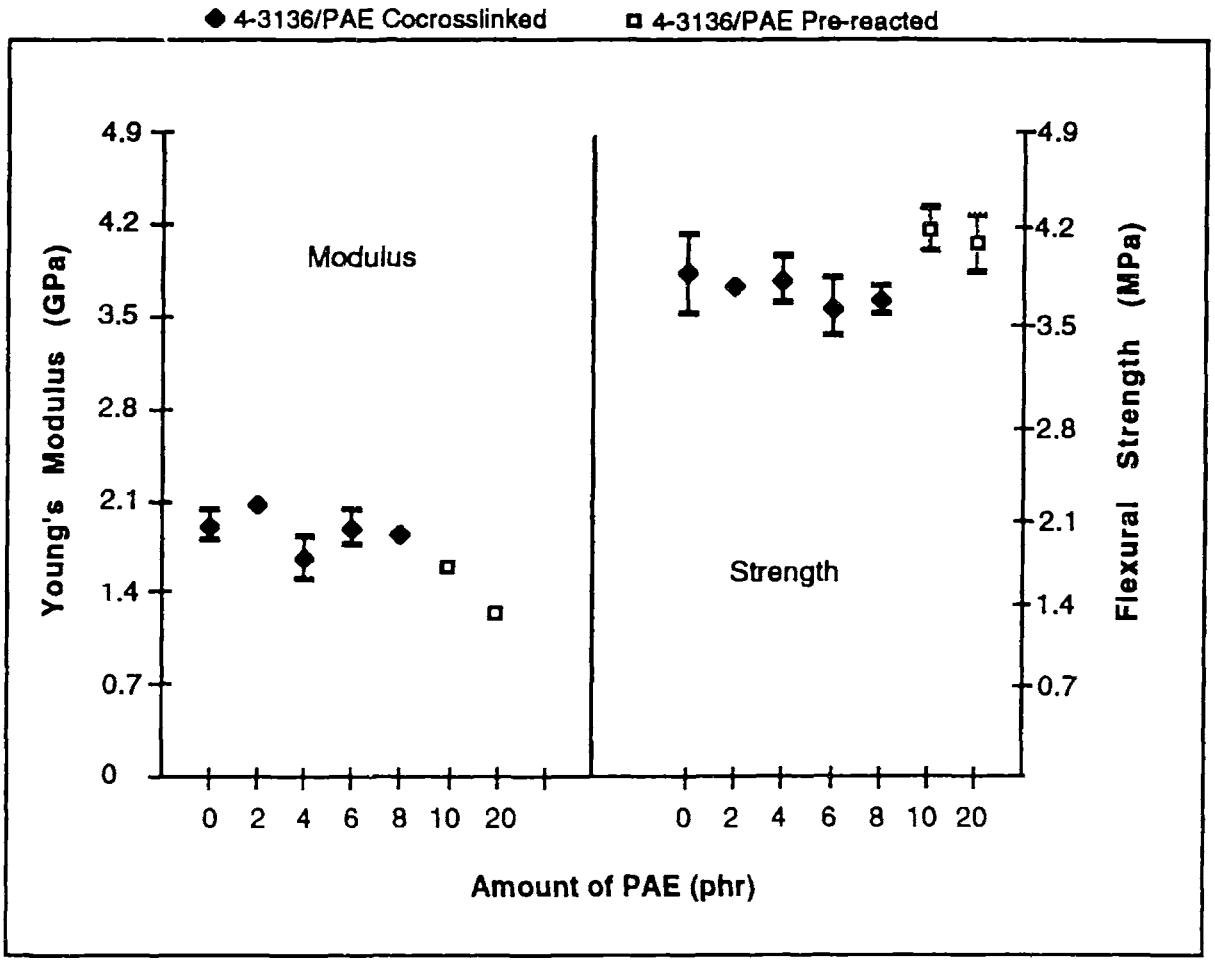

Figure 2.24. Flexural properties of the 4-3136 resin co-reacted or pre-reacted with PAE. Some data points do not have error bars since their error bars coincide with the marks that indicate average value.

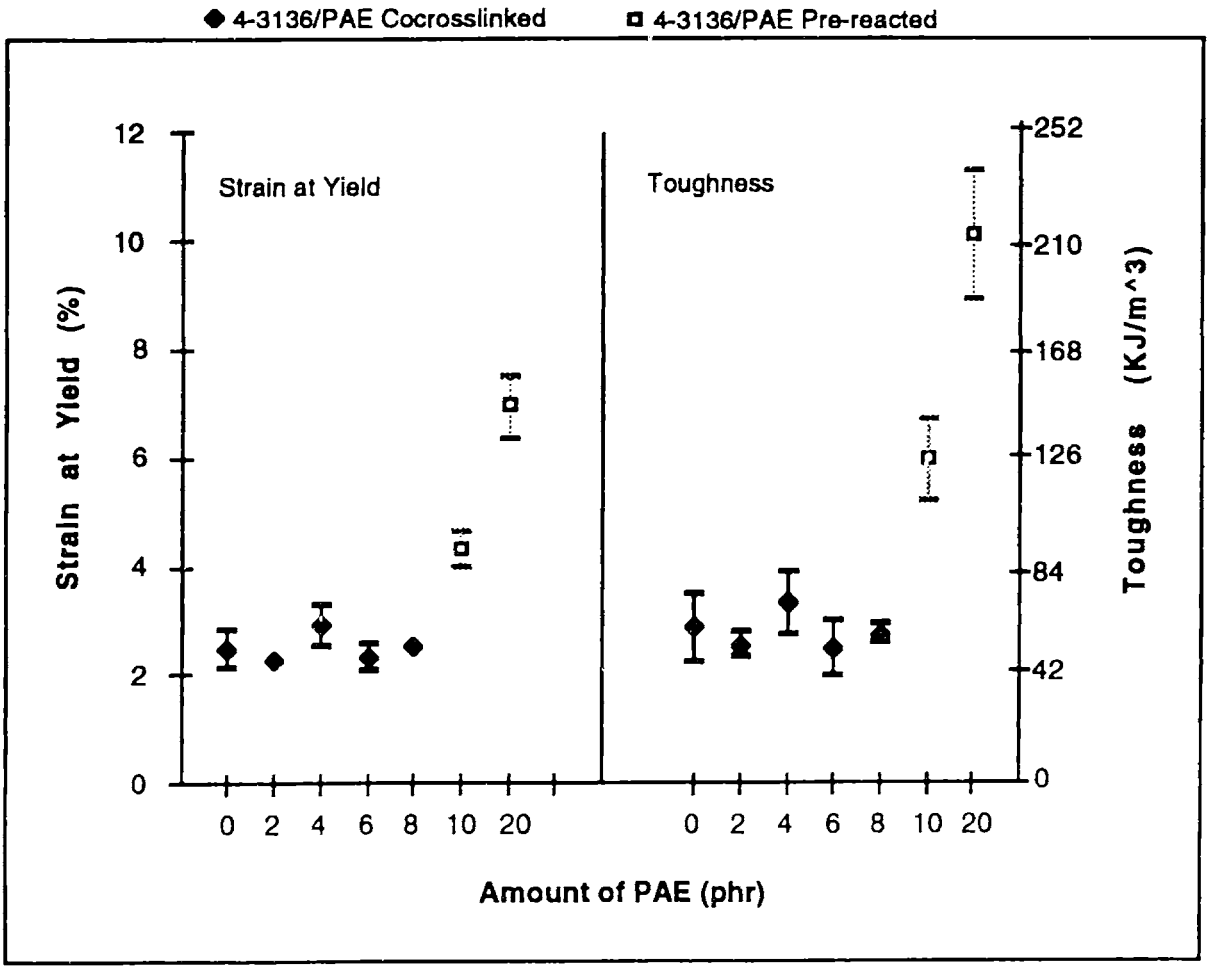

Figure 2.25. Flexural properties of the 4-3136 resin co-reacted or pre-reacted with PAE. Some data points do not have error bars since their error bars coincide with the marks that indicate average value.

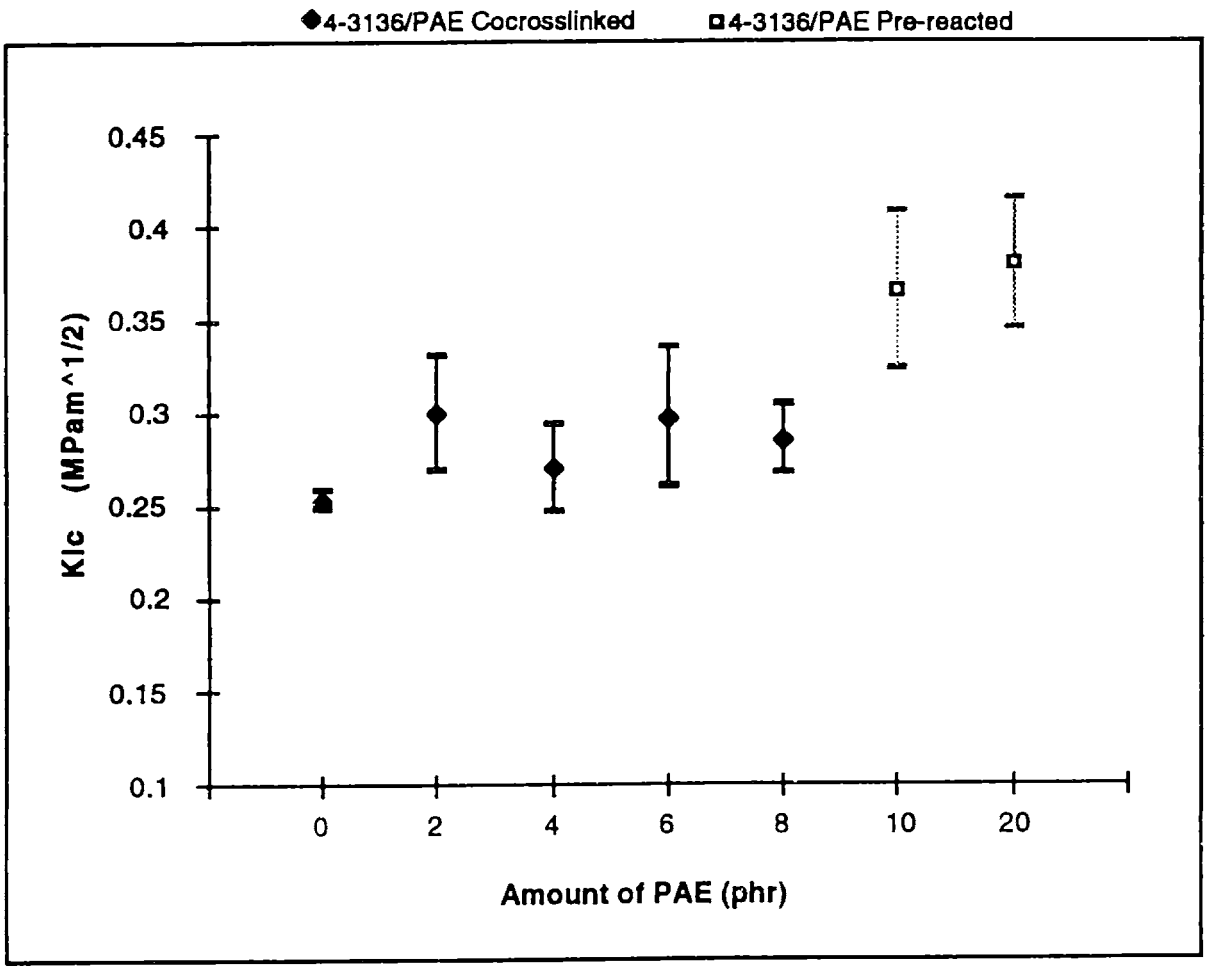

Figure 2.26. KIc of the 4-3136 resin modified with PAE through co-reaction or pre-reaction.

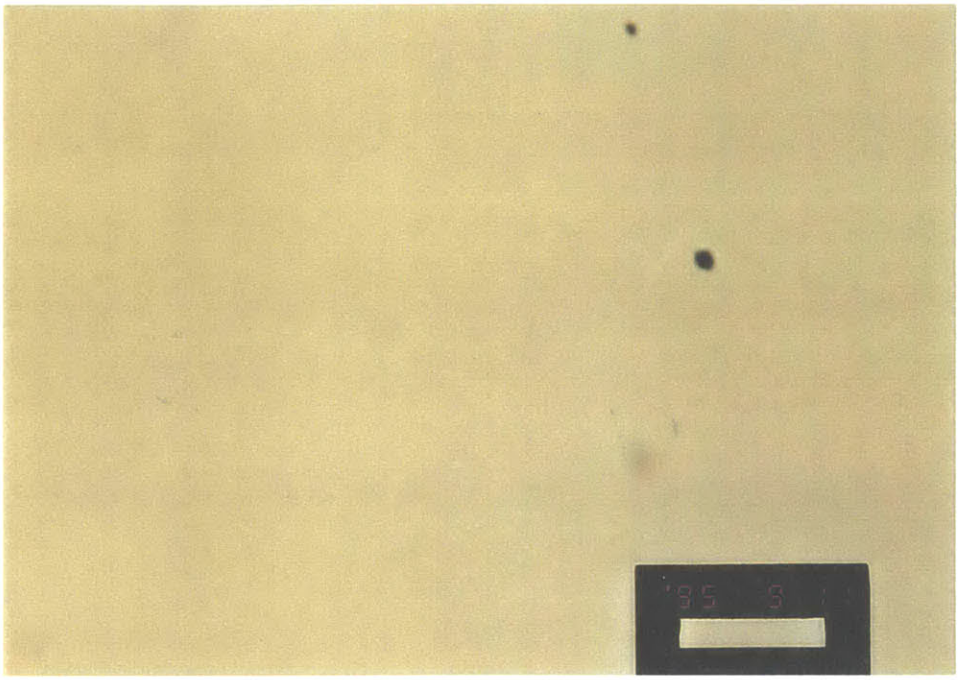

Figure 2.27. Optical microscopy picture taken from inside a casting of the 4-3136 resin pre-reacted with 10 parts of PAE. The casting was transparent and the black spots were impurities. Magnification: 500X.

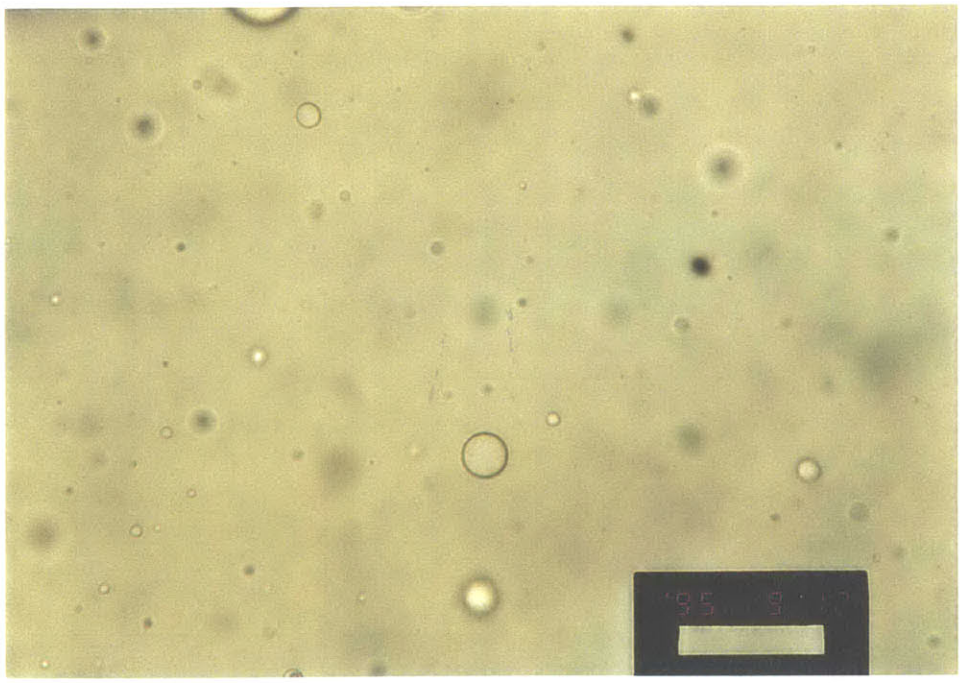

a

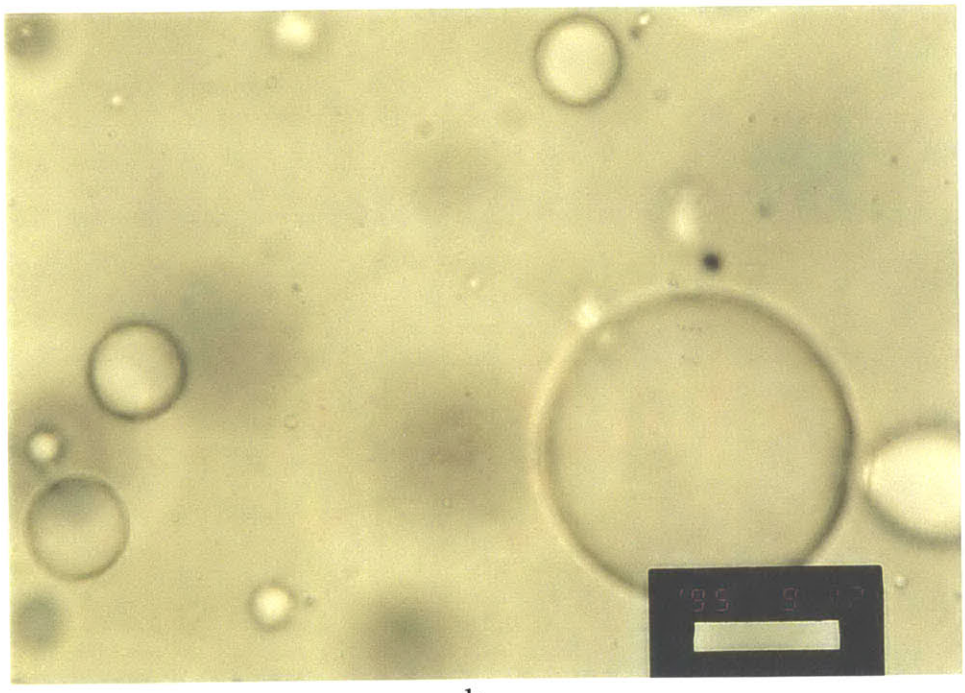

b

Figure 2.28. Optical microscopy pictures taken from inside castings of the 4-3136 resin co-reacted with a: 2 parts of PAE, and b: 8 parts of PAE. Magnification: 500X.

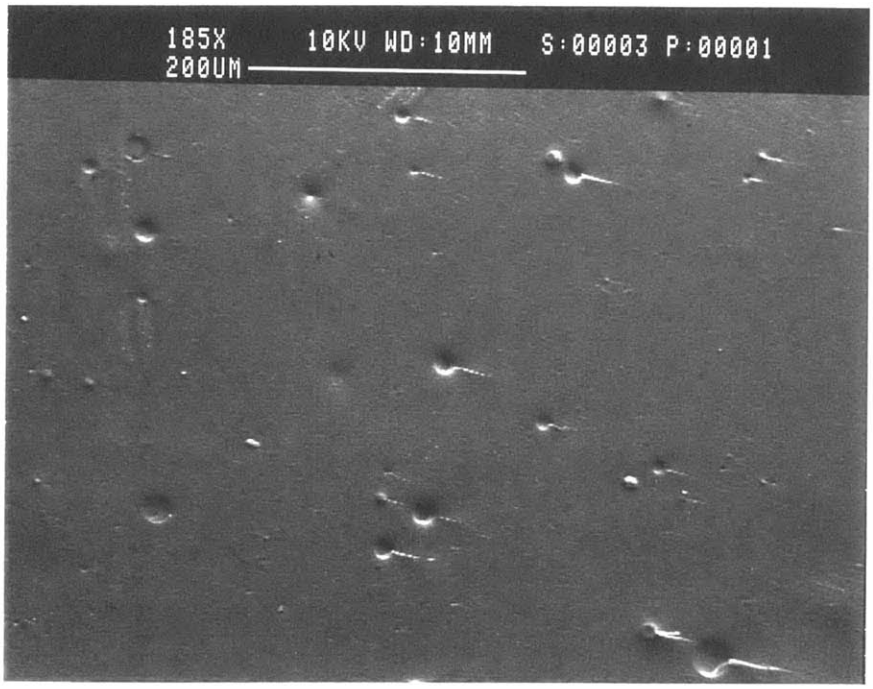

a

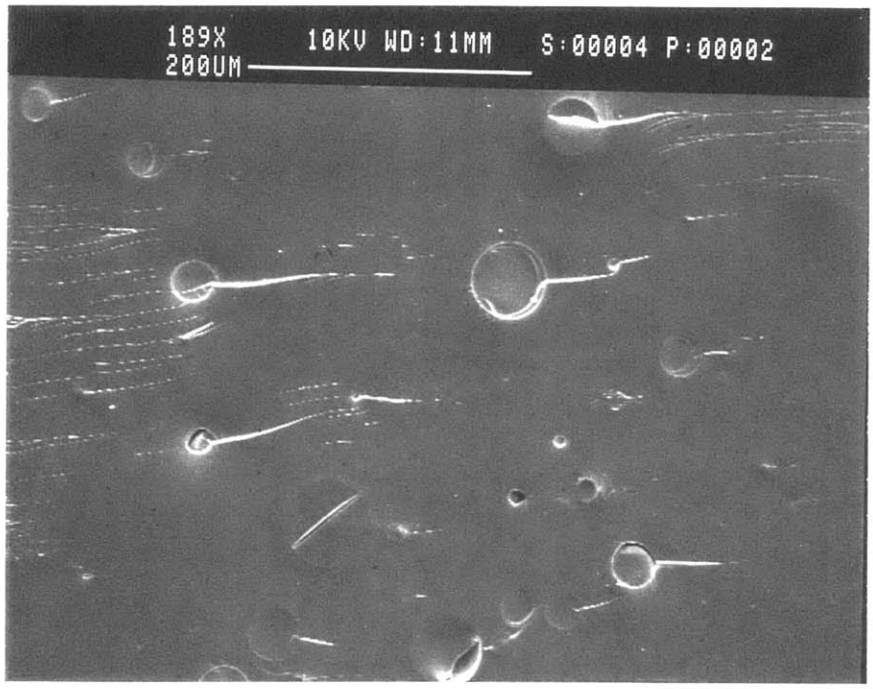

b

Figure 2.29. SEM photos taken from the freshly fractured surfaces of castings of the 4-3136 resin co-reacted with a: 4, b: 8 part PAE, showing second phase particles.

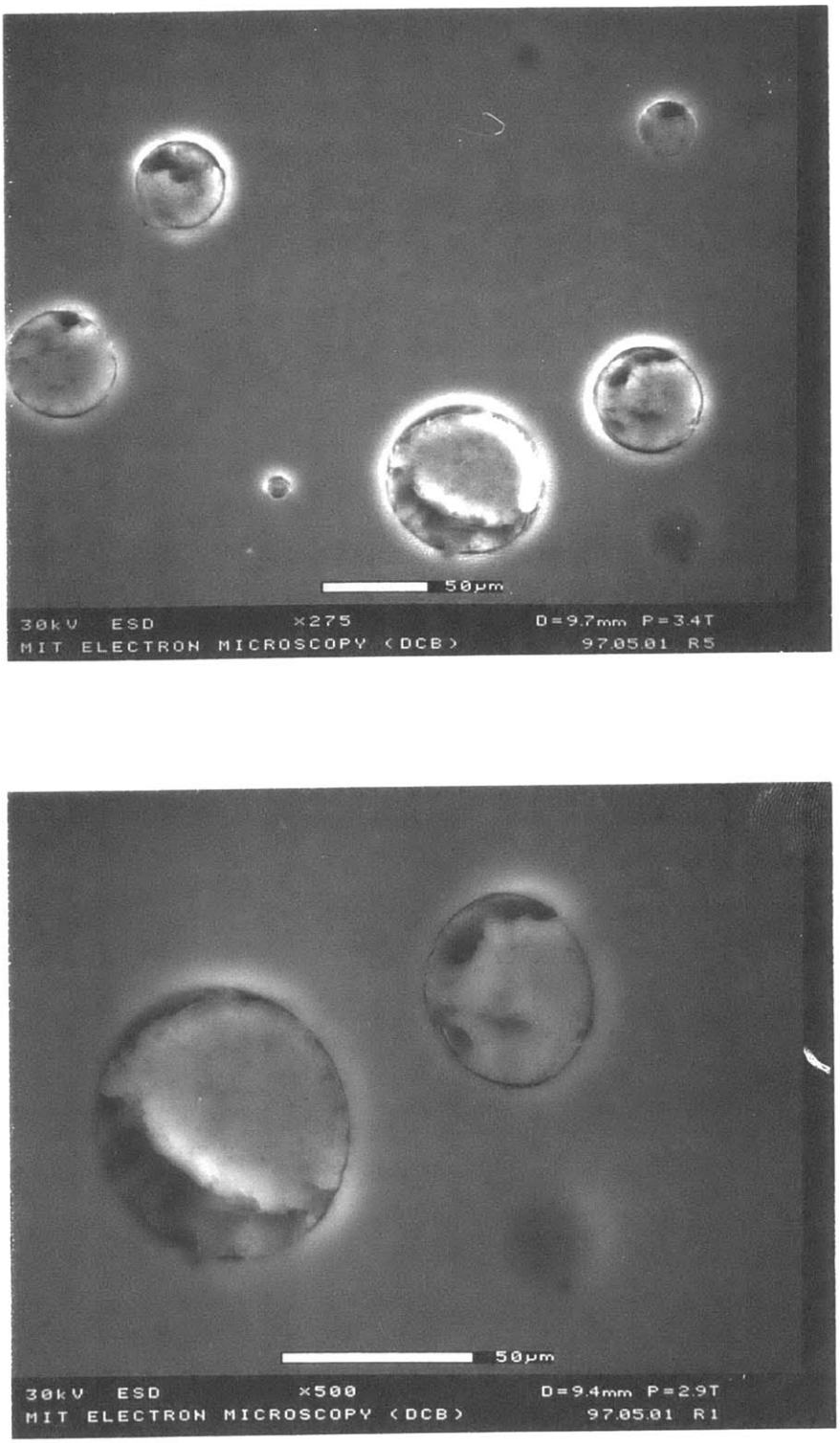

Figure 2.30. Photos taken by an Environmental SEM from the polished surface of a casting of the 4-3136 resin co-reacted with 8 part PAE, showing second phase particles.

Chapter 3. Mechanical Properties of Toughened Rigid Silicone Resins

3.1. Introduction.

Before this study the mechanical properties and fracture behavior of rigid silicone resins have not been fully investigated. No fracture toughness data could be found either in the open literature or in internal research reports of a major manufacturer, although some flexural property data are available in the latter. There are primarily two reasons for this situation: difficulties in making sound, void free thick samples, and the brittleness of rigid silicone resins which prevents their use as structural materials. The preparation of cast plates of condensation cure resins is difficult due to the release of condensation by-products. These are trapped by thick, highly crosslinked surroundings and cause internal bubbles. Of the two major types of rigid silicone resins, however, condensation cures are more versatile and more important than addition cures. To fully evaluate the mechanical and fracture properties of the condensation resins, and to study the toughening effect by Phase I and Phase II modifications, new sample preparation methods had to be developed to avoid the formation of voids.

In the previous chapter it was shown that plastic flow of the cured network was enhanced by pre-reacting a functionalized PDMS into the network. The PDMS chain can have a wide range of lengths, which will affect the mechanical and fracture behavior of the modified resins. An upper limit of chain length can be expected to exist, above which the PDMS can no longer be a Phase I rubber, but rather, a Phase II. This limit, and the chain length effect on mechanical properties, are unknown without experimental investigation.

After the Phase I modification, Phase II rubber particles are introduced into the matrix. Appropriate Phase II particles will promote wider plastic deformation and utilize the enhanced flow capability of the matrix afforded by the Phase I modification. There are requirements, however, which must be

satisfied for the rubber particles to function as effective toughеners. Among them adhesion at the interface of the particles and the matrix, the elastic modulus of the second phase particles, and their diameters are expected to be critical. It was demonstrated in the early stage of this study that commercially available silicone rubber powders do not toughen rigid silicone resins, with or without Phase I modification. Thus a new process was required to form the appropriate Phase II particles in a Phase I modified matrix. In this Chapter, new methods to prepare void free condensation cure silicone resin samples are discussed. This enables the study of their mechanical properties. Toughening by the short chain functionalized PDMS and the effect of chain length are investigated. A new route to form appropriate Phase II rubber particles will be described and the combined toughening effect of the Phase I/II modification will be shown.

3.2. Preparation of cast plates of rigid silicone resins.

3.2.1. Casting Procedure.

To make a void free condensation cure cast plate, it was necessary to prevent the accumulation of water vapor in the casting during cure. At a typical curing temperature, as recommended by the product information sheet supplied by the manufacturer, one gram of solid resin would produce 45 to 60 ml of water vapor within 10 to 20 minutes. If the recommended schedule was followed, a highly foamed plate was obtained.

To eliminate the voids the condensation reaction rate must be lowered, and the diffusion of the water must be accelerated. The general principle was explained by a simple equality (3.1): the production rate of the water vapor, R^*, plus the diffusion rate, $\frac{\partial}{\partial x}(D_i \frac{\partial \rho_i}{\partial x})$, was the accumulation rate, $\frac{\partial \rho_i}{\partial t}$. The first two rates should be matched so that the accumulation rate was zero.

$$\frac{\partial \rho_i}{\partial t} = \frac{\partial}{\partial x}(D_i \frac{\partial \rho_i}{\partial x}) + R^* \qquad (3.1)$$

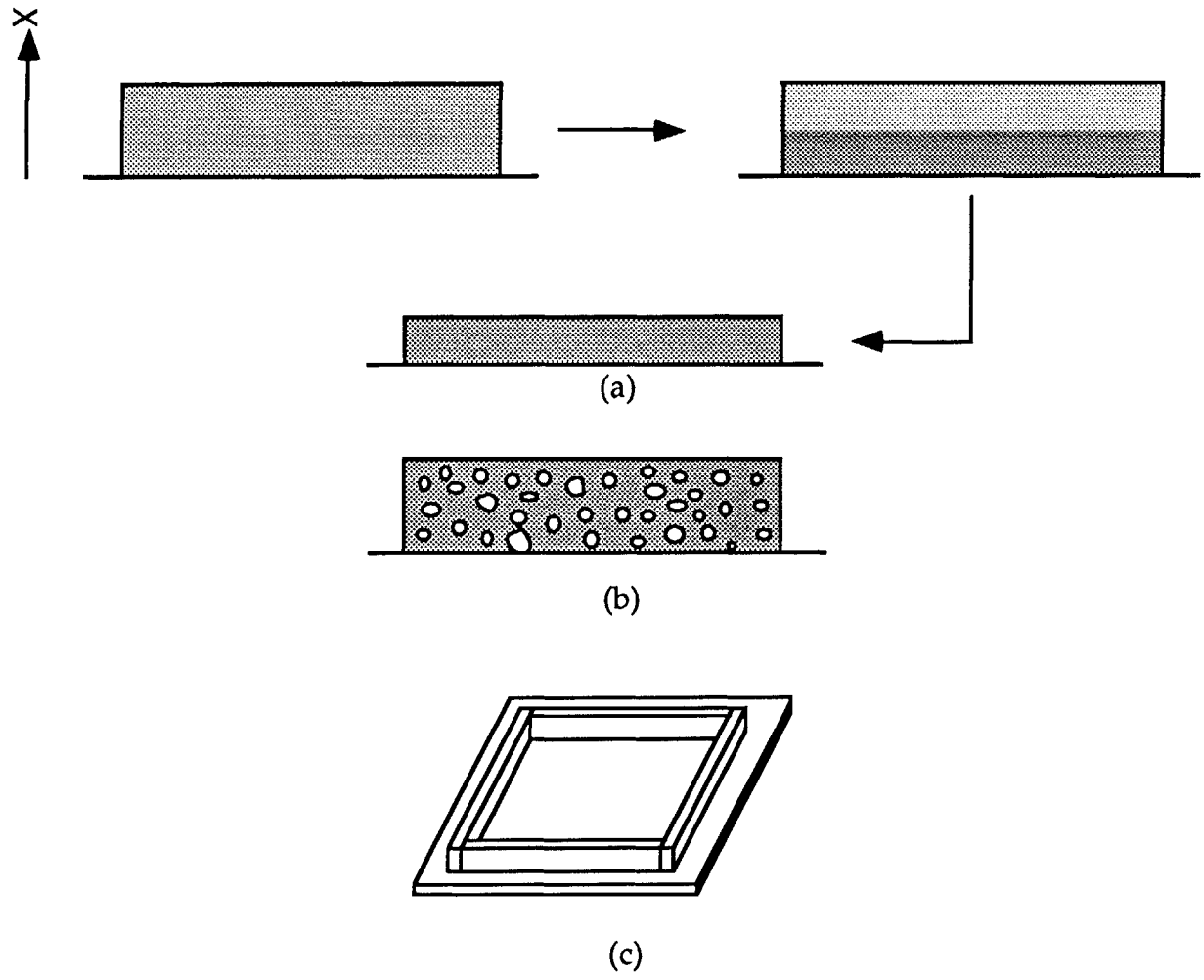

Figure 3.1. Schematic diagram showing: (a) and (b), how the removal of condensation by-product was facilitated; and (c), the mold used for curing the resin.

The initial stage of the curing reaction is the most likely time when bubbles will form and grow, because of the high condensation rate and low viscosity of the resin. When the condensation rate exceeds the diffusion rate, water vapor is accumulated and voids are nucleated which grow to form bubbles. The addition of a small amount of a high boiling point inert solvent at this stage reduces the viscosity and increases the diffusion rate, preventing the accumulation of water vapor. This is illustrated schematically by Figure

3.1(a). The curing process was started at a temperature below the boiling point of the inert solvent. Past the initial stage, when the condensation reaction became slower, the curing temperature was gradually raised, and the high boiling point solvent was evaporated gradually. When the resin matrix was strong enough to resist the nucleation and growth of voids, the temperature could be raised to above the boiling point of the solvent to complete its removal. The curing process was carried further, to completion.

A number of solvents were tried and it was found that N-dimethyl acetamide, with a boiling point at 163 °C, was the best. Usually 5% based on the resin was needed. Xylene, with a boiling point at 144 °C, was also a reasonable choice, but a little more than 5% was needed.

Another way to remove the by-products is to add fillers such as fumed silica, shown by Figure 3.1(b). Due to its very small particle size, only 1 to 2% is needed to obtain a much improved casting.

The addition of an inert solvent or a highly dispersed filler is effective, but they can obscure the mechanical evaluation due to the following reasons: 1). some solvents are not entirely inert, and the precipitation sequence results in a distribution of compositions and structures along the thickness direction; 2). if fillers are used the mechanical properties are altered. Therefore another process, involving no addition of foreign substances, was developed and used in this study.

This process slowed the production rate of by-products by decreasing the catalyst level and using a prolonged curing cycle. The catalyst level was reduced from 0.2 wt.% to 0.05 wt.%, and the curing cycle was started at 70 °C. The temperature was raised gradually and a long curing process, lasting for 13 days, was carried out. In this process, both the resin pre-polymer melt and a solution of the pre-polymer could be used. In the melt process the solid pre-polymer was melted at 90 - 100°C and mixed with other ingredients, typically 0.05% Dow Corning Catalyst Y-177® and modifying agents if needed. The molten mixture was poured into a mold as shown in Figure 3.1(c), which was designed to maximize the surface area and speed the removal of water vapor. The molten resin in the mold was degassed in a vacuum oven at 100 °C for about half an hour and moved to an air circulating oven to cure. In the

solvent process, the solution of modified or unmodified resins was mixed with other ingredients at room temperature. The solution was poured into the mold and placed in a vacuum oven at 100 °C. The solvent was removed by applying vacuum and collected in a trap cooled by liquid nitrogen. When the solvent removal was complete, the mold with the resin was transferred to an air circulating oven to cure. The same temperature sequence was followed for both processes: 70 °C/24 h, 75 °C/24 h, 80 °C/24 h, 85 °C/24 h, 90 °C/24 h, 95 °C/48 h, 110 °C/24 h, 120 °C/24 h, 130 °C/48 h, 150 °C/4 h, 175 °C/4 h, 200 °C/12 h, 230 °C/6 h, and 260 °C/8 h. At the end of this sequence a sound, void free, fully cured plate was obtained.

3.2.2. DMA analysis.

The cast plates were compared with a much thiner casting prepared using the manufacturer recommended curing cycle. DMA was used for this purpose. The experimental details of the DMA are given in Chapter 5. From the recommended curing cycle, only thin samples could be obtained without extensive foaming: they were not suitable for plane strain fracture toughness testing but were used to compare the crosslink density of castings made by different procedures.

Figure 3.2 illustrates that the DMA responses of these two castings are similar. The phenyl rich transition at ~220 °C, the methyl rich transition at ~ 120 °C, the phenyl β transition at -108 °C, the broad transition centered at ~-30 °C, and the transition at ~70 °C, (possibly the phenyl T β transition) are at similar positions and their damping magnitudes are similar, although small structural difference do exist, evidenced by the separation tendency of the 120 °C and the 70 °C peaks in the bottom curve.

In Figure 3.3 the storage modulus is compared. These curves also are similar: a very gradual transition from the glassy state to the softened state, a broad transition temperature range, as well as a small modulus change at the transition. The rubbery plateau modulus is indicative of the crosslink density through the relation $M_C=3dRT/G'$, where G' is the shear modulus taken as E/3, E the storage modulus, M_C the molecular weight between crosslinks, d

the density of the resin casting, R the gas constant, and T the temperature in K. From the storage modulus values at 180 °C it was calculated that $M_{c,lower}=0.75\ M_{c,upper}$, indicating that a higher crosslink density was obtained from the curing procedure used in this study.

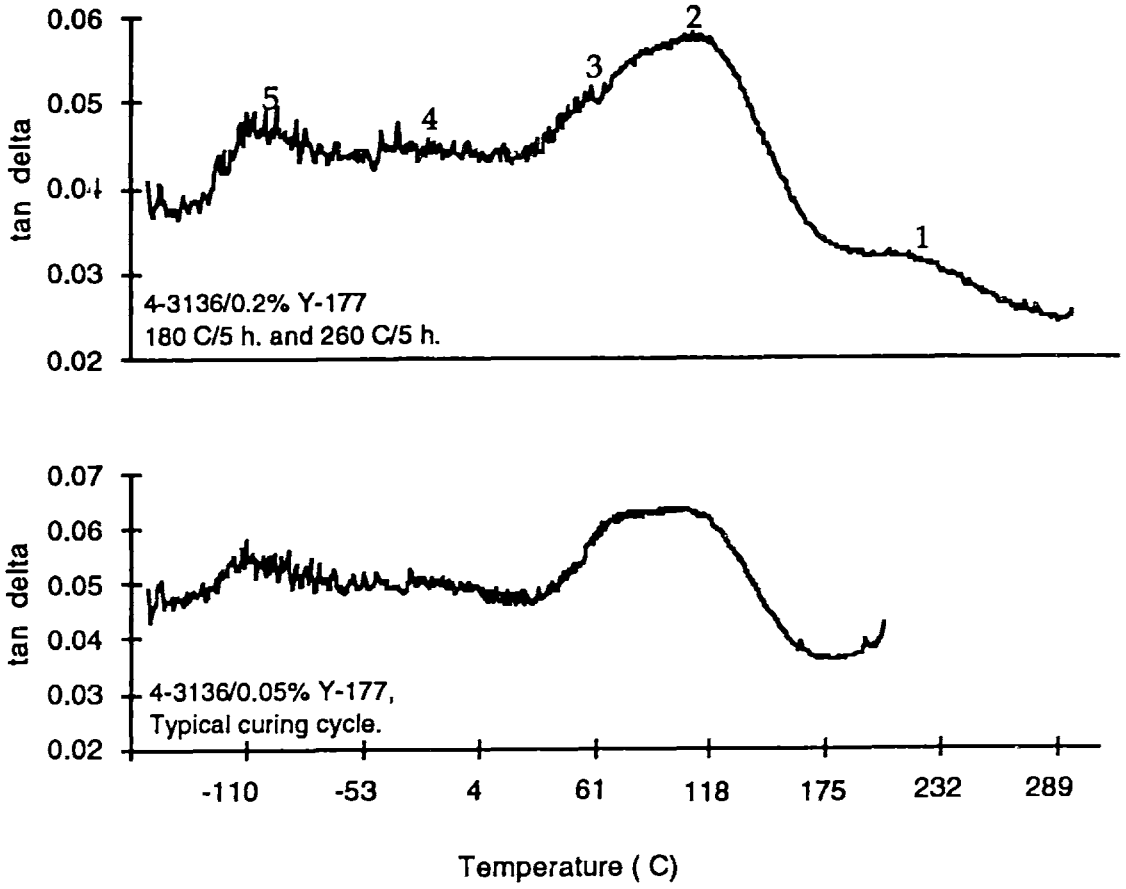

Figure 3.2. Loss factor, tan δ, as determined by DMA analysis, of 4-3136 resin castings cured through 1). upper curve, a conventional process, as recommended by the product information sheet supplied by the manufacturer, and 2). bottom curve, a curing process described in the text.

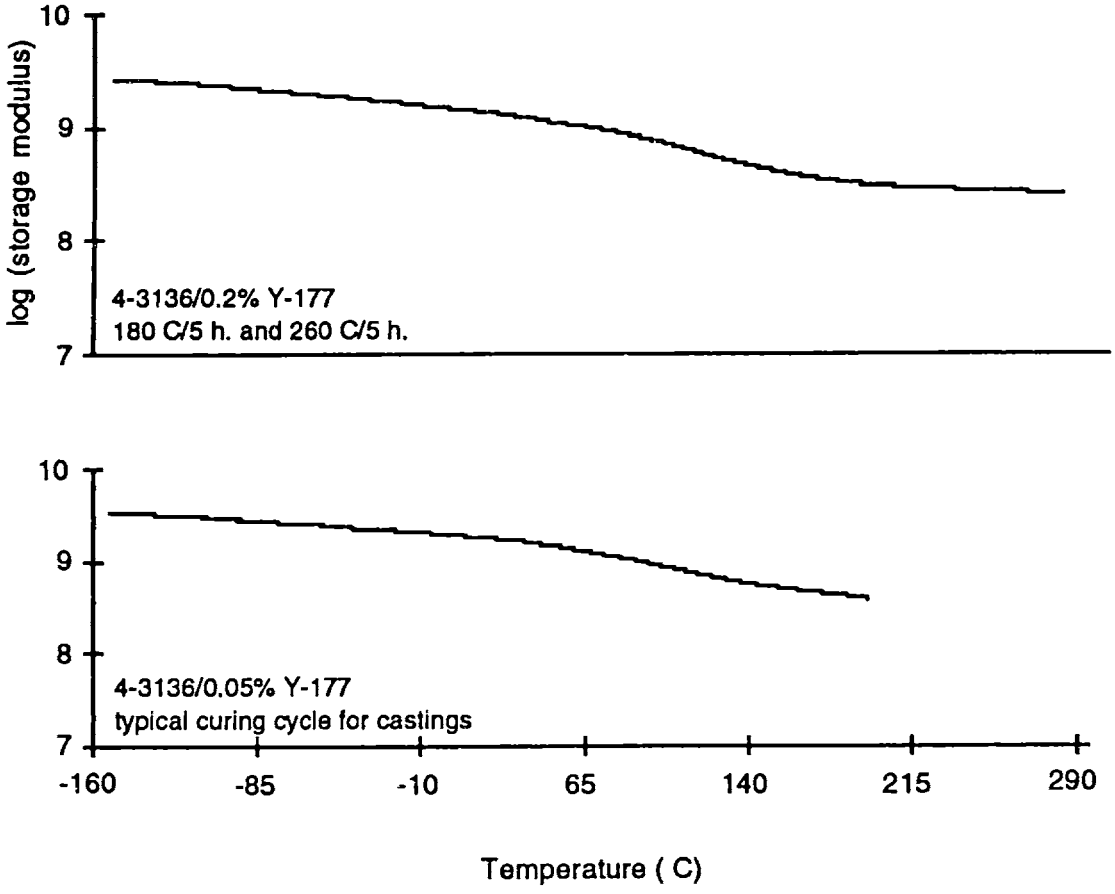

Figure 3.3. Storage modulus, as determined by DMA analysis, of 4-3136 resin castings cured through 1). upper curve, a conventional process, as recommended by the product information sheet supplied by the manufacturer, and 2). bottom curve, a curing process described in the text.

3.3. Mechanical and fracture toughness testing.

Sample Preparation. After curing, the cast plate 0.15" thick was cut and four 0.5"x2" specimens were obtained for the three point bending test and six 0.375"x2" specimens for the fracture toughness test. The three point bending test is very sensitive to surface imperfections so the specimens were polished before testing. The following polishing schedule was satisfactory: sand paper Grid # 320, 600(or 800), 1200, 2400, 4000, then alumina dispersion in water: 1, 0.3, and finally 0.05 μm. The polished specimens were dried at 70 °C overnight and conditioned at 20±2 °C for at least 24 hours before being tested.

Three point flexural test. This was discussed in Chapter 2.

Fracture toughness test. The plane strain fracture toughness, K_{Ic}, was obtained as specified in ASTM D 5045-91a, and the critical strain energy release rate, G_{Ic}, was calculated from K_{Ic} based on LEFM assumptions[1 to 4]. The sample geometry and dimensions are shown in Figure 3.4. The single edge notched geometry was chosen since less material was needed. A natural pre-crack was produced by cutting a 0.1" deep notch at the center and then tapping a razor blade into the notch. The displacement rate of the test was 10 mm/minute. For the geometry and loading conditions shown, with a support to width ratio of 4,

$$K_{Ic}=(P/BW^{1/2})f(x) \tag{3.2}$$

where P is the highest load and:

$$f(x)=6x^{1/2}[1.99-x(1-x)(2.15-3.93x+2.7x^2)]/[(1+2x)(1-x)^{3/2}] \tag{3.3}$$

where x is the pre-crack to specimen width ratio, a/W. After the test the pre-crack length was measured. Only those specimens with x between 0.45 to 0.55 were considered valid. The variation of x across the thickness should be less than 10%. The validity of the test was further ensured by comparing the sample dimensions with the estimated plastic zone size enlarged by approximately 25 times:

$$B, a, (W-a) > 2.5(K_{Ic}/\sigma_y)^2 \tag{3.4}$$

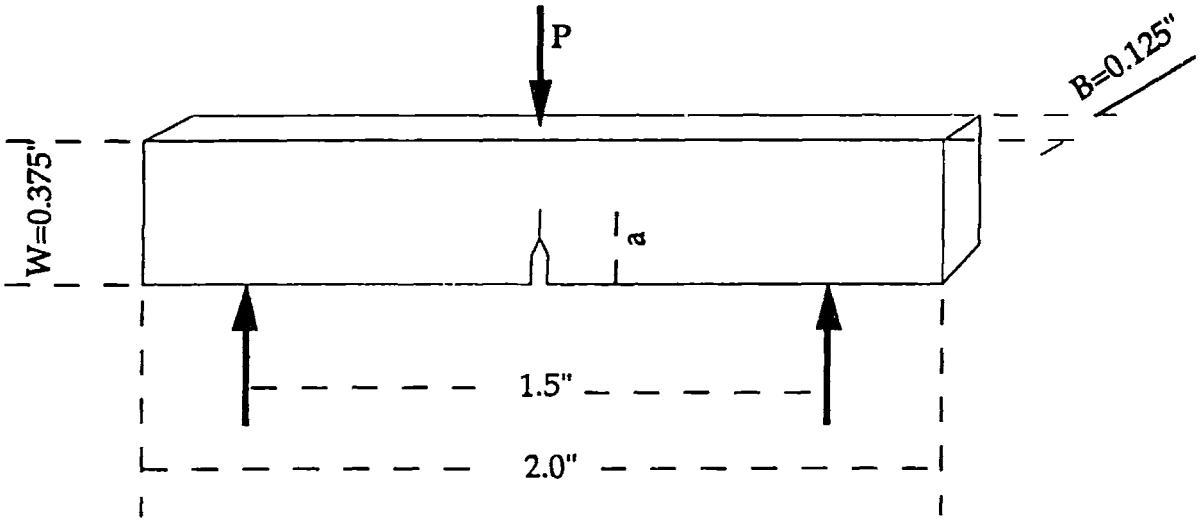

Figure 3.4. Fracture toughness test sample geometry, loading position (upper downward arrow) and support positions (lower upward arrows).

From the K_{Ic}, G_{Ic} was calculated by (3.5):

$$G_{Ic} = K_{Ic}^2(1-\upsilon^2)/E \tag{3.5}$$

where υ, the Poisson's ratio of the resin, was neglected to simplify the experiment. (For a glassy polymer with a Poisson's ratio of 0.4, G_{Ic} was exaggerated by about 16%. However, it was believed that the relative ranking of G_{Ic} values would not be obscured since the change of Poisson's ratio was small after modification.)

3.4. Phase I Toughening.

Table 3.1. Functionalized PDMS and their DP

PDMS	PAE2	PAE	KPE
DP	8	16	57

The functionalized PDMS short segments, listed in Table 3.1, were pre-reacted with the 4-3136 resin and cast plates were made. Specimens were cut from the plates and tested, according to the procedures described. The test results are plotted in Figures 3.5 to 3.10. Numerical values are included in Table A.1 in the Appendix.

The unmodified 4-3136 resin had a strain to break of 2.46%, a Young's modulus of 1.88 GPa, a flexural strength of 37.73 MPa, and a toughness, measured by the area under the stress-strain curve, of 5.9 KJ/m^3. These values were low compared to most untoughened epoxy resins. The K_{Ic} of the unmodified 4-3136 resin was 0.253 $MPam^{1/2}$, and G_{Ic} ~8 J/m^2. Both are about half of most untoughened epoxy resins.

All functionalized PDMS short chains toughened the 4-3136 resin. As seen in Figures 3.5 to 3.10, the incorporation of short PDMS segments increased the strain to break and the toughness. The flexural strength also increased slightly, contrary to experience with toughened epoxy resins. As expected the Young's modulus dropped slowly, however the drop was small. At the optimal composition, with 10 part KPE, the Young's modulus was decreased from 1.88 GPa to 1.37 GPa. The fracture toughness, K_{Ic}, and the critical strain energy release rate, G_{Ic}, increased.

Longer PDMS chains are more effective than shorter ones. With a DP of 8, (Fig. 3.5 to 3.8), 10 part PAE2 improved the mechanical and fracture properties: the strain from 2.46% to 4.20%; the flexural strength from 37.73 MPa to 42.62 MPa; the toughness, measured by the area under the stress-strain

curve, from 58.9 to 121.39 KJ/m^3; K_{Ic} from 0.253 MPa $m^{1/2}$ to 0.310 MPa$m^{1/2}$; and G_{Ic} from 38 J/m^2 to 80 J/m^2. The Young's modulus decreased from 1.88 GPa to 1.51 GPa. With a higher DP of 55, 10 parts of KPE increased the strain to 7.43%; the flexural strength to 48.49 MPa; the toughness, measured by the area under the stress-strain curve, to 261.24 KJ/m^3; the K_{Ic} to 0.453 MPa$m^{1/2}$; and the G_{Ic} to 267 J/m^2. The effect of the chain length is more clearly demonstrated by comparing the G_{Ic} values: 10 parts of KPE increased G_{Ic} by seven fold, while the same amount of PAE2 increased it by only two fold.

The same amount of PAE, with an intermediate DP of 16, improved the G_{Ic} by over three times. The other properties followed the same trend, seen in Figures 3.5 to 3.10: a longer PDMS chain caused an increasing slope of property change with the PDMS content. This behavior was attributable to the mobility of the PDMS chains which were linked to the resin network by their reacted ends. A long chain, such as the KPE with a DP of 55, is less restricted by the ends and freer to move when stressed, whereas the shorter ones are more constrained. The longer Phase I PDMS is also more effective in promoting damping of the high Tg domains of the resin. The combination of higher mobility of the PDMS chains and the more effective promotion of flow in the surrounding matrix make the longer Phase I PDMS better toughgeners.

In Figures 3.5 to 3.7, a maximum is seen at 10 parts of KPE. after which the strain, the strength, and the area under the stress-strain curves dropped, while the K_{Ic} and G_{Ic} continued to increase, but at a slower rate. It is suggested that this is caused by the higher residual stress built up in the higher content KPE formulations. The existence of residual stress was verified by the inspection of the cross section of resin casting under crossed polarizers, as well as by the behavior of castings when a pre-crack was made. In polarized light, birefringence was seen in the castings. It was absent in the unmodified resin and very slight in the shorter chain PDMS toughened resins. When a razor blade was tapped into the notch to make a pre-crack, with an increasing amount of KPE, the cracking of the casting changed from mode I to II and then to III as illustrated in Figure 3.11. In mode III, cracks were initiated at the surfaces and grew towards the center, consistent with a tensile residual stress at the surfaces.

The residual stress was probably related to the increased contraction as a result of cooling. In a DMA experiment, a 14 mm long specimen of any 4-3136 resins contracted when it was cooled to -160 °C from room temperature. A larger contraction was always observed with specimens of KPE toughened resins.

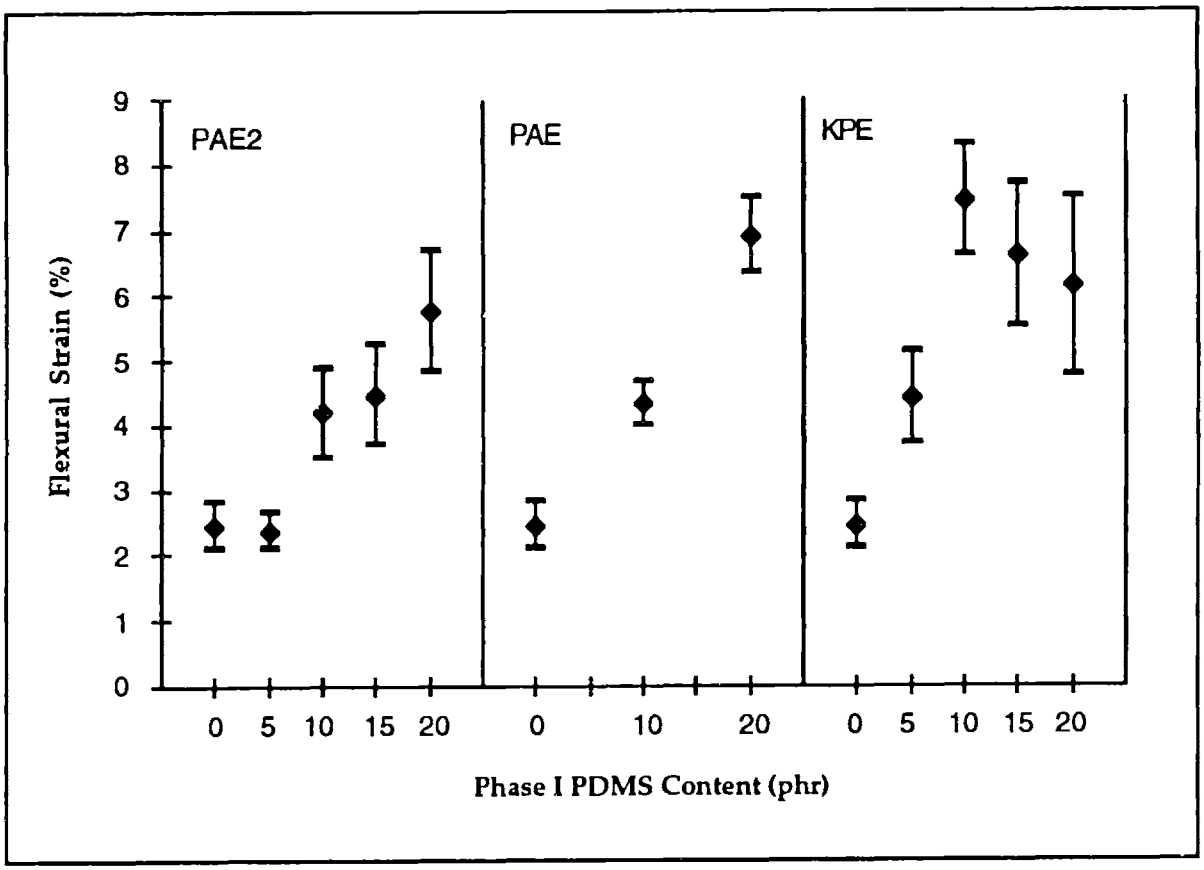

Figure 3.5. Flexural strain of 4-3136 resin modified by pre-reacting with functionalized Phase I PDMS of various chain lengths.

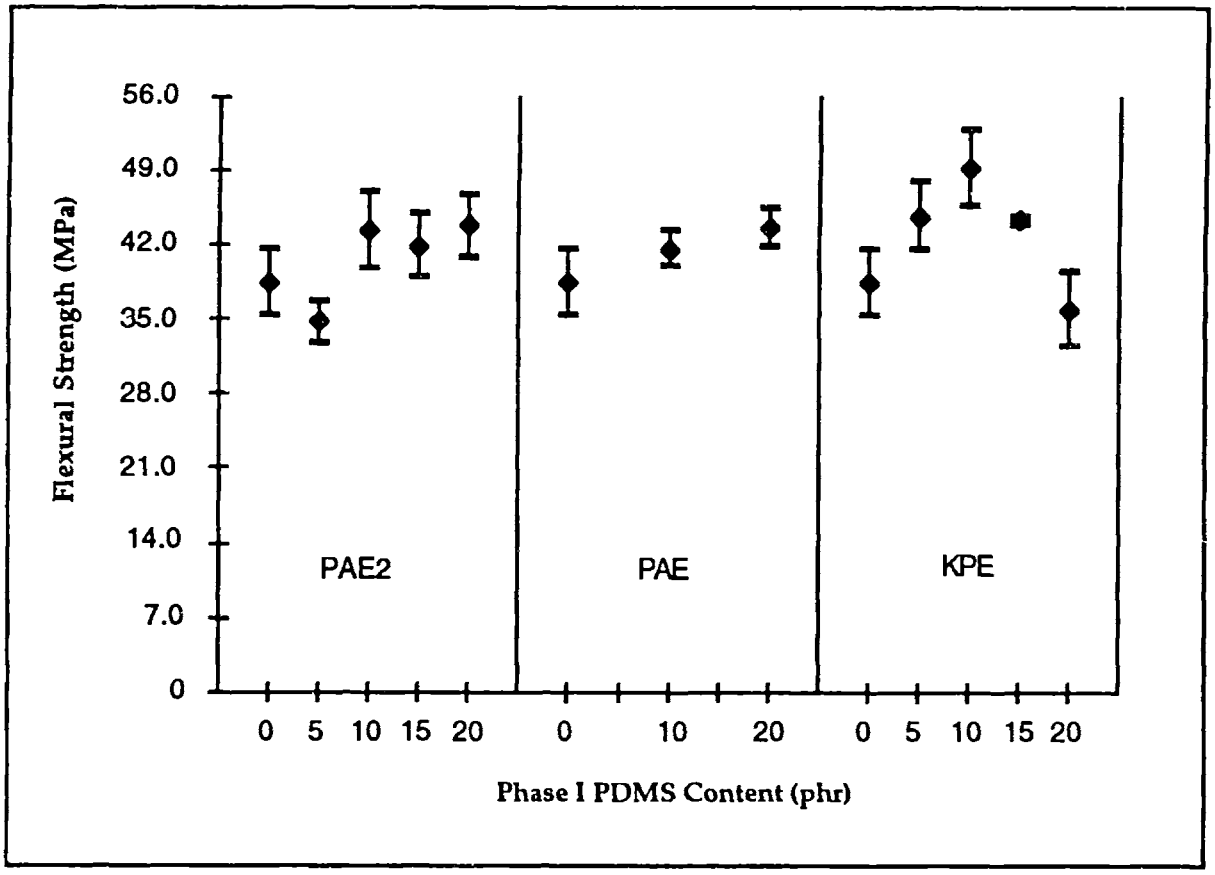

Figure 3.6. Flexural strength of 4-3136 resin modified by pre-reacting with functionalized Phase I PDMS of various chain lengths.

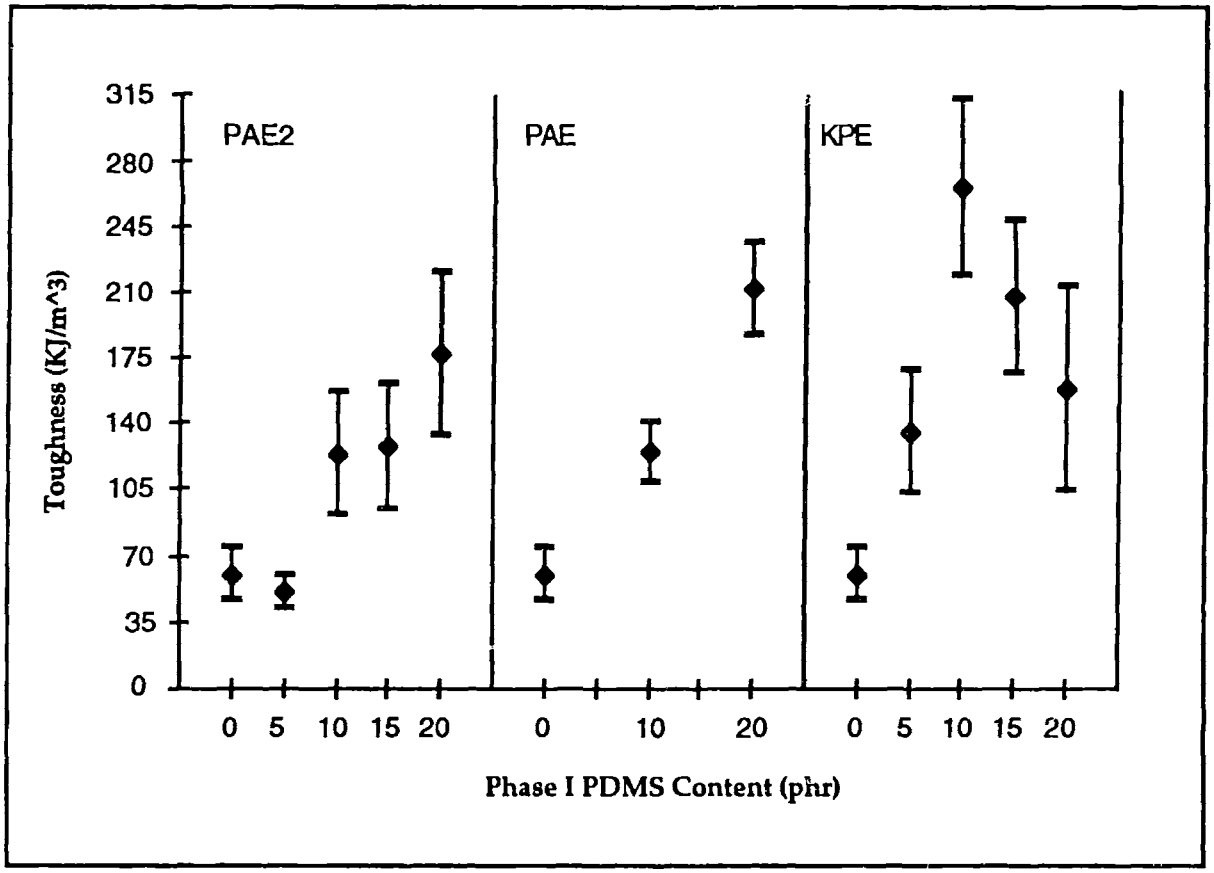

Figure 3.7. Toughness measured by the area under the stress-strain curve of 4-3136 resin modified by pre-reacting with functionalized Phase I PDMS of various chain lengths.

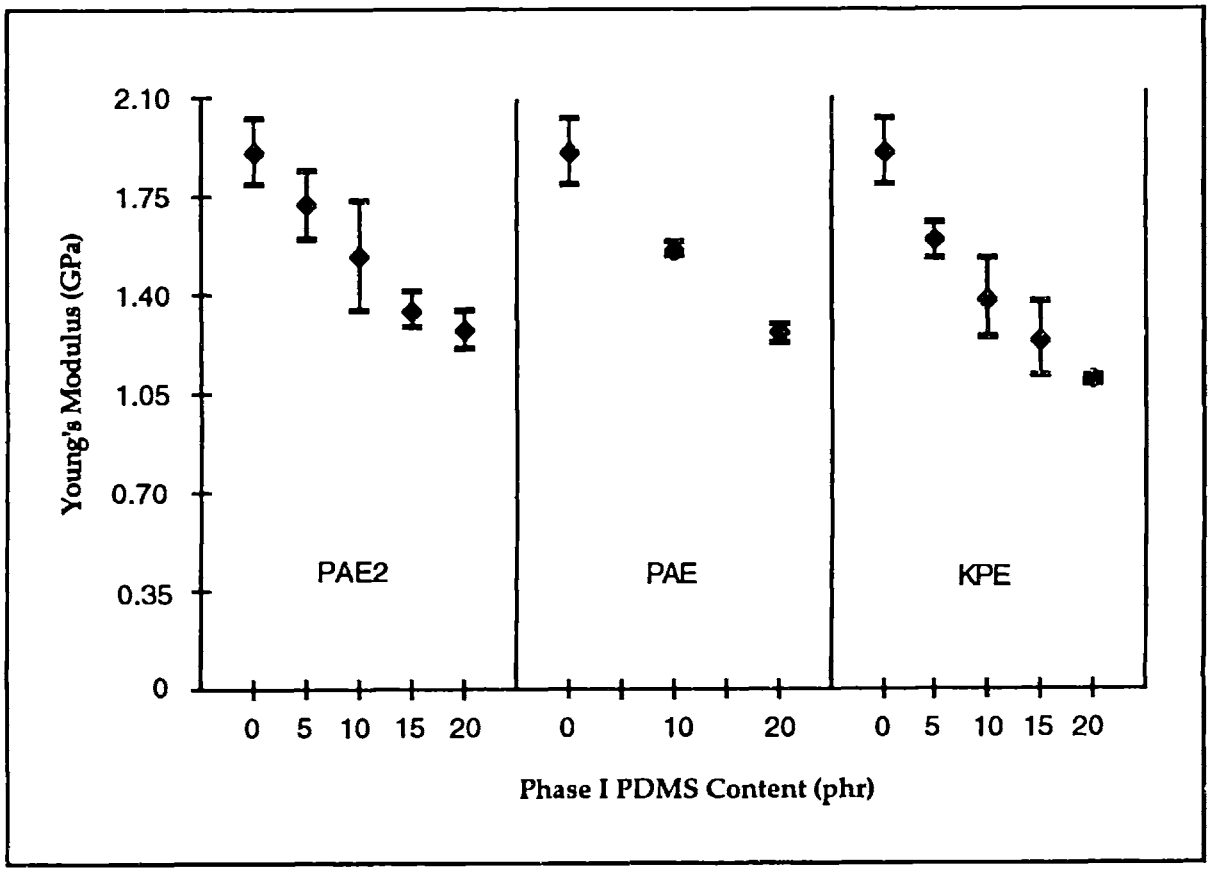

Figure 3.8. Young's modulus of 4-3136 resin modified by pre-reacting with functionalized Phase I PDMS of various chain lengths.

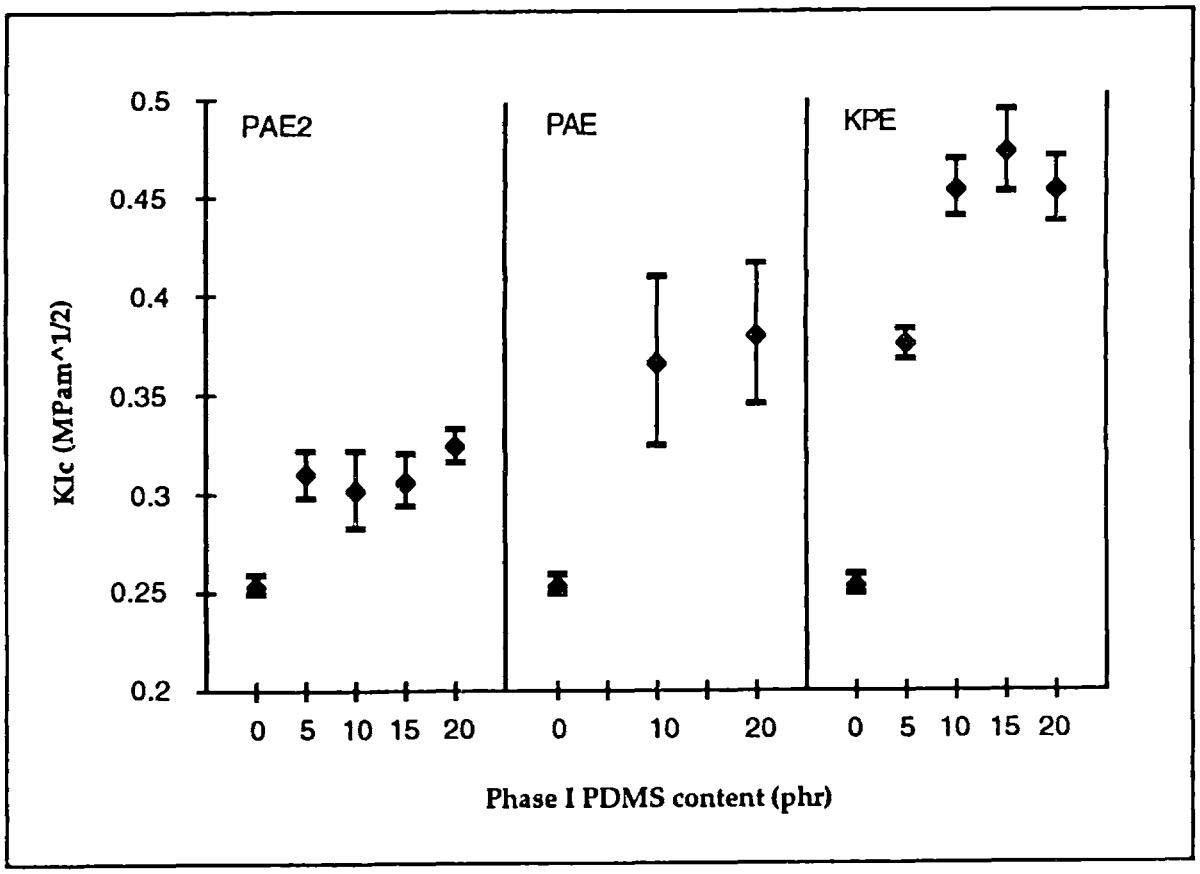

Figure 3.9. K_{Ic}, the fracture toughness, of 4-3136 resin modified by pre-reacting with functionalized Phase I PDMS of various chain lengths.

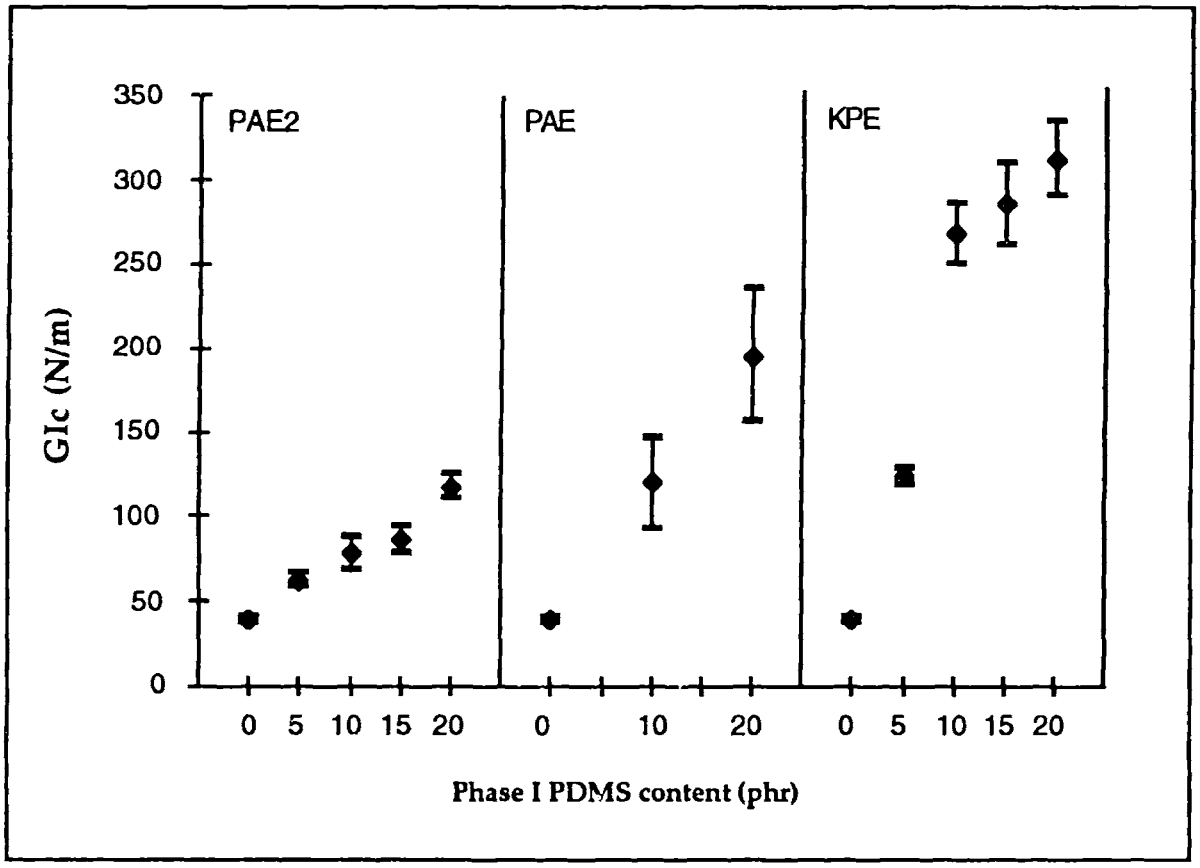

Figure 3.10. G_{Ic}, the critical strain energy release rate, of 4-3136 resin modified by pre-reacting with functionalized Phase I PDMS of various chain lengths.

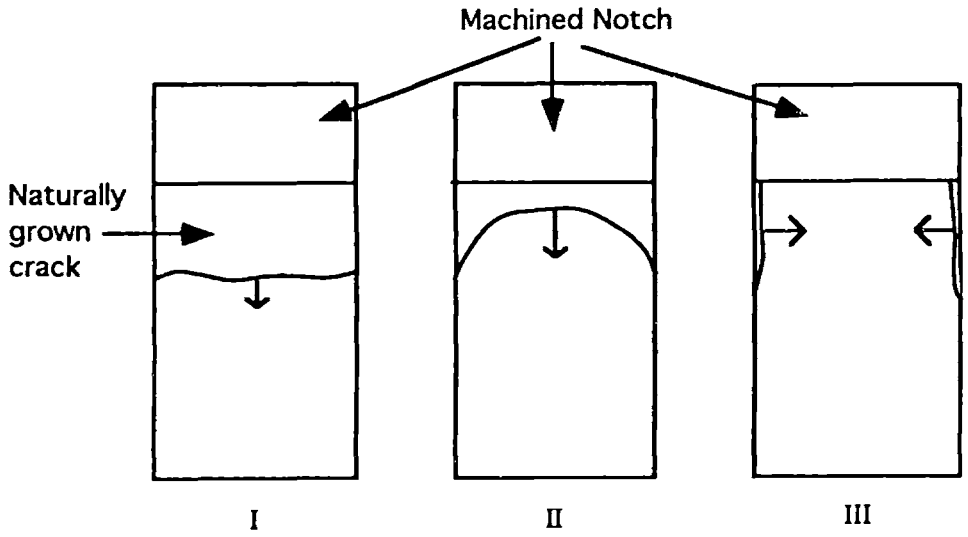

Figure 3.11. Three cases where crack is initiated by tapping a razor blade on the bottom of the machined notch and grows in the direction indicated by the arrow. In each case the cross-section of the rectangular specimen is displayed at the position of notch.

3.5. Phase I/II combination toughening.

3.5.1. Formation of Second Phase Particles (Phase II).

The compatibility of PDMS rubber with the matrix resin is determined by two factors: the chain length and the coupling reaction. A short chain PDMS, Phase I, was compatiblized by establishing chemical linkage at the ends of the chains. When the chain length became long, they tended to segregate from the resin even though an effective coupling was achieved. These became the Phase II rubbers,with a DP of 246, 375, and 586. They were used to form second phase rubber particles.

Figure 3.12 illustrates the process of forming second phase particles. The dots in the boxes represent the silicone resin pre-polymer, pure or mixed with a solvent, the lines the PDMS segments. In the left box short and long lines are coexistent, representing a mixture of the Phase I and II rubbers. If part of the short chains are replaced by longer ones there is an entropy of mixing loss, which favors phase separation. This can be compensated for by adding more solvent or by raising the temperature to perform a coupling reaction, or it can be utilized to form second phase particles after the coupling reaction.

Usually the Phase II PDMS was mixed with the Phase I in a resin solution at an appropriate concentration. A coupling reaction was carried out in the same way as for the Phase I. After the Phase I and Phase II PDMS were reacted with the resin pre-polymer, the solvent was removed and the temperature was lowered. The Phase II PDMS segregated with some Phase I and the rest of Phase I was distributed homogeneously to modify the resin matrix. The rubber particle size was controlled by the length of the Phase II PDMS, the chain length difference between the Phase I and the Phase II, the concentrations of both, and their ratio.

An example of second phase particles thus formed is shown in Figure 3.13, an SEM picture of the freshly fractured surface of a resin toughened by a combination of 10 parts of KPE and 2 parts of DP 586 Phase II PDMS. The coupling reaction of the resin and the Phase I and II rubbers was carried out in a 37 wt.% toluene solution. Phase separated domains of 3 to 20 microns were

formed. In the absence of the Phase II PDMS, 10 parts of KPE were homogeneously distributed in the resin network after the coupling reaction. The use of 2 parts of Phase II PDMS successfully induced phase separation and the formation of rubber particles.

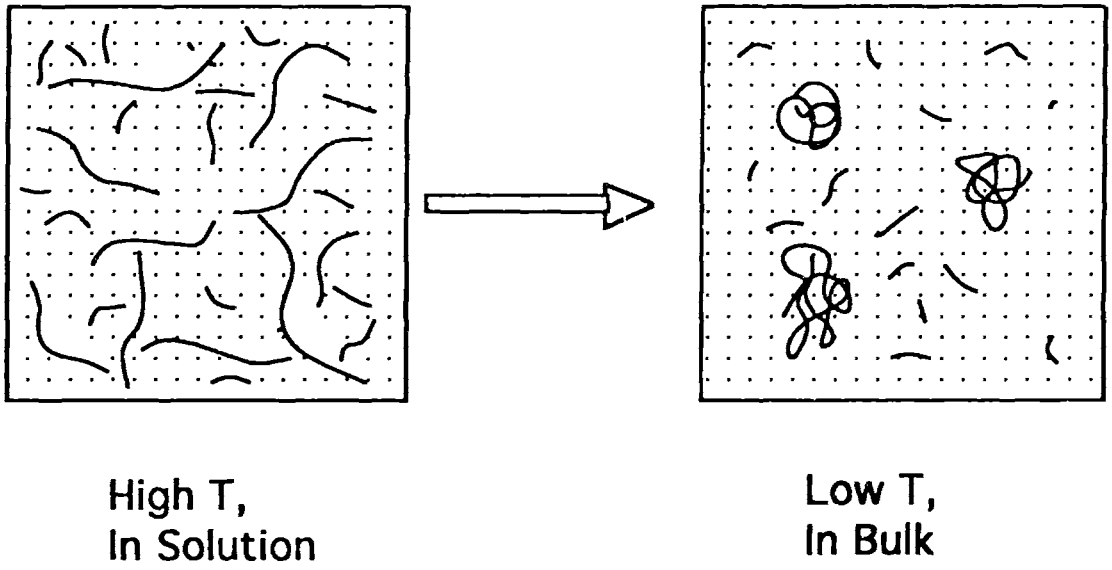

Figure 3.12. Schematic diagram showing the process of forming second phase domains.

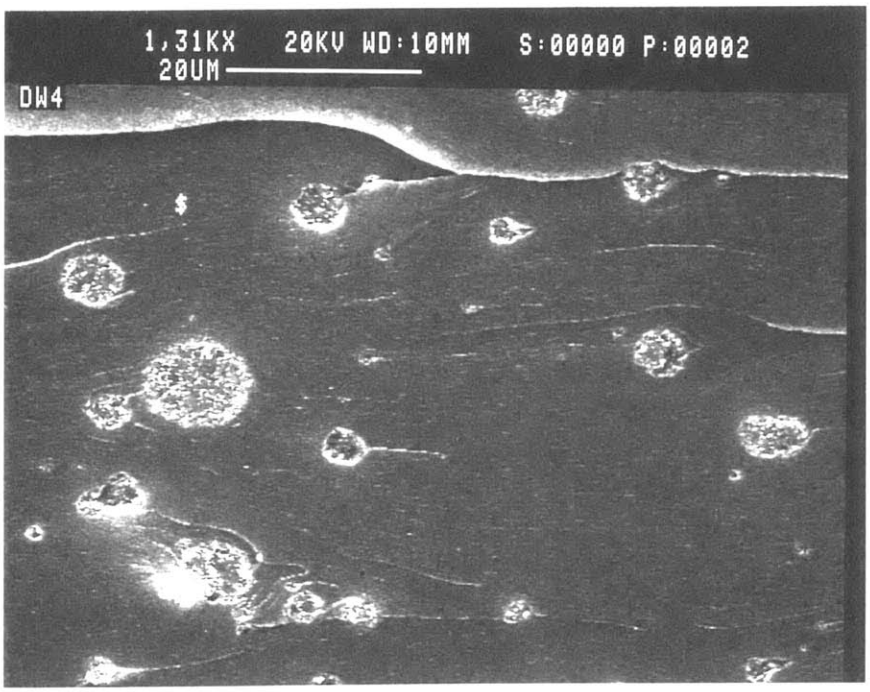

Figure 3.13. SEM picture of the freshly fractured surface of the 4-3136 resin toughened by a combination of 10 part KPE and 2 part DP 586 Phase II PDMS.

3.5.2. Submicron sized particle toughening.

Among the factors which affect the toughening by rubber particles, their size is critical. In this study it has been observed that particles larger than a few microns do not toughen the silicone resins, while the ones in the submiron range do. Some ideas to explain the influence of particle size were reviewed in Chapter 1. It is believed that for rubber particles to toughen a polymer matrix, the size of the stress field disturbance caused by the presence of these particles should be comparable to the scale of the matrix plastic deformation promoted by the particles[5]. The plastic deformation induced by a particle occurs in a yielding zone around the crack tip when the crack advances. According to Irwin, for plane strain condition, the radius of the plastic zone can be estimated by[6, 7]:

$$r_y = \frac{1}{6\pi}\left(\frac{K_{Ic}}{\sigma_{ys}}\right)^2 \tag{3.6}$$

where r_y is the radius of the plastic zone, and σ_{ys} the yield stress. Since a classical yielding has not been observed in the resin, the flexural stress at break is used to approximate σ_{ys}. The values calculated by this method are presented in Table 3.2. The size increases as Phase I rubber toughens the material. The results in Table 3.2 show the sizes of the plastic zone are small. This means the Phase II particles must be small to be effective.

Table 3.2. Calculated plastic zone size in the 4-3136 resin.

Toughener	K_{Ic} (MPam$^{1/2}$)	σ (MPa)	r_y (μm)
None	0.253	37.732	2.4
5 part PAE2	0.310	34.113	4.4
10 part PAE2	0.301	42.633	2.8
15 part PAE2	0.306	41.172	2.9
20 part PAE2	0.324	43.054	3.0
5 part PAE	0.285	48.251	1.9
10 part PAE	0.328	40.917	3.4
15 part PAE	0.333	44.115	3.0
20 part PAE	0.380	41.006	4.6
5 part KPE	0.375	43.964	3.9
10 part KPE	0.453	48.492	4.6
15 part KPE	0.473	43.516	6.3
20 part KPE	0.453	35.368	8.7

In untoughened and Phase I toughened 4-3136 resin, nodules of 60 to 100 nm in diameter have been observed. In a plastic zone a few microns in size, they appear to displace and move but do not distort. To cause distortion

within such nodules, the second phase particles must be very small in size. This will be discussed in the next Chapter.

The mechanical properties of 4-3136 resin toughened by the Phase I/II combinations are plotted in Figures 3.14 to 3.19. The properties of resins toughened by the Phase I alone are included in the same plots. The Phase I PDMS was PAE, and the Phase II was a triethoxylated PDMS of DP 375. In the Phase I/II combinations, the amount of PAE was fixed at 10 parts, and that of Phase II varied from 2.5 to 5 parts. These two rubbers were pre-reacted simultaneously with the resin pre-polymer in a 31 wt.% toluene solution with 0.2 part titanium tetrabutoxide. In Figure 3.14, the lower line represents the effect of Phase I alone on the fracture toughness, K_{Ic}, and the upper line the effect of the Phase I/II combination. The lower has a slope of 0.0065, and the upper a slope of ~0.05. The Phase I/II combination was approximately 8.5 times more effective than the Phase I alone. 10 parts of Phase I alone pre-reacted into the resin increased the fracture toughness from 0.25 $MPam^{1/2}$ to 0.33 $MPam^{1/2}$, and 15 parts increased it to 0.340 $MPam^{1/2}$. If 5 part Phase II was pre-reacted with 10 part Phase I into the resin, the fracture toughness was increased to 0.58 $MPam^{1/2}$. In Figure 3.14, the fracture toughness of a resin toughened by the Phase II alone is shown as an open circle. When the Phase II level was low it was slightly better than the untoughened resin, but with 10 parts of Phase II the resin was too weak to be tested, and no value is shown in the plot.

Figure 3.15 presents the G_{Ic} values for the same compositions. The lower line has a slope of 7.5, and the upper a slope of 47: the Phase I/II combination is 6.5 times more effective in increasing the critical strain energy release rate. Higher amounts of the Phase II alone severely decreased the G_{Ic}, and with more than 2.5 parts of Phase II alone the G_{Ic} values were too low to be measured.

The effects of the two phases on the flexural strain, Figure 3.16, is somewhat complicated. If both phases are present, the strain at break increases with total rubber content. If only the Phase I is present, the strain at break increases with rubber content. If only Phase II particles are present, the limited data shows pronounced embrittlement at 10 parts of rubber and some modest

improvement at 2.5 parts of rubber. Generally, the Phase I material seems to be dominant in producing a more ductile material.

In Figure 3.17, flexural strength data are presented. Both Phase I and Phase I/II combination increase the strength measurably though not monotonically; Phase II alone reduces it quite drastically. Less analogous is the effect of the added rubber on the modulus, Figure 3.18. Here the down trend with increasing rubber content is clear and consistent and again, the 10 part Phase II only material is particularly unattractive. Much the same can be said for the work to fracture data shown in Figure 3.19: it incerases quite consistently with total rubber content but the 10 part Phase II alone material is far below the trend line. It is tempting to speculate on the reason for the effect of 10 parts of Phase II particles alone but until more data are obtained, and the (complicated) system is better understood, such speculation could be misleading.

The particles in the Phase I/II combinations were from 60 to 70 nm in diameter, as shown in Figure 3.20. This size was comparable to that of the resin nodules. Additional evidence obtained from etching study is attached in the appendices.

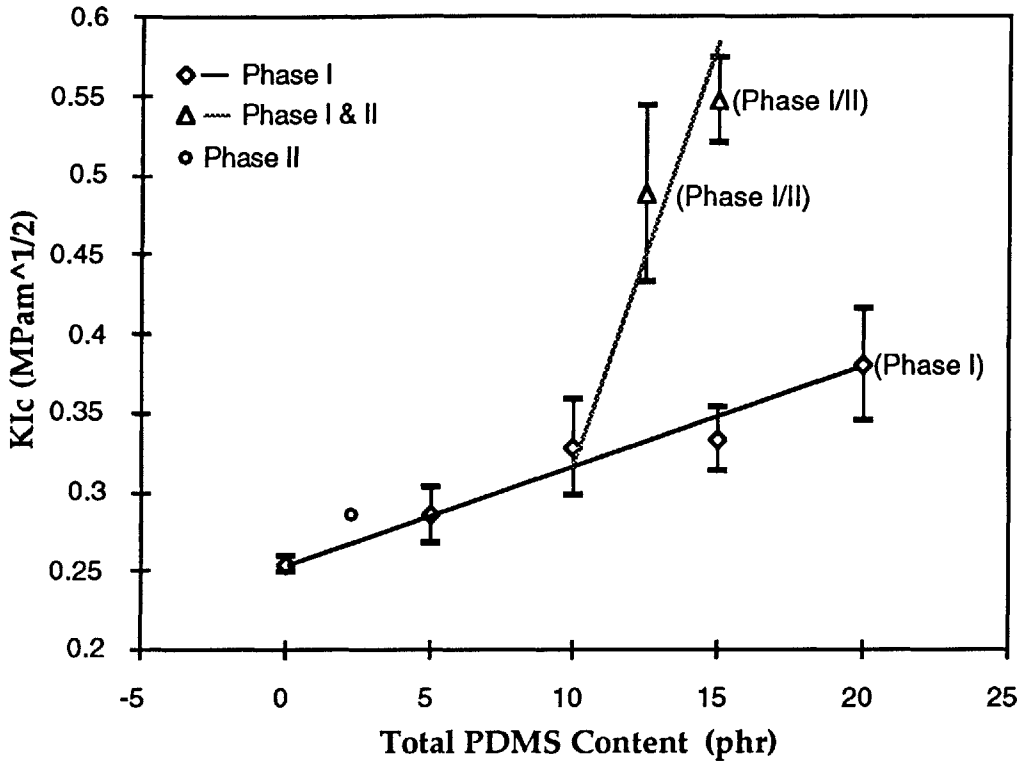

Figure 3.14. Plane strain fracture toughness, K_{Ic}, of the silicone resins toughened by the Phase I PDMS, PAE, alone; by the Phase II PDMS alone; and by the combinations of 10 part Phase I with various amounts of Phase II. The PDMS content shown in the plot was the total amount of PDMS including the Phase I and Phase II. Phase I: DP 16; Phase II: DP 375.

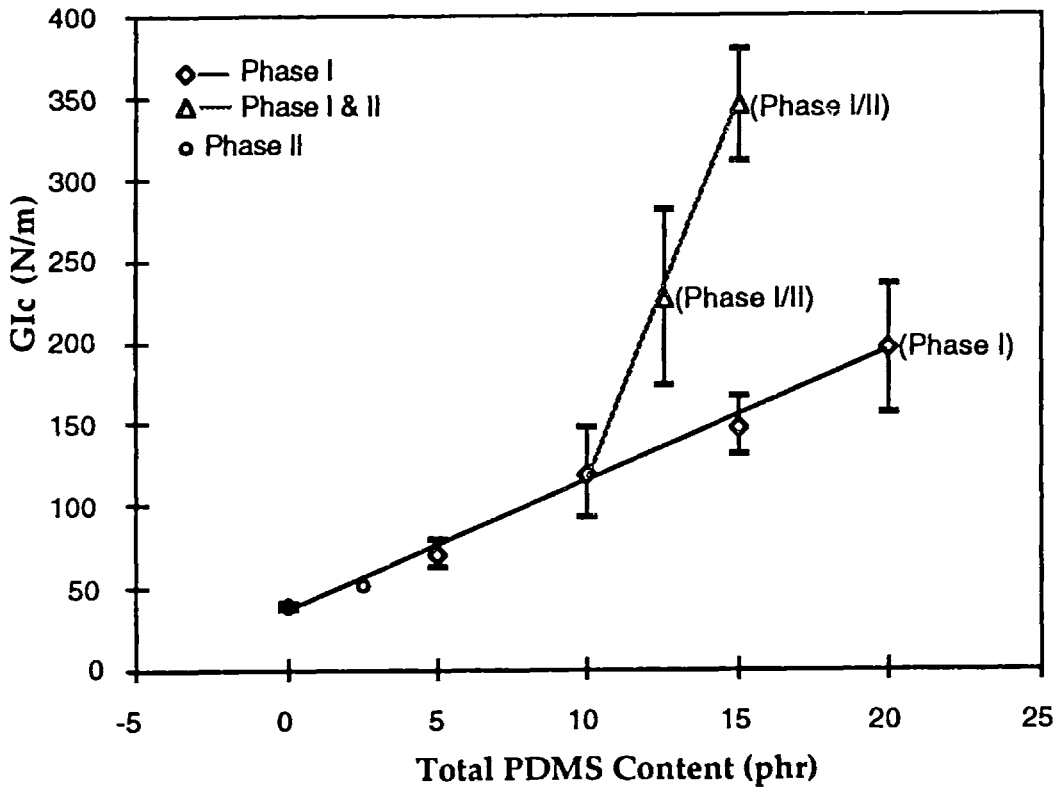

Figure 3.15. Critical strain energy release rate, G_{Ic}, of the silicone resins toughened by the Phase I PDMS, PAE, alone; by the Phase II PDMS alone; and by the combinations of 10 part Phase I with various amounts of Phase II. The PDMS content shown in the plot was the total amount of PDMS including the Phase I and Phase II. Phase I: DP 16; Phase II: DP 375.

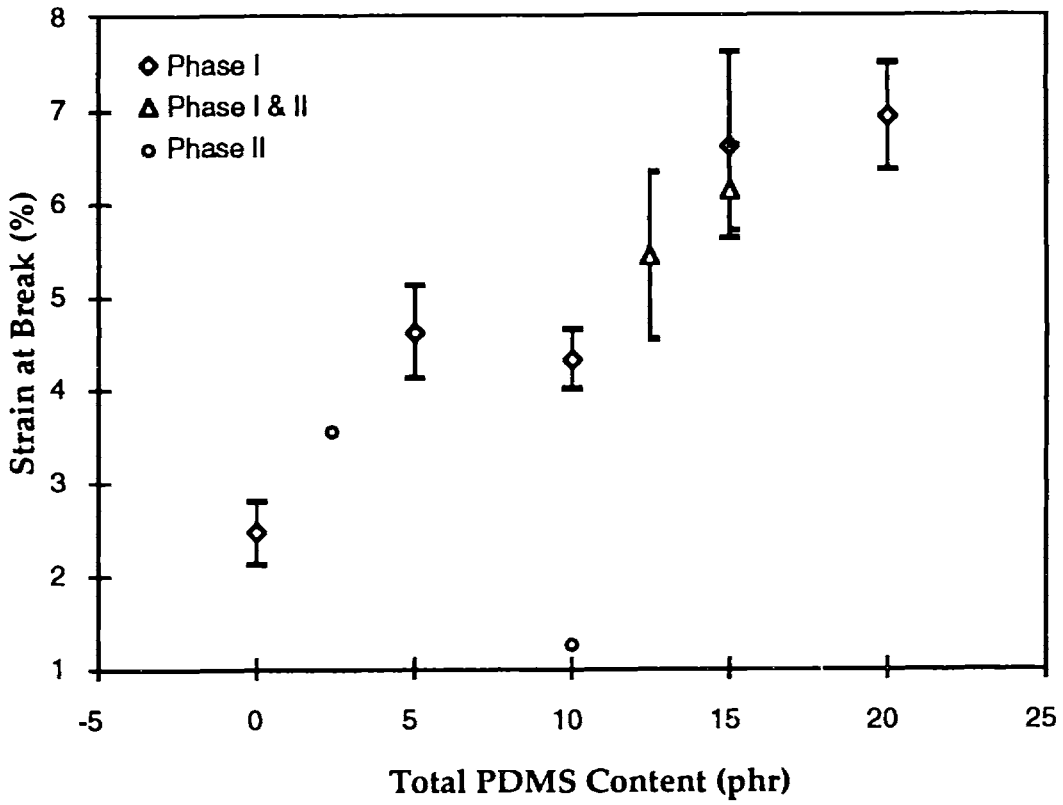

Figure 3.16. Strain at break of the silicone resins toughened by the Phase I PDMS, PAE, alone; by the Phase II PDMS alone; and by the combinations of 10 part Phase I with various amounts of Phase II. Triethoxylated PDMS of DP 375 was used as the Phase II, and was pre-reacted into the resin simultaneously with 10 part PAE. The PDMS content shown in the plot was the total amount of PDMS including the Phase I and Phase II.

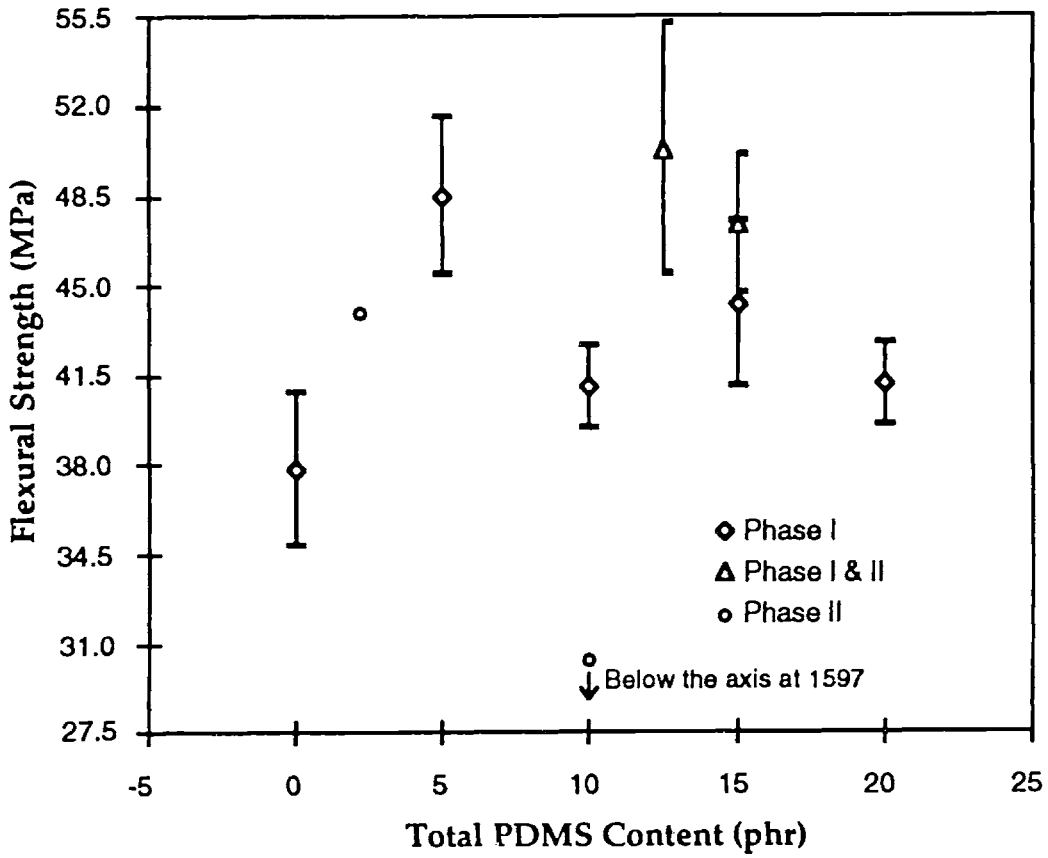

Figure 3.17. Flexural strength of the silicone resins toughened by the Phase I PDMS, PAE, alone; by the Phase II PDMS alone; and by the combinations of 10 part Phase I with various amounts of Phase II. Triethoxylated PDMS of DP 375 was used as the Phase II, and was pre-reacted into the resin simultaneously with 10 part PAE. The PDMS content shown in the plot was the total amount of PDMS including the Phase I and Phase II.

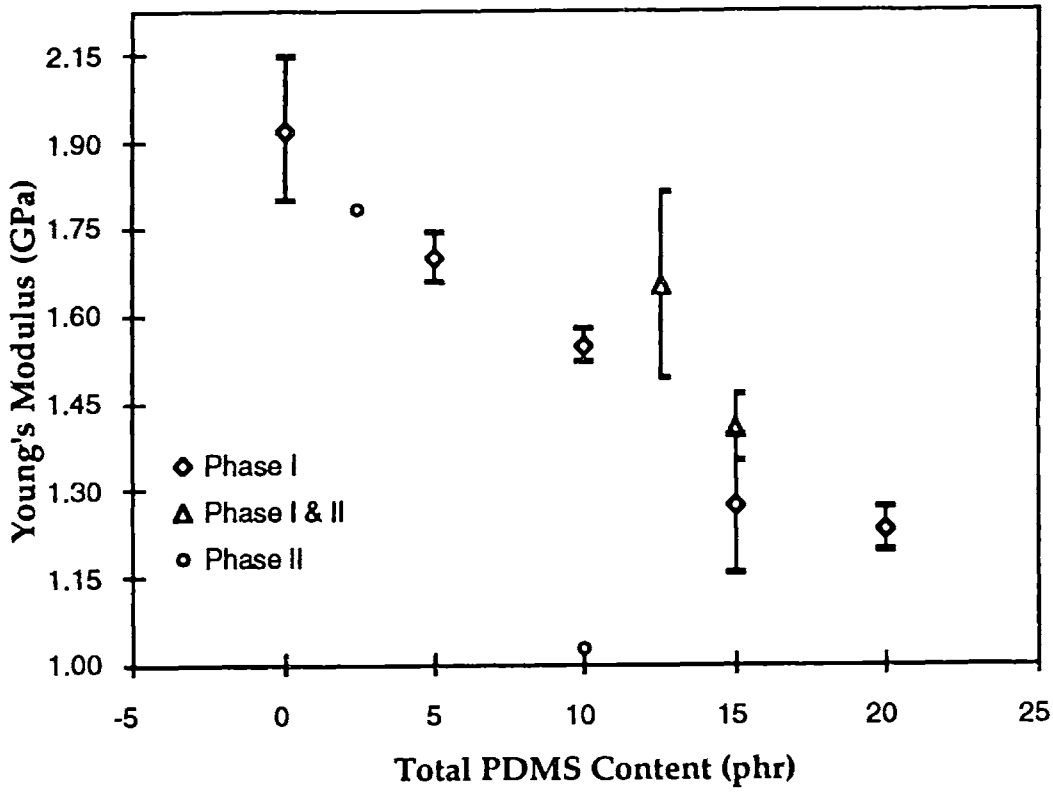

Figure 3.18. Young's modulus of the silicone resins toughened by the Phase I PDMS, PAE, alone; by the Phase II PDMS alone; and by the combinations of 10 part Phase I with various amounts of Phase II. Triethoxylated PDMS of DP 375 was used as the Phase II, and was pre-reacted into the resin simultaneously with 10 part PAE. The PDMS content shown in the plot was the total amount of PDMS including the Phase I and Phase II.

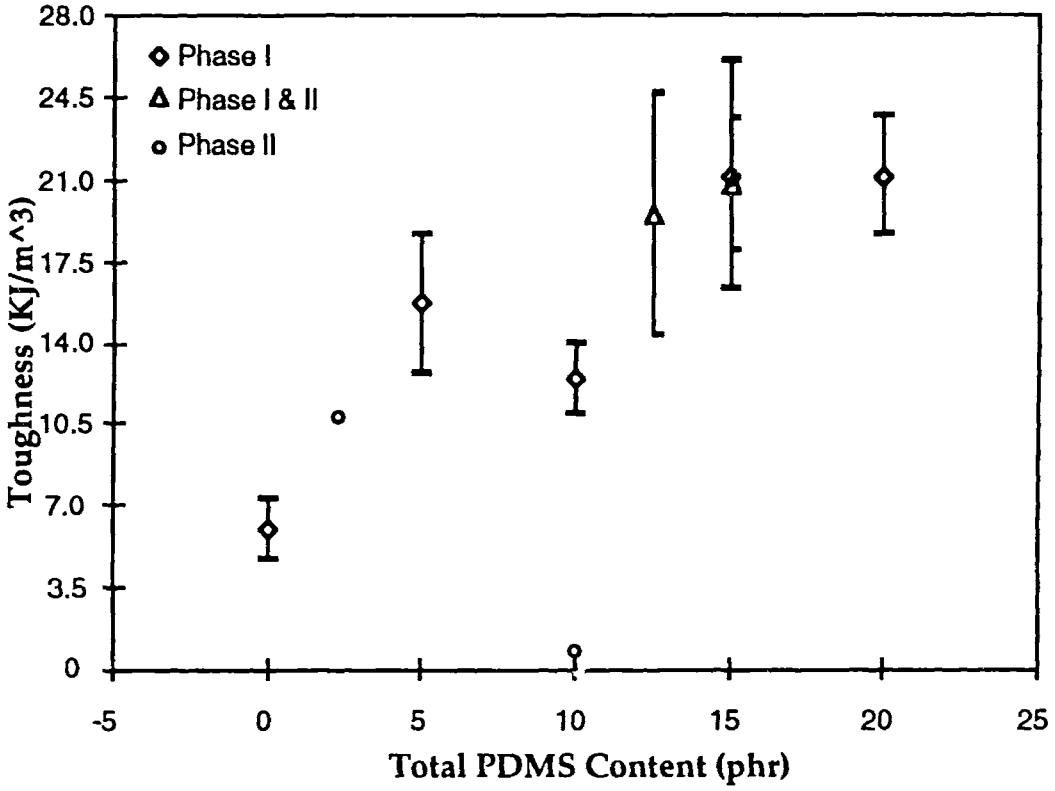

Figure 3.19. Toughness, measured by the area under the stress-strain curve, of the silicone resins toughened by the Phase I PDMS, PAE, alone; by the Phase II PDMS alone; and by the combinations of 10 part Phase I with various amounts of Phase II. Triethoxylated PDMS of DP 375 was used as the Phase II, and was pre-reacted into the resin simultaneously with 10 part PAE. The PDMS content shown in the plot was the total amount of PDMS including the Phase I and Phase II.

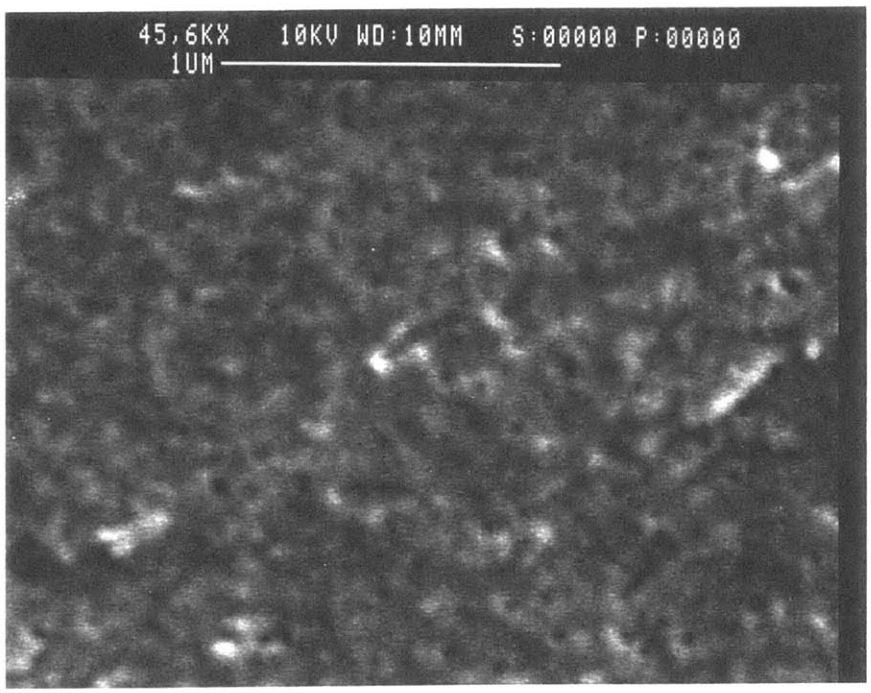

a

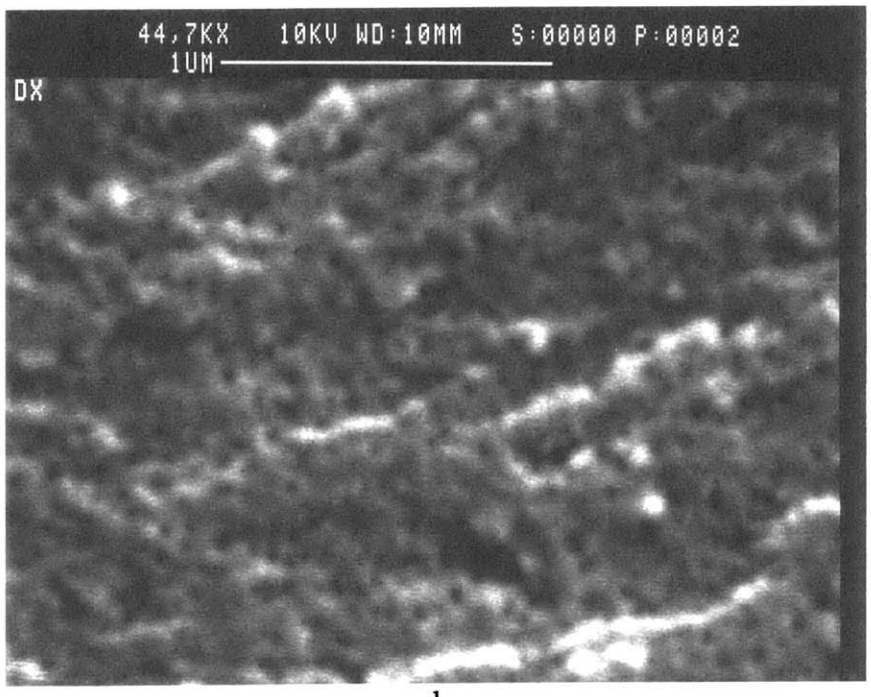

b

Figure 3.20. SEM photos of the freshly fractured surfaces of the Phase I/II combination toughened resins. The Phase I was 10 part PAE, and the Phase II was (a) 2.5, and (b) 5 part triethoxylated PDMS of DP 375.

3.5.3. Large particle toughening.

If the particle size is increased substantially by increasing the pre-reaction concentration, the length of the Phase II rubber segments, or the Phase II PDMS content, the toughening effect is reduced. This is shown by the results summarized in Tables 3.3 and 3.4. In Table 3.3, the compositions, pre-reaction conditions, and estimated particle sizes of a series of samples are listed. The corresponding fracture toughness values are included in Table 3.4. In Table 3.4 the values in parenthesis are standard deviations.

Table 3.3. Sample Compositions and Pre-reaction Concentration.

Sample	4-3136°	PAE°	PDMS of DP 375°	PDMS of DP 586°	Pre-reaction Concentration*	Particle Size, μm
A	100	10	7.5	---	31.0%	∞†
B	100	10	7.5	---	28.6%	1-3
C	100	10	10.0	---	28.6%	1-3
D	100	10	---	2.5	31.0%	∞
E	100	10	---	5.0	31.0%	∞
F	100	10	---	2.5	26.6%	12-37
G	100	10	---	5.0	26.6%	20-50

°Parts per hundred parts of resin.
*Reaction conditions: 0.2% Titanium tetrabutoxide, in a toluene solution of the specified total solid content, 95 °C for 28 hours.
†Large scale separated layers.

Table 3.4. Properties of Phase I/II Toughened Silicone Resins with Large separate domains.

	A	B	C	D	E	F	G
K_{Ic}, $MPam^{1/2}$	0.305	0.439	0.531	0.280	0.286	0.427	0.401
	(0.014)	(0.019)	(0.046)	(0.025)	(0.028)	(0.024)	(0.021)
G_{Ic}, J/m^2	88.60	240.90	391.61	79.19	116.85	186.05	184.83
	(13.35)	(31.50)	(50.24)	(11.87)	(13.85)	(27.54)	(28.80)

Higher amounts of the Phase II PDMS of DP 375 were pre-reacted with the 4-3136 resin simultaneously with 10 parts of PAE. In Table 3.3, sample A contained 7.5 part Phase II. The pre-reaction for A was done in a 31 wt.% solution, as for the previously discussed ones containing 2.5 and 5 parts of Phase II. When cast, the resin separated into two layers. The upper layer was rubbery and the lower layer was brittle. The fracture toughness values of A are included in Table 3.4. They are lower than the resin toughened by the Phase I alone.

To better compatiblize the Phase II and the resin, the pre-reaction concentration was lowered to 28.6%. Samples B and C, in Table 3.3, contained 7.5 and 10 parts of Phase II, in addition to 10 parts of Phase I. They were pre-reacted with the resin pre-polymer in a 28.6 wt.% toluene solution. When cast, no separation of layers was seen, and particles from 1 to 3 microns in diameter were obtained. The fracture toughness of B was higher than A, but lower than when 60 - 70 nm particles were produced by 5 parts of Phase II. At this particle size, it took 10 parts of Phase II to produce a toughening result close to that from 5 parts of Phase II present as 60-70 nm particles.

In addition to the PDMS of DP 375, the one with a DP 586 was also used as the Phase II. Again, the pre-reaction of the resin with 10 parts of Phase I and various levels of Phase II was first done in a 31 wt.% toluene solution. When cast, a separate rubbery layer formed on top of the casting. The obtained castings with 2.5 and 5 parts of the Phase II were D and E in Table 3.3. In Table 3.4, the fracture toughness values are listed. They were slightly higher than the unmodified resin but lower than the resin modified by the Phase I alone. The pre-reaction of these two compositions was then carried out in a lower concentration solution of 26.6 wt.%. Separate domains of 12 to 50 microns in size were formed in the castings. The fracture toughness values of F and G, containing 2.5 and 5 parts of the Phase II, were improved but they were lower than when the particles were 1-3 microns or 60-70 nm in diameter.

3.6. Conclusions.

Methods have been developed to prepare sound cast plates of condensation cure rigid silicone resins. They included the addition of a small amount of inert solvents, the use of highly dispersed fillers, and slow long curing cycles. This has enabled the investigation of the mechanical properties and fracture behavior of the resins.

When properly reacted into the resin network, PDMS short segments always toughen 4-3136 resin. The longer the Phase I PDMS chains, the more effective they are as long as they can be properly incorporated into the resin network. When toughened by the Phase I PDMS, the resins have slightly higher flexural strength, higher strain, K_{Ic}, and G_{Ic}. The elastic modulus slowly goes down but the decrease is small. With the optimal chain length and Phase I content, K_{Ic} can be increased by 180%, and G_{Ic} by 600%, with a 25% reduction of modulus.

Proper combinations of the Phase I and the Phase II toughen rigid silicone resins much more effectively than the Phase I alone; the the Phase II alone does not toughen the resins. The effectiveness of the Phase I/II combinations is determined by the particle size. Submicron sized particles are more effective than particles of a few microns in diameter. The particle size can be controlled by changing the pre-reaction concentration, the amount of Phase II, the Phase II chain length, and the chain length ratio of Phase I/II. With appropriate Phase I/II combinations, the K_{Ic} is increased by up to 220% and the G_{Ic} by up to 900%, with less loss of elastic modulus as compared to toughening by the Phase I alone.

Chapter 4. Toughening Mechanisms: Fractography.

4.1. Introduction.

The fracture surface morphology of the 4-3136 resins depends on the position and the shape of the initial pre-crack, the loading rate, and the resin composition. An analysis of these features reveals the toughening mechanisms.

In this chapter the fracture surface features of the modified and unmodified 4-3136 resin, produced by a SEN three point bending fracture toughness test, will be presented. The formation of these features will be discussed, leading to the understanding of the toughening phenomenon.

It should be emphasized that only the fracture surfaces produced by performing a fracture toughness test, in the mode specified above, will be discussed. The fracture surfaces obtained from a three point flexural test are very complex, and the formation of them often involves the shattering of a certain volume of material at the center of specimens. They will not be discussed here.

4.2. Fractographic features of brittle solids.

The morphology of the fractured surface gives valuable insights to the fracture mechanisms. Although it is not always easy to associate a specific type of surface feature with a specific fracture mode, a number of surface features commonly appearing in the fracture of a brittle solid have been recorded and explained by accepted mechanisms. These features include striations, steps, welds, river markings, basic longitudinal textures, and so on. There is confusion in the field because the same type of feature may be called a different name and different authors may use the same name for different

features. In this study those terms deemed most descriptive and relevant to the fracture surface features of rigid silicone resins will be used.

Preston[1] showed that in a brittle solid a crack endeavors to be perpendicular to the direction of the principle tension. This simple rule has been observed in a great variety of essentially brittle materials and become widely accepted. The change of fracture path is a result of the rotation of the principle tension direction. The direction of the principle tension can rotate in two ways: around an axis parallel to the crack advancing direction in the crack plane; or around an axis perpendicular to the crack advancing direction in the crack plane. The former is called a tilt and the latter a twist. They are shown schematically in Figure 4.1.

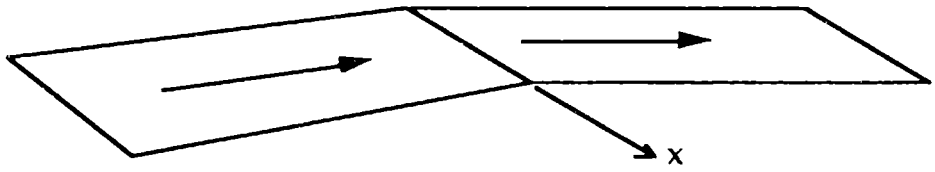

Tilt

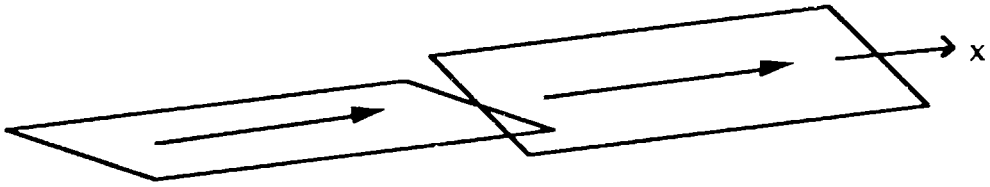

Twist

Figure 4.1. Schematic diagram showing the change of crack propagating direction as a result of the rotation of the principle tension direction around axis x.

When a crack plane is twisted, the plane is not able to adjust to the normal direction of the tension as a whole and is subdivided into many narrower planes perpendicular to the tension[2, to 5], as drawn schematically in Figure 4.2b. Serrated striations with steps are formed as the crack travels

through. When a plane is tilted differently at different locations, the plane is also divided into many narrower planes and each sub plane travels into a different elevation (Figure 4.2c).

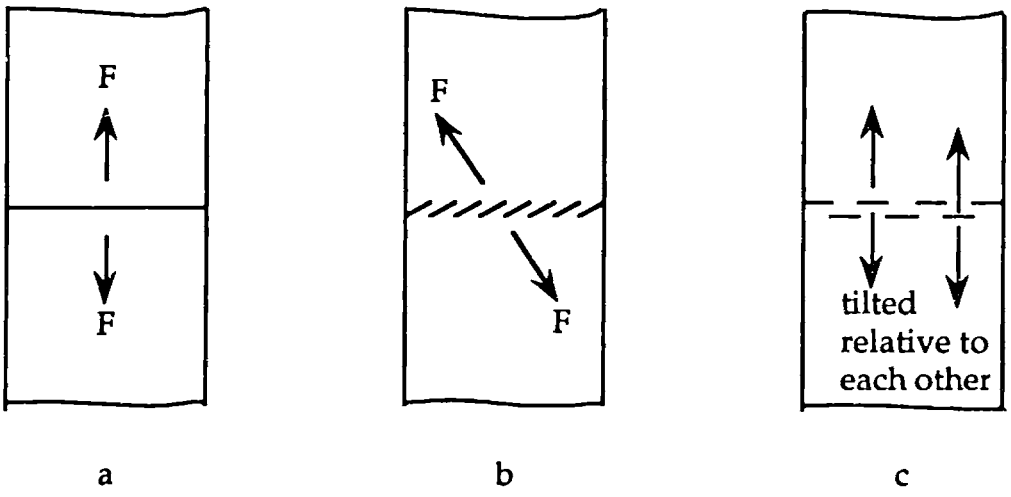

Figure 4.2. Schematic diagram showing the development of a single crack plane (a), into multiple planes as a result of the twisting of the principle tension (b); into multiple planes because of different tilting of the tension (c).

The fracture surface of brittle thermosetts bears many similarities to that of a brittle glass. The above discussed striations and steps are examples. Another example is the fibrils, or welds, separated from or semi-attached to the steps. As shown by Figure 4.3, these are formed when two crack sub planes at different elevations meet. Both find their way to the crack surfaces as the tension is twisted locally in the ligament between these two crack sub planes. The sub planes meeting otherwise, shown in Figure 4.4, may form a wedge.

At higher magnifications, a longitudinal texture is seen in each sub crack plane. This basic texture is sometimes called river markings but the term is also used for the much larger striation features. To avoid confusion, the simple term "basic longitudinal texture"[6] is preferred. The direction of this texture is a record of the crack traveling direction.

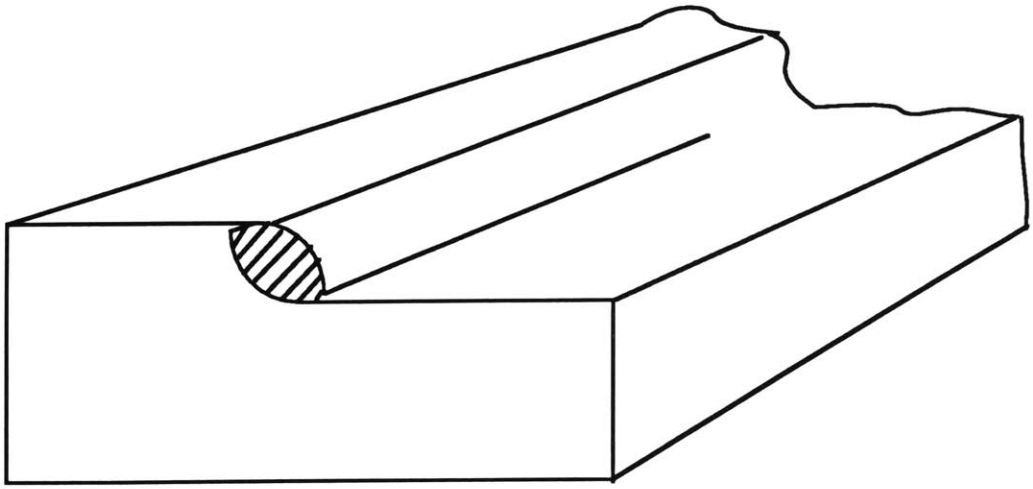

Figure 4.3. Schematic diagram showing two crack planes at different elevations meet and form a weld.

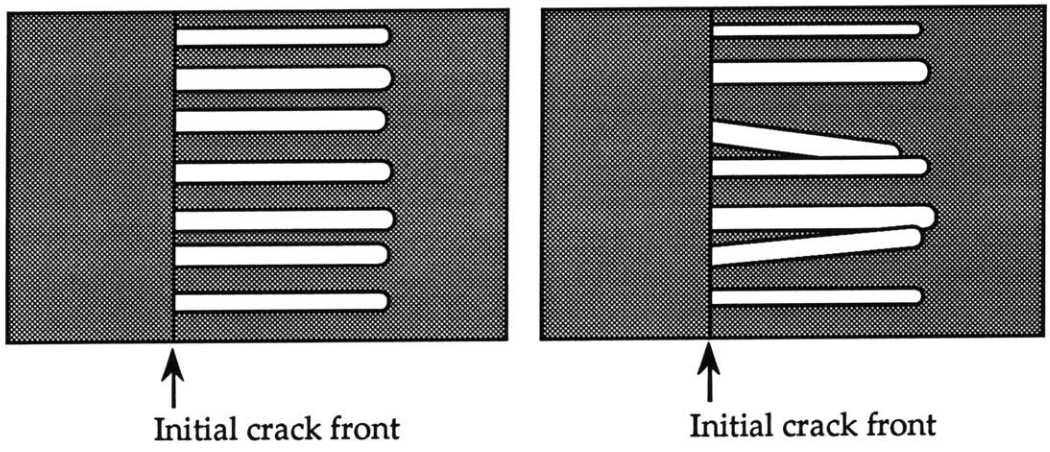

Figure 4.4. Crack fingering and formation of wedges due to the merge of fingers.

The texture has also been observed on the fracture surface of epoxy resins and explained by some authors in terms of a meniscus instability mechanism[7, 8]. The meniscus instability phenomenon was first mathematically predicted by Geoferey Taylor[9] for two fluids with very low

viscosity and different densities. It was later demonstrated by D.J. Lewis[10]. When two fluids are accelerated along the direction perpendicular to the interface and towards the higher density fluid, disturbances of certain wave lengths at the interface grow in amplitude and finger into the higher density fluid. It has been demonstrated that this is a general phenomenon for a meniscus interface between a low density and a high density fluid, whether they are accelerated or flowing in a steady state. An idealized model, a two dimensional laminar flow between two parallel plates, helps understand the physics of this phenomenon. This is schematically shown in Figure 4.5. The curvature of the meniscus creates a negative pressure in the denser fluid which forces the meniscus interface to move with the fluids. A negative pressure gradient exists in the flow direction, x, but the pressure gradient in Z direction is zero. The wave disturbance causes a drop in pressure in the higher density fluid at the interface where there is a valley of the disturbance wave, due to the new curvature which helps balance the external pressure, shown by Figure 4.6. If this pressure drop is smaller than the flow field pressure drop across a distance equal the amplitude of the wave, a pressure gradient in Z direction is created. Therefore P' is greater than P", which drives flow from the position of the wave valley to that of the wave peak. The meniscus thus becomes unstable and fingers into solids or liquids[11 to 14].

This mechanism of crack growth was directly observed[15] in some thermoplastics, where a craze traveled by voids fingering into the glassy polymer. However it remained doubtful for highly crosslinked thermosetts. In highly crosslinked thermosetts flow of material is severely restricted by covalent bonding. In fairly ductile thermosetts, it is possible to explain the fracture surface feature by this mechanism[16], but only under idealized conditions will a crack tip resemble a meniscus in shape.

The basic longitudinal texture on the fracture surfaces of epoxy resins was also explained by a nodular structure of the resin[17]. It will be shown in the next section that rigid silicone resins also have a nodular structure. When untoughened or toughened with very short Phase I rubber segments, the basic longitudinal texture is associated with the nodular structure; and when toughened by longer Phase I rubber and the effective Phase I/II combinations,

the basic longitudinal texture is not controlled by the nodular structure but by a meniscus instability mechanism.

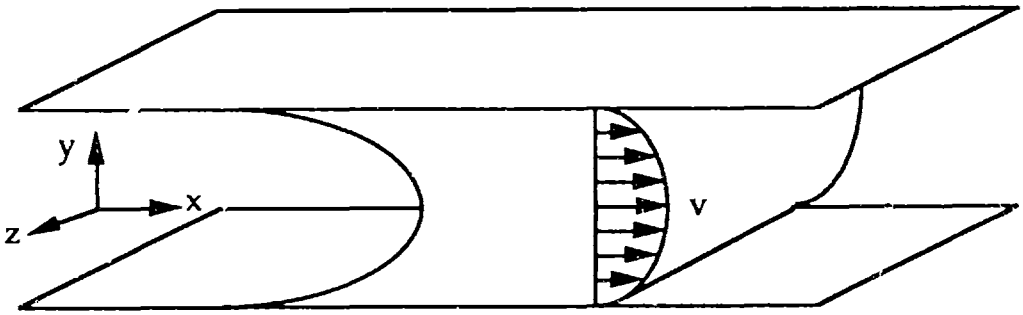

Figure 4.5. Two fluids with a meniscus interface flowing between two parallel plates.

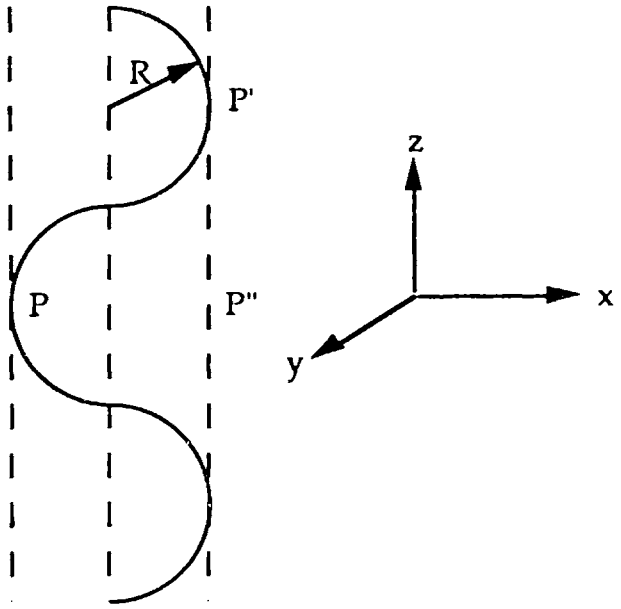

Figure 4.6. Disturbance of the meniscus and pressure at different locations.

4.3. Fractographic features of rigid silicone resins.

Modifications of 4-3136 resins produced dramatic changes in the fracture surface morphology. These features, summarized and explained below, revealed the toughening mechanisms.

4.3.1. Evidence of slow crack growth and crack acceleration.

The fracture surfaces of the unmodified, and the PAE2 or PAE modified resins always have a rough area immediately after the pre-crack tip. This rough zone forms when the crack propagates at a relatively slow speed. After the rough area, a mirror smooth area followed. The mirror smooth area was associated with fast crack growth. This was supported by the following two observations.

First, at the end of each rough zone, a sudden acceleration of the crack was clearly indicated, as shown by Figure 4.7, a photo taken at the end of a rough zone at the center of the specimen. The crack front started to accelerate at the center of the specimen due to highest elastic constraint, changing the velocity direction of the crack front and creating the fan shaped striations in the region connecting the rough and mirror smooth zones. The two photos shown in Figure 4.8 were taken on both sides of the crack center: the striations fanned away from the center of the crack. As the crack speed increased further, the multi-plane feature was diminished and finally disappeared.

Second, in a separate experiment, a 10 part PAE2 toughened resin was tested at a speed a decade slower than the normal test speed. The fracture surface was mostly rough except for a very small smooth zone at the end. If the test was performed at the normal speed, the fracture surface showed four bands containing two mirror smooth regions.

In the fast propagation region, material heterogeneity played an less important role due to the time dependence of its properties and the resin essentially fractured in a brittle fashion, leaving mirror smooth fracture surfaces.

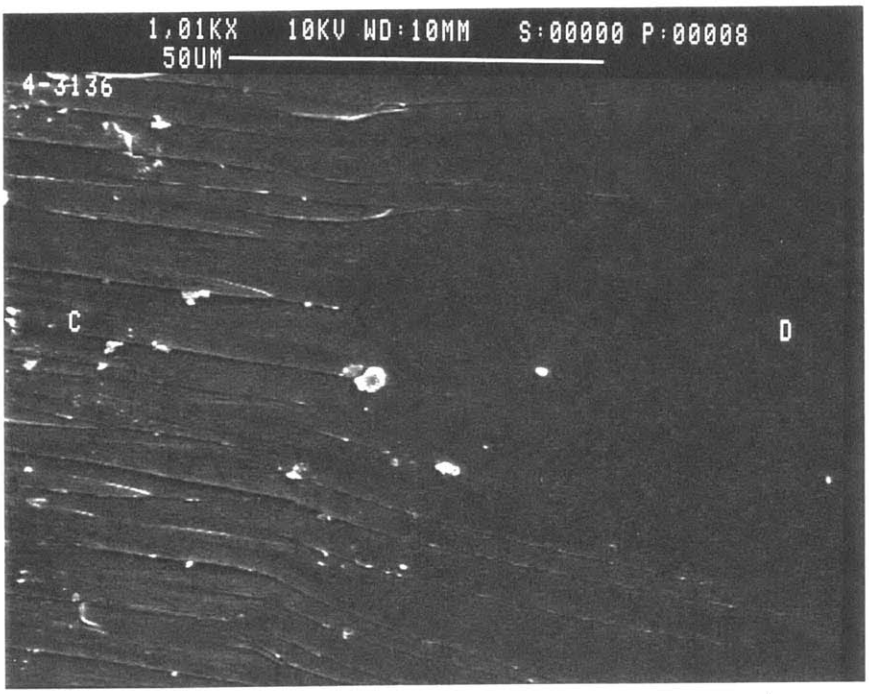

Figure 4.7. SEM photos of the fracture surface of the unmodified 4-3136 resin. C: the end of slow propagation zone; D: the beginning of fast propagation zone.

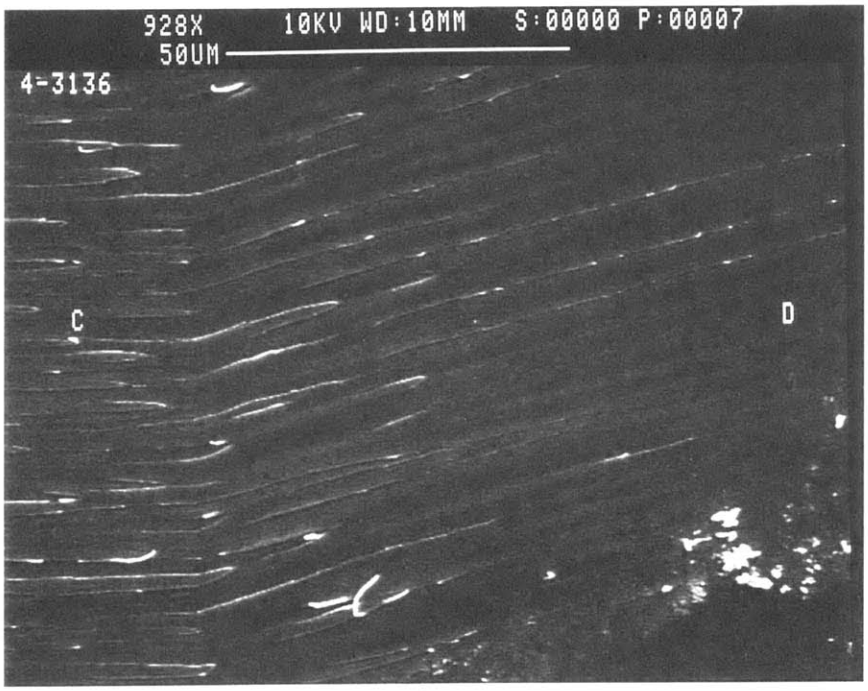

a

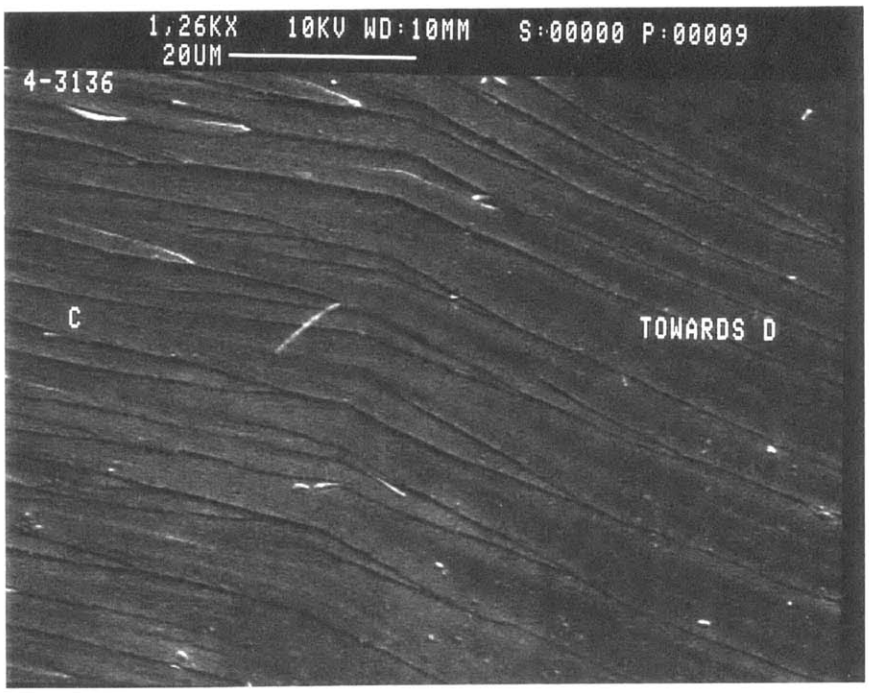

b

Figure 4.8. SEM photos of the fracture surface of the unmodified 4-3136 resin. C: the end of a slow propagation zone; D: the beginning of a fast propagation zone. For more explanation see text.

4.3.2. Crack propagation at different speeds.

The SEN specimen was notched by a diamond saw. From the root of the saw cut a pre-crack was produced by tapping a razor blade. The specimen was then loaded to fracture. The fracture surfaces of specimens are schematically shown in Figure 4.9. The crack was re-initiated from the pre-crack tip and driven through the sample during the test. After the pre-crack tip the fracture surfaces could be either alternatingly rough and mirror smooth, or rough all the way through.

Shown in Figure 4.9, when tested at a constant displacement rate, i.e. 0.4 inch/min., unmodified 4-3136 resin always showed alternating rough and mirror smooth bands on the fracture surface. Since the number of bands depended on the initial position of the pre-crack tip, all the crack surfaces discussed here had a initial pre-crack tip position close to the center of the specimen. When a razor blade was tapped into the root of the saw cut to make the pre-crack, most of the time it was not practical to make a perfectly straight and even crack front. When loaded, this uneven front grew slowly first and a parabolic crack front was obtained, symmetric about the center line of the cross section of the specimen. This, illustrated by the first rough zone on the fracture surface of the unmodified resin, was consistent with the more severe plane strain constraint at the center of the specimen. At the end of this rough zone, the crack started accelerating at the center of the specimen, producing a mirror smooth zone. It was slowed down after traveling a distance. The slow to fast transition was then repeated.

When the resin was modified with 10 part PAE2, the crack surface was also divided into four regions, alternatingly rough and mirror smooth, but the area of the mirror smooth region became smaller (Figure 4.9). If 10 part PAE was pre-reacted into the 4-3136 resin, the fracture surface was largely rough with an even smaller mirror smooth region flanked by a small slow growth initiation region and a large rough final zone. The 10 part KPE modified resin did not show any band like feature on the fracture surface. There was no mirror smooth region and the whole crack surface was relatively rough. It was evident that as more effective toughenners were incorporated, a higher fraction of the fracture surface was occupied by rough

areas, and the mirror smooth area became smaller, until the entire surface was relatively rough when 10 part KPE was pre-reacted in. The number of bands also decreased when more effective toughenerers were used.

The fracture surfaces were rougher when the resin was toughened by the effective Phase I/II combinations than when unmodified or modified by the Phase I rubber alone. The last two plots in Figure 4.9 illustrated the appearance of the fracture surfaces of two resins toughened by 10 part PAE with 2.5 and 5 part Phase II of DP 375. There was no mirror smooth zone on the fracture surfaces. The one containing 2.5 part Phase II had four bands on the fracture surface: a rough initiation region, a less rough propagation region, a relatively rough, narrow re-initiation region, and a final rough tear region. The one containing higher amount of the Phase II had only two bands: a rough initiation region, and a rough tear region.

To explain these features, a detailed energy analysis is desired. But such an analysis requires information about the actual speeds of the crack propagation, the kinetic energy as a function of time, the R curve, etc. No such information can be obtained from a standard fracture toughness test and therefore such an analysis will not be attempted. On the other hand, a simple qualitative explanation will be given below.

The force-displacement curves of the fracture toughness test, plotted in Figure 4.10, display the loading history corresponding to crack propagation in different regions. In Figure 4.10, the scale of all plots were made the same to facilitate comparison. Plot a, for the unmodified 4-3136 resin, showed that the load went up linearly and then bent towards the peak. It was possible that this bend corresponded to the initiation and slow propagation indicated by a small rough zone immediately after the pre-crack tip. Such a bending of the force-displacement curve was always seen whenever there was a slow growth initiation zone appearing on the fracture surfaces. During this slow propagation, the load increased much more slowly and when the highest point was reached, it suddenly dropped. This sudden drop corresponded to the accelerated propagation which produced a smoother fracture surface. After traveling a distance the crack was slowed or arrested and the mirror smooth zone was ended. Then this slow growth-acceleration-deceleration

process was repeated, recorded on the force-displacement curve as a tail after the load dropped from the peak. This multi-step fracture process left rough and smooth area bands on the fracture surface.

A simple energy balance, showing the interchange of energy input and potential energy, kinetic energy and dissipation, may be written as:

$$U_1 = U_2 + U_3 + U_4, \qquad \frac{dU_1}{dA} - \frac{dU_3}{dA} = \frac{dU_2}{dA} + \frac{dU_4}{dA} \tag{4.1}$$

where U_1 is the energy input, U_2 the dissipated energy, U_3 the stored potential energy, U_4 the kinetic energy of the specimen, and A the crack area. The energy release rate G and the crack propagation resistance R are defined by[18]:

$$G = \frac{dU_1}{dA} - \frac{dU_3}{dA}, \qquad R = \frac{dU_2}{dA} \tag{4.2}$$

As the crack propagated fast the load dropped quickly because the load was applied at a constant displacement rate, which resulted in a decrease of the energy input rate. When the energy input rate, dU_1/dA, and the strain energy release rate, $-dU_3/dA$, were reduced further as a result of fast propagation, kinetic energy could be used to help drive crack propagation by deceleration.

The energy storage before fast propagation corresponds to the area under the corresponding part of the force-displacement curve. With specimens of about the same dimensions and crack length, the unmodified 4-3136 resin was able to store the least amount of energy before fast crack propagation, shown by Figure 4.10. During acceleration of the crack, the stored potential energy and the continued input energy were being dissipated and converted to kinetic energy. It is reasonable to expect that the higher the strain energy storage before fast propagation, the farther the crack can travel before it is arrested or slowed down. As a result a wider mirror smooth area should be left behind. On the other hand if the energy dissipation was higher, the crack would be able to travel a shorter distance and deceleration would begin earlier. Higher strain energy storage of the toughened resins before fast crack

propagation, as shown by Figure 4.10, and narrower mirror smooth zones on the surfaces of toughened resins, suggested higher dissipation.

When the resin was toughened by the most effective Phase I toughener KPE or the Phase I/II combinations, the mirror smooth region disappeared. A difference was also observed on the force-displacement curve. After the peak, a fast propagation corresponded to a steep drop, as shown by Figure 4.10a-e. With the more effective tougheners, e.g. the KPE (Fig. 4.10d) and the 10 part Phase I/5 part Phase II combination (Fig. 4.10g), the load dropped more slowly and the specimens were continuously torn apart, indicating higher ductility. This was also evidenced by the progressively larger energy input, measured by the area under the force-displacement curve, into the tougher specimens of the same shape and dimensions.

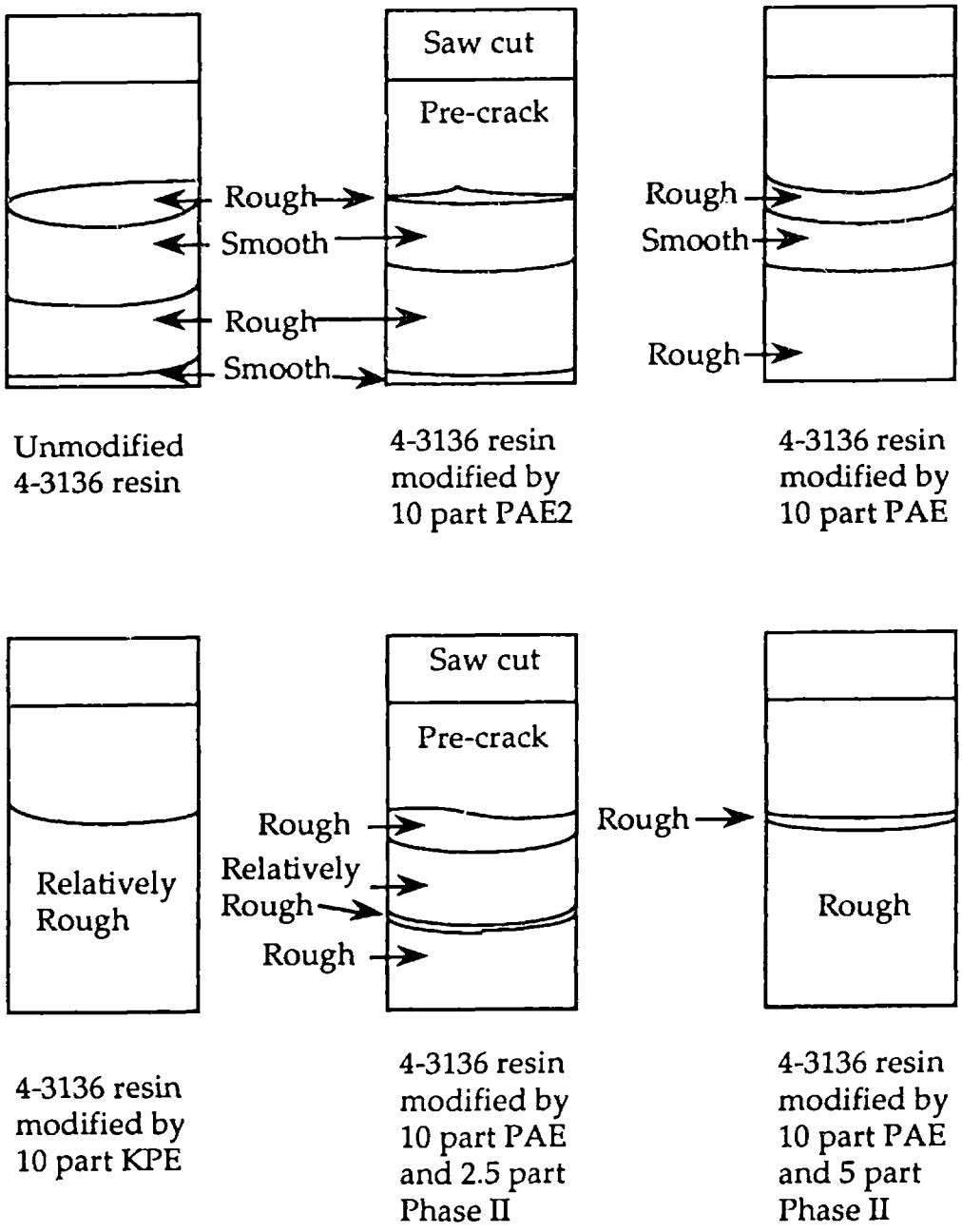

Figure 4.9. Schematic drawing of fracture surfaces of the modified and unmodified 4-3136 resins.

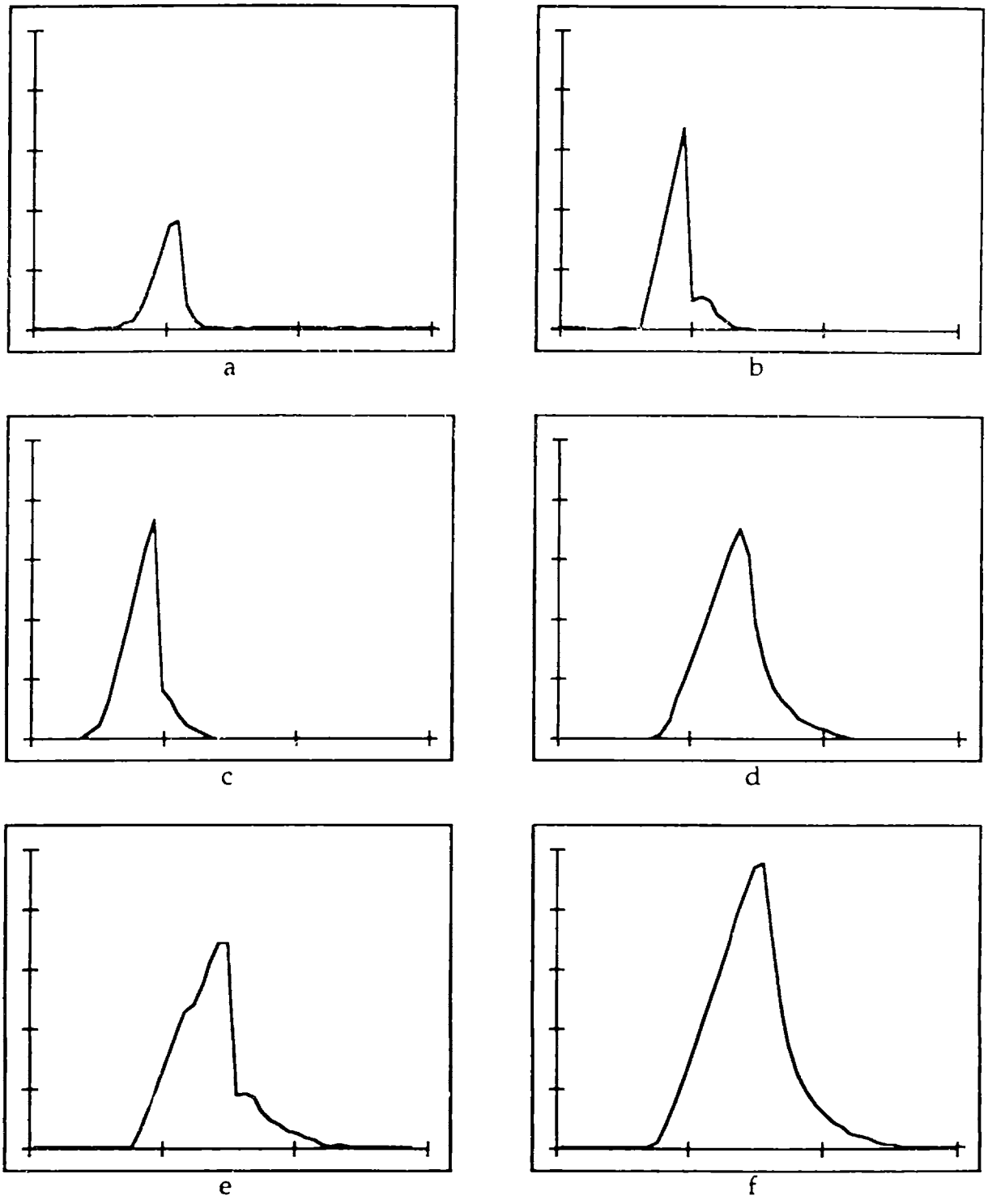

Figure 4.10. Force-displacement curves of the unmodified and modified 4-3136 resins, from a fracture toughness test. Toughners: a, none; b, 10 part PAE2; c, 10 part PAE; d, 10 part KPE; f, 10 part PAE and 2.5 part PDMS of DP 375; g, 10 part PAE and 5 part PDMS of DP 375.

4.3.3. Multiple planes, steps, welds, and wedges.

When the rough zones on the fracture surface of the unmodified resin were examined at relatively high magnifications under SEM, striations were seen. They were formed by the main crack being divided into many sub crack planes and each plane traveling at different elevations. There were three possible causes for this: the imperfection of the initial crack; the twisting and titling of the tension when the crack was traveling; and material heterogeneity.

Possible causes of a irregularly shaped, or skewed pre-crack front included the waviness of the razor tip imprinted to the root of the notch, and the misalignment of the razor blade when it was used to make the pre-crack. In Figure 4.11, the original serrated crack front continued to grow when re-initiated and the elevation difference between adjacent crack planes was augmented. Even if the pre-crack front was smooth, a multi-plane feature was developed immediately after the crack was re-initiated, as seen in Figure 4.12.

Serrated crack planes usually exist only in the region close to the pre-crack tip, strongly suggesting a twisted tension mechanism. As the crack traveled away from the pre-crack tip, serrated multiple planes were replaced gradually by multiple planes parallel to the main crack plane, as shown in Figure 4.13. This was observed with not only the unmodified 4-3136 resin but also the PAE2 or PAE toughened resins.

After the multi-plane feature was fully developed, there seemed to be a characteristic periodicity associated with each type of resin. The unmodified resin, most brittle, had the smallest average width of each individual plane, about 2 microns. This width increased slightly when 10 parts of PAE2 were pre-reacted into the resin, shown by Figure 4.14a. When 10 parts of PAE were incorporated, it increased further to 8 microns, shown by Figure 4.14b. The step height between planes decreased progressively from the unmodified to the 10 part PAE2 and then to the 10 part PAE toughened resins. If 2.5 or 5 parts of Phase II were pre-reacted with 10 parts of PAE into the resin, the plane width increased further to about 20 microns and the step height was reduced further, shown by Figures 4.24 and 4.25. This multi-plane feature completely disappeared when 10 parts of KPE were incorporated, shown by Figure 4.21.

Between two adjacent planes, a step (Figure 4.13) and a weld (Figure 4.8) were formed. When two planes came close to each other, the tension direction was continuously twisted in the ligament between the two planes and a fibril shaped weld was cut off. These welds were either completely detached or semi-attached to one crack plane. The size of a weld indicated the height of the step associated with it.

Multiple planes, welds, and steps were more often seen in the unmodified and the PAE2 toughened resins. They were mostly from a brittle fracture process without extensive plastic flow. It was found that there was no permanent deformation retained in the fracture surfaces showing multi-plane features. The fractured specimen of the unmodified resin was observed under SEM and then heated at 120 °C for 2 hours and observed again. Figure 4.15 compares the same location on the fractured surface before and after heat treatment. There was no change caused by the heat treatment. No change was produced by a further heat treatment of the specimen at 200 °C for 2 hours.

Sometimes the elevation difference between adjacent planes became progressively larger as the crack was advancing, one sub plane was narrowed and a wedge was formed, as seen also in Figure 4.13. The increasing step height was clearly seen in Figure 4.13 where a wedge formed and was pulled out.

4.3.4. Plastic zone in the KPE toughened resin.

A highly distinctive feature of the fracture surface of the 10 part KPE toughened resin was the presence of a band left by the ruptured plastic zone ahead of the pre-crack tip. The shape of the band is shown schematically in Figure 4.16. This band was divided into two parts, each extending from the surface to the center of the specimen. They overlapped at the center of the fracture surface but did not connect. Pictures of the upper part were included in Figure 4.17. 4.17a was taken at a location close to the side of the specimen and 4.17b close to the center of the specimen. The plastic zone became progressively narrower towards the center. Pictures of the lower part of the plastic zone in Figure 4.16 are included in Figure 4.18. This part of the plastic

zone had a zone width comparable to the upper part except for the locations close to the center of the specimen, where the wide band was divided into a few sub bands, resembling a stick slip crack growth process, shown by Figure 4.18a. These variations were consistent with the more severe plane strain constraint at the center of the specimen.

This plastic zone, left by the rupture of the plastically deformed materials and the snapping back to the surface by ruptured strands, was a conclusive evidence of increased plastic flow in the 10 part KPE modified resin. There was, however, no permanent deformation in this band. The fractured specimen was heat treated at 120 °C for 2 hours and the shape of the strands in this band did not change. The photos presented in Figure 4.19 were taken from the fracture surface after heat treatment. Photo 4.19a should be compared with Figure 4.17a, both of which were taken at the same location. Photo 4.19b should be compared with Figure 4.18b, for the same reason. The wide glass transition temperature range, a temperature rise due to energy dissipation, and the small scale of the plastic deformation might have contributed to the full recovery of the plastic deformation.

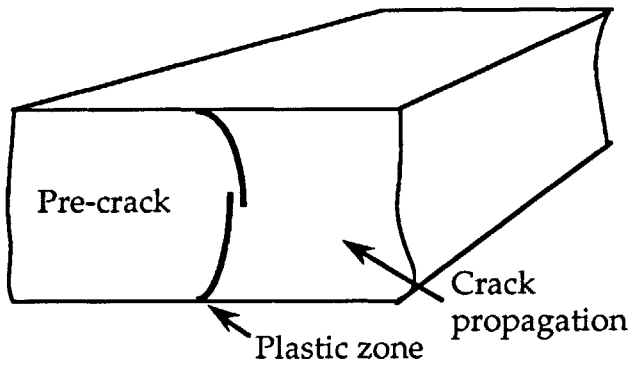

Figure 4.16. Schematic drawing of the shape of the band left on the fracture surface by the rupture of the plastic zone ahead of the pre-crack tip. Crack travels from left to right.

The size of the plastic zone compares very favorably to the calculation included in Table 3.2. In Figures 4.17 and 4.18, it was seen that the width of the plastic zone was from 8 to a little over 10 microns, depending on the location. This size is almost the same as the calculated value: a half size of 4.6 microns.

4.3.5. Basic longitudinal textures: meniscus instability and nodules.

At higher magnifications a consistent longitudinal texture was seen on the fracture surfaces of all the resins, although occasionally not in the mirror smooth zones. Shown in Figures 4.21 to 4.25, the characteristic longitudinal texture was always present. The longitudinal texture is also schematically illustrated in Figure 4.26. Figure 4.21 contains photos taken from the fracture surface of the 10 part KPE toughened resin. In 4.21b, the periodicity of the longitudinal texture was about 600 nm. The fracture surface of the unmodified resin also showed a basic longitudinal texture(Figure 4.22b). The spacing between adjacent crests was approximately 100 nm on the average, shown by Figure 4.22a. A similar basic longitudinal texture was also seen on the fracture surfaces of the 10 part PAE2 or PAE toughened resins, shown in Figure 4.23. The average periodicity was also approximately 100 nm.

In the resins toughened by the Phase I/II combinations, such a basic longitudinal texture became more prominent, shown by Figures 4.24 and 4.25. Photo b of the two Figures show an increase of periodicity and higher ductility of the resins. When 2.5 part Phase II rubber was present, the periodicity increased to over 1000 nm. It increased further to ~2000 nm with 5 parts of Phase II.

A meniscus instability mechanism[3] can be used to explain the observed longitudinal texture. When a meniscus instability grows the periodicity increases with the crack opening displacement and decreases with the crack velocity[9, 10, 11, 12]. Therefore the increased periodicity in effectively toughened resins indicates more extensive plastic flow. When the resin was not modified, there was no extensive plastic flow so the periodicity was controlled by the inter nodule spacing. This was maintained even when the

resin was moderately toughened. More discussion on the nodular structure will be given in the next section.

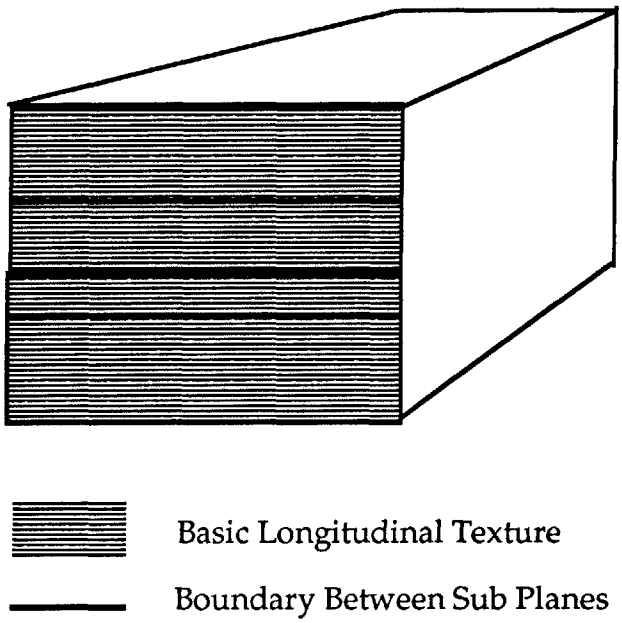

Figure 4.26. Schematic illustration of the basic longitudinal texture seen in individual sub crack planes. Crack travels from left to right.

4.3.6. Nodular structure and the role of rubber particle size.

4-3136 resins, both unmodified and modified, have a nodular structure, as shown by Figures 4.27 and 4.28. The nodular size for the unmodified 4-3136 resin is about 80 to 100 nm, comparable to the nodular size found in epoxy resins[17]. The nodular size in the PAE2 and PAE toughened resins was comparable to the unmodified 4-3136 resin, while that in the KPE toughened resin decreased to about 60 nm. These nodules appear to be stiffer than the surrounding connecting materials. A crack appears to go around them and leave bumps or dents on the fracture surface, see Figures 4.27 and 4.28.

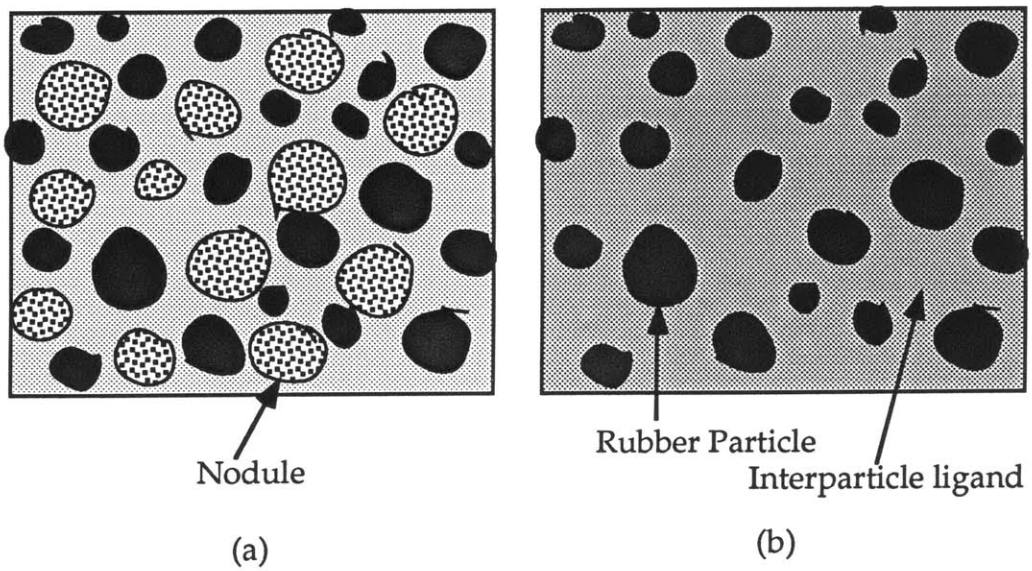

Figure 4.31. Schematic illustration of the nodules and the second phase particles. (b) is the same as (a) except for the nodules which are omitted.

Close examination of the Phase I/II combination shows the second phase particle size is comparable to that of the nodules. As shown by Figures 4.29 and 4.30, in the Phase I/II combination toughened resins, such nodular structure is not seen on the fracture surface. Instead, drawn inter particle ligands are observed. This suggested that in an elevated stress field caused by the presence of the rubber particles the individual nodules were substantially deformed. A proposed structure of the Phase I/II combination is schematically shown in Figure 4.31, where the nodules, rubber particles, and inter particle ligands are labeled. The nodules are in the inter particle ligands. This may explain why the size of the rubber particles has to be very small, comparable to or smaller than the nodular size: it is necessary to reduce the inter particle ligand thickness and engage the individual nodules in a deformation process. When large rubber particles are present, the inter particle ligand thickness is large and the stress elevation can be relieved by the deformation of material between stiff nodules. Such a system failed to cause distortion of individual nodules and as observed, did not toughen the resin effectively.

4.4. Conclusions.

Multiple planes, steps, welds, wedges, basic longitudinal textures, and rough/mirror smooth bands are the common features found on the fractured surfaces of 4-3136 resins, both modified and unmodified. Possible formation mechanisms of these include a tilting/twisting of the principle tension, the presence of meniscus instability, and a resin nodule modulated flow.

The increased plastic flow was indicated in the effectively toughened resins by the basic longitudinal texture, and by a plastic zone ahead of the pre-crack tip in the KPE toughened resin. It was also evidenced by drawn ligands on the fracture surfaces seen at high magnifications, as well as the reduced area of the mirror smooth zones with toughening. More tougheners introduced more extensive plastic flow to the fracture process.

The unmodified and Phase I modified resins show a nodular structure, with a nodular size from 60 to 100 nm. The KPE Phase I modification seemed to reduce the nodular size.

The Phase I/II combinations were effective perhaps because the second phase successfully engaged the resin nodules in plastic deformation. This required that the second phase particle size be comparable to or smaller than the nodular size. Larger particles would produce a concentrated stress field a few times the size of the particles and far larger than the nodular size, and cause a large inter particle ligand thickness. Therefore they did not effectively promote plastic flow involving individual nodules and as observed, did not toughen the resin.

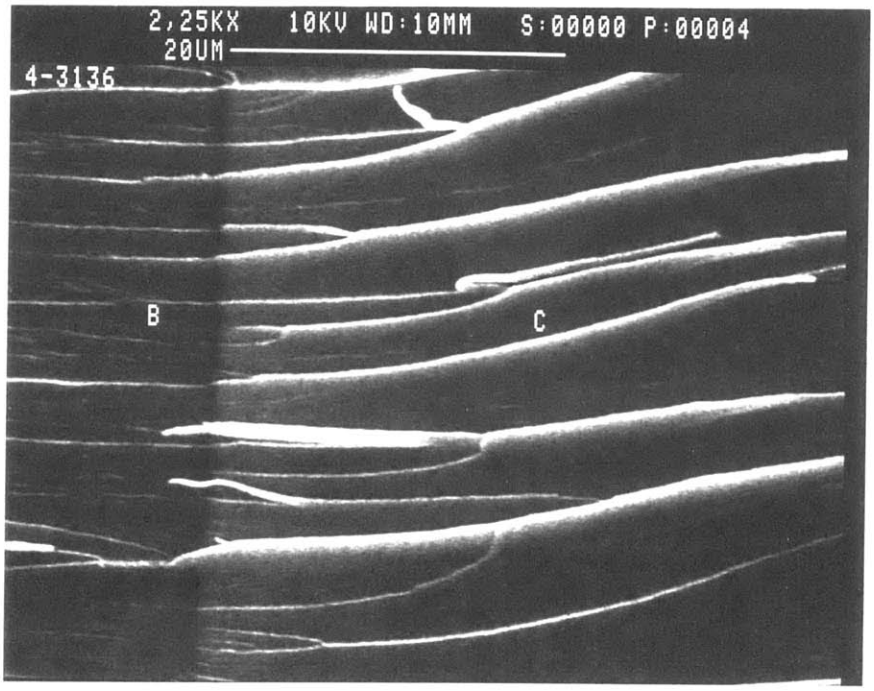

a

b

Figure 4.11. Fracture surface of the unmodified 4-3136 resin showing multi-plane features. B: pre-crack; C: slow propagation rough zone.

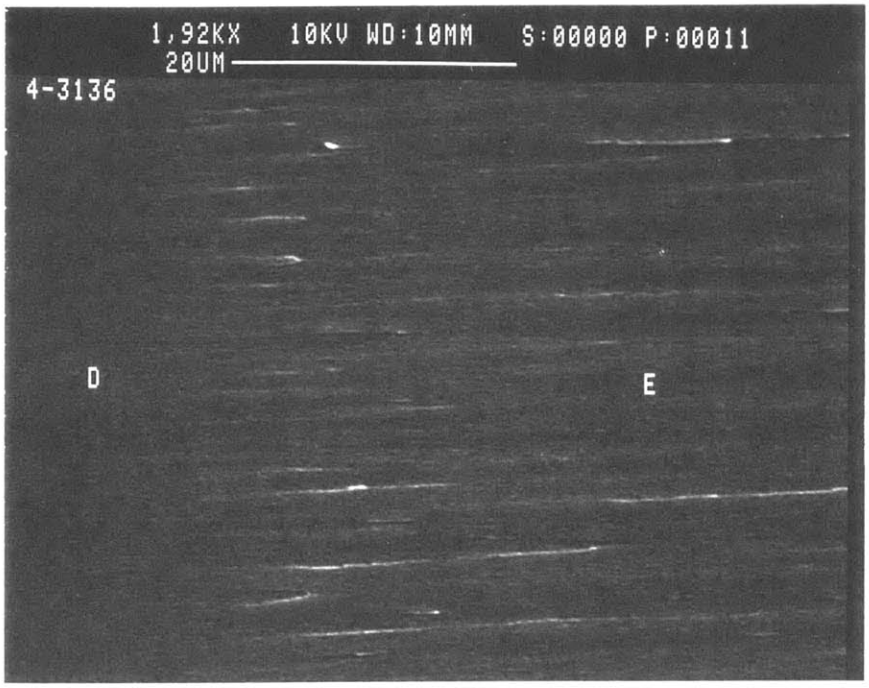

Figure 4.12. Fracture surface of the unmodified 4-3136 resin showing gradual development of multi-plane features. D: mirror smooth region; E: beginning of a slow propagation rough zone. Crack travels from the left to the right.

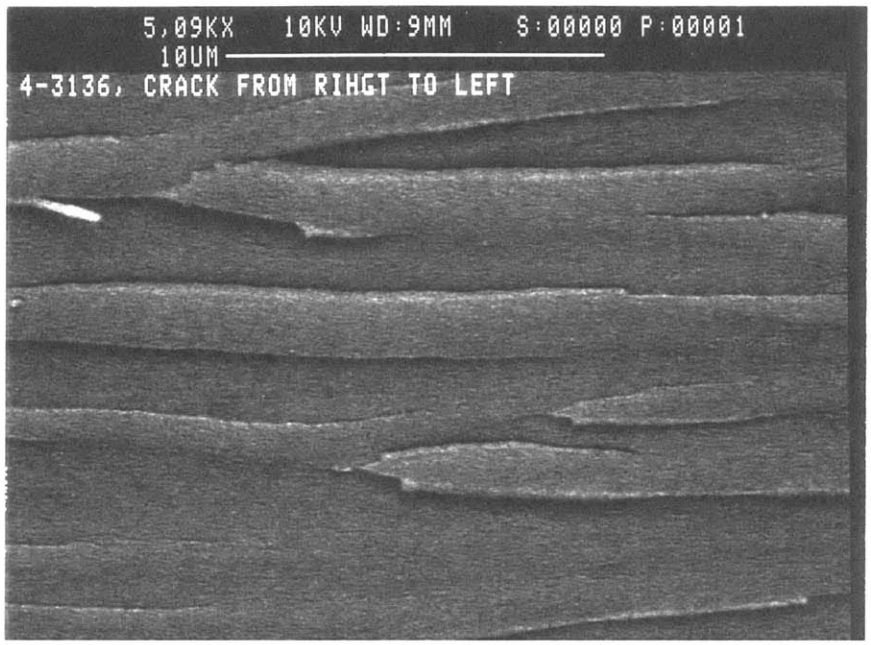

Figure 4.13. Fully developed slow propagation, multi-plane rough zone on the fracture surface of 4-3136 resin. Crack travels from the right to the left.

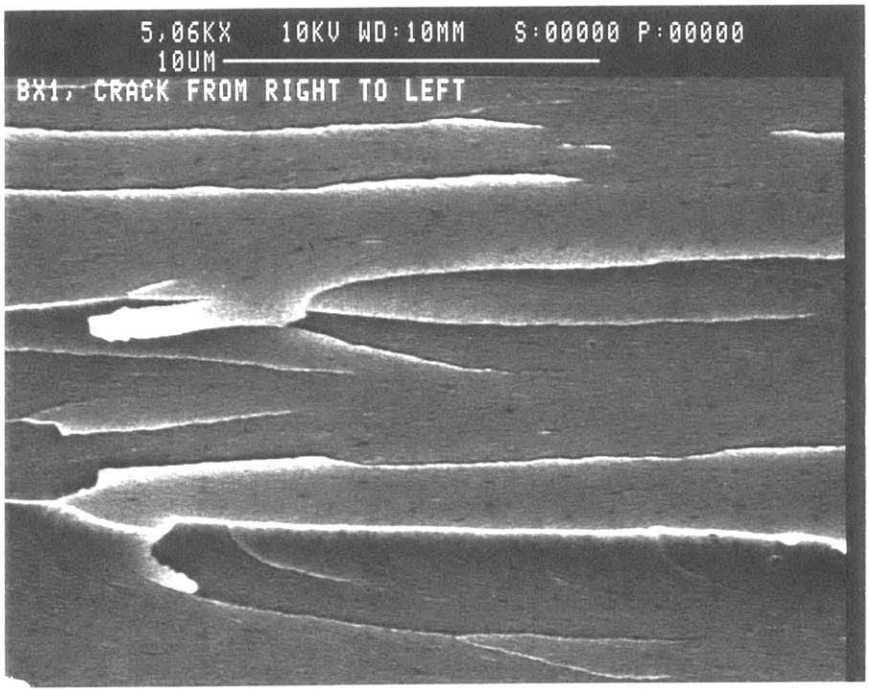

a

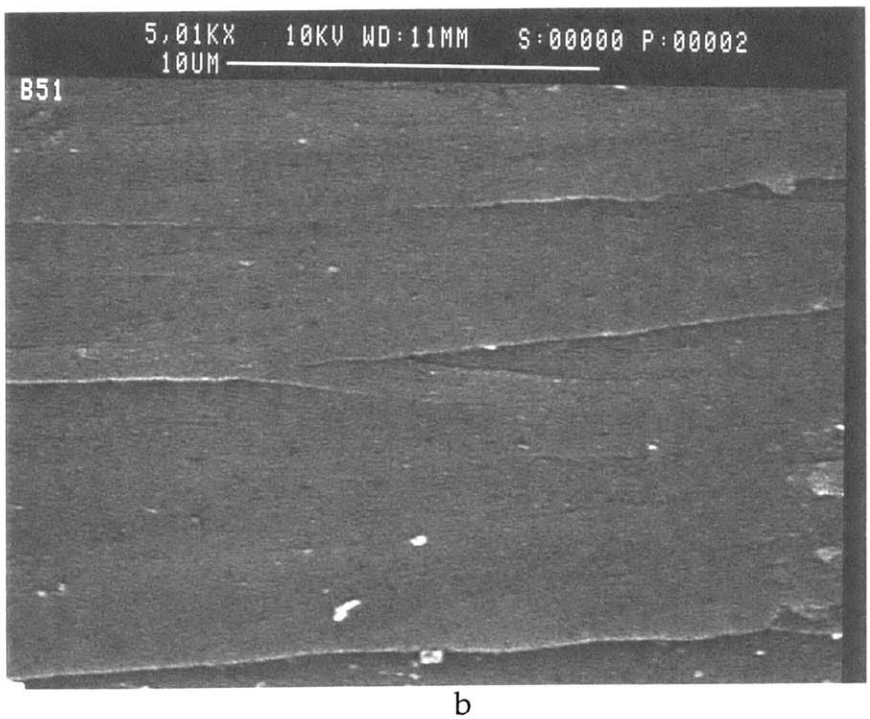

b

Figure 4.14. Fully developed slow propagation, multi-plane rough zone on the fracture surface of the 10 part PAE2 toughened (a), and the 10 part PAE toughened 4-3136 resins (b). Crack travels: a, from right to left; b, the opposite.

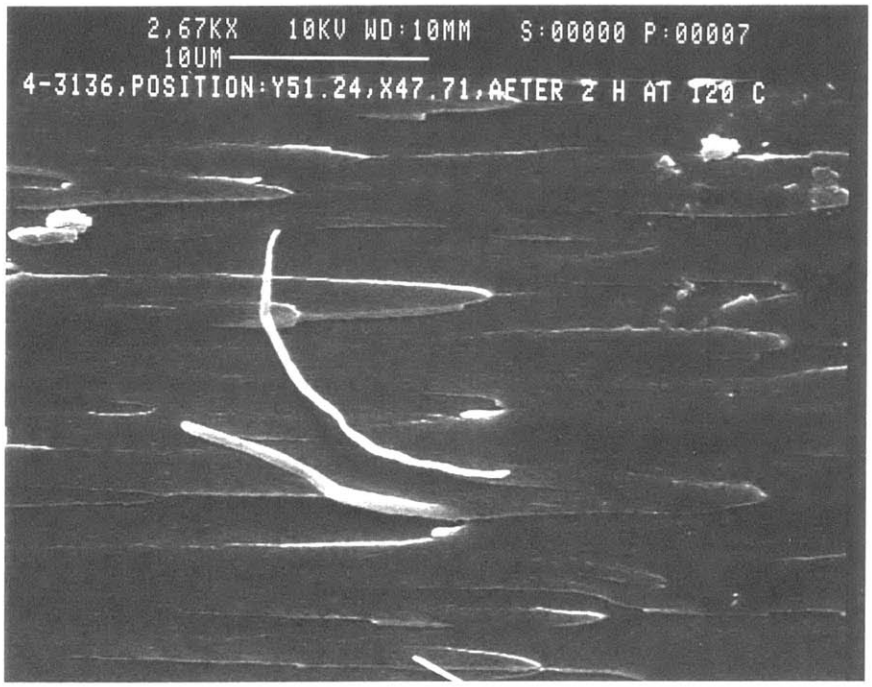

a

b

Figure 4.15. Fracture surface of the unmodified 4-3136 resin after heat treatment (a), and before heat treatment (b). Crack travels from the left to the right.

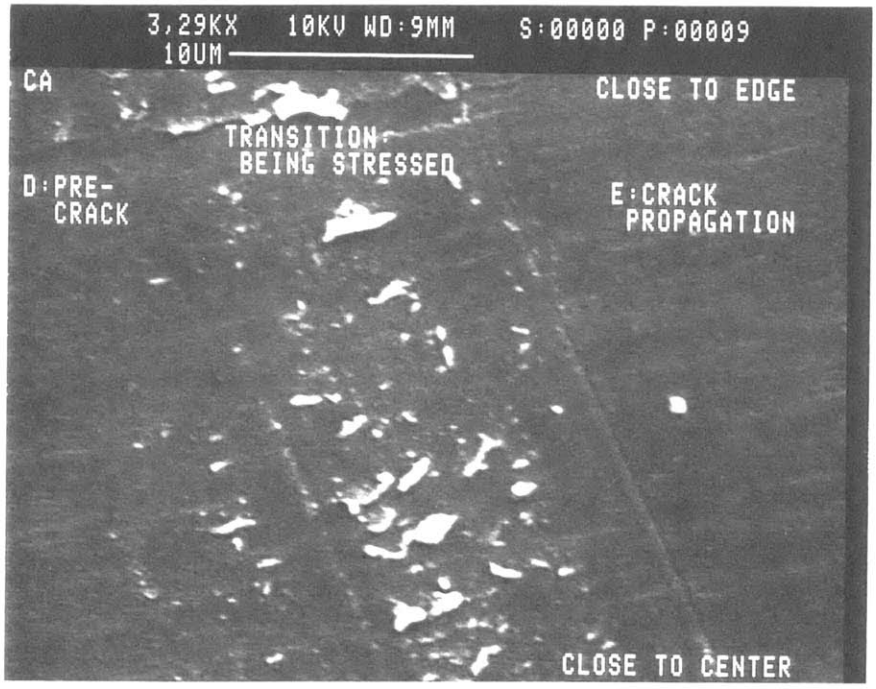

a

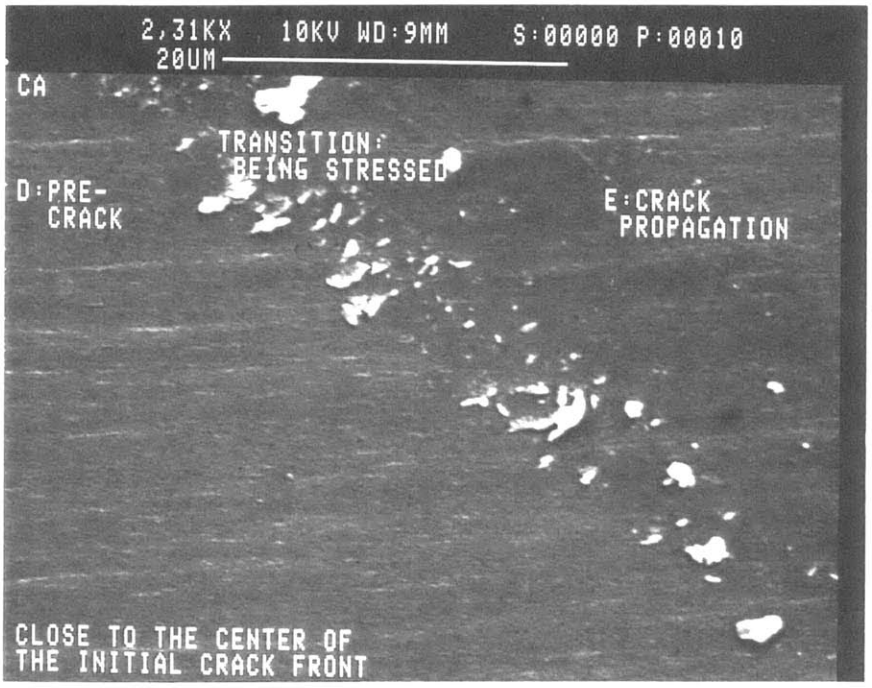

b

Figure 4.17. SEM photos of the fracture surface of the 10 part KPE toughened 4-3136 resin showing the plastic zone. D: end of the pre-crack; E: beginning of crack propagation. Crack travels from the left to the right.

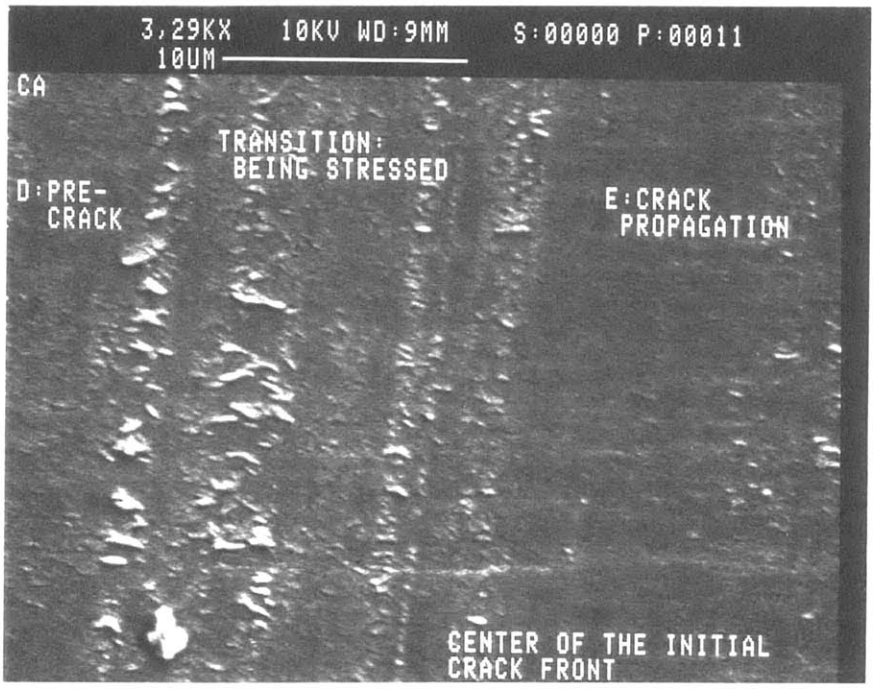

a

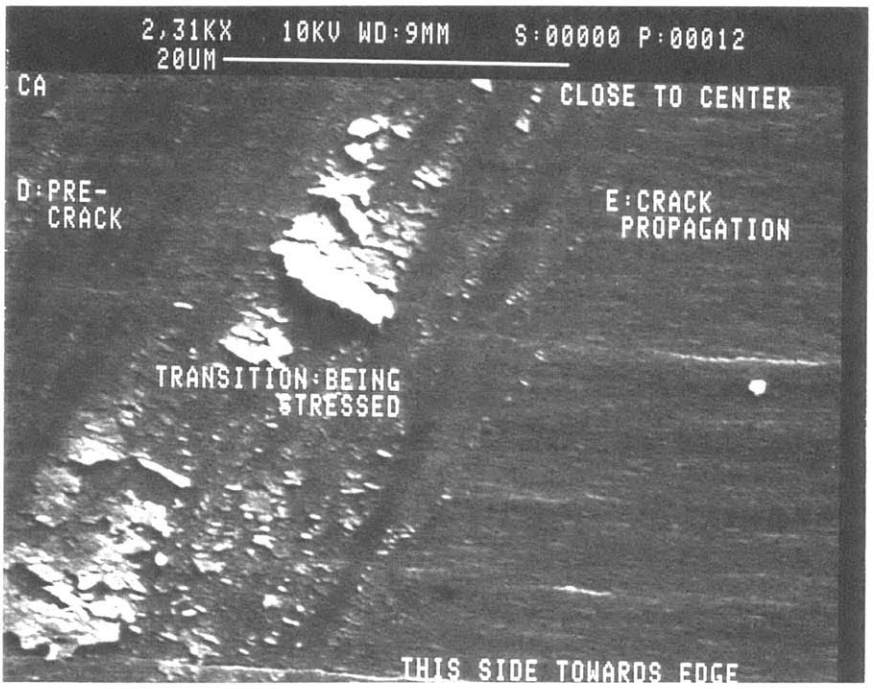

b

Figure 4.18. SEM photos of the fracture surface of the 10 part KPE toughened 4-3136 resin showing a plastic zone. D: end of the pre-crack; E: beginning of crack propagation. Crack travels from the left to the right.

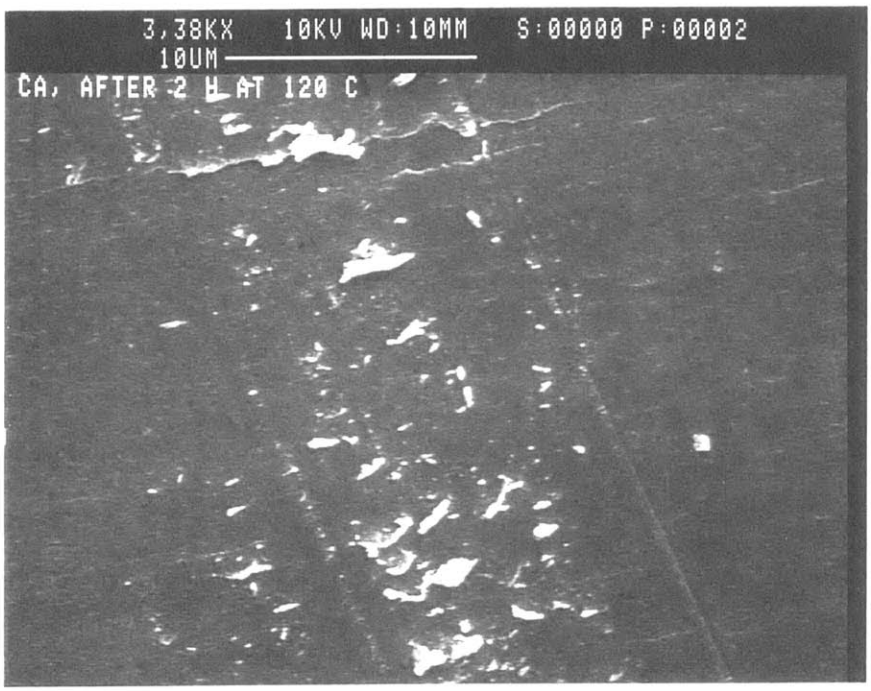

a

b

Figure 4.19. SEM photos of the fracture surface of the 10 part KPE toughened 4-3136 resin showing a plastic zone after heat treatment at 120 °C for 2 hours. Crack travels from the left to the right.

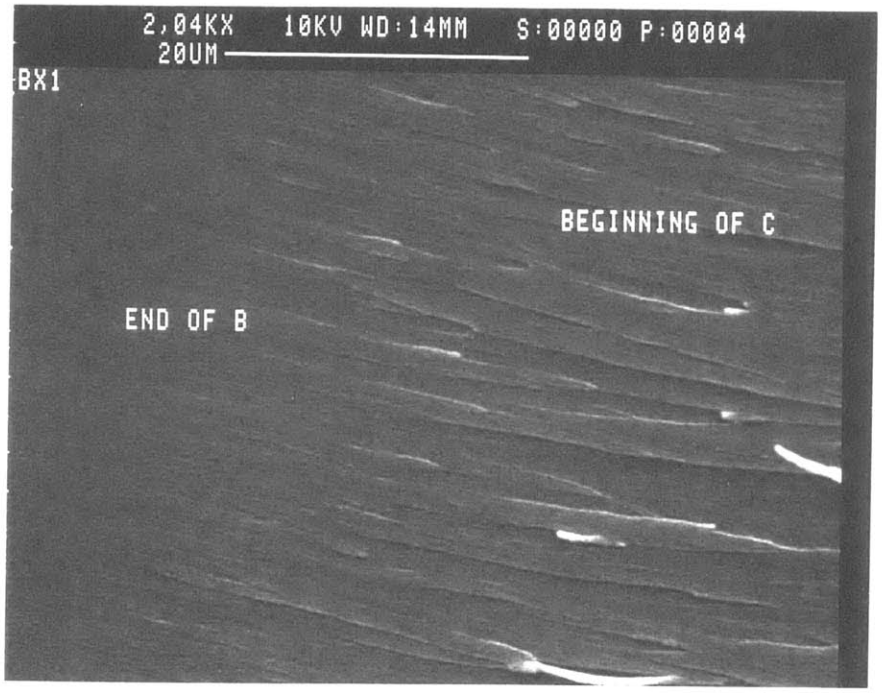

a

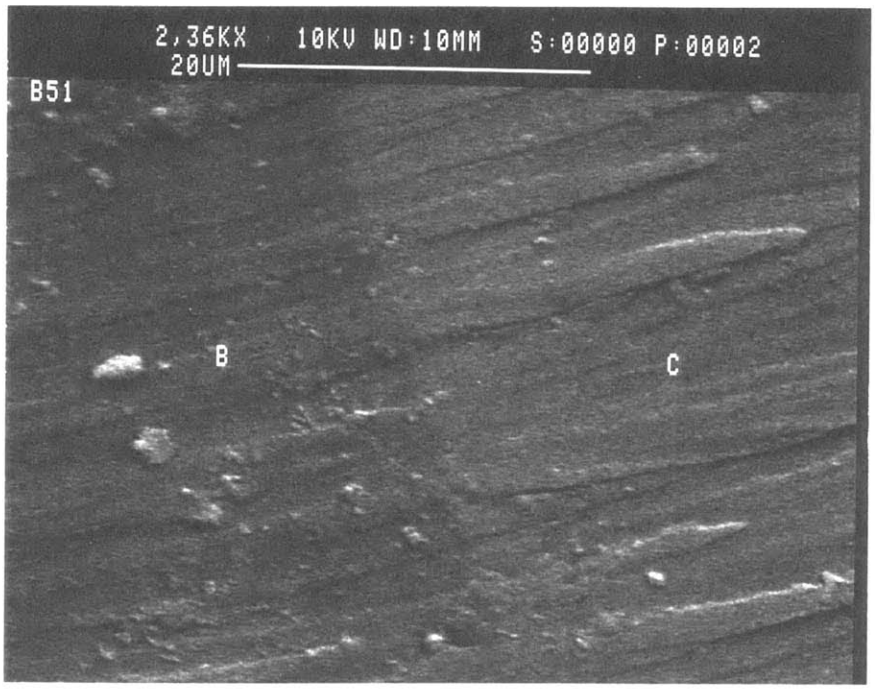

b

Figure 4.20. SEM photos of the fracture surfaces of the 10 part PAE2 (a), and the 10 part PAE (b) toughened 4-3136 resins. B: end of the pre-crack; C: beginning of slow propagation. Crack travels from the left to the right.

a

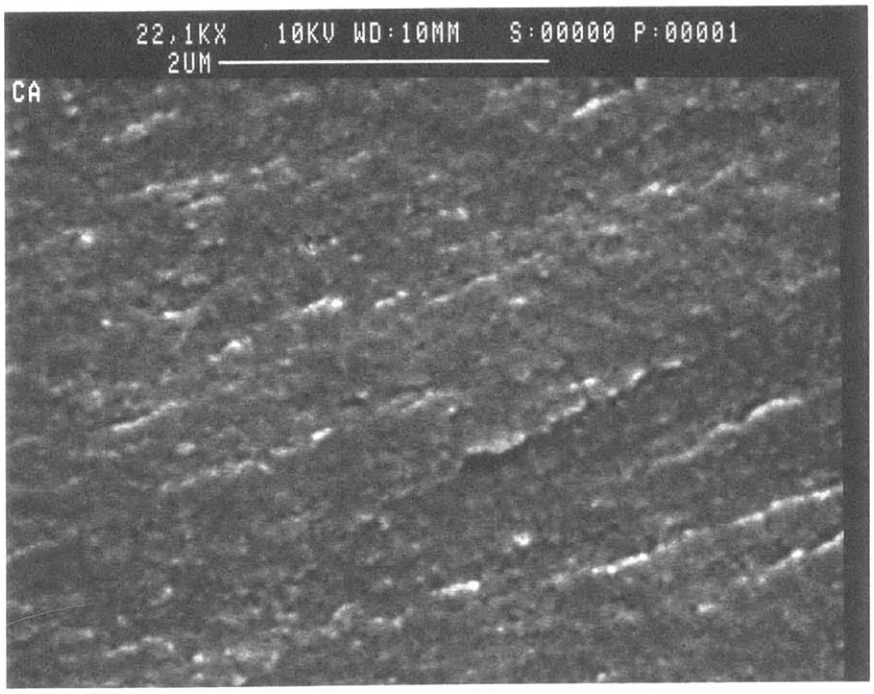

b

Figure 4.21. SEM photos of fracture surface of the 10 part KPE toughened 4-3136 resin showing a basic longitudinal texture and its periodicity. Crack travels from the left to the right.

a

b

Figure 4.22. SEM photos of a slow growth zone on the fracture surface of the unmodified 4-3136 resin showing, a: nodular structure; b: a basic longitudinal texture. Crack travels from the left to the right.

a

b

Figure 4.23. SEM photos of a slow propagation zone on the fracture surfaces of the 10 part PAE2 (a) and the 10 part PAE (b) toughened 4-3136 resin, showing a basic longitudinal texture. Crack travels from the lower left to the upper right.

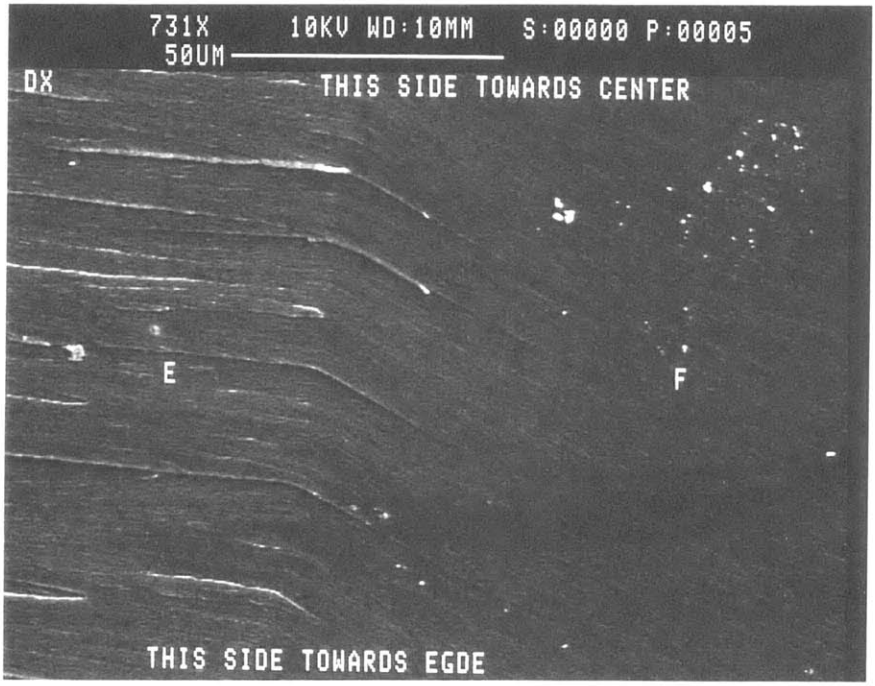

a

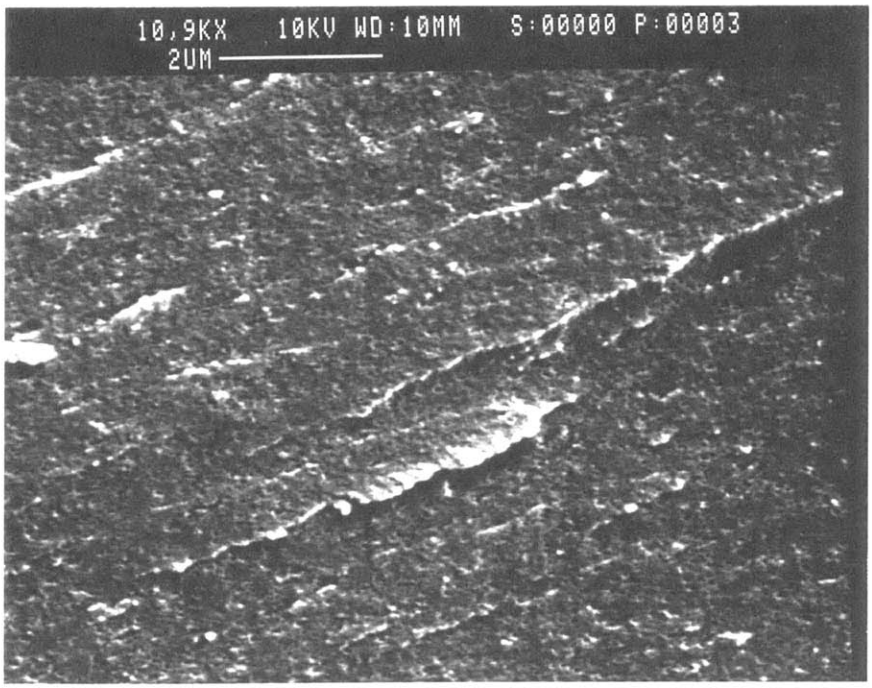

b

Figure 4.24. Basic longitudinal texture on the fracture surface of the resin toughened by 10 part PAE in combination with 2.5 part DP 375 PDMS. Crack travels: a, from the left to the right; b, from the lower left to the upper right.

a

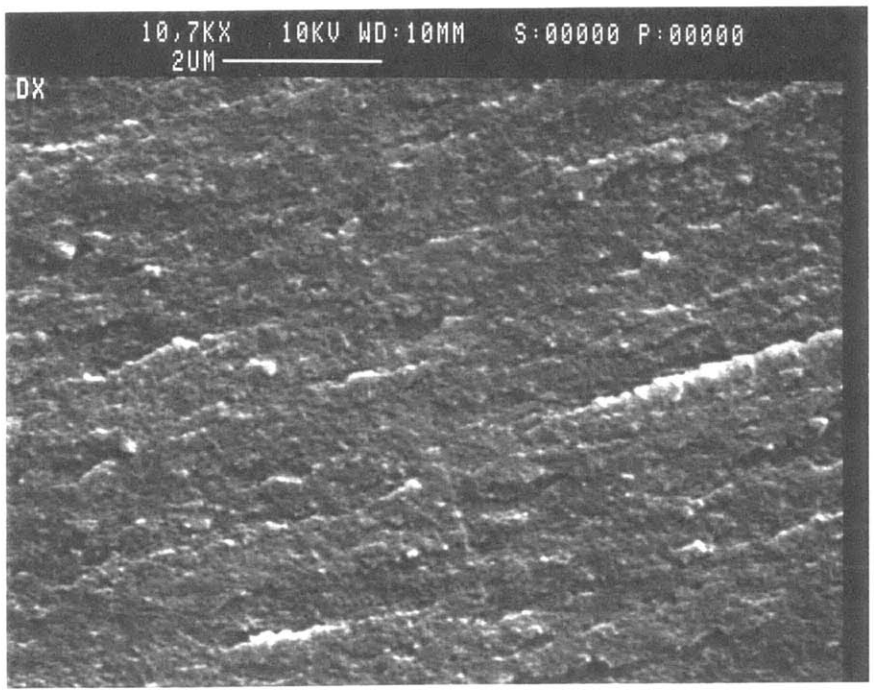

b

Figure 4.25. Basic longitudinal texture on the fracture surface of the resin toughened by 10 part PAE in combination with 5 part DP 375 PDMS. Crack travels: a, from the left to the right; b, from the lower left to the upper right.

a

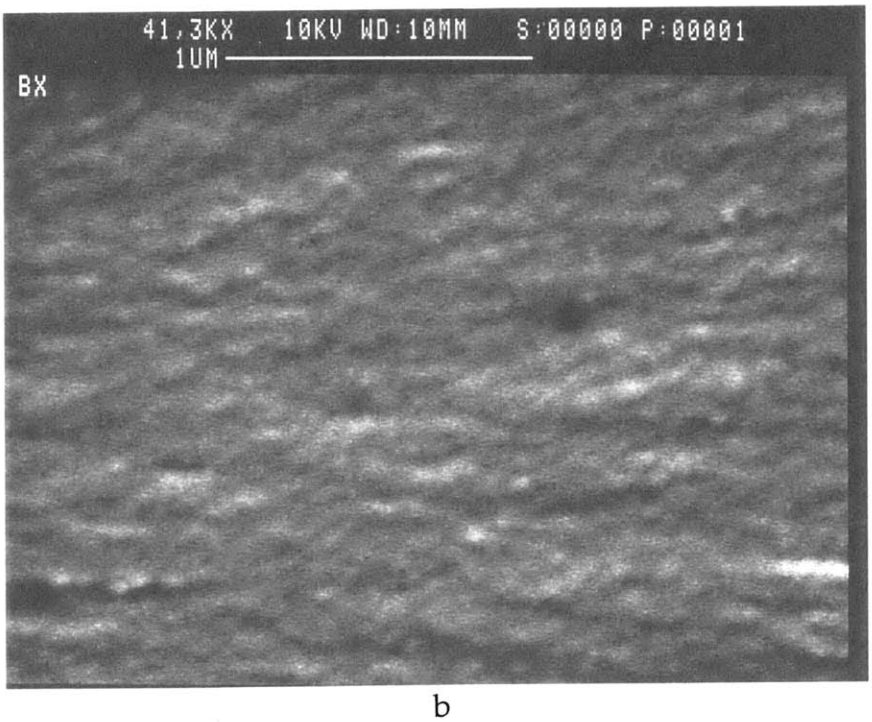

b

Figure 4.27. SEM photos showing the nodular structure of the unmodified 4-3136 resin (a); and the 10 part PAE2 toughened resin (b). Crack travels from the left to the right.

a

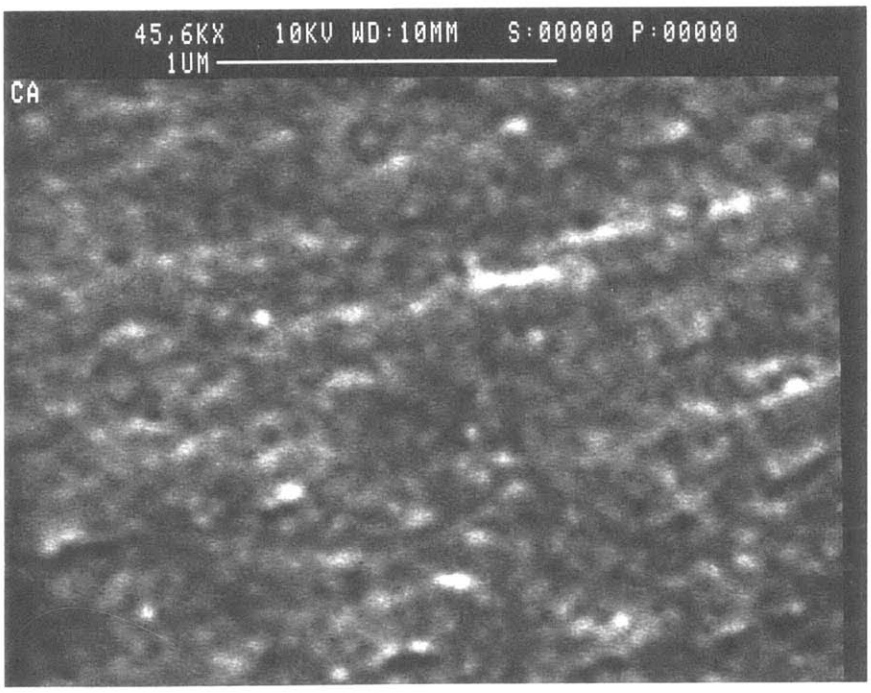

b

Figure 4.28. SEM photos showing the nodular structure of the 10 part PAE toughened 4-3136 resin (a); and the 10 part KPE toughened resin (b). Crack travels from the left to the right.

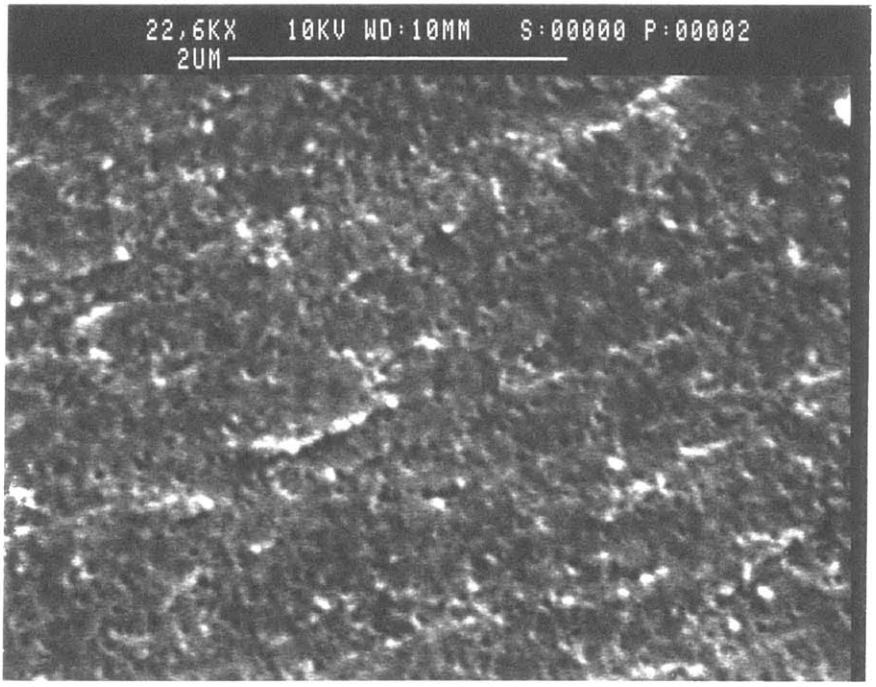

a

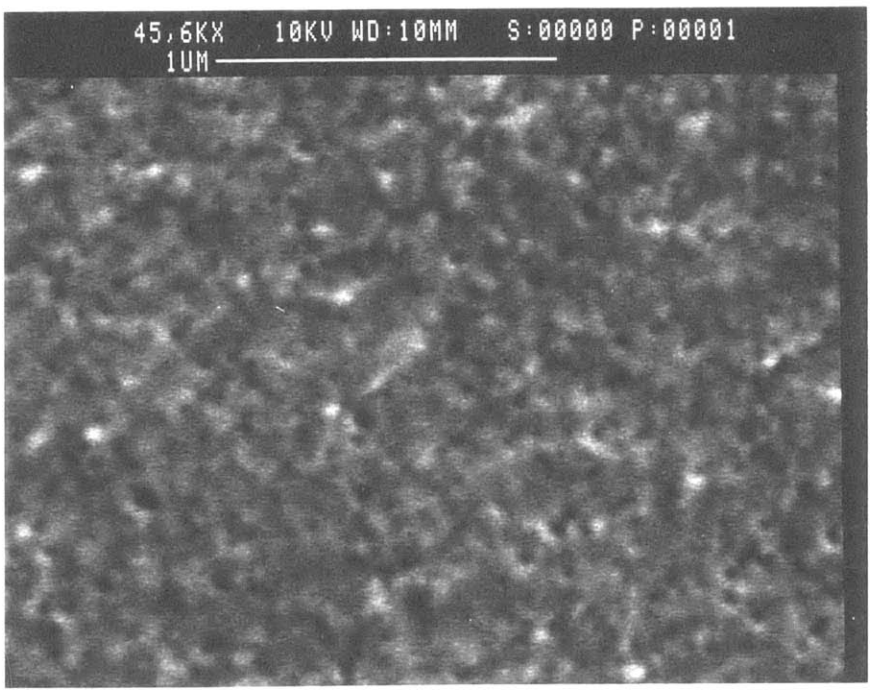

b

Figure 4.29. SEM photos of the fracture surface of the 10 part PAE/2.5 part DP 375 PDMS toughened resin, showing second phase particles and drawn ligands between close particles. Crack travels from the left to the right.

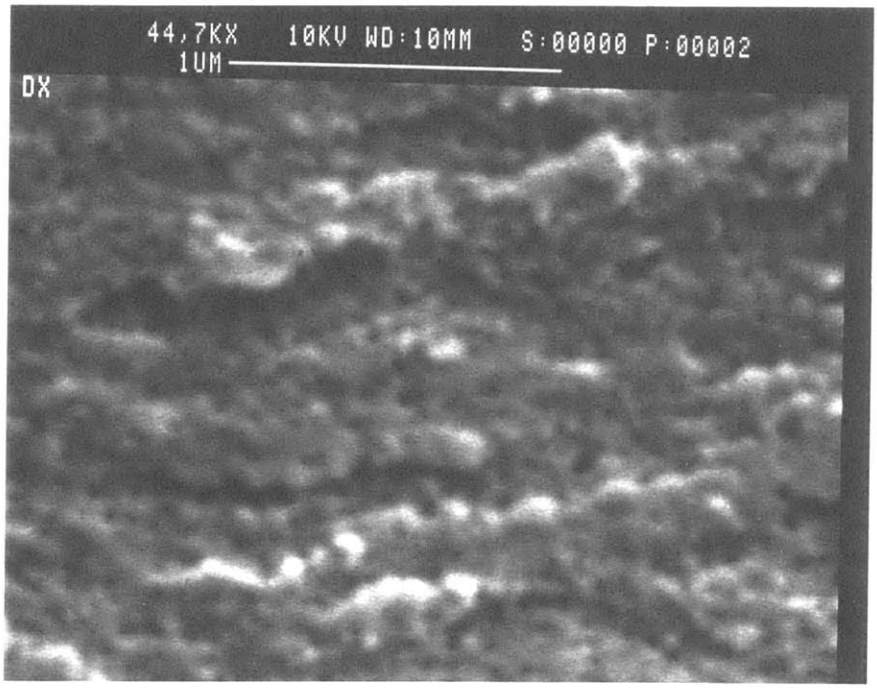

a

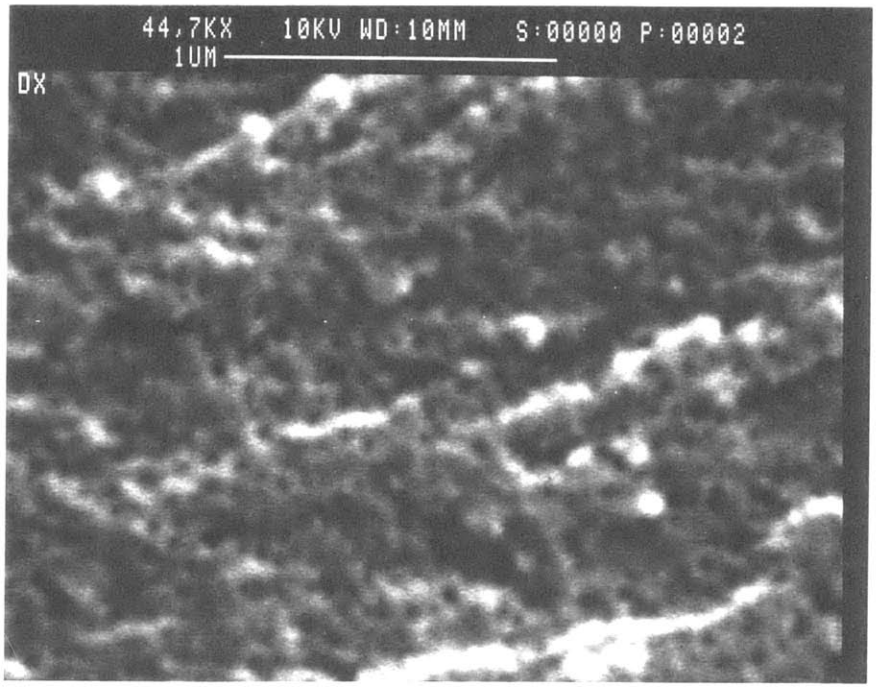

b

Figure 4.30. SEM photos of the fracture surface of the 10 part PAE/5 part DP 375 PDMS toughened resin, showing second phase particles and drawn ligands between particles. Crack travels from the left to the right.

Chapter 5. Molecular Origin of Enhanced Network Mobility: DMA Analysis.

5.1. Introduction.

Previously it was shown that rigid silicone resin was toughened both by Phase I short chain PDMS and by effective combinations of Phase I short chain and second phase long chain PDMS. The toughening mechanism was identified as the enhanced plastic deformation due to the presence of the Phase I and Phase II rubbers. It was also found that the longer Phase I PDMS chain was more effective than shorter ones, provided that it was homogeneously reacted into the resin network.

However it was not obvious why the longer Phase I PDMS was more effective. In this Chapter, dynamic mechanical analysis (DMA) was used to probe the relative mobility of the rubber segments of different lengths in the resin network and their influence on the network mechanical damping. The analysis showed that the longer chains were less restricted by the network, more mobile, and more effectively increased the energy dissipation of the originally low damping, high Tg domains.

5.2. Experimental.

The DMA used a Seiko Dynamic Mechanical Rheology Station DMS 200 in the tension mode. A specimen 20 mm long, 4 mm wide and 1 mm thick was mounted in two grips 14 mm apart. The test temperature range was -155 °C to 350 °C. The specimen was cooled to -160 °C and subjected to a tensile displacement changing sinusoidally at a frequency of 1 Hz while the temperature was raised at 2 °C per minute. The tension was measured and the storage and loss moduli were calculated. Some untoughened and less effectively toughened resins did not survive the whole process and failed before 350 °C, but in most cases the useful part of the spectra, from -150 to 280 °C, was successfully collected.

The 4-3136 resin samples were cured with different levels of Catalyst Y-177®. When 0.4% or 0.2% catalyst was used, the DMA specimens were made by drying a 1.5 mm thick casting at 60 °C for 16 hours and curing it at 180 °C for 5 hours and then 260 °C for 5 hours. This casting was thin so that the removal of by-products was fast enough to ensure the absence of bubbles in the majority of the casting, and DMA specimens could be obtained. For thick castings suitable for plane strain fracture toughness test, the catalyst level was lowered to 0.05% and a prolonged curing cycle was used. All Phase I toughened resin samples were cured with 0.05% Catalyst Y-177® via the prolonged curing cycle. DMA specimens of these samples were made by cutting a small piece and polishing it to the correct dimensions.

In Table 5.1, the codes of Phase I PDMS and their meanings are repeated.

Table 5.1. Phase I PDMS.

Code	Degree of Polymerization	Terminal Functionality
PAE2	8	Triethoxy
PAE	16	Triethoxy
KPE	55	Triethoxy

5.3. Results and Discussions.

5.3.1. Major transitions of silicone resins.

Silicone resins have several major transitions in a DMA spectrum, depending on their composition and structure. Although the structure of the resins has not been fully understood, an assignment of the DMA peaks at different temperatures to different compositions is possible.

It has been documented[1] that pure methyl T resin has a major glass transition at about 40 °C[1]. This was verified by Figure 5.1, the DMA spectrum of a methyl T resin MetFlex, made by hydrolyzing pure methyl trichlorosilane and then polymerizing the hydrolyzate. It showed a major glass transition from 40 to 50 °C, and a secondary transition at a lower temperature, ~ -25 °C. In Figure 5.2, the DMA spectrum of a phenyl T resin, a broad glass transition from 180 to 225 °C was seen. It also had a secondary transition at 70 °C. They overlapped and formed an extremely broad peak. The DMA spectra of the network polymers, formed by co-hydrolyzing different amounts of KP-80 with 100 part phenyl trichlorosilane and 10 part phenyl methyl dichlorosilane and then polymerizing the hydrolyzate were included in Figure 5.3. They showed two or three peaks, depending on the composition. The highest temperature transition was for the phenyl T structure, and the lowest temperature transition for the PDMS. The transition in the intermediate position was possibly due to the phenyl methyl di units connected with other components, but other assignments may be possible. The PDMS transition at -120 to -125 °C is well documented, as was the phenyl secondary transition, near -100°C.

5.3.2. Unmodified 4-3136 resin.

In Chapter 3 the DMA spectra of these castings were compared to validate the prolonged curing cycle. In this section the resin network structure, rather than the similarities among different castings, will be emphasized.

The loss factor, tan δ, and the storage modulus of unmodified 4-3136 resin castings are shown in Figures 5.4 and 5.5 as functions of temperature. Each damping mechanism in the material, including long range chain/network motions, and localized chain/network or side group motions, was detected by a peak in the tan δ curve[2,3]. The former was termed the glass transition, and the latter a secondary transition. In the DMA spectrum of 4-3136 resin a glass transition of a domain also corresponded to a sudden drop in storage modulus, while secondary transitions did not significantly vary the overall decreasing trend of the storage modulus with rising temperature.

In the DMA spectra of 4-136 resin there are five damping peaks. The first, second and third comprise the broad glass transition. This transition spanned a temperature range from ~50 °C to ~160 °C and the modulus drop across the transition is small. The third peak is actually a shoulder on the second. It became more prominent for the specimen made with the prolonged curing cycle using a low catalyst level. At a lower temperature, peak 4 was very broad and not easy to distinguish from the others, but it appeared consistently and in modified resins it became more prominent. The fifth peak, at -107.6 °C, appeared consistently in all the samples.

These spectra indicate a non uniform distribution of composition in the resin network. The highest temperature peak, at 190 °C, reflected regions containing more phenyl T units which promoted a rigid network. Peak 2 was believed to be due to less rigid domains containing more methyl T structure. Peak 3 could be the secondary damping of the Phenyl T structure, or the damping of phenyl methyl di or diphenyl units. Peak 4 was assingned to the secondary transition of the methyl T rich region, and peak 5 the phenyl group β transition.

The non uniform distribution of composition was also inferred from the ^{29}Si NMR studies. The peak positions and their integrals of ^{29}Si NMR spectra were included in Table 5.2 for the unmodified 4-3136 resin. Those of KPE toughened resins were also included. In the unmodified 4-3136 resin pre-polymer, 20.1% (mole, the same in the following) silicon nuclei were phenyl T units and 32.7% were methyl T. The initial monomer mixture contained 40% phenyl T monomer and 45% methyl T monomer. It was clear that the conversion of methyl T monomer to T structure, at the pre-polymer stage, was more complete than the phenyl T monomer. The resin blocks formed first had a higher amount of methyl T units. At the pre-polymer stage, substantial amount of di phenyl units remained dangling as active ends, in the form of $M^{(Ph_2,OZ)}$, along with larger amounts of $D^{[ph,oz]}$ and $D^{[Me,oz]}$. Smaller amounts of other types of ends also existed. The amount of $D^{[ph,oz]}$ ends, as a result of partial reaction of the phenyl T monomer, was twice that of the $D^{[Me,oz]}$ ends, the result of partial condensation of the methyl T monomer. This again verified the easier transformation of the methyl T monomer to an actual T structure. Therefore it was expected that the domains

formed at the pre-polymer stage had more methyl T units, and those formed subsequently had more phenyl T units. The latter, with the highest Tg, comprised the resin nodules that were not involved in plastic deformation without toughening.

5.3.3. Phase I PDMS modified 4-3136 resin.

Phase I toughened resins also showed a non uniform structure, indicated by multiple transitions in a DMA spectrum. This was also verified by the ^{29}Si NMR studies, included in Table 5.2. The peak integrals of KPE toughened resins were representative of all Phase I toughened resins, and those of other Phase I toughened resins were not included.

Similar to the unmodified resin, PAE2 toughened 4-3136 resins displayed five peaks in their DMA spectrum (Figure 5.6). No glass transition was seen at -125 °C, where the unrestricted PDMS glass transition should be, but the secondary transition at -108 °C increased in height and was broadened. With an increasing amount of PAE2, peaks 1 and 2 shifted to lower temperatures, while their heights increased.

The increasing height of the damping peaks reflects the increased toughness of the resin with increasing PAE2 content. The absence of the PDMS transition below room temperature showed that long range motion of the short PDMS segments was severely restricted by the surrounding resin network. These short chains were, as shown earlier, less effective toughener.

When a longer chain Phase I PDMS, the KPE, was reacted into the network, the chain motion was less restricted. In Figures 5.7 and 5.8, a glass transition at -126 °C, was seen in addition to the major glass transition at much higher temperature. This was attributed to the PDMS segments. The position of the peak was unaffected by the connection between the PDMS and the network, yet it was evident that the PDMS chains were reacted into the network. With an increasing amount of KPE, the height of peak 1 increased, but the height of the PDMS damping peak at -126 °C remained constant. The presence of low temperature damping, and the increased damping of the highest Tg domains, contributed to the increased toughness of the polymer.

When PAE, with an intermediate DP of 16, was reacted in, the PDMS transition appeared again, but at -109 °C (Figure 5.9); because of the restriction of the network on the long range motion of the PAE chain, its transition was moved up by 17 °C and merged with the secondary transition at -108 °C. A modulus drop at this temperature helped distinguish a different mechanism in addition to the -108 °C β transition (Figure 5.10). In Figure 5.9, the dynamic mechanical spectra of the unmodified resin and other Phase I modified resins were also included. The height of the damping peak in the vicinity of 200 °C increased when the Phase I rubber was introduced into the resin, but KPE increased it the most. The more effectively increased damping of high Tg domains and the less restricted mobility of the PDMS chain correlated with the better toughening effect of KPE.

5.4. Conclusions.

4-3136 resins, both toughened and untoughened, are non uniform and contain domains of relatively higher methyl T or phenyl T level. In the unmodified resin the damping of the higher Phenyl T domains, with a high Tg, was low.

The mobility of the pre-reacted Phase I PDMS segments in the modified 4-3136 resin depended on the segment length. At DP 8, the segments were severely restricted; at DP 16, the segments were less restricted; at DP 55, the mobility of the segments was least affected by the resin network. The less restricted mobility of the Phase I PDMS chains related to the better toughening effect in the 4-3136 resin.

When pre-reacted with the resin, the less restricted PDMS segments increased energy dissipation of the high Tg domains. The increased damping of these domains, along with the mobility of PDMS segments, appeared to be directly related to the improved fracture toughness of the resin. Most probably these high Tg domains were the undeformed nodules, and the increased mechanical damping of these nodules toughened the 4-3136 resin.

DMA analysis also showed that the mechanical properties of rigid silicone resins had a very low temperature dependence. The glass transition

was extremely broad and the modulus drop over the glass transition was extremely small compared with other resins such as epoxies.

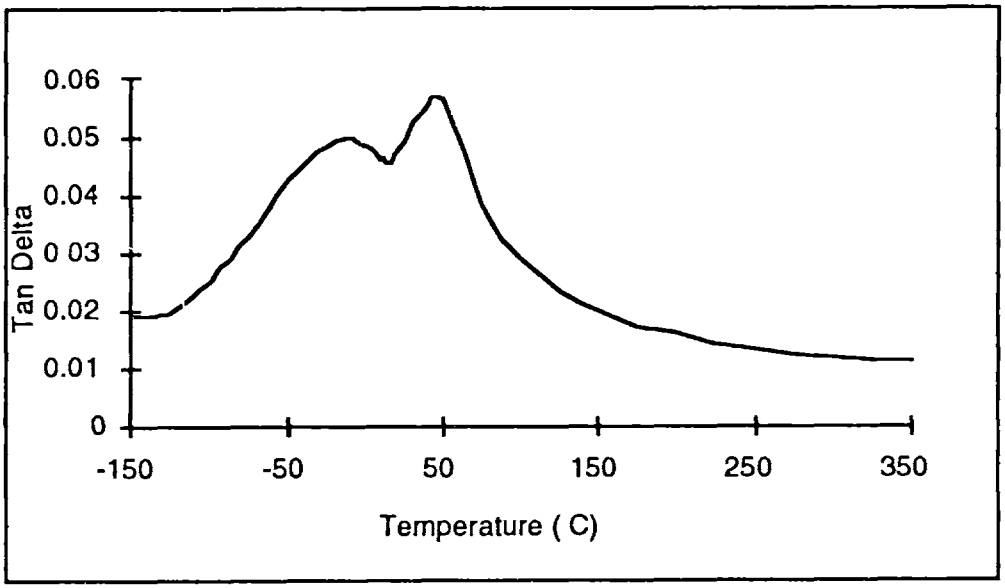

Figure 5.1. Loss factor, tan δ, of a methyl T resin, Metflex.

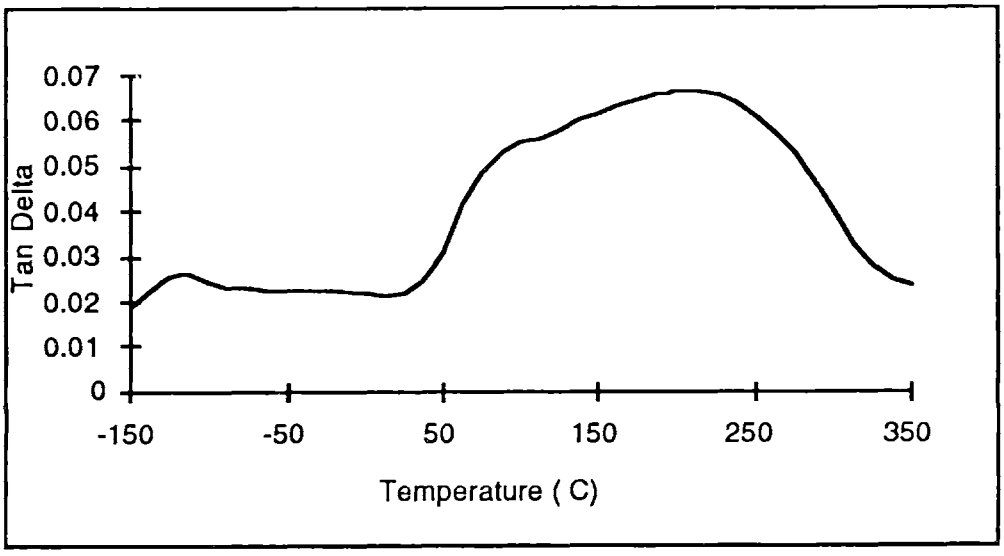

Figure 5.2. Loss factor, tan δ, of a Phenyl T resin.

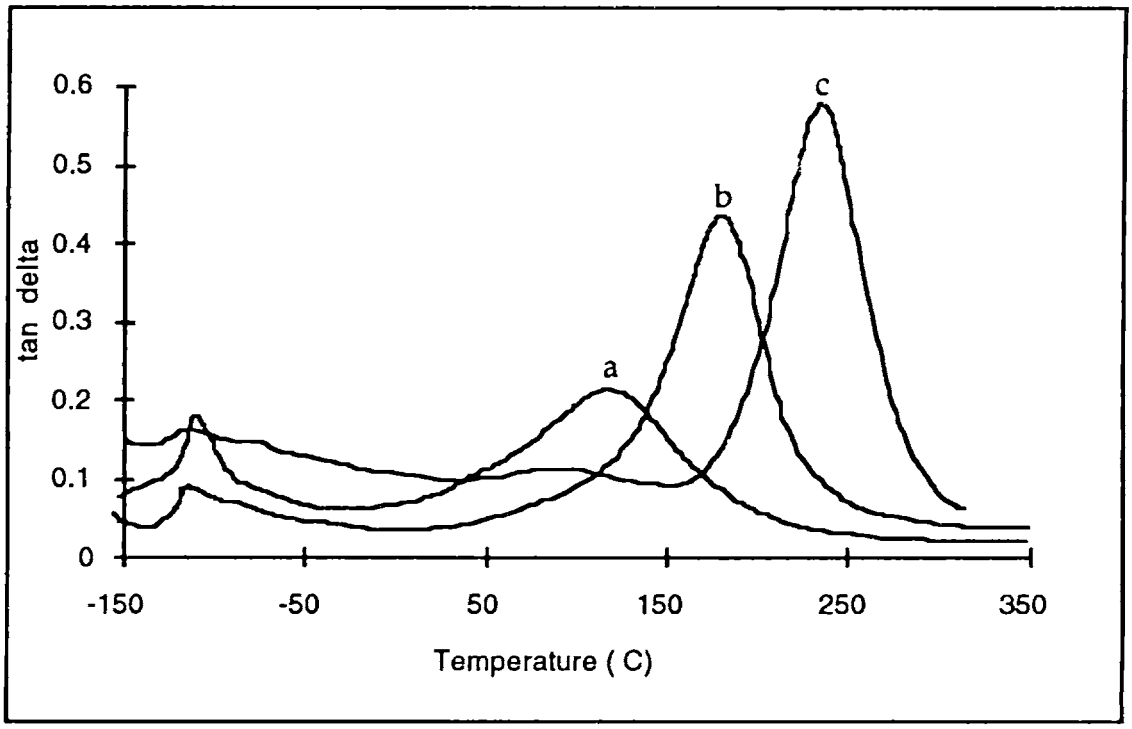

Figure 5.3. Loss factor, tan δ, of the network polymers. KP-80 content, a: 46; b: 29; c: 18 parts.

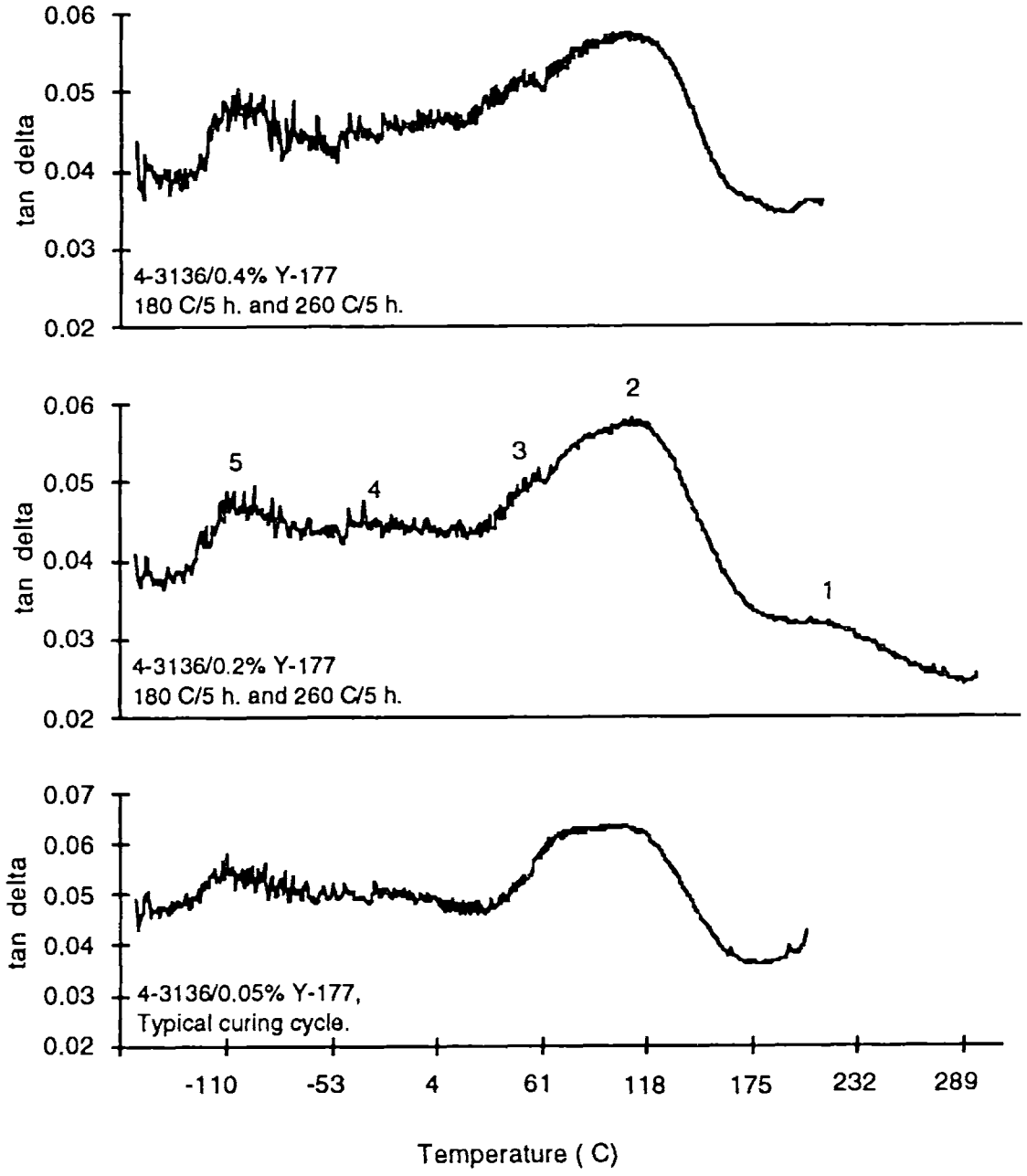

Figure 5.4. tan δ of unmodified 4-3136 silicone resin cured with various amounts of Catalyst Y-177 and under different conditions as specified in the plots.

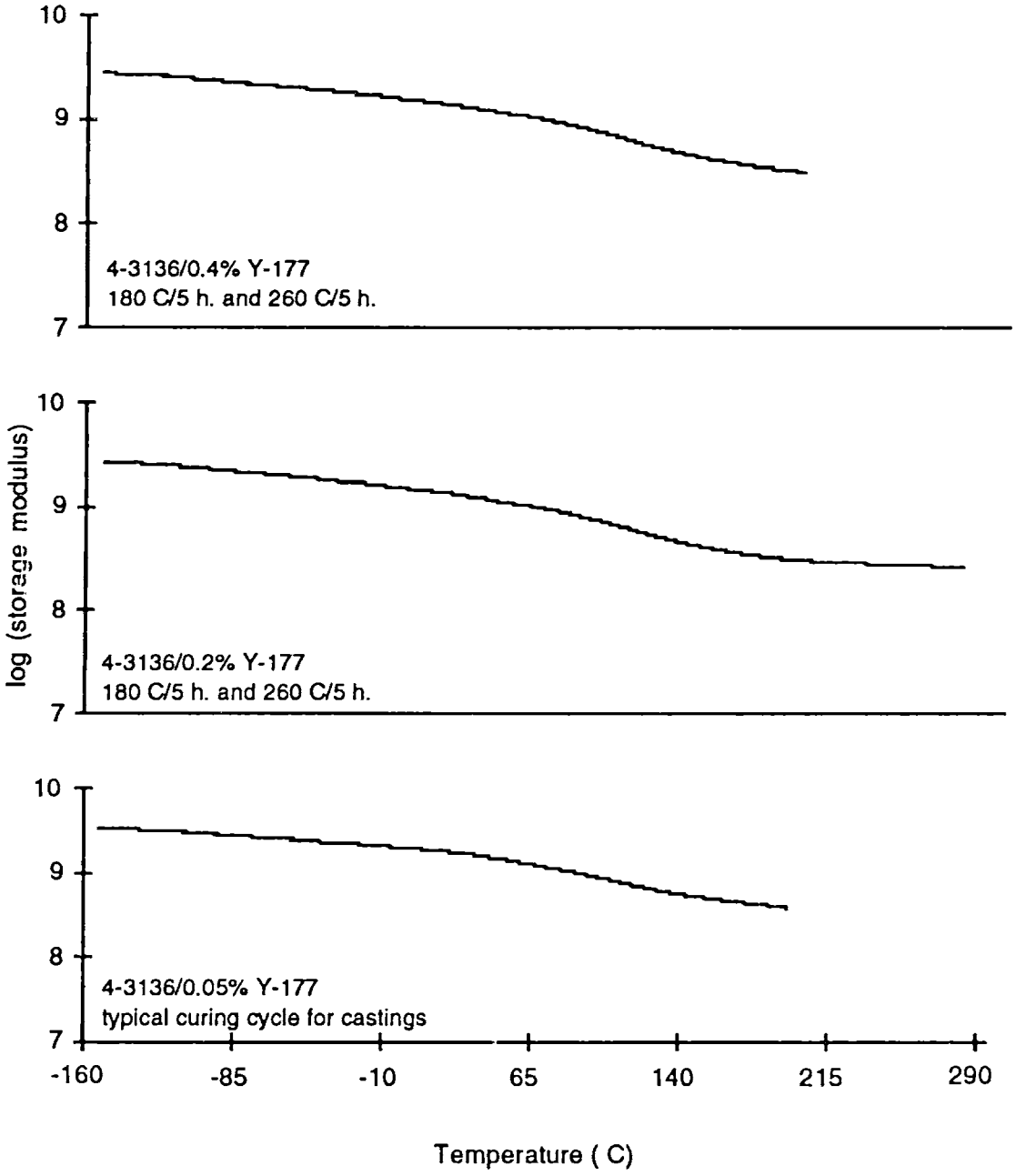

Figure 5.5. Dynamic modulus of unmodified 4-3136 resin cured with various amounts of Catalyst Y-177 and under different conditions. DMA was done at a frequency of 1 Hz.

Table 5.2. ^{29}Si **NMR peaks and their integrals (units: %)**

position (ppm)	Type of Nucleus	4-3136 resin	5% KPE modified	10% KPE modified	15% KPE modified	20% KPE modified
-78.7	phenyl T	20.1	21.60	22.05	22.09	22.08
-69.9	$D^{[ph,oz]}$	20.8	22.14	19.73	19.67	20.14
-63.9	methyl T	32.7	32.34	33.06	33.63	35.05
-58.1	$M^{[ph,(oz)_2]}$	2.3	2.11	2.92	2.80	13.46*
-55.6	$D^{[Me,oz]}$	10.8	10.21	10.09	10.11	
-45.9	D^{Ph_2} + $M^{(OZ)_2}$	2.9	2.96	3.37	3.58	2.98
-37.4	$M^{(Ph_2,OZ)}$	4.9	4.31	4.33	3.88	3.11
-31.7	$D^{(Me,Ph)}$	4.5	4.34	4.49	4.21	3.17
-21	D^{Me_2}		6.91	13.08	20.03	28.40

* $M^{[ph,(oz)_2]}$ and $D^{[Me,oz]}$ combined.

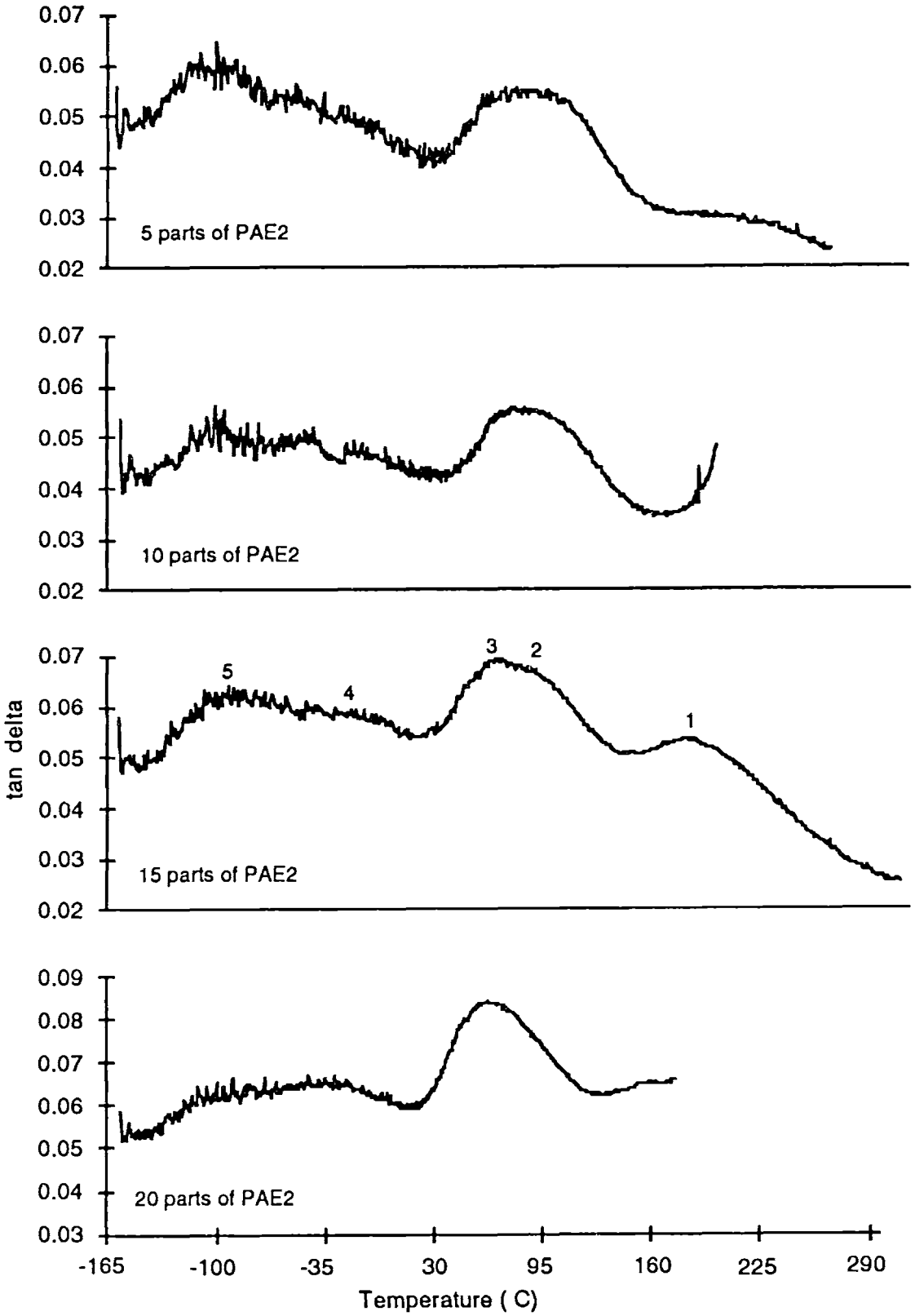

Figure 5.6. tan δ of 4-3136 resin modified by pre-reacting with various amounts of PAE2.

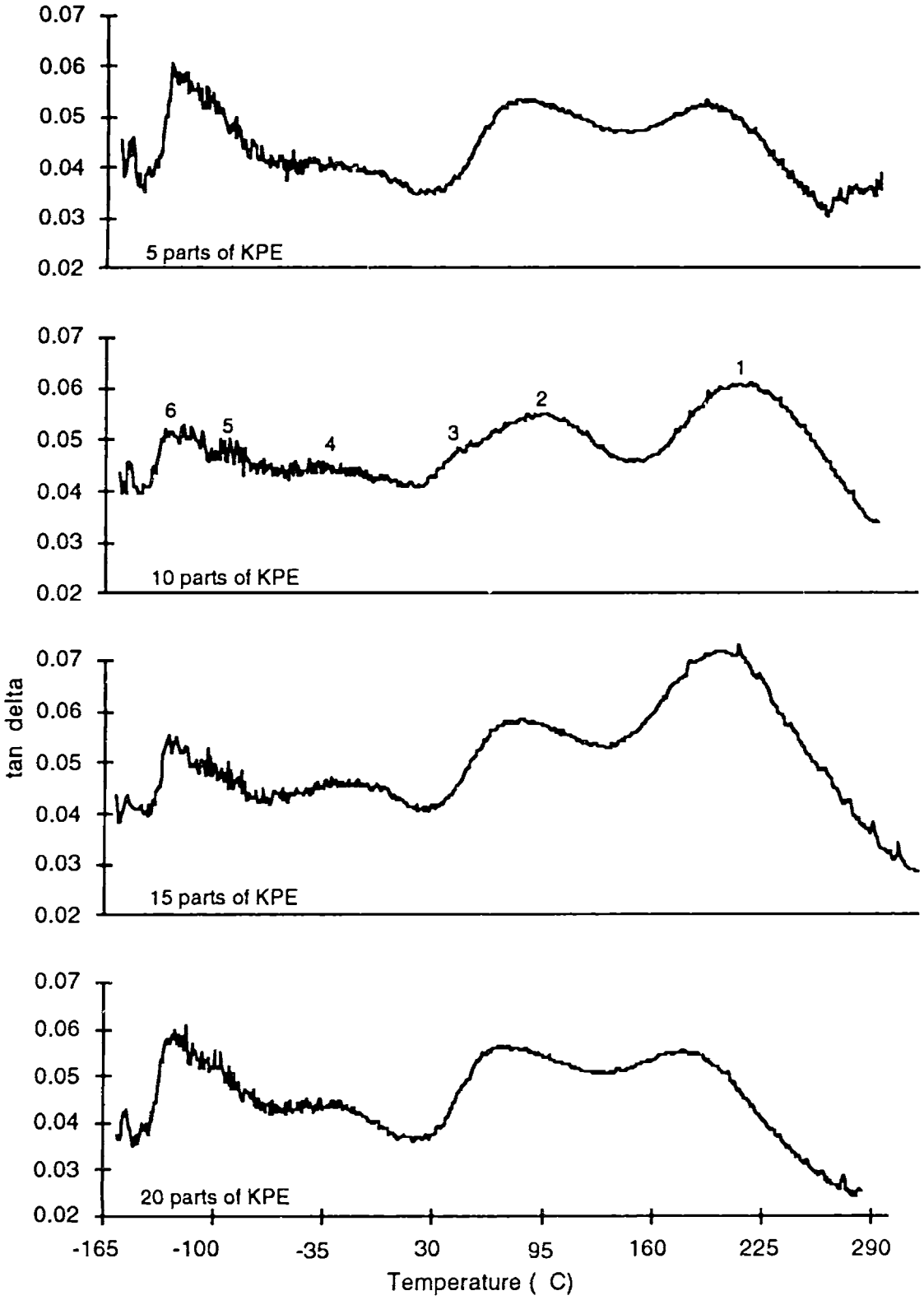

Figure 5.7. tan δ of 4-3136 resin modified by pre-reacting with various amounts of KPE.

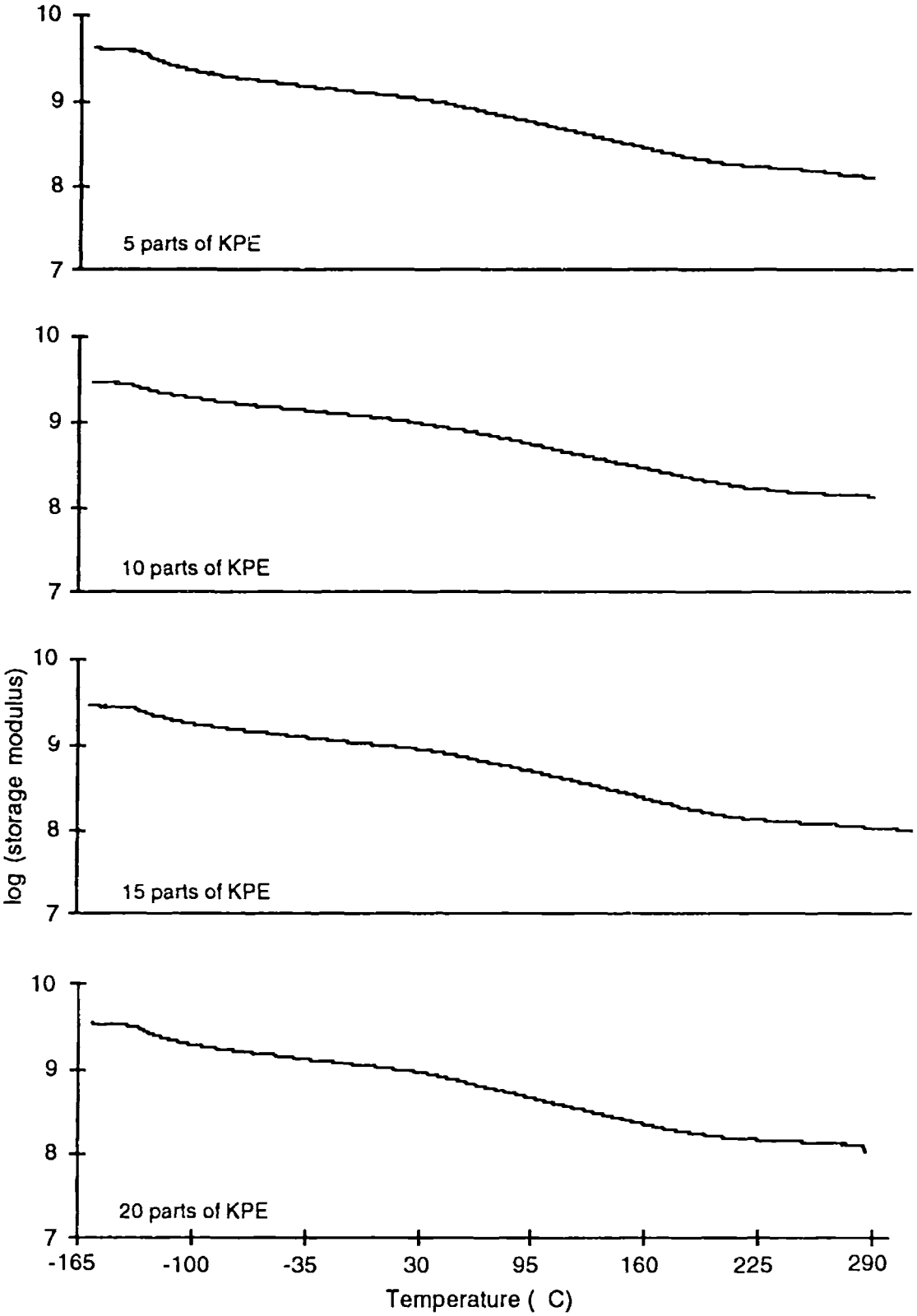

Figure 5.8. Storage modulus of 4-3136 resin modified by pre-reacting with various amounts of KPE.

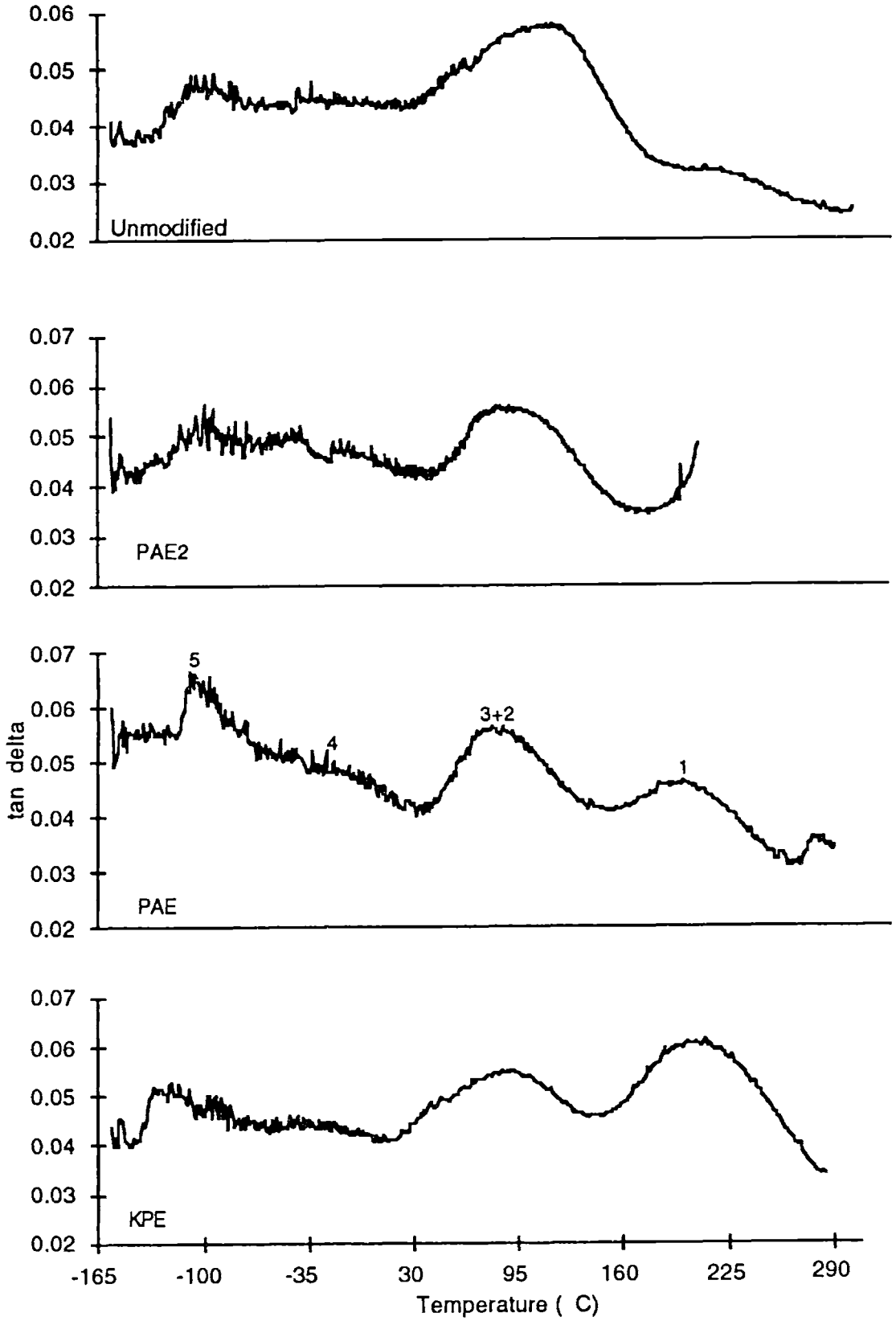

Figure 5.9. tan δ of 4-3136 resin modified by pre-reacting with 10 phr functionalized PDMS of different chain lengths.

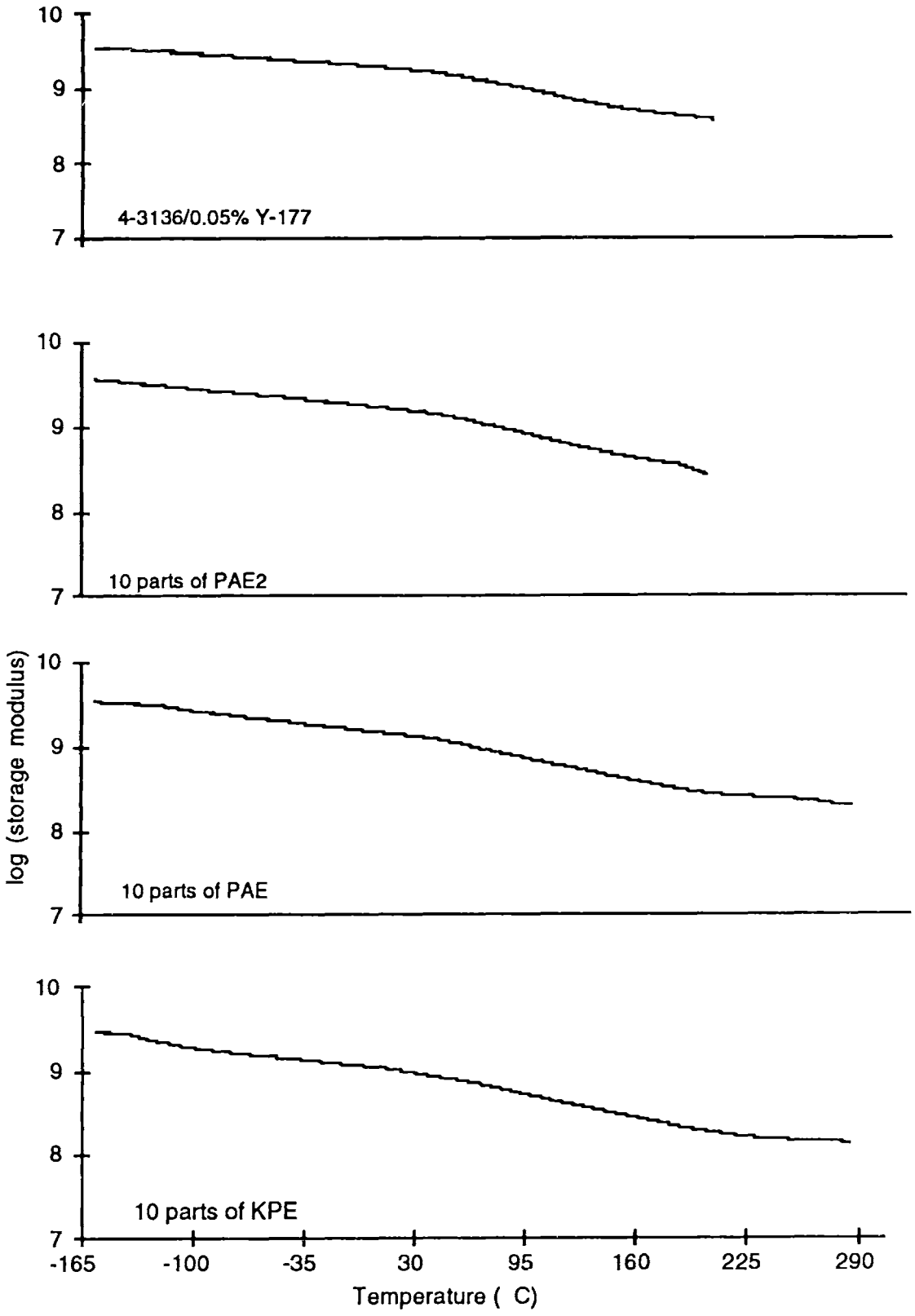

Figure 5.10. Storage modulus of 4-3136 resin modified by pre-reacting with functionalized PDMS of various chain lengths.

Chapter 6. Thermal Stability.

6.1. Introduction.

Usually the heat resistance of a polymer will be degraded when it is toughened by the addition of rubber. This is especially important if high temperature applications are sought.

In a toughened silicone resin, two factors may degrade its thermal stability after toughening: the residue catalyst in the cured resins, and the easier degradation of toughenersl[1-9]. Small amounts of certain catalysts are extremely detrimentall[10]. For example, trace KOH, the residue of a common polymerization catalyst, may lower the degradation temperature of silicone rubber by more than 100 °C. Tin catalyst is believed to facilitate the degradation also. However titanium tetrabutoxide has been shown to do no harm to the thermal stability of silicone rubbers. Therefore titanium tetrabutoxide has been used as the catalyst for the coupling reaction.

While organic rubbers have been successful tougheners for polymers used at room or slightly elevated temperatures, they are not suited for rigid silicone resins because of their oxidation at high temperature. A semi-inorganic rubber, PDMS, has been chosen as toughener for rigid silicone resins. It has a slightly stronger backbone bond and is much more resistant to thermal oxidation. Compared to the resin its linear structure and high methyl content may still cause some sacrifice in thermal stability, but the oxidation of methyl also depends on oxygen transport, and the depolymerization of the linear structure on the mobility of the chain. Both can be manipulated by end linking of the Phase I chain and by the mophorlogy in a Phase I/II toughened system.

Based on the results of TGA analysis, the effect of toughening, by Phase I or by Phase I/II combinations, on the thermal stability will be discussed in this Chapter. The impact of chain length on thermal stability of Phase I toughened resins, and that of phase separation in Phase I/II combination toughened resins will be shown. The degradation due to oxidation and that due to thermal dissociation are differentiated by TGA analysis in different

types of environment, i.e. air or argon. It will be seen that the heat resistance of the rigid silicone resin is unaltered after toughening with PDMS.

6.2. Experimental.

TGA was run on a Seiko SSC/5200 TGA/DTA 320 system. Purging gas was air or argon flowing at 150 ml/minute. The temperature was raised 10 °C/minute from room temperature to 800 °C. Precautions were taken to ensure that approximately the same amount of material, 13.5±0.2 mg in this test, was used for each sample. And the sample should be one piece, to eliminate the possibility of being blown away and ensure that the sample specific surface area did not vary from run to run. From the record of weight retention with time a 5% weight loss temperature was identified.

6.3. Results and Discussion.

6.3.1. Phase I toughened resins aged in air.

In Figure 6.1 is plotted the weight retention curve of the unmodified 4-3136 resin. It started losing weight slowly around 400 °C and the weight loss accelerated around 550 °C. Most weight loss occurred in a temperature range from 400 to 660 °C. Outside this range no obvious weight loss was detected. After 660 °C, 58% of the original weight was retained. The two major weight loss peaks, one at 540 °C and another at 640, are shown in Figure 6.2.

Figure 6.3 shows the weight retention of unmodified resin and two resins modified by 10 and 20 part PAE2 (DP 8). The curves overlap and no significant difference is seen. In Figure 6.4, the two weight loss peaks were actually shifted slightly toward higher temperatures by the PAE2 toughening.

The modification by PAE (DP 16) did not significantly change the thermal weight loss. As shown by Figures 6.5 and 6.6, the weight retention curves of unmodified resin and the resins modified by PAE are not distinguishable, and the weight loss peaks actually move slightly toward higher temperatures.

If the DP of the Phase I PDMS is 55 (KPE), the thermal stability of the resin is slightly degraded. See Figures 6.7 and 6.8. In Figure 6.7, the weight of the KPE toughened resin starts to decrease earlier and faster, but the absolute difference between them and the unmodified resin is very small. The final weight retention in all Phase I toughened resins was slightly higher than the unmodified resin, consistent with the slightly higher silicon content in PDMS. In Figure 6.8, a small weight loss peak appeared at 420 °C when 10 to 20 parts of KPE were incorporated. This peak was absent in the PAE2 or PAE toughened resins and is believed to be attributable to the depolymerization of the PDMS chain. A longer chain, linked to the resin network only at the ends, is more mobile and the depolymerization of it becomes easier. The thermal depolymerization of PDMS involved the cooperation of inter or intra molecular segments to form cyclic intermediate states and then small cyclics. The higher mobility of the chain and the proximity of neighboring chains would facilitate this process. (The increased mobility of the chain segments of larger DP was shown in Chapter 5 by DMA analysis). The increased depolymerization is more clearly seen in Figure 6.9, where the weight loss rate of unmodified resin and the resins modified by 20 part Phase I PDMS of various DP are plotted. In Figure 6.8 the other two major weight loss peaks are shifted first toward higher temperatures and then with the addition of more KPE in the opposite direction. The easier depolymerization is believed to have caused the small degradation in thermal stability.

The effect of Phase I modification on thermal stability is best summarized by the 5% weight loss temperature plotted in Figure 6.10. It is seen that longer chains decrease thermal stability faster, but the absolute difference is small. Except for the resins containing high levels of KPE, the 5% weight loss temperatures of Phase I toughened resins are not significantly different from that of the unmodified resin.

6.3.2. Phase I/II combination toughened resins in air.

In Table 6.1, the compositions of the Phase I/II combination toughened samples, and the corresponding Phase I toughened samples, are listed. The

5% weight loss temperature of the Phase I/II combination toughened resins are included.

The introduction of Phase II into a Phase I toughened resin, shown by samples DP to DY, raised the 5% weight loss temperature. The representative samples of this Phase I/II combination toughened resins, DX and DY, had the same 5% weight loss temperature as the unmodified resin. When the Phase II PDMS was absent, the 5% weight loss temperature was 13 °C lower(BAA).

The weight retention curves in Figure 6.11 are plotted to compare resins toughened in different ways. These include the unmodified one and the ones modified by 10 part Phase I PDMS PAE, and by a combination of 10 part PAE with 2.5 or 5 part Phase II PDMS of DP 375. They were aged in air. As seen in the Figure, the Phase I modification lowers the curve slightly, but the Phase I/II modification raises it to above the unmodified one. In Figure 6.12, the weight loss peaks of the Phase I/II combination toughened resins are moved to higher temperature. Generally the incorporation of Phase II PDMS lowers the weight loss of the Phase I toughened resins.

The TGA curves of the Phase I/II toughened resins are independent of the Phase II PDMS chain length within the experimented range. In Figure 6.13, the weight retention curves of 4-3136 resin toughened by 10 part KPE and 2 part Phase II PDMS are plotted for comparison. The Phase II PDMS were of DP 246, 375 or 586. The Phase I and Phase II PDMS were pre-reacted with the 4-3136 resin pre-polymer in a 31 wt.% toluene solution. Practically, no difference is seen in Figure 6.13, and in Figure 6.14, the weight loss rates are very similar.

The pre-reaction concentration only slightly affects the thermal weight loss of the Phase I/II combination resins. In Figures 6.15 and 6.16 the resin samples modified by 10 part KPE and 2 part Phase II PDMS of DP 375 were compared. The Phase I and II PDMS were pre-reacted with the 4-3136 resin pre-polymer in a 28 wt.% (DR), 31 wt.%(DT), and 37 wt.%(DV) toluene solution. Higher pre-reaction concentrations did not significantly change the weight retention and the weight loss rate. In Figure 6.17 and 6.18 the resin samples containing 10 part KPE and 2 part Phase II PDMS of DP 586 are compared. The KPE and Phase II PDMS were pre-reacted in a 26 wt.%(DS), 31

wt.%(DU), or 37 wt.%(DW) toluene solution. Again a trend similar to that observed in Figures 6.15 and 6.16 is seen.

6.3.3. Toughened resins aged in argon.

As seen in Table 6.1, in argon the 5% weight loss temperature of the unmodified resin and the Phase I modified resins are about 20 to 30 degrees higher than in air. This gap narrows slightly in Phase I/II combination resins.

In Figure 6.19 the weight retention of 4-3136 resin in air and argon is plotted. The final weight retention of the resin in argon was 85%, much higher than 58% in air. In argon the resin initially decomposed slightly faster at around 460 °C but much more slowly after 500 °C. In Figure 6.20, where the rate of weight loss is plotted, this trend is seen. In argon a small weight loss peak appears earlier at around 460 °C. This peak is believed to be attributed to the easier depolymerization due to the absence of oxidation. The two major weight loss peaks in air became one in argon, in a position intermediate between the two peaks in air. This probably results from the suppression of the oxidation of the hydrocarbon substituents. Oxidation is believed to increase crosslink density and slow the release of small cyclics or cages at 460 °C, but facilitate decomposition at higher temperature.

In Figures 6.21 and 6.22, two resins toughened by 10 part Phase I PDMS of different lengths are compared. They were aged both in air and in argon. Figure 6.21 shows that the weight retention curves of toughened and untoughened resins are similar in both types of environment. Figure 6.22 shows the shape change of the weight loss peak in the two environments. One distinct feature is evident: in argon the weight loss peak of KPE toughened resin, which was more prone to depolymerization, moved to a lower temperature and it coincided with the position of the first weight loss peak in air.

In Figures 6.23 and 6.24, the TGA curves of two resins toughened by Phase I/II combinations, both in air and in argon, are plotted. The final weight retention of the resin in argon was much higher, although the initial weight loss curves are similar. In air two weight loss peaks appear, in argon

these two become one, but the position of it is at a temperature slightly lower than the first peak in air. As discussed, the longer chain and proximity of neighboring PDMS chains in a phase separated system facilitate depolymerization, whereas in such a phase separated system more methyl groups are shielded by the tightly crosslinked matrix from oxygen in air. The shielding of linear chains from oxygen by the matrix in a Phase I/II toughened resin improves the thermal resistance in air, but the easier deploymerization in the same resin lowers the thermal resistance in argon.

6.4. Conclusions.

The heat resistance of the 4-3136 resin is retained after toughening by both Phase I and Phase I/II PDMS. Longer chain Phase I PDMS slightly lower thermal resistance in air. Shorter ones barely produce any significant difference. Phase I/II combination toughened resins show unaltered thermal stability as compared to the unmodified resin. Due to the phase separated structure, PDMS is protected from oxygen in air. In argon oxidation is suppressed, and thermal depolymerization is facilitated, probably due to the lack of oxidation which at moderately elevated temperatures increased crosslink density and retarded depolymerization.

Table 6.1. Compositions and 5% Weight Loss temperatures of silicone resins in Air and Argon.

Sample ID	4-3136	PAE2	PAE	KPE	PDMS DP 246	PDMS DP 375	PDMS DP 586	Reactant Concentration*	5% Weight Loss Temp., in Air†	5% Weight Loss Temp., in Argon†
4-3136	100	—	—	—	—	—	—	—	528.3	548.9
BU	100	10	—	—	—	—	—	50%	517.3	548.9
BAA	100	—	10	—	—	—	—	50%	515.2	546.6
CA	100	—	—	10	—	—	—	38%	510.1	535.5
CO	100	–	—	—	—	2	—	unknown	—	—
DP	100	—	–	8	2	—	—	unknown	524.3	535.4
DQ	100	—	—	10	2	—	—	31%	526.4	—
DR	100	–	—	10	—	2	—	28%	528.7	—
DS	100	—	–	10	—	—	2	26%	539.8	—
DT	100	—	—	10	–	2	—	31%	517.6	—
DU	100	–	—	10	—	—	2	31%	530.9	—
DV	100	–	–	10	—	2	—	37%	519.7	—
DW	100	—	–	10	–	—	2	37%	519.8	544.4
DX	100	–	10	—	—	2.5	—	31%	533.2	526.5
DY	100	–	10	—	—	5	—	31%	528.8	542.1

*weight percentage.
†°C.

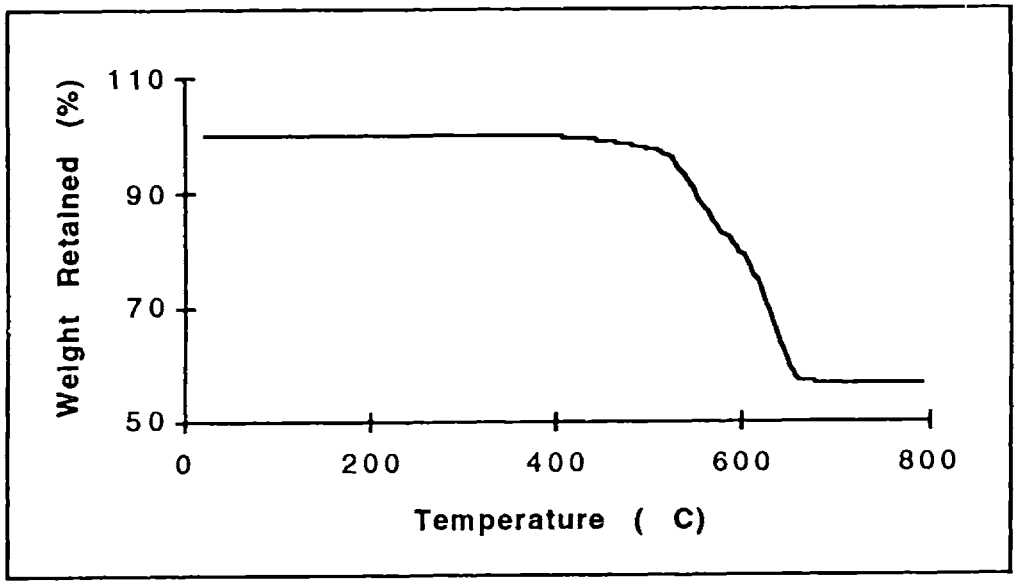

Figure 6.1. Weight retention of 4-3136 resin in air.

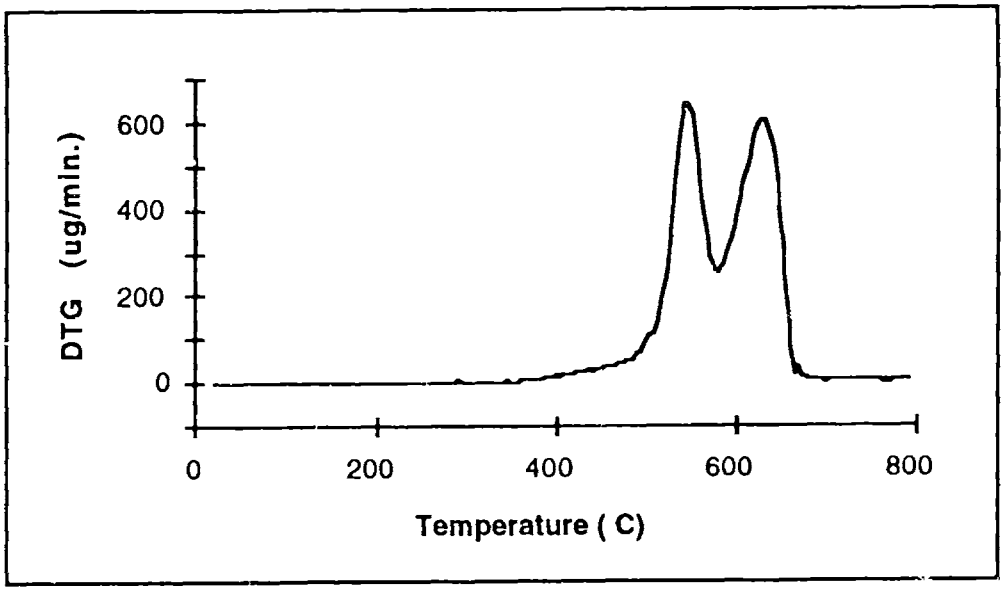

Figure 6.2. Weight loss rate (DTG) of 4-3136 resin in air.

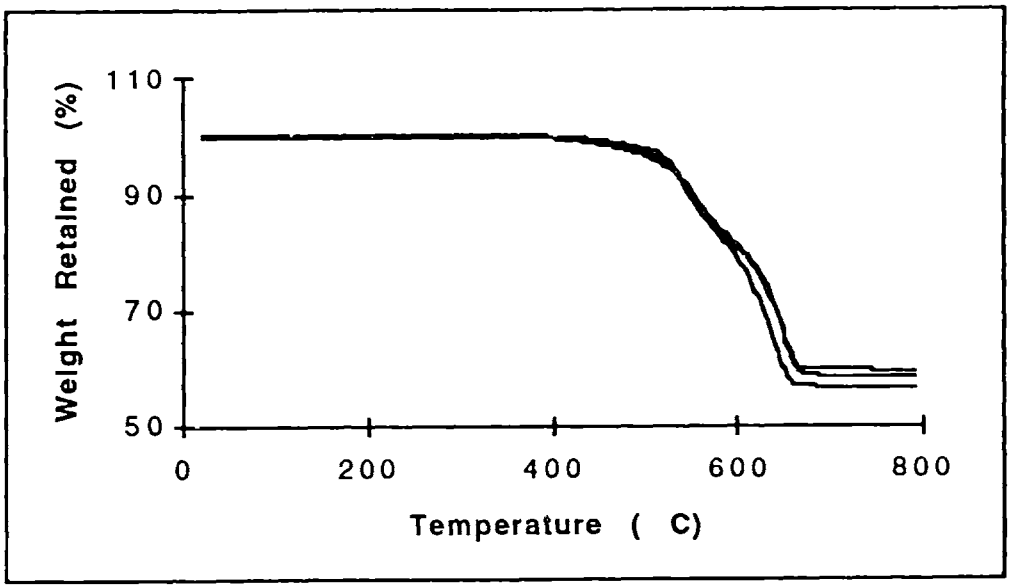

Figure 6.3. Weight retention in air of 4-3136 resin modified by 0, 10, 20 part PAE2. Above 600 °C curves from bottom to top.

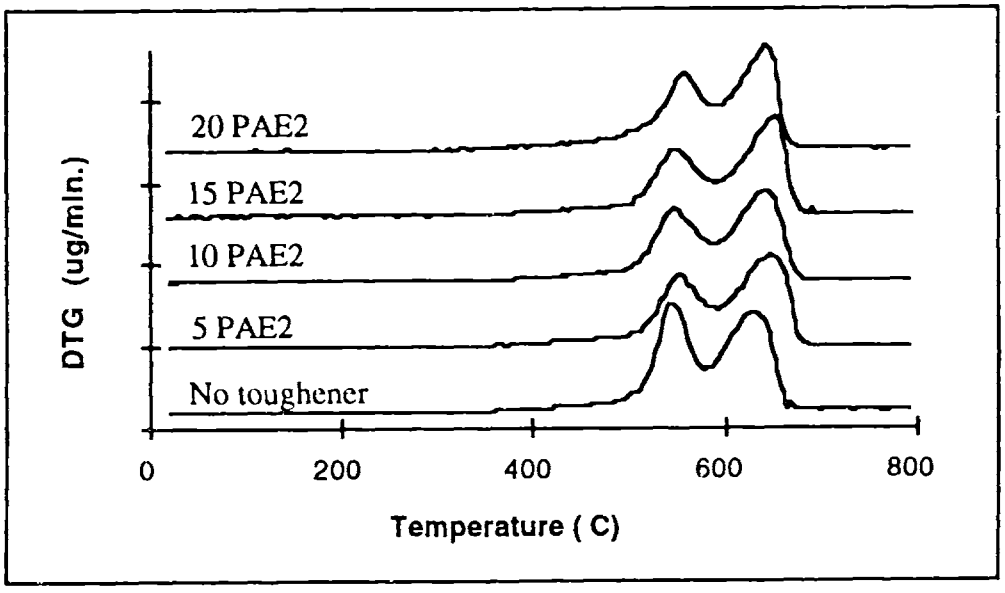

Figure 6.4. Weight loss rate (DTG) in air of 4-3136 resin modified by 0, 5, 10, 15, 20 part PAE2. Vertical axis: 500 per division.

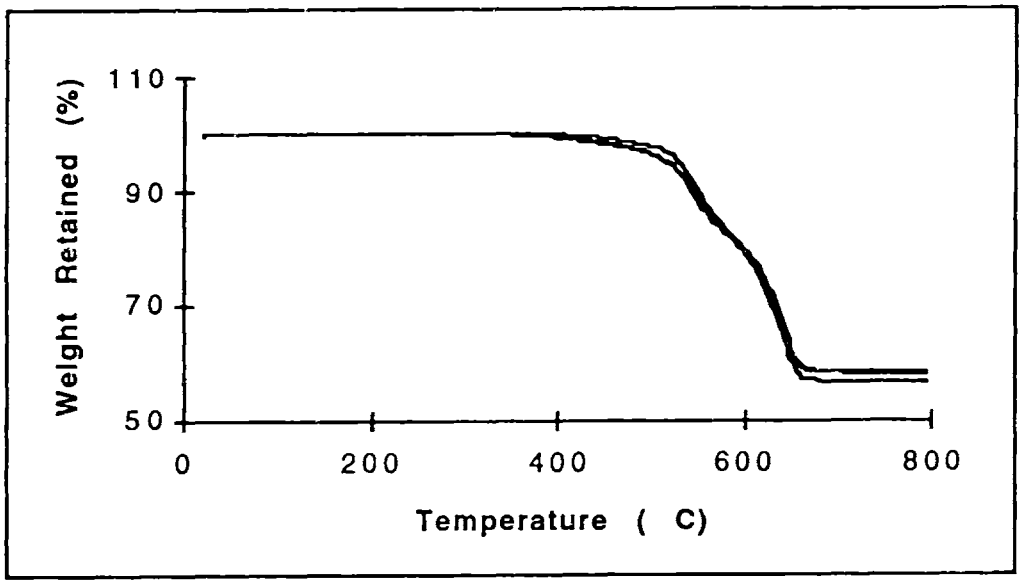

Figure 6.5. Weight retention in air of 4-3136 resin modified by 0, 10, 20 part PAE. Above 600 °C, curves from bottom to top.

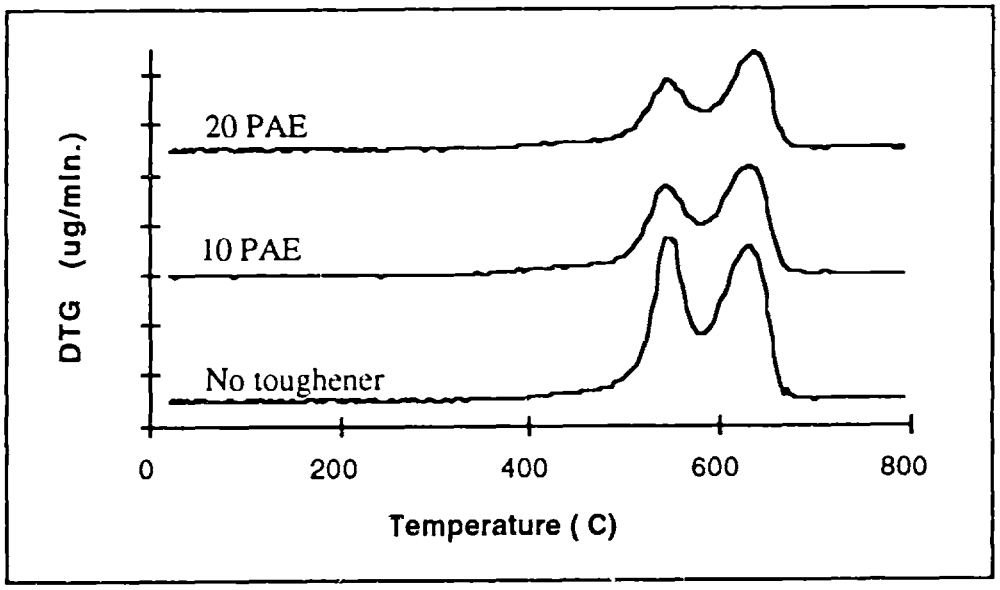

Figure 6.6. Weight loss rate (DTG) of 4-3136 modified by 0, 10, 20 part PAE. Vertical axis: 200 per division.

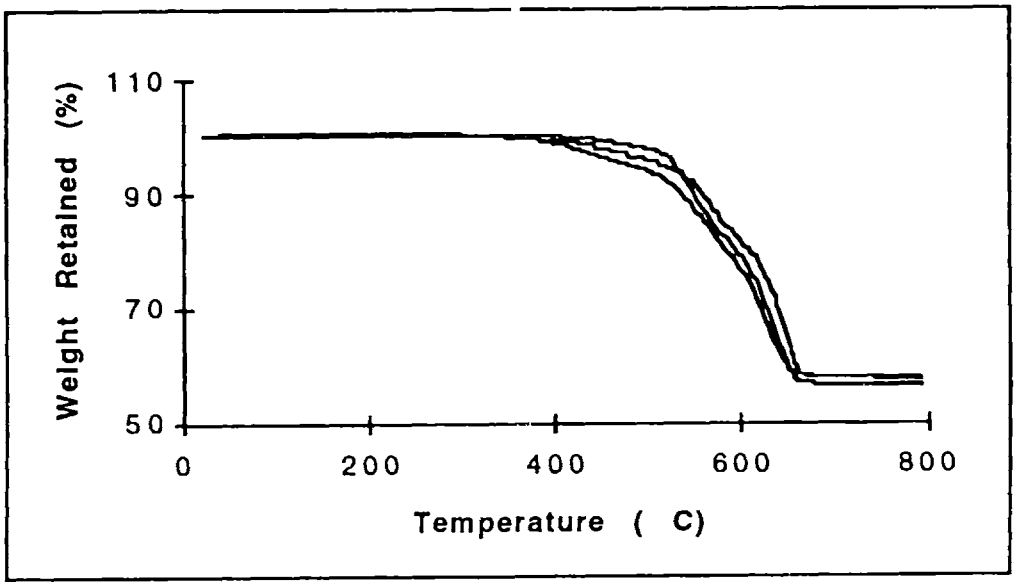

Figure 6.7. Weight retention in air of 4-3136 resin modified by 0, 10, 20 part KPE, from top to bottom.

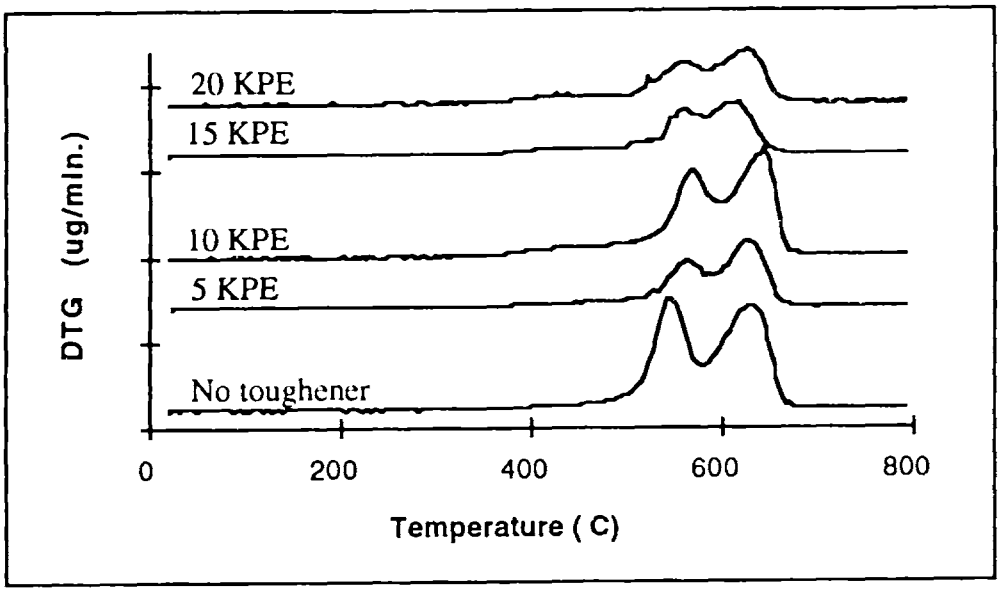

Figure 6.8. Weight loss rate (DTG) in air of 4-3136 resin modified by 0, 5, 10, 15, 20 part KPE, from bottom to top. Vertical axis: 500 per division.

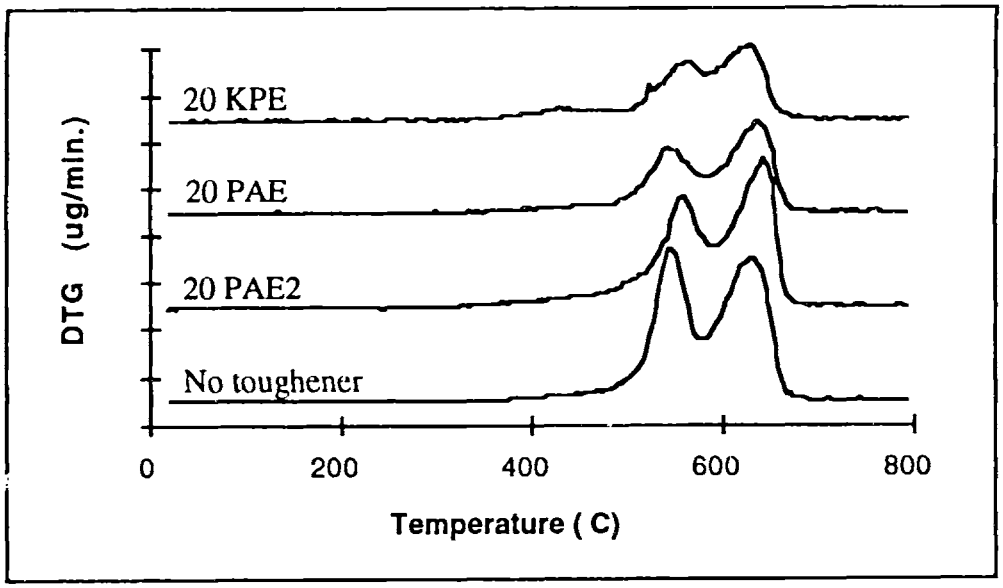

Figure 6.9. Weight loss rate (DTG) in air of 4-3136 resins, unmodified and modified by 20 part PAE2, PAE and KPE, from bottom to top. Vertical axis: 200 per division.

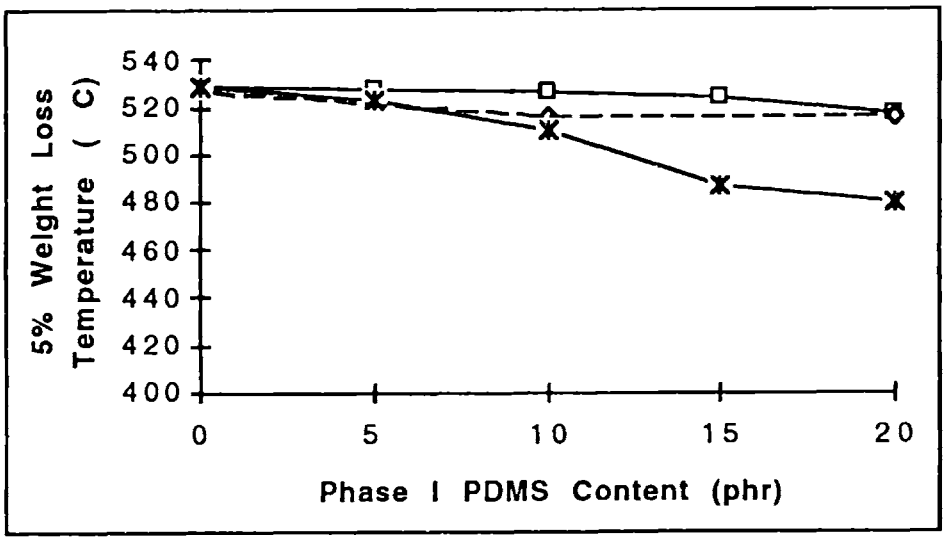

Figure 6.10. 5% weight loss temperature of Phase I toughened 4-3136 resins, from top to bottom: PAE2, PAE, KPE toughened.

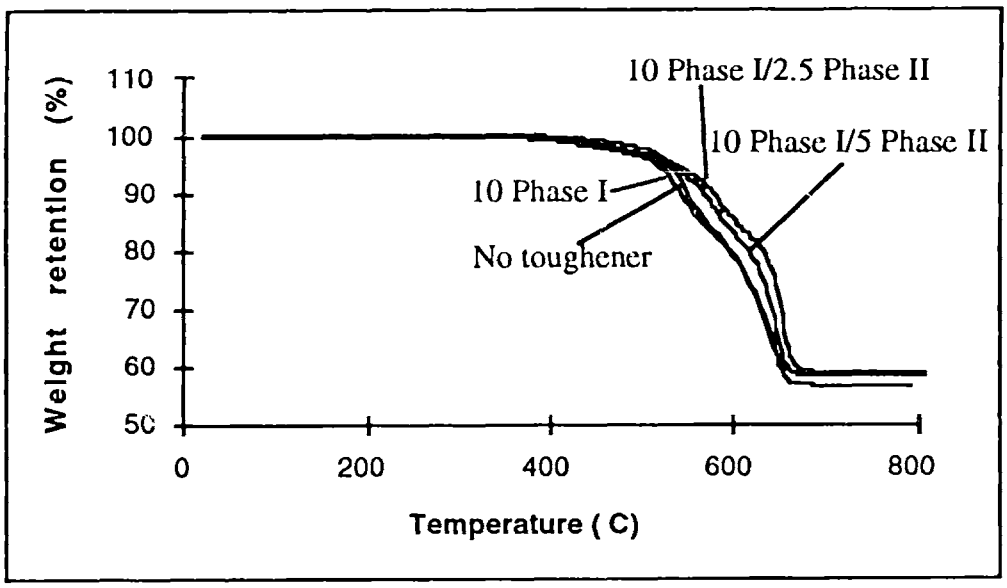

Figure 6.11. Weight retention in air of untoughened 4-3136 resin, and resins toughened by 10 part PAE, and a combination of 10 part PAE/2.5 or 5 part Phase II PDMS of DP 375.

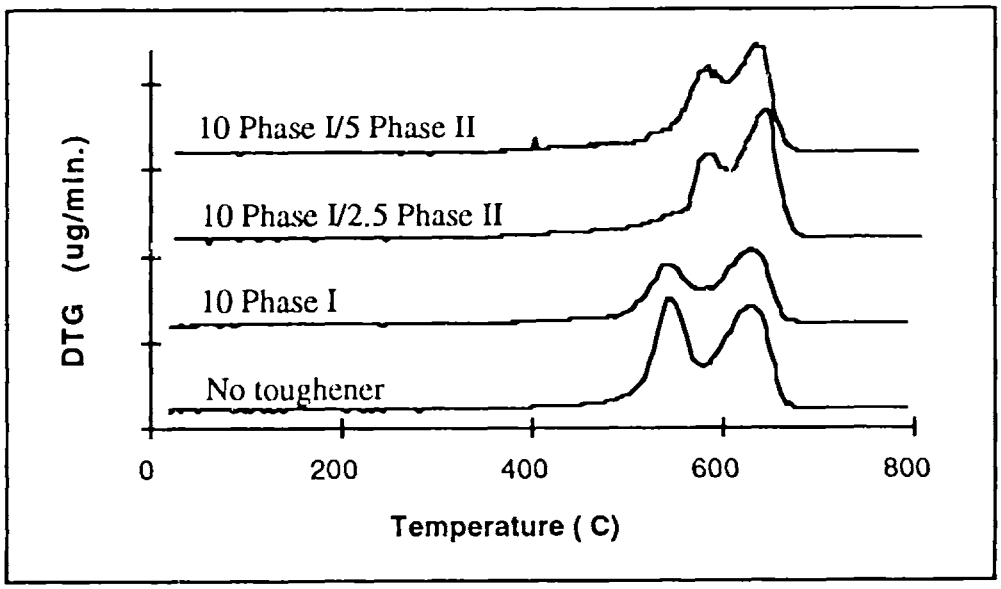

Figure 6.12. Weight loss rate (DTG) in air of untoughened 4-3136 resin, and resins toughened by 10 part PAE, and a combination of 10 part PAE/2.5 or 5 part Phase II PDMS of DP 375. Vertical Axis: 500 per division.

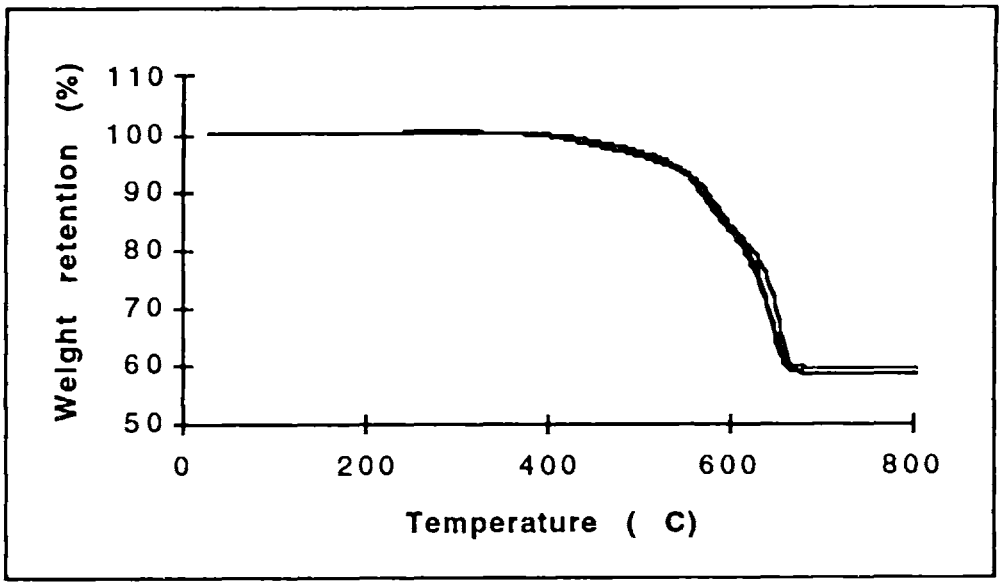

Figure 6.13. Weight retention in air of the 4-3136 resins toughened by a combination of 10 part KPE and 2 part Phase II PDMS of DP 246 (DQ), 375(DT), and 586(DU). The pre-reaction was done in a 31 wt.% solution.

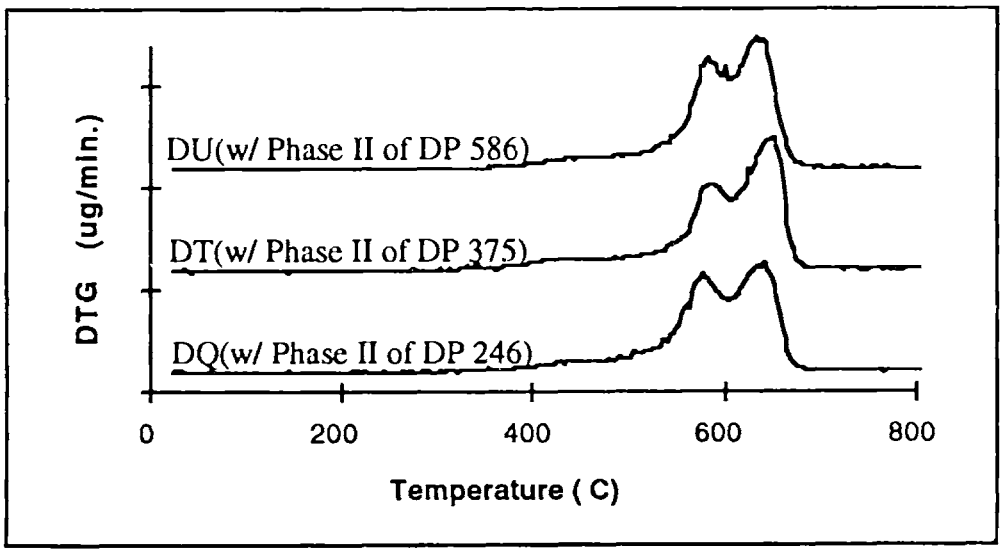

Figure 6.14. Weight loss rate (DTG) in air of the 4-3136 resins toughened by a combination of 10 part KPE and 2 part Phase II PDMS of DP 246 (DQ), 375(DT), and 586(DU). The pre-reaction was done in a 31 wt.% solution. Vertical axis: 500 per division.

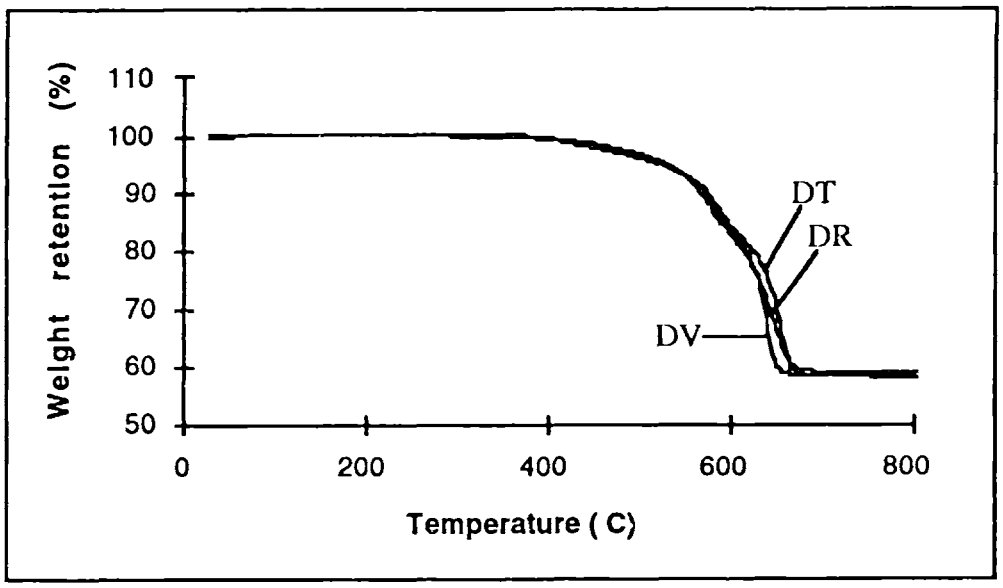

Figure 6.15. Weight retention in air of the 4-3136 resin toughened by a combination of 10 part KPE and 2 part Phase II PDMS of DP 375. The pre-reaction was done in a 28 wt.%(DR), 31 wt.%(DT), and 37 wt.%(DV) solution.

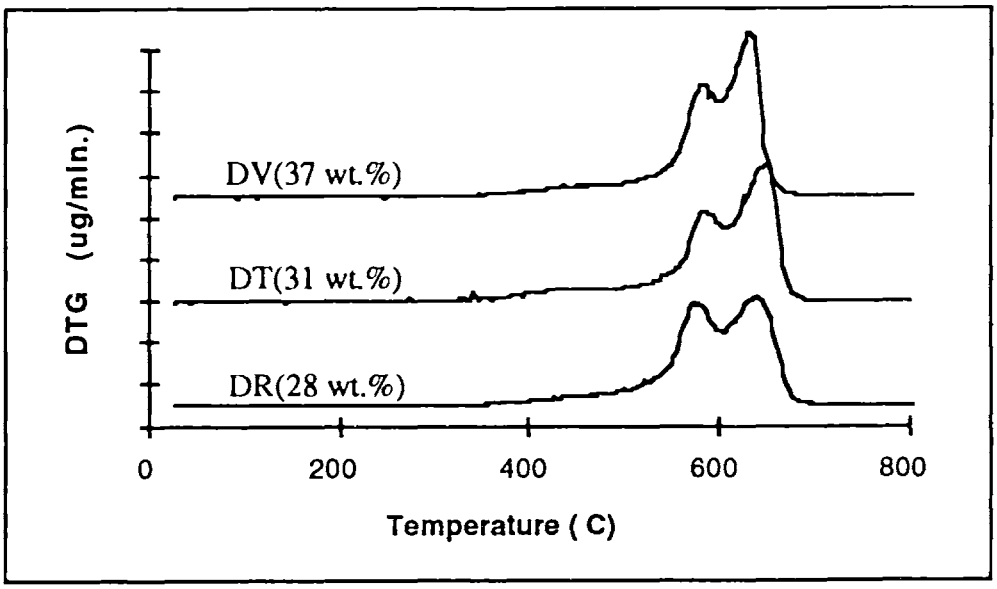

Figure 6.16. Weight loss rate (DTG) in air of the 4-3136 resin toughened by a combination of 10 part KPE and 2 part Phase II PDMS of DP 375. The pre-reaction was done in a 28 wt.%(DR), 31 wt.%(DT), and 37 wt.%(DV) solution. Vertical axis: 200 per division.

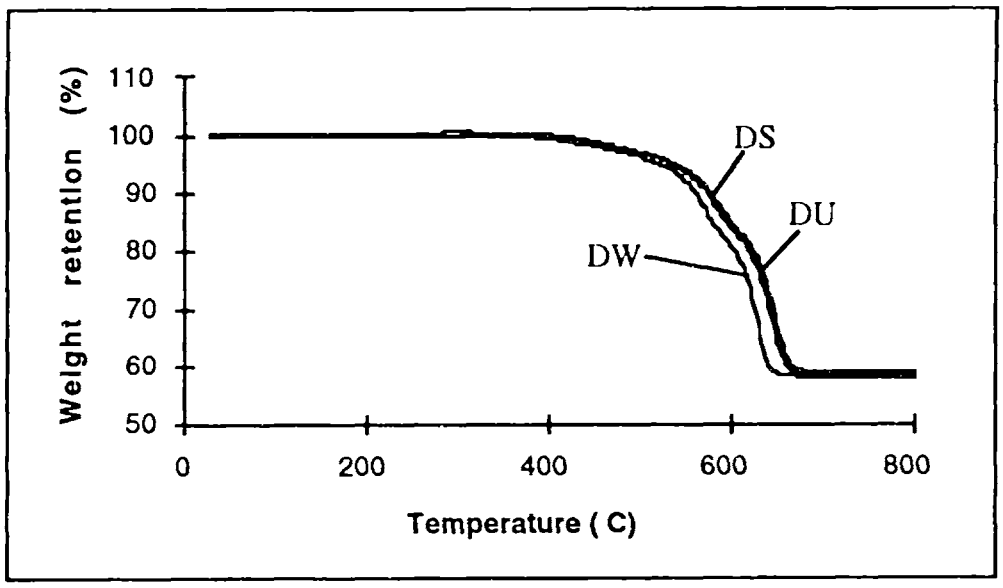

Figure 6.17. weight retention in air of the 4-3136 resin toughened by 10 part KPE and 2 part Phase II PDMS of DP 586. Pre-reacted in a solution of 26, 31 and 37 wt.% (DS, DU, DW).

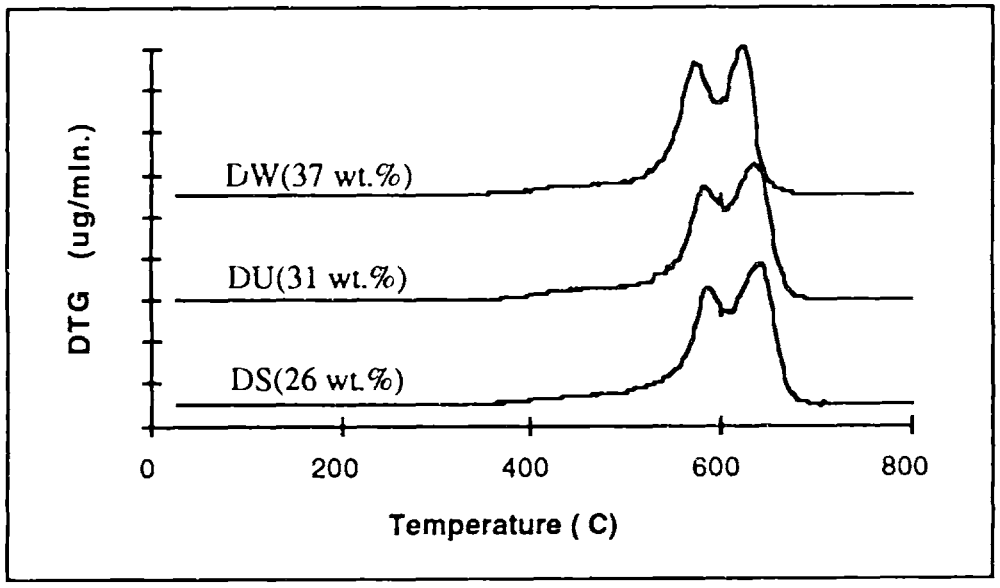

Figure 6.18. Weight loss rate (DTG) in air of the 4-3136 resin toughened by 10 part KPE and 2 part Phase II PDMS of DP 586. Pre-reacted in a solution of 26, 31 and 37 wt.% (DS, DU, DW). Vertical axis: 200 per division.

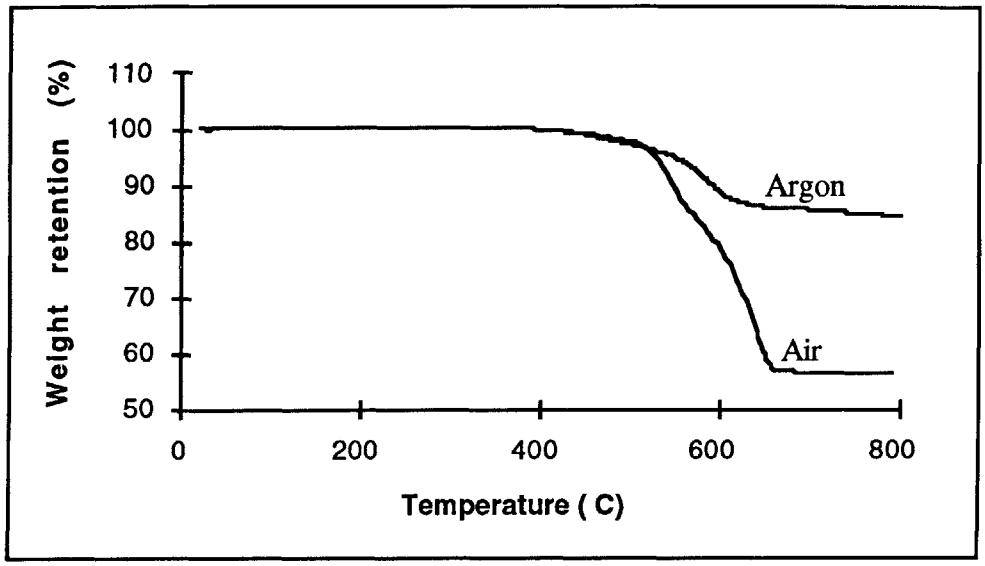

Figure 6.19. Weight retention of unmodified 4-3136 resin in air and argon.

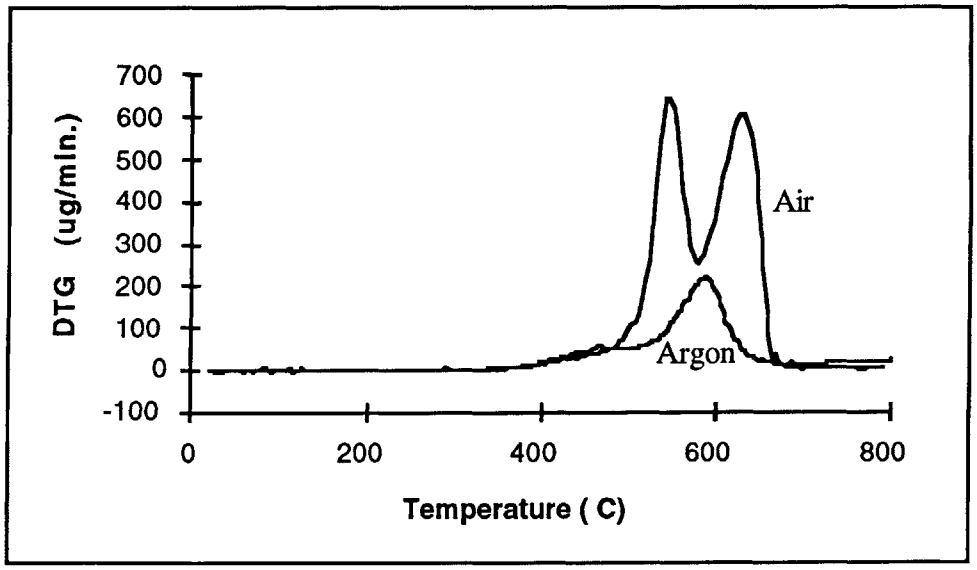

Figure 6.20. Weight loss rate (DTG) of unmodified 4-3136 resin in air and argon.

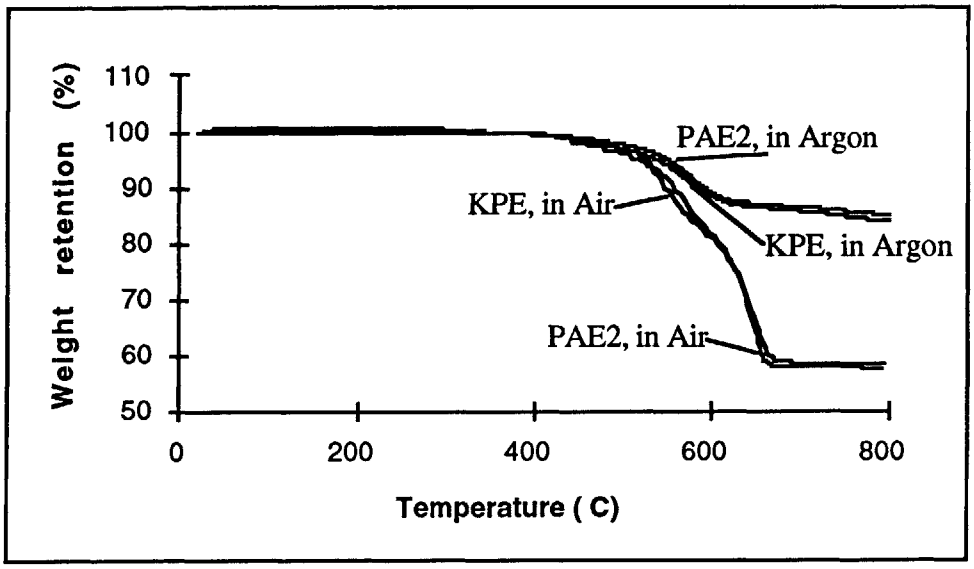

Figure 6.21. Weight retention, in air and argon, of 4-3136 resin toughened by 10 part Phase I rubbers of different chain lengths.

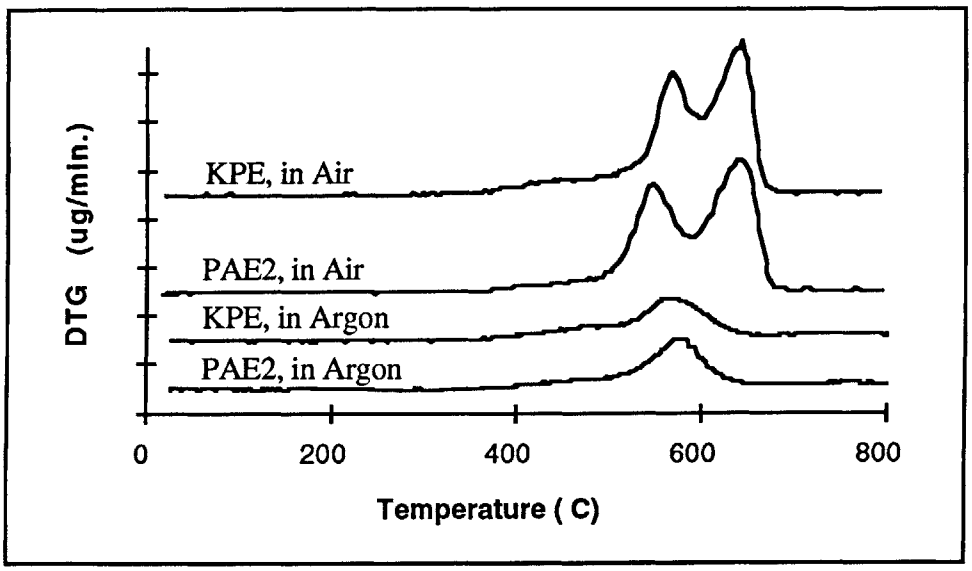

Figure 6.22. Weight loss rate (DTG), in air and argon, of 4-3136 resin toughened by 10 part Phase I rubbers of different chain lengths. Vertical axis: 200 per division.

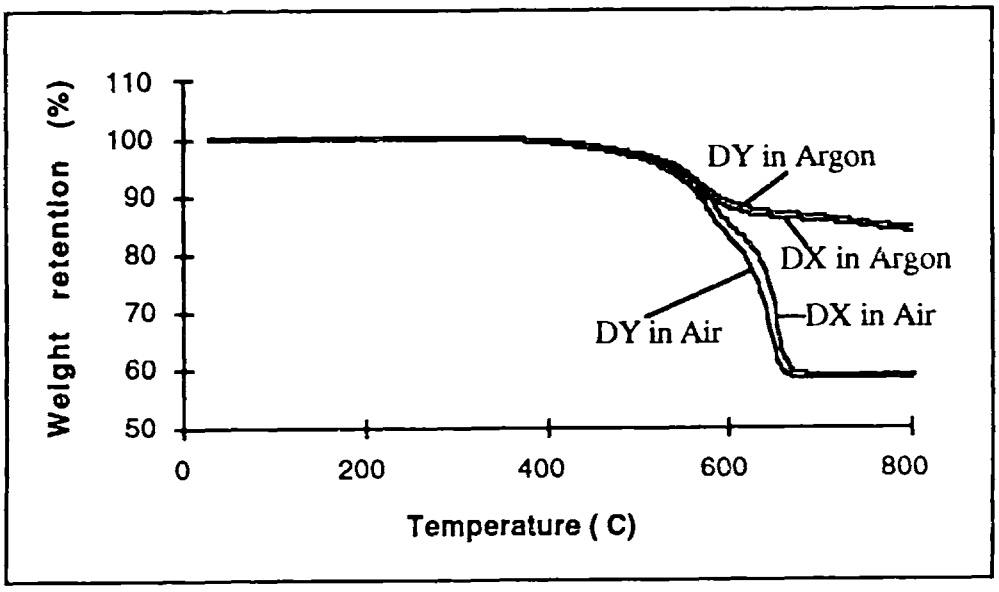

Figure 6.23. Weight retention, in air and argon, of DX and DY, the resins toughened by 10 part PAE and 2.5 or 5 part Phase II PDMS of DP 375.

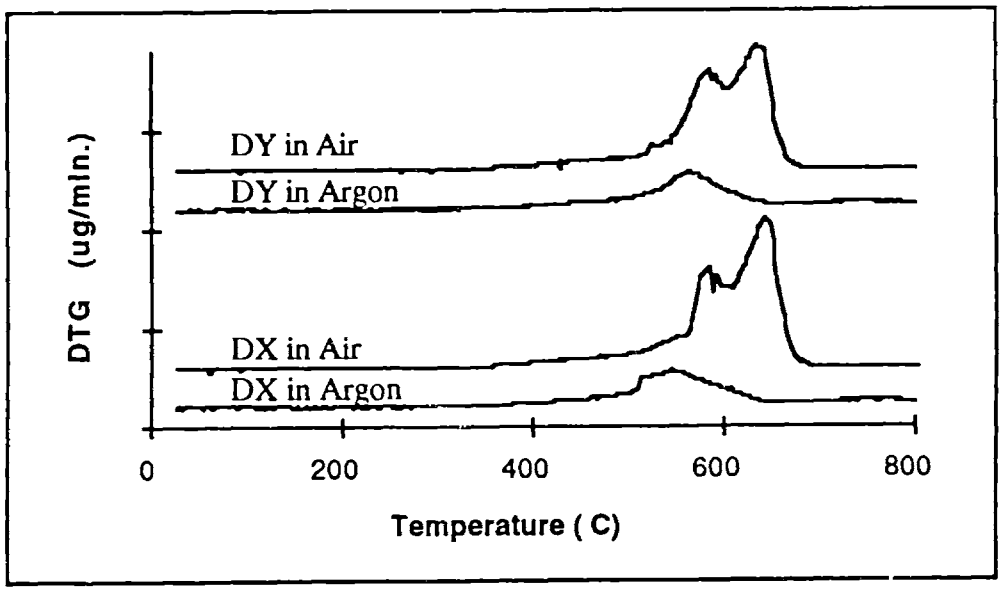

Figure 6.24. Weight loss rate (DTG), in air and argon, of DX and DY, the resins toughened by 10 part PAE and 2.5 or 5 part Phase II PDMS of DP 375. Vertical axis: 500 per division.

Appendices

Appendix I

Table A1. Mechanical properties of modified and unmodified 4-3136.

Modifier	Strain @ Yield (%)	Flexural Strength (MPa)	Young's Modulus (GPa)	Toughness (KJ/m^3)*	K_{Ic} ($MPam^{1/2}$)	G_{Ic} (J/m^2)
none	2.46 (0.34)	37.73 (3.01)	1.88 (0.11)	5.89 (1.30)	0.253 (0.005)	38.31 (1.46)
5 wt.% PAE2	2.37 (0.27)	34.11 (1.81)	1.70 (0.12)	4.98 (0.90)	0.310 (0.012)	61.75 (4.19)
10 wt.% PAE2	4.20 (0.69)	42.62 (3.66)	1.51 (0.19)	12.14 (3.20)	0.301 (0.019)	77.62 (9.80)
15 wt.% PAE2	4.48 (0.79)	41.17 (2.85)	1.33 (0.06)	12.50 (3.27)	0.306 (0.013)	86.44 (7.27)
20 wt.% PAE2	5.76 (0.94)	43.05 (2.97)	1.26 (0.07)	17.38 (4.27)	0.324 (0.008)	116.90 (7.32)
10 wt.% PAE	4.32 (0.33)	40.92 (1.61)	1.54 (0.03)	12.27 (1.52)	0.366 (0.042)	119.34(27.47)
20 wt.% PAE	6.92 (0.58)	41.01 (1.56)	1.24 (0.04)	20.86 (2.44)	0.380 (0.035)	195.44(39.46)
5 wt.% KPE	4.43 (0.71)	43.96 (3.12)	1.57 (0.06)	13.30 (3.22)	0.375 (0.008)	123.65 (5.18)
10 wt.% KPE	7.43 (0.84)	48.49 (3.62)	1.37 (0.14)	26.12 (4.56)	0.453 (0.015)	267.83(17.26)
15 wt.% KPE	6.62 (1.09)	43.52 (0.50)	1.22 (0.13)	20.47 (4.00)	0.473 (0.020)	285.41(24.49)
20 wt.% KPE	6.13 (1.38)	35.37 (3.41)	1.08 (0.02)	15.55 (5.36)	0.453 (0.016)	312.18(22.43)

*area under the stress-strain curve.

Appendix II. Etching of Rubber Particles in the Resin Matrix

Etching of the polished surfaces of the 4-3136 resin containing rubber particles by a KOH aqueous solution provides useful information about the particle size and serves to verify the rubbery composition of the particles.

This method is based on the principle that siloxane bonds can be broken in the presence of KOH and water, and the rubber, with a linear structure and two ends tied to the network, will be easier to remove than the resin, with a predominantly branched structure and three or more ends at each silicon atom chemically anchored to the surroundings. A diffusion rate difference also exists to augment the decomposition rate disparity. This principle has been verified: a piece of silicone rubber loses twice the fraction of its weight compared to a piece of silicone resin after both are boiled in a KOH solution for the same period of time.

The resin samples were polished according to the same procedure used for a three point bending test sample. The polished sample was dipped into a boiling KOH aqueous solution for a period of time; it was then washed in water thoroughly and observed under the SEM.

Figure A1a was taken from the polished surface of a sample before etching. It contained 10 parts of KPE Phase I and 2 parts of Phase II rubber of DP 586. The unetched surface was smooth and featureless. After etching in a 30 wt.% KOH solution for 10 minutes, as shown by Figure A1b, the rubbery particles were partially removed. If this is compared to Figure 3.13, an image of the freshly fractured surface of the same sample, it can be seen that the particle size is the same as that of the holes produced by etching. If the sample is etched in a 40 wt.% solution for 10 minutes, the rubbery particles are completely removed; see Figure A2.

The etching process does not produce holes on the surface if there are no rubber particles present. Figure A3 shows the unetched and etched surfaces of the unmodified resin. It is evident that etching produces a smoother

surface: a form of chemical polishing takes place. Figure A4 shows the PAE Phase I toughened resin surface roughened by the etching.

Other experiments confirmed that the PDMS is preferentially etched by this process. In Figure A5, pre-formed silicone rubber particles which had been mixed with the 4-3136 resin are seen agglomerated. They were attacked and removed by the etch; see Figure A6.

The etching behavior of a sample containing 10 parts of PAE Phase I and 5 parts of Phase II PDMS of DP 375, discussed in Chapter 3, verified the rubbery composition of the small Phase II particles. Figure A7 shows the surface after being etched in a 40 wt.% KOH solution for 10 seconds. Holes of approximately 150 nm in diameter are seen. The boundary between the holes is blurred, indicating a decomposition of the inter particle ligands. This cannot be ignored because of the small ligand thickness. In Figure A8, two images taken from an area with relatively fewer particles are shown. Holes approximately 200 nm in diameter are seen. As a result of the degradation of the inter particle ligands, the holes are larger than the actual particles.

a

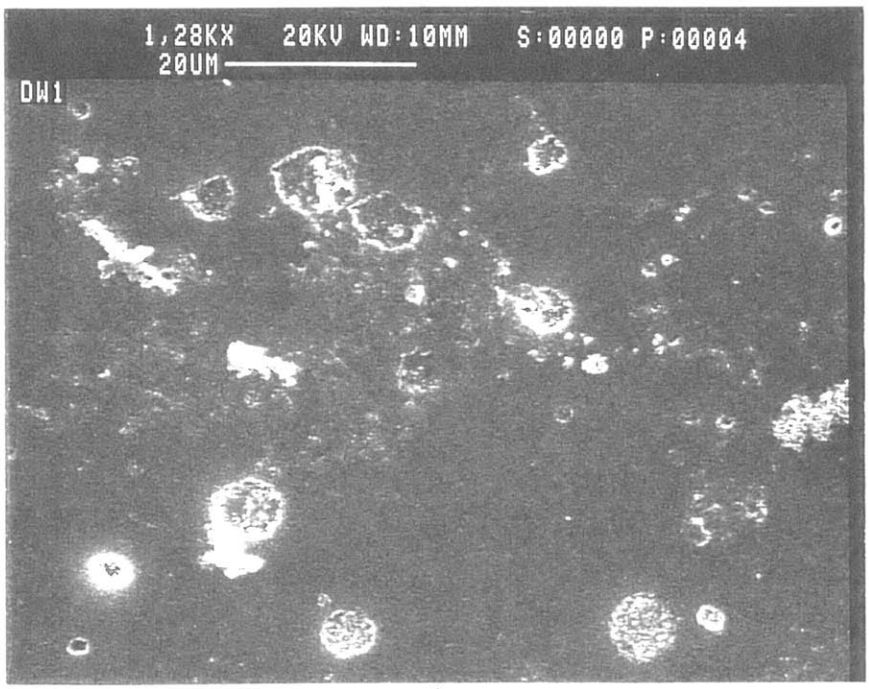

b

Figure A1. SEM photos of, a: polished surface of the 4-3136 resin modified by 10 parts of KPE and 2 parts of Phase II PDMS of DP 586; and b: the surface etched by a 30 wt.% KOH aqueous solution for 10 minutes at the boiling point.

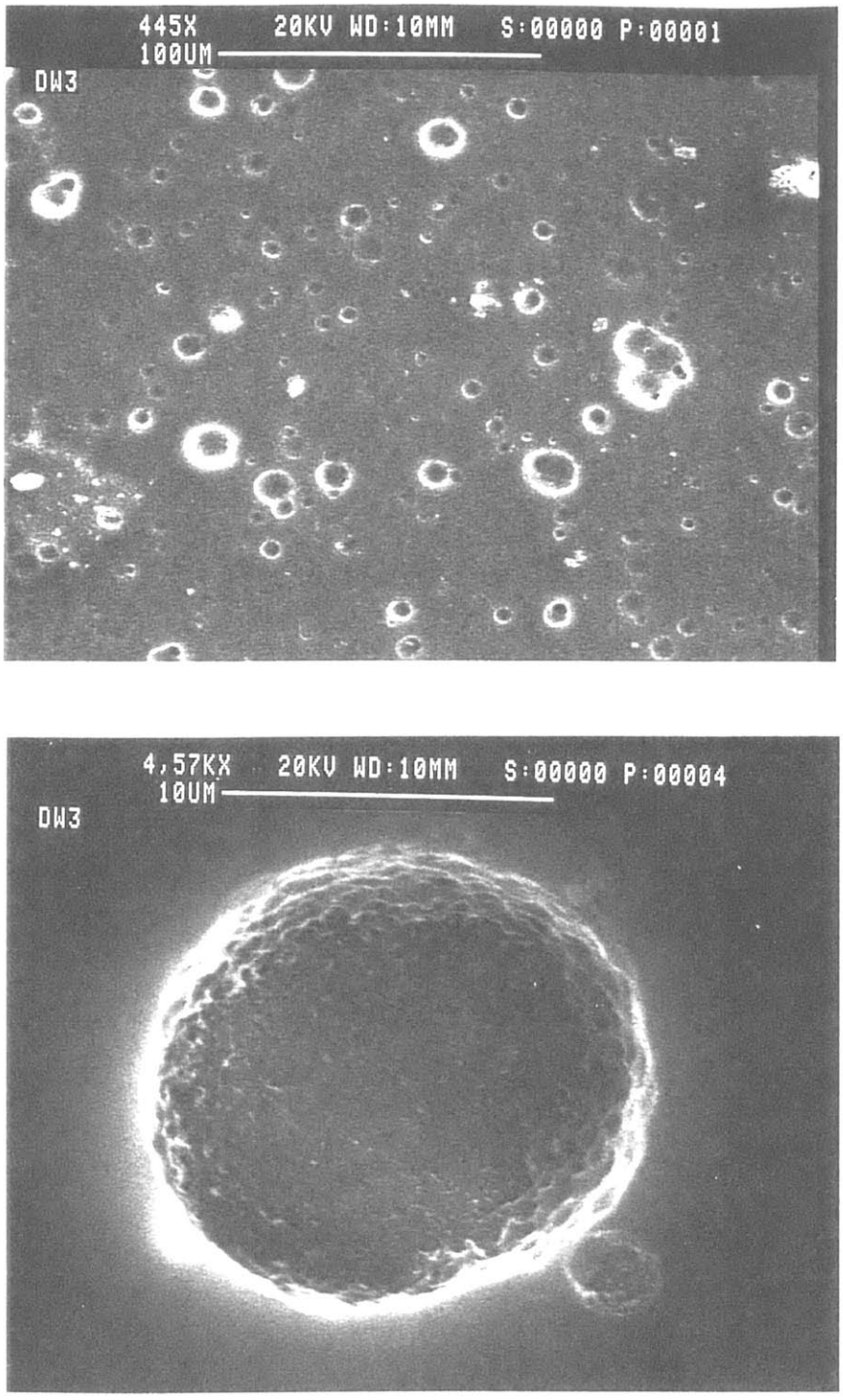

Figure A2. SEM photos of the etched surface of the 4-3136 resin modified by 10 parts of KPE and 2 parts of Phase II PDMS of DP 586. Etching conditions: 40 wt.% KOH aqueous solution for 10 minutes at its boiling point.

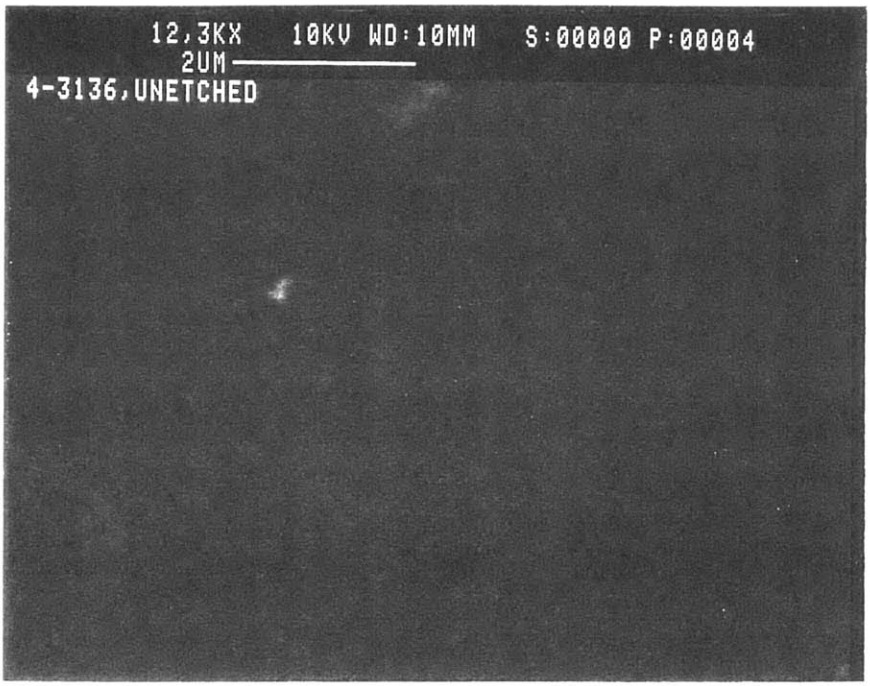

a

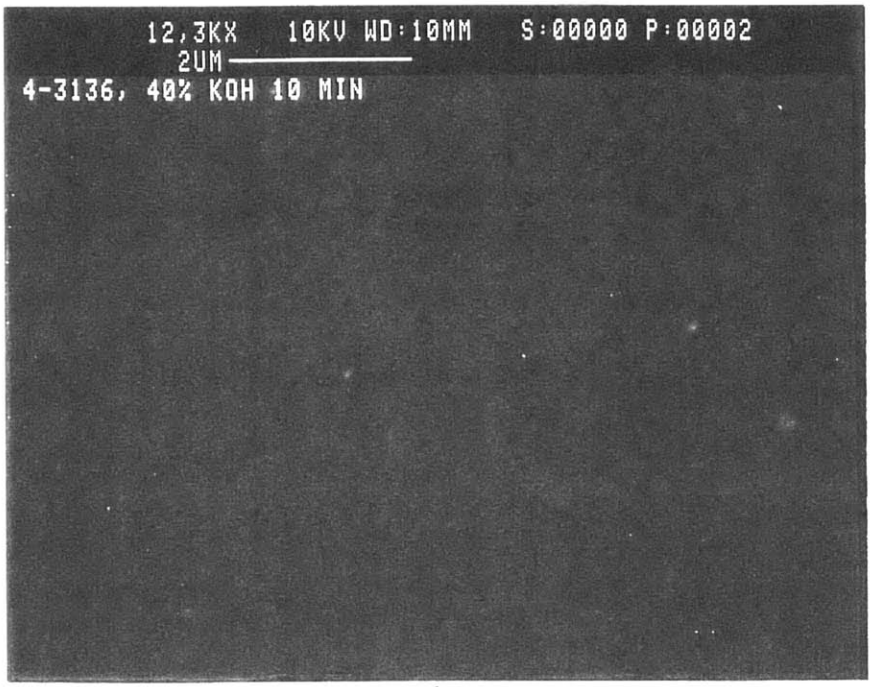

b

Figure A3. SEM photos of the surface of the unmodified 4-3136 resin. a: unetched; and b, etched in a 40 wt.% KOH aqueous solution for 10 minutes at the boiling point.

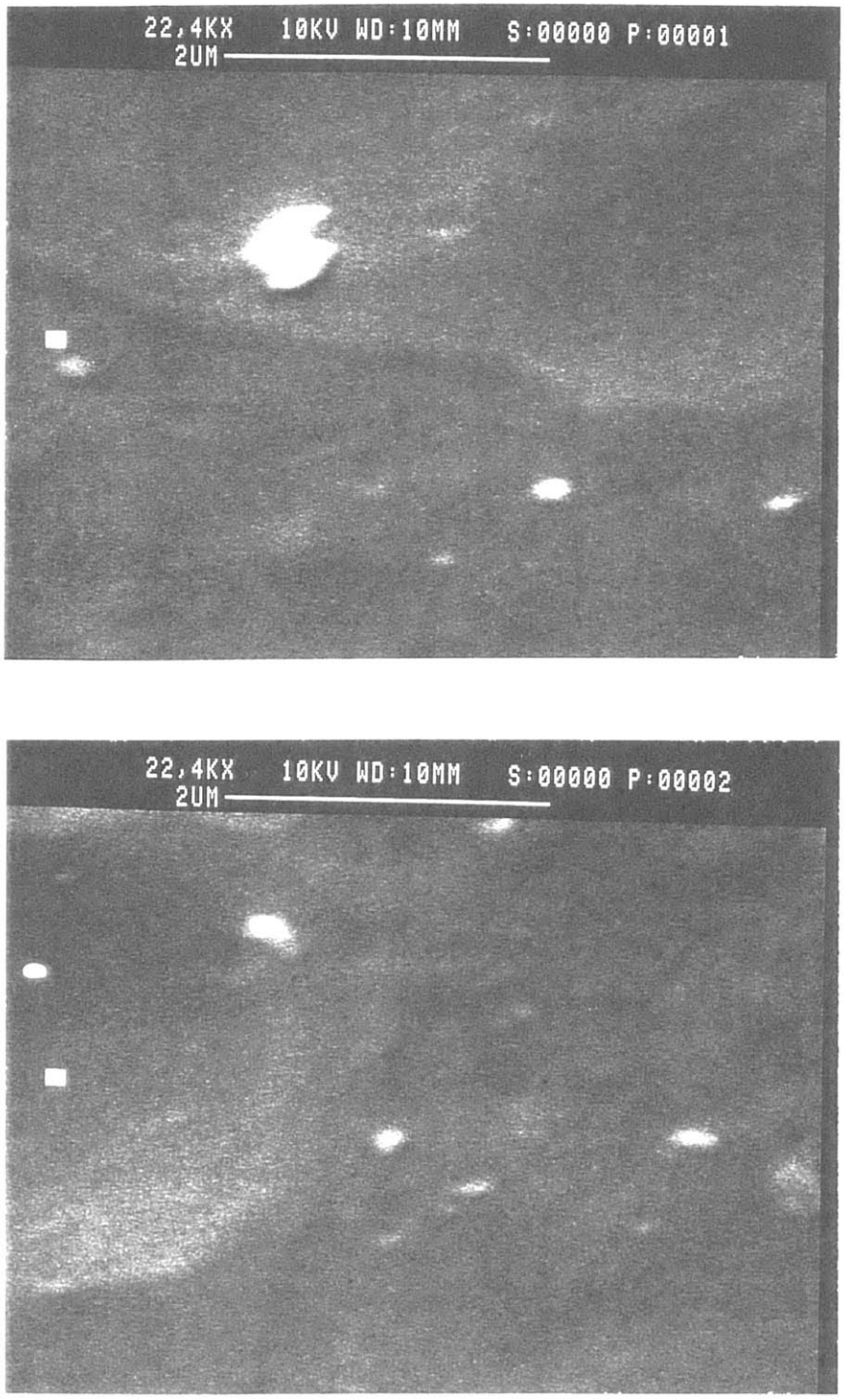

Figure A4. SEM photos of the etched surface of the 4-3136 resin modified by 10 parts of PAE, a Phase I PDMS. Etching conditions: 40 wt.% KOH aqueous solution for 10 minutes at its boiling temperature.

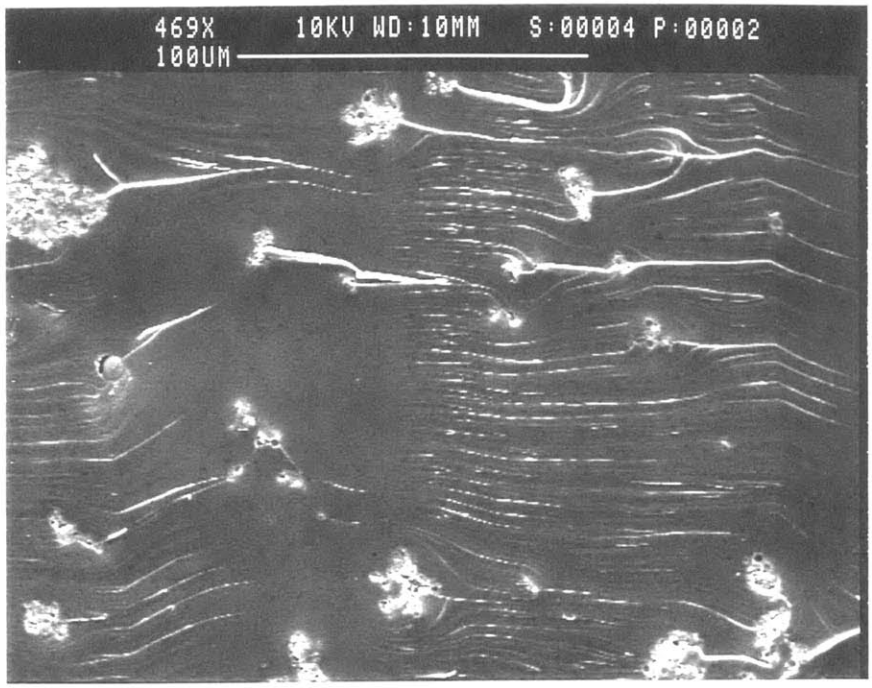

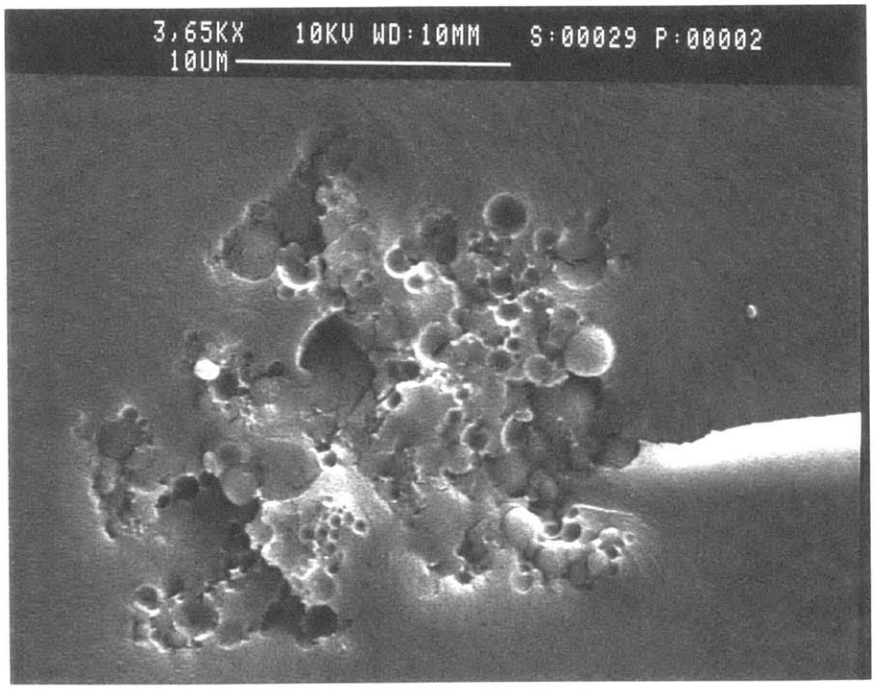

Figure A5. SEM photos of the freshly fractured surface of the 4-3136 resin containing 1 part silicone rubber powders.

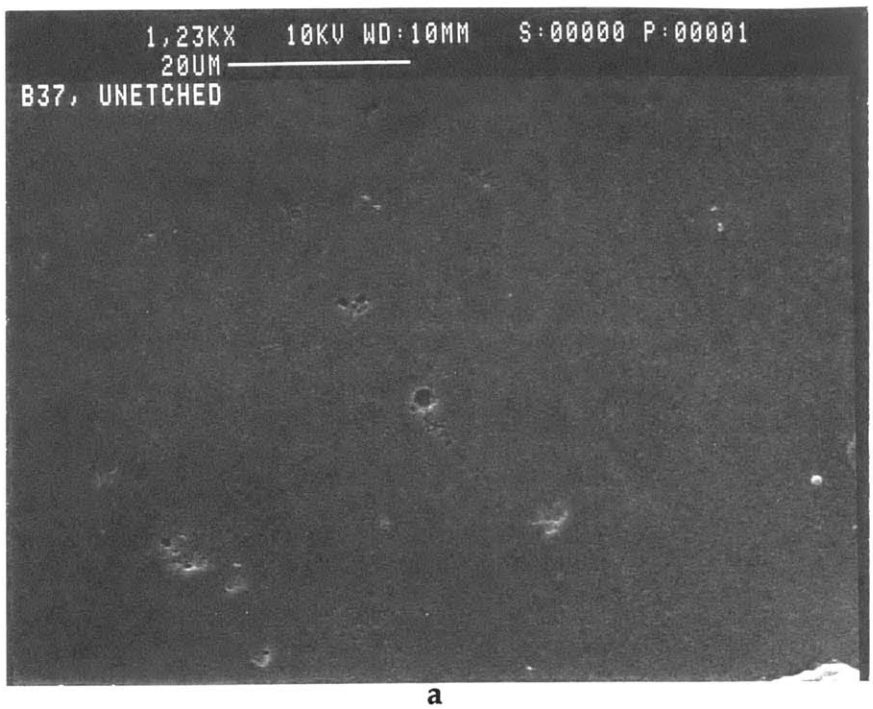

a

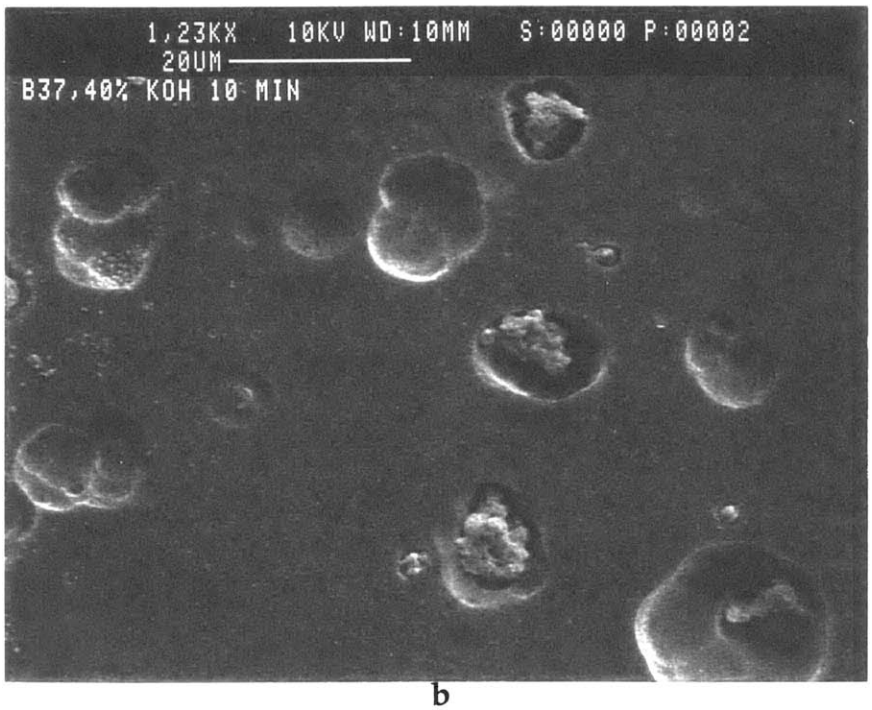

b

Figure A6. SEM photos of the surface of the 4-3136 resin containing 1 part silicone rubber powders. a: unetched; b: etched in a 40 wt.% KOH solution for 10 minutes at the boiling point.

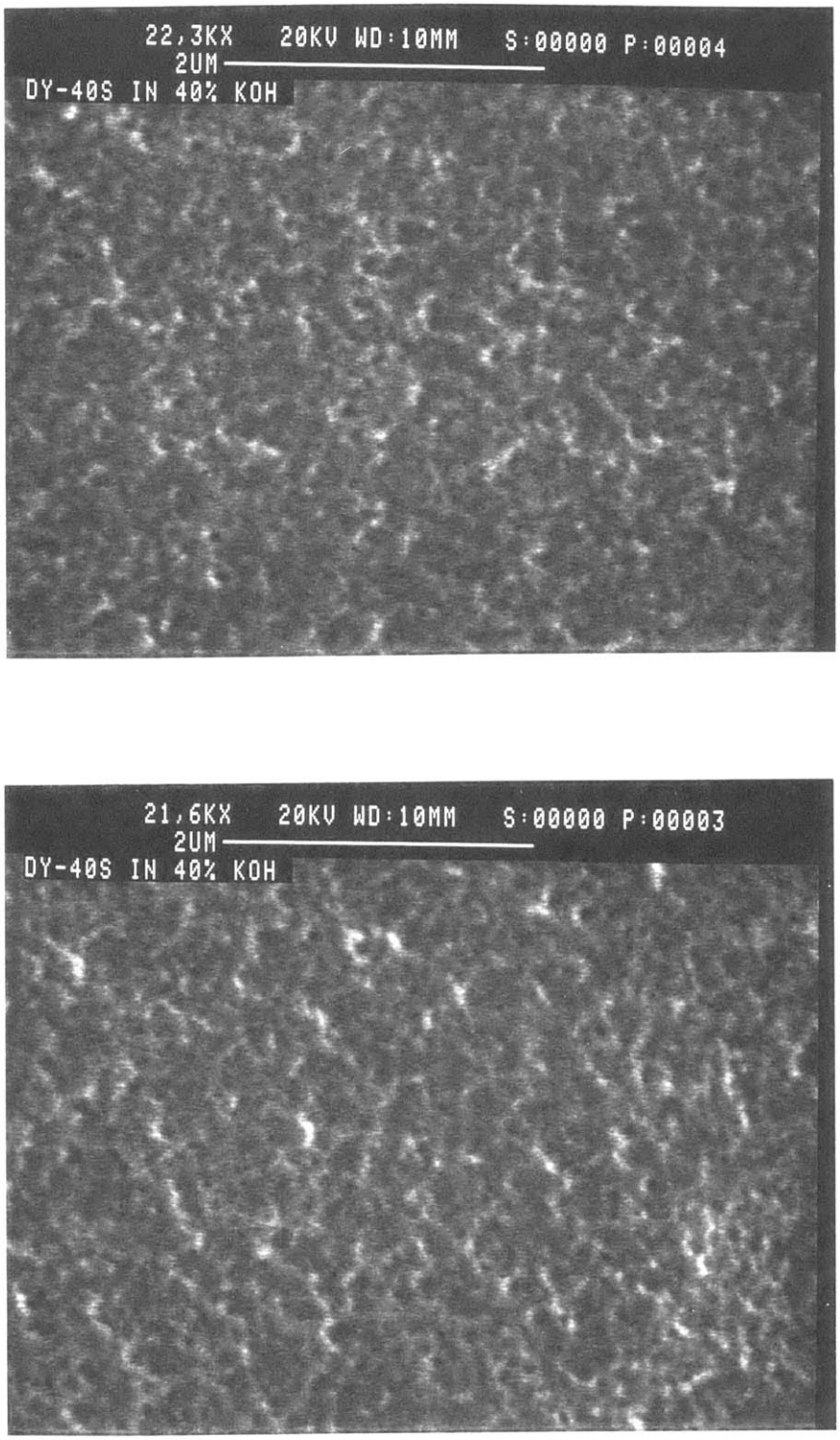

Figure A7. SEM photos of the 4-3136 resin modified by a combination of 10 parts of PAE with 5 parts of Phase II PDMS of DP 375. Etching conditions: 40 wt.% KOH solution, 10 seconds at the boiling point.

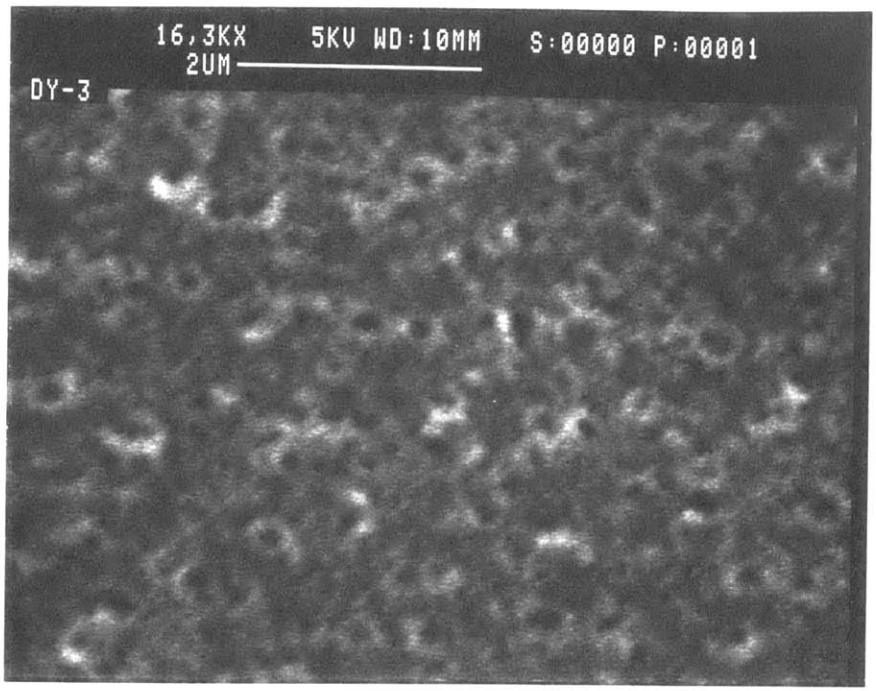

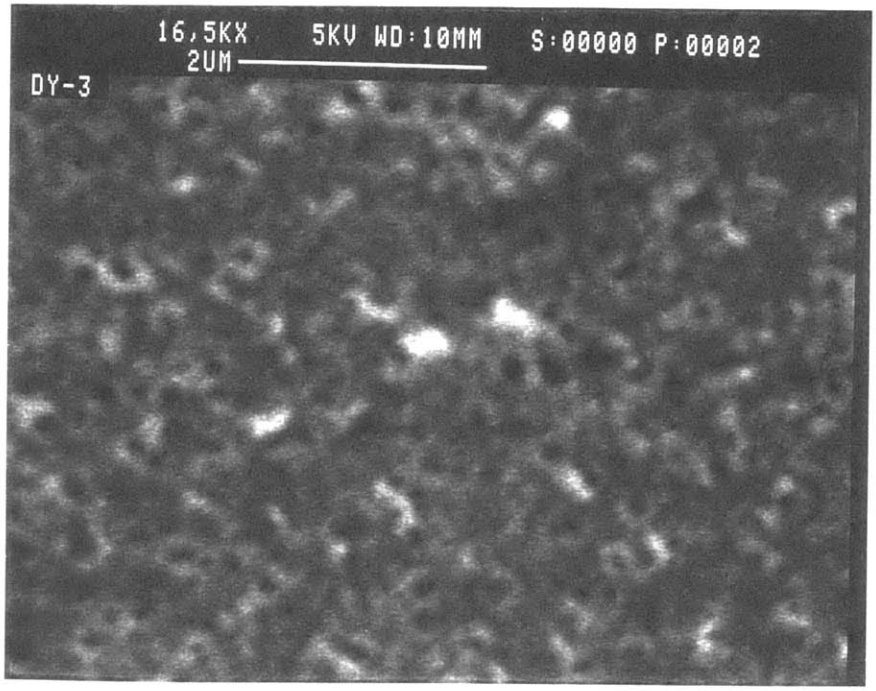

Figure A8. SEM photos of the 4-3136 resin modified by a combination of 10 parts of PAE with 5 parts of Phase II PDMS of DP 375. Etching conditions: 40 wt.% KOH solution, 10 seconds at the boiling point.

Bibliography

Chapter 1.

1. Hourston, D. J., Lane, S., and Zhang, H. X., *Polymer*, 1991, **32**, 2215.
2. Sullivan, V. J., *ANTEC '93*, May 1993, p96.
3. Chung, J. Y. J., and Lazear, N. R., *ANTEC '94*, May 1994, San Francisco, p1728.
4. Chung, M., -F., Golovoy, A., Mindroiu, V. E., Plummer, H. K., and van Oene, H., *Polymer*, 1993, **34**, 3809.
5. Kramer, E. J., *MMM Press Symposium Series: Polymer Compatibility and incompatibility, Principles and Practices: Papers Presented at the 10th Midland macromolecular Meeting*, 1982, **V2**, Midland, MI., MMM Press by Harwood Acedamic Publ., New York, p251.
6. McGarry, F. J., *Polymer Toughening*, edited by Charles B. Arends, Marcel Dekker, Inc., New York, p175.
7. Huang, Y., Hunston, D. L., Kinloch, A. J., and Riew, C. Keith, *Rubber Toughened Plastics, ACS Advances in Chemistry Series 233*, 1993, p1.
8. Bucknall, C. B., *Toughened Plastics*, Applied Science Publishers Ltd., 1977.
9. Seymour, R. B., *Rubber Toughened Plastics, ACS Advances in Chemistry Series 222*, edited by Riew, C. K., 1989.
10. Hedrick, J. L., Allen, R. D., Diaz, A., Hilborn, J. G., and Hendrick, J. C., *Polymer Bulletin*, 1993, **31**, 715.
11. Majumdar, B., Keskkula, H., and Paul, D. R., *Polymer*, 1994, **35**, 1399.
12. Kumar, G., Neelakantan, N. R., Subramanian, N., *J. Mater. Sci.*, 1995, **30**, 1480.
13. Hobbs, S. Y., Bopp, R. C., and Watkins, V. H., *Polym. Eng. Sci.*, 1983, **23**, 380.
14. Arends, C. B., editor, *Polymer Toughening*, Marcel Dekker, Inc., New York, 1989.
15. Howard, R. N., *The Physics of Glassy Polymers*, John Wiley & Sons, New York, 1973, Chapters 5, 6, and 7.
16. Echte, A., *Rubber-Toughened Plastics, ACS Advances in Chemistry Series 222*, 1989, p15.
17. Gebizlioglu, O. S., Argon, A. S., and Cohen, R. E., *Polymer*, 1985, **26**, 519.
18. Braun, D., Klein, M., and Hellmann, G. P.,*J. Appl. Polym. Sci.*, 1996, **60**, 981.
19. Gebizlioglu, O. S., Argon, A. S., and Cohen, R. E., *Polymer*, 1985, **26**, 529.
20. McGarry, F. J., and Rosner, R. B., *Rubber Toughened Plastics, ACS Advances in Chemistry Series 233*, 1993, p305.
21. Sultan, J. N., McGarry, F. J., *Polym. Eng. Sci.*, 1973, **13**, 29.
22. Iljima, T., Tomoi, M., Suzuki, A., and Kakiuki, H., *Euro. Polym. J.*, 1991, **27**, 851.

23. Lanzetta, N., Laurienzo, P., Malinconico, M., Martuscelli, E., Ragosta, G., and Volpe, M. G., *J. Mater. Sci.*, 1992, **27**, 786.
24. Pearce, P. J., Siebert, A. R., Egan, D. R., Guiley, C. D., and Drake, R. S., *J. Adhesion*, 1995, **49**, 245.
25. Vallo, C. I., Hu, L., Frontini, P. M., and Williams, R. J. J., *J. Mater. Sci.*, 1994, **29**, 2481.
26. Maazouz, A., Sautereau, H., and Gerard, J. F.,*Polymer Bulletin*, 1994, **33**, 67.
27. Geisler, B., and Kelley, N., *J. Appl. Polym. Sci.*, 1994, **54**, 177.
28. McGarry, F. J., *Proc. Roy. Soc. London*, 1970, **A319**, 58.
29. Sultan, J. N., and McGarry, F. J., *Microstructural Characteristics of Toughened Thermosett Polymers*, MIT School of Engineering, Research Report R69-59, October 1969.
30. Yanagase, A., Ito, M., Yamamoto, N., and Ishikawa, M., *J. Appl. Polym. Sci.*, 1996, **62**, 1387.
31. Bakar, M., Djaider, F., and Feghouli, A., *ANTEC '94*, May 1994, San Francisco, p1724.
32. Abbate, M., Martuscelli, E., Musto, P., Ragosta, G., and Leonardi, M., *J. Appl. Polym. Sci.*, 1996, **62**, 2107.
33. Lowell, P. A., McDonald, J., Saunders, D. E. J., and Young, R. J., *Polymer*, 1993, **34**, 61.
34. Das, B., Gangopadhyay, T., and Sinha, S., *J. Appl. Polym. Sci.*, 1994, **54**, 367.
35. Kyu, T., Kennedy, J. P., and Richard, G. C., *Macromolecules*, 1993, **26**, 572.
36. Kennedy, J. P., and Richard, G. C., *Macromolecules*, 1993, **26**, 567.
37. Vazquez, F., Schneider, M., Pith, T., and Lambla, M., *Polymer International*, 1996, **41**, 1.
38. Archer, A. C., Lovell, P. A., McDonald, J., Sherratt, M. N., and Young, R. J.,*Macromolecular Reports*, 1994, **A31(Suppls. 6&7)**, 901.
39. Oshinski, A. J., Keskkula, H., and Paul, D. R., *J. Appl. Polym. Sci.*, 1996, **61**, 623.
40. Oshinski, A. J., Keskkula, H., and Paul, D. R., *Polymer*, 1996, **37**, 4909.
41. Liu, Y., and Donovan, J. A., *ANTEC '94*, May 1994, San Francisco, p1746.
42. Liu, Y., and Donovan, J., *ANTEC '95*, May 1995, Boston, p1530.
43. Harding, J. A., *ANTEC '95*, May 1995, Boston, p1526.
44. Ishikawa, M., Sugimoto, M., and Inoune, T., *J. Appl. Polym. Sci.*, 1996, **62**, 1495.
45. Wand, Z., *J. Appl. Polym. Sci.*, 1996, **60**, 2239.
46. Gupta, A. K., Ratnam, B. K., and Srinivasan, K. R., *J Appl. Polym. Sci.*, 1992, **45**, 1303.
47. Tanrattanakul, V., Baer, E., Hiltner, A., Hu, R., Dimonie, V. L., El-Aasser, M. S., Sperling, L. H., and Mylonakis, S. G., *J. Appl. Polym. Sci.*, 1996, **62**, 2005.

48. Seibel, S. R., and Moet, A., *ANTEC '95*, May 1995, Boston, p3966.
49. Carte, T. L., and Moet, A., *J. Appl. Polym. Sci.*, 1993, **48**, 611.
50. Rakoutz, M., and Balme, M., *Polymer Journal*, 1987, **19**, 173.
51. Hedrick, J. L., Hilborn, J. G., Prime, R. B., Labadie, J. W., Dawson, D. J., Russell, T. P., and Wakharker, V., *Polymer*, 1994, **35**, 291.
52. Kinloch, A. J., and Willaims, J. G., *J. Mater. Sci.*, 1080, **15**, 987.
53. Kinlock, A. J., and Shaw, S. J., *Polymer*, 1983, **24**, 1355.
54. Yamini, S., and Young, R. J., *J. Mater. Sci.*, 1980, **15**, 1823.
55. Dugdale, D. S., *J. Mech. Phys. Solids*, 1960, **8**, 100.
56. Creager, M., and Paris, P. C., *J. Geoph. Res.*, 1968, **73**, 247.
57. Williams, J. G., *Stress Analysis of Polymers*, Longman, London, 1977, p242.
58. Griffith. A. A., *Phil. Trans. R. Soc.*, 1920, **A221**, 163.
59. Irwin, G. R., *J. Appl. Mechanics*, 1957, September, 361.
60. Irwin, G. R., *Proc. the Seventh Sagamore Ordnance Materials Research Conference*, August 1960, IV-63.
61. Selsing, J., *J. American Ceramics Soc. -Discussions and Notes*, August 1961, 419.
62. Goodier, J. N., *Appl. Mechanics*, 1933, 39.
63. Argon, A. S., Cohen, R. E., Gebizlioglu, O. S., and Schwier, C. E., *Advances in Fracture Research, (Fracture 84)*, 1984, **1**, 427.
64. Konczol, L., Doll, W., and Michler, G. H., *Colloid & Polym. Sci.*, 1992, **270**, 972.
65. Narisawa, I., *190th ACS National Meeting, Division of Polymer Chemistry*, Chicago, September 1985, paper 122.
66. Argon, A. S., Cohen, R. E., and Qin, J.,*190th ACS National Meeting, Division of Polymeric Materials: Science and Engineering, Inc.* paper 1.
67. Qin, J., Argon, A. S., and Cohen, R. E., *ibid.*, paper 2.
68. Okamoto, Y., Miyagi, H., Uno, T., and Amemiya, Y., *Polym. Eng. Sci.*, 1993, **33**, 1606.
69. Cheng, C., Hiltner, A., Baer, E., Soskey, P. R., and Mylonakis, S. G., *J. Appl. Polym. Sci.*, 1994, **52**, 177.
70. Ishikawa, M., *Polymer*, 1995, **36**, 2203.
71. Dompas, D., and Groeninckx, G., *Polymer*, 1994, **35**, 4743.
72. Liang, H., Jiang, W., Zhang, J., and Jiang, B., *J. Appl. Polym. Sci.*, 1996, **59**, 505.
73. Magalhaes, A. M. L., and Borggreve, R. J. M., *Macromolecules*, 1995, **28**, 5841.
74. Ijichi, Y., Kojima, T., Suzuki, Y., Nishio, T., Kakugo, M., and Amemiya, Y.,*Macromolecules*, 1993, **26**, 829.
75. Ishikawa, M., Sato, Y., Yanagase, A., Ito, M., and Yamamoto, N., *Polymer*, 1996, **37**, 5583.
76. Bagheri, R., and Perason, R. A., *Polymer*, 1996, **37**, 4529.
77. Pan, J., Jeong, H.-Y., and Chang, W. J., *ANTEC '95*, May 1995, Boston, p1516.

78. Sue, H. -J., and Yee, A. F., *ibid.*, p1517.
79. Cruz, C. A., and Haviriliak, S., *ibid.*, p1521.
80. Dompas, D., Groeninckx, G., Isogawa, M., Hasegawa, T., and Kadokura, M., *Polymer*, 1994, **35**, 4750.
81. Hill, R. G., *J. Mater. Sci.*, 1994, **29**, 3062.
82. Muratoglu, O. K., Argon, A. S., Cohen, R. E., and Weinberg, M., *Polymer*, 1995, **36**, 921.
83. Okamoto, M., Shinoda, Y., Kojima, T., and Inoue, T., *Polymer*, 1993, **34**, 4868.
84. Dompas, D., Groeninckx, G., Isogawa, M., Hasegawa, T., and Kadokura, M.,*Polymer*, 1994, **35**, 4760.
85. Kunz-Douglass, S., Beaumont, P. W. R., and Ashby, M. F., *J. Mater. Sci.*, 1980, **15**, 1109.
86. Wu, S., *J. Appl. Polym. Sci.*, 1988, **35**, 549.
87. Wu, S., *J. Polym. Sci.*, 1983, **21**, 699.
88. Margolina, A., and Wu, S., *Polymer*, 1988, **29**, 2170.
89. Wu, S., *Polymer*, 1990, **31**, 972.
90. Wu, S., *Polymer*, 1985, **26**, 1855.
91. Sjoerdsma, S. D., *Polymer Communications*, 1989, **30**, 106.
92. Wu, S., *Polymer*, 1985, **26**, 1855.
93. van der Sanden, M.C.M., Meijer, H.E.H., and Lemstra, P. J., *Polymer*, 1993, **34**, 2148.
94. van der Sanden, M.C.M., Meijer, H.E.H., and Tervoort, T. A., *Polymer*, 1993, **34**, 2961.
95. van der Sanden, M.C.M., Meijer, H.E.H., *ibid.*, 1993, **34**, 5063.
96. van der Sanden, M.C.M., Meijer, H.E.H., *ibid.*, 1994, **35**, 2774.
97. van der Sanden, M.C.M., Buijs, L. G. C., de Bie, F. O., and Meijer, H.E.H.,*ibid.*, 1994, **35**, 2791.
98. van der Sanden, M.C.M., Meijer, H.E.H., *ibid.*, 1994, **35**, 2991.
99. van der Sanden, M.C.M., de Kok, J. M. M., and Meijer, H.E.H., *ibid.*, 1994, **35**, 2999.
100. van der Sanden, M.C.M., Meijer, H.E.H., and Crevecoeur, J. J., *Advanced Composites '93*, edited by Chandra, T and Dhingra, A. K., The Minerals, Metals & Materials Society, 1993, p829.
101. Koo, K. K., Inoue, T., and Miyasaka, K., *Polym. Eng. Sci.*, 1985, **25**, 741.
102. Angola, J. C., Fujita, Y., Sakai, T., and Inoue, T., *J. Polym. Sci., Part B: Polym. Phys.*, 1988, **26**, 807.
103. Kurauchi, T., and Ohta, T., *J. Mater. Sci.*, 1984, **19**, 1699.
104. Karger-Kocsis, J., *Polymer Bulletin*, 1996, **36**, 119.
105. Bucknall, C. B., *Makromol. Chem., Macromol. Symp.*, 1988, **16**, 209.
106. Alan S. W., *Plasticizers: Principles and Practice*, The institute of Materials, The University Press, Cambridge, 1995.
107. Bos, H. L., and Nusselder, J. H., *Polymer*, 1994, **35**, 2793.
108. Kim, H., Keskkula, H., and Paul, D. R., *Reinforcement, Impact Modification and Nucleation of Polymers.* Society of Plastic Engineers,

Regional Technical Conference, Houston, 1990, p33.
109. Chen, T. K., and Jan, Y. H., *Polym. Eng. Sci.*, 1995, **35**, 778.
110. Huo, C., *Tu Liao kung Yeh*, 1986, **3**, 19.
111. Kato, Y., *Shikizai Kyiokai Shi*, 1988, **61**, 699.
112. Ando, N., *Kiogyio Zairyio*, 1996, **44**, 90.
113. Akashi, M., *Kaobunshi Kakao*, 1996, **45**, 124.
114. Chida, K., Sakaguchi, S., Wagatsuma,, M., and Kimura, T., *Electronics Letters*, 1982, **18**, 713.
115. Shibata, S., Kimura, T., Sakaguchi, S., and Ohmori, Y., *Electronics Letters*, 1984, **20**, 662.
116. Bogatyrjov, V. A., Bubnov, M. M., *Electronics Letters*, 1986, **22**, 1013.
117. Gutek, B. I., and vanWert, B., *Ind. Eng. Chem. Prod. Res. Dev.*, 1982, **21**, 601.
118. Weyenberg, D. R., *Silicon Chemistry*, edited by Corey, E. R., Corey, J. Y, and Gaspar, P. P., Ellis Horwood Limited, 1987, Chapter 27.
119. Laubender, T., *Technol. Dev. Coat.: Their Appl. Uses, Middle East Conf., 2nd*, 1995, Paper 9.
120. Bhute, R. S., and Aggarwal, J. S., *J. Scient. Ind. Res.*, 1968, **27**, 181.
121. Suzuki, T., *Netsu Kiokasei Jushi*, 1994, **15**, 9.
122. Chen, P. Y., *Kung Yeh Chi Shu*, 1978, **54**, 30.
123. Sato, A., Ushigome, M., and Matsumura, F., *IEEE*, 1985, p9.
124. Collins, W. R., and powell, D. B., *ibid.*, 1985, p14.
125. Ritchie, B., *Converting to Solvent-Free Conformal Coating Process*, 485.
126. Trego, B. R.,*European hybrid Microelectronics Conference*, 1979, Ghent, p499.
127. Narula, D., Be, A., and Yamada, H., *Proceedings of the twenty-first Waterborne, higher-solids, and Powder Coatings Symposium*, 1994, New Orleans, p114.
128. Ban, H., Tanaka, A., Kawai, Y., and Imamura, S., *Polymer*, 1990, **31**, 564.
129. Oikawa, A., Fukuyama, S. -I., and Yoneda, Y., *J. Electrochem. Soc.*, 1990, **137**, 3223.

Chapter 2.

1. Ho, T. H., and Wang, C. S., *J. Appl. Polym. Sci.*, 1994, **54**, 13.
2. Tong, J. D., Bai, R., Pan, C. Y., and Goethals, E. J., *J. Appl. Polym. Sci.*, 1995, **57**, 895.
3. Tong, J. D., Bai, R., Zou, Y. F., Pan C. Y., and Ichimura, S., *J. Appl. Polym. Sci.*, 1994, **52**, 1373.
4. Riffle, J. S., Yilgor, I., Banthia, A. K., Wilkes., G. L., and McGrath, J. E., *Org. Coat. Appl. Polym. Sci. Proc.*, 1981, **46**, 397.

5. Konczol, L., Doll, W., Buchholz, U., and Mulhaupt, R., *J. Appl. Polym. Sci.*, 1994, **54**, 815.
6. Bergstrom, D. F., Burns, G. T., Decker, G. T., Durall, R. L., Fyrear, D., and Gornowicz, G. A., *37th Intern. SAMPE Symposium*, March 1992, p278.
7. DeLollis, N. J., *25th National SAMPE Symposium and Exhibition*, May 1980, p507.
8. Ho, T. H., and Wang, C. S., *Polymer*, 1996, **37**, 2733.
9. Lin, S. T., and Huang, S. K., *J. Polym. Sci., Part A: Polym. Chem.*, 1996, **34**, 1907.
10. Castellanos, F., Fouassier, J. P., and Cavezzan, J., *J. Appl. Polym. Sci.*, 1996, **60**, 705.
11. Lin S. T., and Huang, S. K., *J. Polym. Sci., Part A: Polym. Chem.*, 1996, **34**, 869.
12. Matsukawa, K., HASEGAWA, K., Inoue, H., Fukuda, A., and Arita, Y., *J. Polym. Sci., Part A: Polym. Chem.*, 1992, **30**, 2045.
13. Nakamura, Y., Uenishi, S., Kunishi, T., Miki, K., Tabata, H., Kuwada, K., Suzuki, H., and Matsumoto, T., *IEEE*, 1987, p187.
14. Kuwada, K., Iko, K., and Tabata, H., *IEEE*, 1985, p18.
15. Miwa, M., Takeno, A., Hara, K., and Watanabe, A., *Composites*, 1995, **26**, 371.
16. Ho, T. H., and Wang C. S., *J. Appl. Polym. Sci.*, 1994, **51**, 2047.
17. Lee. C. J., *SAMPE Journal*, 1985, **July/August**, 34.
18. Arnold, C. A., Summers, J. D., Chen, Y. P., Yoon, T. H., McGrath, B. E., Chen. d., and McGrath, J. E., in *Polyimides: Materials, Chemistry and Characterization*, edited by Feger, C., Khojasteh, M. M., and McGrath, J.E., Elsevier Science Publishers B. V., Amsterdam, 1989, p69.
19. John. T. V., and Valenty, V. B., *ibid.*, 1989, p91.
20. Bolon, D. A., Hallgren, J. E., Eddy, V. J., Codella, P. J., Davis, G. C., and Regh, K. A., *ibid.*, 1989, p103.
21. Packirisamy, S., in *Polyimides and other High-Temperature Polymers*, edited by Abadie, M.J.M., and Sillion, B., Elsevier Publishers B.V., Amsterdam, 1991, p255.
22. Sillion, B., and Verdet, L., *ibid.*, 1991, p363.
23. Bureau, J-M., Graciet, M., and Bernard, F., *ibid.*, 1991, p387.
24. Nair, C. P. R. and Clouet, G., *Macromolecules*, 1990, **23**, 1361.
25. Hedrick, J. L., Haidar, B., Russell, T. P., and Hofer, D. C., *Macromolecules*, 1988, **21**, 1967.
26. Yilgor, I., Steckle, W. P., Yilgor, Emel, Freelin, R. G., and Riffle, J. S., *J. Polym. Sci., Part A: Polym. Chem.*, 1989, **27**, 3673.
27. Matsumoto, T., Koinuma, Y., Waki, K., Kishida, A., Furuzono, T., Maruyama, I., and Akashi, M., *J. Appl. Polym. Sci.*, 1996, **59**, 1067.
28. Lu S., Pearce, E. M., and Kwei, T. K., *J. Polym. Sci., Part A: Polym. Chem.*, 1994, **32**, 2597.

29. Hamurcu, E. E., Hazer, B., Misirli, Z., and Baysal, B. M., *J. Appl. Polym. Sci.*, 1996, **62**, 1415.
30. Oiatt, H. W., Shea K. J., Kalluri, S., Shi, Y., and Steier, W. H., *Chem. Mater.*, 1995, **7**, 493.
31. Sung, C., Sobarzo, M. R., and Merrill, E. W., *Polymer*, 1990, **31**, 556.
32. Okada, T., and Ikada, Y., *Makromol. Chem.*, 1991, **192**, 1705.
33. Pillot, J., Dunogues, J., Gerval, J., The, M. D., and Thanh, M. V., *Eur. Polym. J.*, 1989, **25**, 285.
34. Lee, C. J., *IEEE*, 1989, p896.
35. Noll. W., *Chemistry and Technology of Silicones*, Academic Press, London, 1968.
36. Zeigler, J. M., and Feraron, F. W. G., (editors), *Silicon Based Polymer Science: A Comprehensive Resources, ACS Advances in Chemistry Series 224*, Washington, D. C., 1990.
37. Tomanek, A., *Silicones & Industry; A compendium for practical use, instruction and reference*, Hanser, 1991.
38. Auner, N., and Weis, J., (editors), *Organosilicon Chemistry: from Molecules to Materials*, VCH, New York, 1994.
39. Clarson, S. J., and Semlyen, J. A., *Siloxane Polymers*, Ellis Horwood-PTR Prentice Hall, New Jersey, 1993.
40. ASTM Standard D 790-92.
41. Smith, A. L., *Spectrochimica Acta*, 1960, **16**, 87.
42. Smith, A. L., *ibid.*, 1963, **19**, 849.
43. Smith, A. L., editor, *The Analytical Chemistry of Silicones*, John Wiley & Sons, Inc., New York, 1991, Chapter 11.
44. Durig, J. R., editor, *Chemical, Biological and Industrial Applications of Infrared Spectroscopy*, John Wiley & Sons, New York, 1985, p73-85.
45. Aldrich Library of FT-IR.
46. Akiff, J. W., *NMR and Chemistry: An Introduction to the Fourier Transformation-Multinuclear Era*, second edition, Chapman and Hall, New York, 1983.
47. Williams, E. A., Cargioli, J. D., *Annual Reports on NMR Spectroscopy*, 1979, **9**, 221.
48. Williams, E. A., *Annual Reports on NMR Spectroscopy*, 1983, **15**, 235.
49. Williams, E. A., Donahue, P. E., and Cargioli, J. D., *Macromolecules*, 1981, **14**, 1016.
50. Williams, E. A., Cargioli, J. D., and Hobbs, S. Y., *Macromolecules*, 1977, **10**, 782.
51. Zicmane, E. L. I., and Lukevics, E., *J. Organometall. Chem.*, 1986, **306**, 167.
52. Franck, J., and Sponer, H., *The J. Chem. Phys.*, 1956, **25**, 172.
53. Brandt, P. J. A., Subramanian, R., Sormani, P. M., Ward, T. C., and McGrath, J. E., *Polym. Preprints*, 1985, **26**, 213.

54. Levy. G. C., and Cargioli, J. D., *Nuclear Magnetic Resonance, Spectroscopy of Nuclei Other Than Protons*, edited by Axenrod, T and Webb, G. A., 1974, p251.
55. Flory, P. J., *Principles of Polymer Chemistry*, Cornell University Press, Ithaca, New York, 1953, p509, 549.

Chapter 3.

1. Williams, J. G., *Fracture Mechanics of Polymers*, Ellis Horwood Limited, New York, 1984.
2. Anderson, T. L., *Fracture Mechanics, Fundamentals and applications*, CRC Press, Ann Arbor, 1995.
3. Williams, J. g., *Stress Analysis of Polymers*, 2nd edition, Ellis Horwood Limited, New York, 1980.
4. ASTM Standard D5045-91a.
5. Argon, A. S.., Cohen, R. E., Gebizlioglu, O. S., and Schwier, C. E., *Crazing in Block Copolymers and Blends, Advances in Polymer Science*, **52/53**.
6. Anderson, T. L., *Fracture Mechanics: Fundamentals and Applications*, 2nd edition, CRC press, Ann Arbor, 1995, p74.
7. Anderson, T. L., *ibid.*, p77, 326.

Chapter 4.

1. Preston, F. W., *J. Amer. Ceram. Soc.*, 1931, **14**, 419.
2. Atsuta, M., and Turner, D. T., *J. Mater. Sci. Letters*, 1982, **1**, 167.
3. Pan, T. Y., Robertson, R. E., and Filisko, F. E., *J. Mater. Sci.*, 1989, **24**, 3635.
4. Hull, D., *Intern. J. Fracture*, 1993, **62**, 119.
5. Kerlins, V., and Phillips, A., *Modes of Fracture, in Metals Handbook*, 9th edition, vol 12, *Fractography*, Metals Park, Ohio.
6. Robertson, R. E., Mindroiu, V. E., and Cheung, M. F., *Composites Science and Technology*, 1985, **22**, 197.
7. Robertson, R. E., and Mindroiu, V. E., *J. Mater. Sci.*, 1985, **20**, 2801.
8. Robertson, R. E., and Mindroiu, V. E., *Polym. Eng. Sci.*, 1987, **27**, 55.
9. Taylor, G., *Proc. Roy. Soc. London, A*, 1950, **201**, 192.
10. Lewis, D. J., *Proc. Roy. Soc. London, A*, 1951, **202**, 81.
11. Fields, R. J., and Ashby, M. F., *Philosophical Magazine*, 1976, **33**, 33.
12. Argon, A. S., and Salama, M., *Mater. Sci. Eng.*, 1976, **23**, 219.

13. Nittmann, J., Daccord, G., and Stanley, H. E., *Nature,* 1985, **314**, 141.
14. Pitts, E., and Greiller, J., *Fluid Mech.,* 1961, **11**, 33.
15. Donald, A. M., and Kramer, E. J., *Philosophical Magazine,* A, 1981, **43**, 857.
16. Kinloch, A. J., Gilbert, D., and Shaw, S. J., *Polymer Communications.* 1985, **26**, 290.
17. Mijovic, J., and Koutsky, J. A., *Polymer,* 1979, **20**, 1095.
18. Williams, J. G., *Fracture Mechanics of Polymers,* John Wiley & Sons, New York, 1984, Chapter 1.

Chapter 5.

1. Schneider, O., *Thermochimica Acta,* 1988, **134**, 269-274.
2. Murayama, T., *Dynamic Mechanical Analysis of Polymeric Materials,* Elsevier Scientific Pub. Co., New York, 1978.
3. Murayama, T., *Encyclopedia of Polymer Science and Engineering,* Vol. 5, p299.

Chapter 6.

1. Lacoste, J., Israeli, Y., and Lemaire, J., *Polymer Durability, ACS Advances in Chemistry Series,* **249**, 1993, p77.
2. Baker, H. R., Kagarise, R. E., O'Rear, J. G., and Sniegoski, P. J., *J. Chemical Eng. Data,* 1966, **11**, 111.
3. Murphy, C. M., Saunders, C. E., and Smith, D. C., *Ind. Eng. Chem.,* 1950, **42**, 2462.
4. Atkins, D. C., Murphy, C. M., and Saunders, C. E., *ibid.,* 1947, **39**, 1395.
5. Clarson, S. J., and Semlyen, J. A., *Siloxane Polymers,* Ellis Horwood-PTR Prentice Hall, New Jersey, 1993, Chapter 5.
6. Grassie, N., and Macfarlane, I. G., *Euro. Polym. J.,* 1978, **14**, 875.
7. Grassie, N., Macfarlane, I. G., and Francey, K. F., *ibid.,* 1979, **15**, 415.
8. Grassie, N., and Francey, K. F., *Polymer Degradation and Stability,* 1980, **2**, 53.
9. Grassie, N., Francey, K. F., and Macfarlane, I. G., *ibid.,* 1980, **2**, 67.
10. Private communications.